Frank N. Crespilho *Editor*

Advances in Bioelectrochemistry Volume 5

Emerging Techniques and Materials, Biodevice Design and Reactions

Springer

Advances in Bioelectrochemistry Volume 5

Frank N. Crespilho
Editor

Advances in Bioelectrochemistry Volume 5

Emerging Techniques and Materials, Biodevice Design and Reactions

Springer

Editor
Frank N. Crespilho
University of Sao Paulo
São Carlos, Brazil

ISBN 978-3-031-10831-0 ISBN 978-3-031-10832-7 (eBook)
https://doi.org/10.1007/978-3-031-10832-7

This Springer imprint is published by the registered company Springer Nature Switzerland AG
The registered company address is: Gewerbestrasse 11, 6330 Cham, Switzerland

Contents

Trends and Validation in Impedimetric Immunosensors in the Application of Routine Analysis

Sthéfane Valle de Almeida, Maria Lurdes Felsner, Juliana Cancino Bernardi, Mauro Chierici Lopes, and Andressa Galli

Abstract In this chapter, the use of statistical tools that can be applied to determine recommended validation parameters is explored, aiming at the application of impedimetric devices in routine analysis. In addition, this section brings published reviews focused on specific areas, such as the development and characteristics of impedimetric immunosensors applied to the analysis of biological and chemical contaminants in foods, pesticides, hormones, and medicines as environmental pollutants and for clinical analysis for the prevention and detection of diseases and pathogenic infections. First, the fundamentals of electrochemical impedance are presented, and then, the applications of the devices and their advantages are discussed in detail. The future perspectives for the use of analytical validation in these systems, the different levels of validation, and the main figures of merit evaluated in immunosensors were also discussed. In addition, future perspectives for the use of these devices with properly validated methodologies are discussed.

Keywords Immunosensor · Electrochemical impedance spectroscopy · Validation · Routine analysis

S. V. de Almeida
Department of Chemistry, Federal University of São Carlos, São Carlos, São Paulo 13565-905, Brazil

M. L. Felsner
Department of Chemistry, State University of Londrina, Londrina, Paraná 86065-970, Brazil

J. C. Bernardi
Chemistry Department, Faculty of Philosophy, Sciences and Letters of Ribeirão Preto - FFCLRP, University of São Paulo, Ribeirão Preto 14040-901, Brazil

M. C. Lopes
Interfaces and Electrochemistry Laboratory, Department of Chemistry, State University of Midwest Paraná, Campus CEDETEG, Guarapuava 85040-167, Brazil

A. Galli (✉)
Electroanalytical and Nanostructured Materials, Department of Chemistry, State University of Midwest Paraná, Campus CEDETEG, Guarapuava 85040-167, Brazil
e-mail: agalli@unicentro.br

F. N. Crespilho (ed.), *Advances in Bioelectrochemistry Volume 5*,
https://doi.org/10.1007/978-3-031-10832-7_1

1 Introduction

Currently, many impedimetric immunosensors have been developed for routine analysis in several matrices [1–4]. In this chapter, we will address the focus for the different samples (food, environmental, and clinical) that have been analyzed using these devices and what is needed for them to be commercialized.

1.1 Immunosensors

Biosensors are analytical devices characterized by the use of a biological material (bioreceptor) coupled to a transducer surface, responsible for converting the biological response into an analytical signal [5, 6]. These devices can be classified according to the type of bioreceptor and the type of transducer, and among the most common bioreceptors are antibodies/antigens, in so-called immunosensors [6, 7]. They are based on the immunological interaction between antigen and antibody, which generate an immune complex (Fig. 1a). In general, immunosensors have advantages such as high sensitivity, speed in obtaining results, simplicity of handling, and the possibility of miniaturization, so that analyses depend on small volumes of samples and reagents [8, 9]. Furthermore, immunosensors can be combined with electrochemical techniques, being the most economically viable due to the low cost of instrumentation and minimal consumption of reagents when compared to other analysis methods [8, 10].

The detection strategy of these devices can vary according to the interaction mechanism between the bioreceptor and the analyte, which can be direct or indirect detection (Fig. 1b). Direct immunosensors utilize the bioreceptor (antibody or antigen) directly anchored to the transducer surface, and the labeled analyte is then recognized and monitored. Although this strategy is faster and simpler than indirect detection, there is little amplification of the analytical signal, leading to lower sensitivity. Furthermore, in direct detection, the choice of the marker is limited. In addition to the surface-anchored bioreceptor, indirect immunosensors use a second labeled antibody that specifically recognizes the analyte and generates the response. This strategy features a wide variety of labeled antibodies available on the market capable of amplifying the analytical signal, increasing the sensitivity of the analysis. However, the labeling step can be time-consuming and increase the cost of the analysis, besides that cross-reactions with the secondary antibody are common, decreasing its specificity [11–14].

Although it is common that both detection strategies (direct and indirect) use markers (enzymes, nanoparticles, fluorophores, etc.), it is also possible to monitor the formation of the immune complex through a label-free detection (Fig. 1c). These devices feature one less preparation step (antibody/antigen labeling), reducing analysis time and cost. This increases the analytic frequency and makes the device more affordable. Also, not using a marker minimizes cross-reactions, leading to

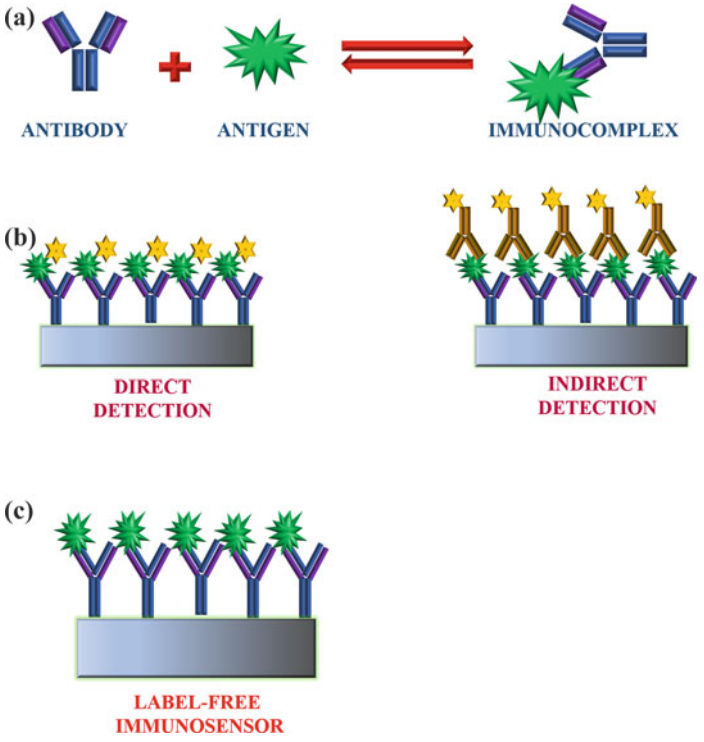

Fig. 1 Representation of immunosensor detection strategies. **a** Immune complex formation. **b** Immunosensor with direct and indirect detection. **c** Immunosensor with label-free detection. [*Source* The authors (2022)]

better accuracy and selectivity [15, 16]. In this context, impedimetric immunosensors, which use the technique of electrochemical impedance spectroscopy (EIS), are advantageous, as they measure the variation in the electrical properties of the electrode surface, providing data about the impedance and resistive properties of the system [15, 17].

1.2 Fundamentals of Impedimetric Measurements

Electrochemical impedance spectroscopy (EIS) consists of applying a low-amplitude sinusoidal input over a given frequency range and analyzing the output signal. The method borrows several concepts from the field of electrical engineering for the analysis of electrical circuits. Due to this, we will first analyze the impedance of some electrical circuits in which the impedance is expressed in terms of electrical properties of the circuit elements, like resistance and capacitance, but is important to understand that impedance is not an electrical property itself. It is, more generally, a

transfer function, that is, a relation between input and output signals in the frequency domain. In the field of electrochemistry, the impedance is formally defined as [18, 19]:

$$Z(\omega) \equiv \frac{\mathcal{F}\{E(t)\}}{\mathcal{F}\{i(t)\}} \tag{1}$$

where $E(t)$ and $i(t)$ are the alternating potential and current, respectively. $\mathcal{F}$ denotes the Fourier transform that is a change of variables defined by:

$$\mathcal{F}\{f(t)\} = \int_{-\infty}^{\infty} f(t)e^{-j\omega t}\mathrm{dt} = F(j\omega) \tag{2}$$

After substituting the limits into the definite integral, the variable t, the time, disappears, and a complex function of ω, the frequency, is obtained. It is simple to show that if the input and output signals are sinusoidal functions with the same frequency, the real and imaginary parts of this complex function can be obtained from the amplitude of the signals and the phase shift between them [20, 21]. Due to non-idealities in the potentiostat and nonlinearities in the system response, the measured signals are more complex than a simple sinusoidal function. In practice, they are represented as a sum of sines and cosines with frequencies that are integer multiples of the fundamental frequency (Fourier series), and due to the low amplitude of the input signal, only the first term of the series is retained [21, 22].

On the other hand, we can obtain theoretical expressions for the impedance of a system by applying the Fourier transform to the time-dependent equations that describe the relationship between input and output. For a resistor of a resistance R, the current follows Ohm's law, $i(t) = \frac{E(t)}{R}$. Applying Fourier transform to both sides of this equation results in $\overline{i}(s) = \frac{\overline{E}(s)}{R}$. Finally, from definition (1):

$$Z(\omega) = R \tag{3}$$

For a capacitor of a capacitance C, the current follows $\frac{\mathrm{dE}}{\mathrm{dt}} = \frac{i(t)}{C}$. Applying Fourier transform, $j\omega\overline{E}(s) = \frac{\overline{i}(s)}{C}$. From definition (1):

$$Z(\omega) = \frac{1}{j\omega C} = -\frac{1}{\omega C}j \tag{4}$$

Note that the impedance of a resistor is a purely real number, while the impedance of a capacitor is a purely imaginary number. Thus, the real and imaginary parts of a complex impedance are associated, respectively, with the resistive and capacitive portions of the system response. Although the response of an electrochemical system is not purely electrical, the resistive part is commonly interpreted as the resistance to

the flow of current, while the capacitive part is commonly interpreted as the storage of charge in the system [18].

The particular form of the complex impedance depends on the relationship between the input and output signal in the time domain. If this relationship is linear, it can be assured that the application of definition (1) will result in a complex impedance that depends only on the frequency and systems parameters [21]. Therefore, linearity between input and output signals is an important requirement for both the measurement and theoretical derivation of impedance.

The equivalent impedance for any electrical circuit containing passive elements (resistors, capacitors, and inductors) can be directly obtained by applying Kirchhoff's laws in the same way as in routine circuit analysis. That is, the equivalent impedance of the elements associated in series is the sum of the impedances of each element $\left(Z_{\text{eq}} = \sum Z_i\right)$ while the inverse of the equivalent impedance of the elements associated in parallel is the sum of the inverses of the impedance of each element $\left(Z_{\text{eq}}^{-1} = \sum Z_i^{-1}\right)$ [19, 21, 22].

The impedance spectra of two simple circuits are represented in Fig. 2 by their Nyquist plots, the representation of the impedance in the complex plane, i.e. the negative of the imaginary part versus the real part.

For the circuit on the left, the impedance spectrum is a vertical line with a constant real part. This circuit can be compared to an ideally polarizable electrode, assuming that the double-layer capacitance is C_{dl} and the uncompensated resistance is R_u. From the equation in the figure, notice that the imaginary part vanishes for $\omega \to \infty$ and increases unlimitedly for $\omega \to 0$, which explains the blocking characteristic of the circuit.

For the circuit on the right, the Nyquist plot is a semi-circle with a radius R_{ct} centered at $\{R_u + R_{\text{ct}}/2, 0\}$. Two semi-circles for two different R_{ct} values are plotted.

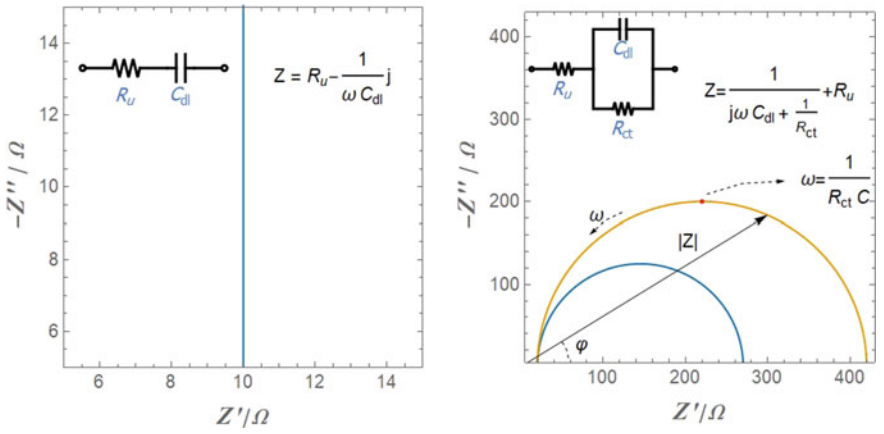

Fig. 2 Nyquist plot of the impedance spectra of two common circuits. The circuits and impedance spectra are shown in the figure. The vector representation of a given impedance point is shown in the graph on the right, identifying the impedance module and phase. [*Source* The authors (2022)]

This circuit can be compared to an electrode that undergoes a kinetically controlled charge transfer. Note that the limit of impedance for $\omega \to \infty$ is a real impedance $Z = R_u$ and the limit of impedance for $\omega \to 0$ is a real impedance $Z = R_u + R_{ct}$. Then, as frequency increases, the impedance goes through the semi-circle from the right to the left as indicated by the red arrow in the figure. The maximum point (redpoint in the figure) located at $\{R_u + R_{ct}/2, R_{ct}/2\}$ is equal to $\frac{1}{R_{ct}C_{dl}}$. So, for this circuit, capacitance and the resistances can be obtained directly from the Nyquist plot. In more complex circuits, however, a numerical fit of the theoretical curve to the experimental points is used to extract the parameters.

There are two other graphs, called Bode plots, commonly used to represent impedance data as a function of frequencies. One of the Bode plots consists of a plot of the logarithm of the impedance modulus versus the logarithm of frequency, and the other consists of a plot of the impedance phase versus the logarithm of the frequency. Often both curves are shown on dual *y*-axis graphs.

The response of electrochemical systems is determined by several phenomena, not exclusively of an electrical nature, so the approach described above is not sufficient to interpret the impedance measurement of electrochemical systems. The most rigorous and powerful approach is to derive the impedance expression from the partial differential equations that model the system, which is mathematically challenging [21, 22]. The transient response of electrochemical systems is intrinsically nonlinear due to the exponential dependence of current on potential. To obtain a linear model, a steady state is assumed, and the perturbation due to the low-amplitude sinusoidal input is analyzed. The oscillating response is expressed by a Taylor series, and under the assumption of linearity, only the first-order term of the series is considered. As it takes several minutes or more to acquire an impedance spectrum, a common cause of problems is that the steady-state condition is not maintained throughout the experiment [23].

In practice, a simpler approach based on equivalent circuits is applied, as exemplified in Fig. 2. Equivalent circuits are composed of the passive circuit elements described above and some generalized circuit elements that mimic the impedance response of non-electrical phenomena such as diffusion, adsorption, and so on [24]. Such an analogy approach has been criticized by some authors [25], but for impedimetric measures, they are completely satisfactory. Caution should be exercised, however, in choosing circuit elements, keeping in mind that the impedance response of these elements is derived for a specific set of experimental conditions.

One generalized element particularly useful is the so-called constant phase element (CPE), whose impedance is $\frac{(j\omega)^{-\alpha}}{Q}$ where α is an empirical parameter ranging from 0 to 1. Returning to the circuits in Fig. 2, the impedance responses of the corresponding electrochemical cells are quantitatively different. To account for this non-ideality, the capacitor must be replaced by a constant-phase element (CPE), as shown in Fig. 3.

The Nyquist plots in Fig. 3 reproduce better what is observed experimentally. When $\alpha \neq 1$, inclined lines appear in the left plot showing the phase angles less then

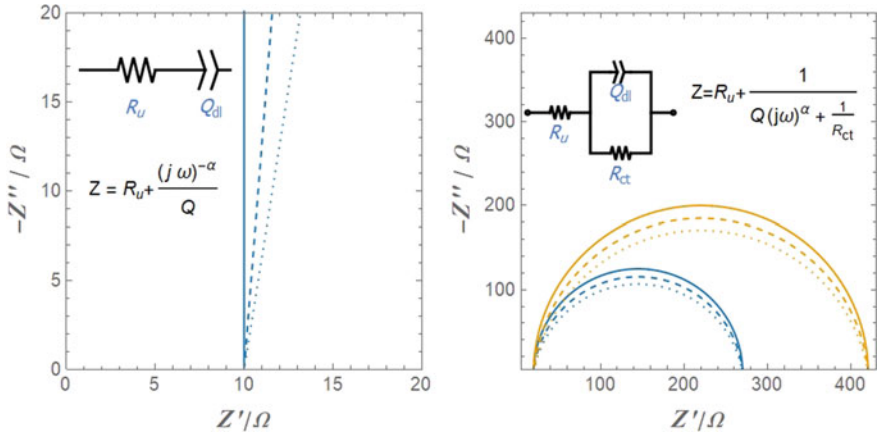

Fig. 3 Nyquist plot for the circuits in Fig. 2 modified by a CPE. Three values of are used: $\alpha = 1$(continuous), $\alpha = 0.95$(dashed) and $\alpha = 0.9$ (dotted). [*Source* The authors (2022)]

90°, and the depressed semi-circles appear in the right plots. When $\alpha = 1$, Q has units of capacitance, and the impedance of the ideal circuits is recovered.

For a system under mixed kinetic and diffusional control, a diffusional impedance must be associated in series with the charge transfer resistance. For semi-infinite linear diffusion, the so-called Warburg element [24] can be inserted into the circuit, forming the Randles circuit. The Nyquist plot calculated for the Randles circuit with two different Warburg parameters is shown in Fig. 4.

The inclined line in the low-frequency region is due to Warburg impedance. The higher the parameter σ, the lower the diffusion coefficient of the electroactive species. For slowly diffusing species, the Warburg impedance merges with the charge transfer semi-circle.

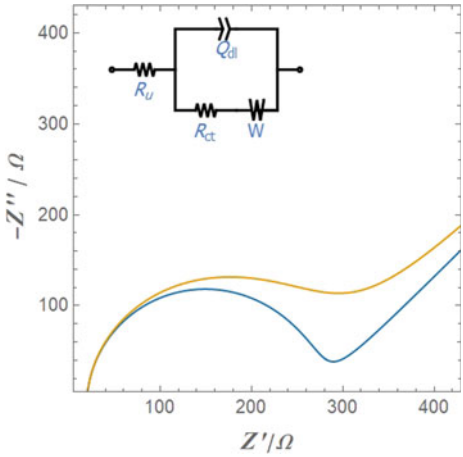

Fig. 4 Nyquist plot for the Randles circuit with $\sigma = 50$ (blue) and $\sigma = 250$ (orange). [*Source* The authors (2022)]

Often, the Randles circuit or some modification of it [26] is used to model the impedance response of immunosensors. For this, the impedance parameters must be correlated with the concentration of the analyte. Note that R_u and Z_W represent the bulk process and should not be affected by changes to the electrode surface. On the other hand, C_{DL}(or Q) and R_{ct} represent, respectively, the double layer and the charge transfer process that is affected by the formation of immune complexes.

1.3 Impedimetric Immunosensors

Immunosensors that use the EIS technique are called impedimetrics. Although EIS is a fundamentally electrochemical technique, used to characterize systems, providing information about their interfacial processes, studies have been carried out regarding its application as an analytical technique, especially in biosensor detection, due to its precise, non-perturbing, and non-destructive nature.

The formation of an immune complex, however, does not involve electron transfer, then the so-called faradaic EIS can be carried through the variation of the electrochemical response of a redox pair, being the ferri/ferrocyanide $\left(\left[Fe(CN)_6\right]^{4-/3-}\right)$ pair the most commonly used. Furthermore, the formation of the immune complex alters the electrode surface configuration, blocking the charge transfer sites, increasing the surface film thickness, and changing the dielectric constant, resulting in an increase in double-layer capacitance that can be correlated with the concentration of antigen in the so-called non-faradaic EIS [27, 28]. The greater the number of immune complexes formed, the greater the R_{ct} of the system, since there is blockage of the electrode for charge transfer resulting from the new redox processes. Thus, EIS can be used to detect the presence of antigens/antibodies and also to quantify them.

2 Trends in Impedimetric Immunosensors for Different Samples

Impedimetric immunosensors have been developed with potential applications for different fields. Figure 5 presents the cluster map of keywords, generated by the VOSViewer software, based on data obtained from the Web of Science database. Author-provided keywords mentioned more than five times were selected in the 726 articles published between February 2002 and February 2022. In all, eight clusters were obtained, represented by different colors. The size of the frames represents the number of times in which the term was mentioned, while their proximity indicates the relationships with the other terms. It is possible to observe the main characteristics and applications of these devices, from materials used (nanoparticles, graphene

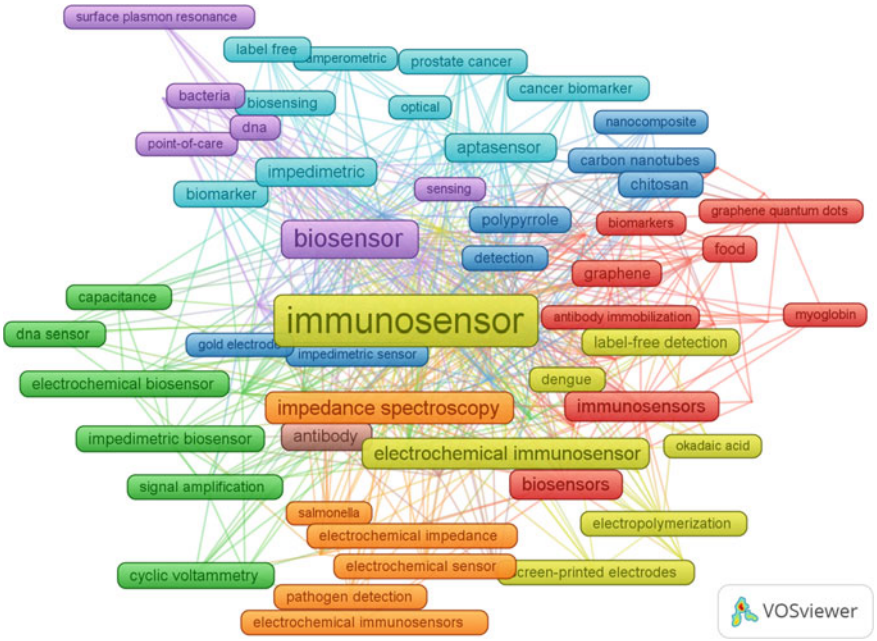

Fig. 5 Subject cluster refers to the incidence of the main keywords of Web of Science articles on impedimetric immunosensors published between Feb/2002 and Feb/2022. [*Source* The authors (2022)]

oxide, conducting polymers, nanocomposites, and quantum dots) to analytes (toxins, pesticides, biomarkers, and especially pathogens).

Furthermore, complex matrices (water, human serum, and food) are commonly mentioned especially for recovery and proof-of-concept studies, being the closest a method can come to routine analysis before it is fully validated. The choice of matrix varies according to the purpose of the analysis, the sensor's characteristics, and its analytical performance. For example, a device intended for clinical diagnosis may use blood, urine, or sweat samples, while a device designed for environmental analysis uses soil, water, or air samples. Additionally, factors such as pH, ionic strength, and possible sample interferences must be carefully evaluated, as they can affect the formation of the immune complex [29, 30].

In this section, we will highlight the application of impedimetric immunosensors in real matrices, discussing the particularities of the main types of analysis: food quality control, environmental monitoring, and clinical diagnosis.

2.1 Food Analysis

With the increasing demand for food worldwide, the need for stricter control over its production and storage is essential to guarantee its quality. Food and beverages that are inappropriately consumed can cause serious damage to health and in some cases lead to death. Contamination can occur through several mechanisms: failures in the manufacturing/storage process, such as poor quality of raw material and poorly performed cleaning of facilities and equipment; careless, ill-disposed, out of temperature or poorly sanitized transport; and storage for longer than indicated or in inappropriate places [1, 31]. Currently, analyses for quality control in food and beverages are complex and expensive, since it is a complex matrix, with many contaminants that can interfere with an accurate result. In addition, certain microorganisms can cause irreversible damage to health even in tiny amounts, so their detection must be extremely sensitive [32].

Contaminations in food can be biological (viruses, bacteria, fungi, protozoa, and worms) or chemical (pesticides, toxins, and allergens). Biological, especially bacterial, corresponds to most cases of foodborne infection [33, 34]. Bacteria are conventionally detected by culture methods in a process that takes between 3 and 10 days for results, or by enzyme-linked immunosorbent assays (ELISA) that takes between 1 and 3 days [35, 36]. Thus, with the main advantage of being quick to obtain the result, impedimetric immunosensors are being developed to detect them in food samples. As an example, Mutreja et al. [37] developed an impedimetric immunosensor based on screen-printed carbon electrodes (SPCE) for the detection of *Salmonella typhimurium* (responsible for most cases of food contamination worldwide [38]) in water and de lichi and orange juices. OmpD was used as a surface biomarker and the anti-OmpD antibody as a detection probe, both extracted and purified by the authors themselves. Systems like this give the result in less than 1 h and tend to have low cross-reactivity with other pathogens. Furthermore, liquid samples (water, juice, and milk) only need to be diluted before analysis [39, 40], eliminating costly processes and time-consuming pre-treatment and enrichment.

Devices to detect bacteria in solid samples, especially meat, can also be found. Unlike liquids, these samples must be pre-treated. For meat in general (including pork, fish, and chicken), a process of digestion in saline solution and filtration can be carried out [40, 41], lasting about 15 min. In some cases, it is still necessary to enrich the sample (24 h) followed by centrifugation and/or filtration [42, 43]. However, it is noteworthy that even being more time-consuming, the enrichment process can increase the sensitivity of the analysis, making it more effective in detecting small amounts of bacteria that would not be observed in samples without this pre-treatment.

The most common chemical contaminants come from the environment and the manufacturing, packaging, and shipping process. Meat is commonly contaminated with compounds from pasture (e.g., pesticides) and water (e.g., drugs for human use) ingested by the animal, as well as drugs and supplements for animal use (e.g., antibiotics). Agricultural foods, on the other hand, are mainly contaminated with pesticides used to improve production. Chemical additives can also be found in most

processed foods, and even though they are necessary, some of these compounds can be toxic [44]. Although most countries and regions determine acceptable concentration limits for these compounds for food to be considered suitable for consumption, some compounds are not yet legislated. In addition, there are chemicals such as pesticides that are banned in a certain country, but that does not mean that food produced is completely free of it [44, 45]. For the detection of chemical contaminations in food, laborious and expensive techniques (HPLC, ELISA) are used, which generally require a sample extraction step [46, 47]. Besides, the detection of these compounds is at the trace level, so the methods used need to be sensitive, with detection limits below those established by current legislation.

In the case of chemical contaminants, beverage analysis by impedimetric immunosensors generally does not require preparation [48, 49]. Solid agricultural samples, such as fruits, cereals, or vegetables, however, undergo minimal pre-treatment, which generally takes less than 1 h. For this, the sample needs to be washed and dried to remove surface contaminants, ground or kneaded for homogenization, and extracted with an organic solvent (usually acetone [50, 51]) [52]. Some works also report the use of centrifugation and ultrasonic treatment instead of extraction with organic solvent [53]. An example, Malvano et al. [54] developed an impedimetric immunosensor for the detection of the mycotoxin ochratoxin A in cocoa samples, with pre-treatment using the addition of phosphoric acid and chloroform, followed by filtration, the addition of sodium bicarbonate, and centrifugation. Furthermore, recovery studies carried out on the samples present results with an accuracy comparable to traditional methods, with detection limits below those stipulated by legislation [54, 55].

In addition to toxins and pesticides, allergens (substances capable of causing allergic reactions) are chemical compounds that can be present in food samples, natural from the production process, or consequences of contamination. Allergen detection is of paramount importance for the food industry, to avoid accidental exposure to consumers who may have severe allergic reactions. Even when not present in the food formulation, it is possible to find these substances due to cross-contamination or poor quality of the raw material used. In addition, the manufacturer must indicate on the product label which allergens are present so that an allergic person can avoid consuming them. Little explored so far, the detection of allergens employing immunosensors would make it possible to carry out analyzes outside of centralized laboratories, making the result faster and more accessible [56, 57]. Although there are voltammetric [58] and amperometric [59] immunosensors reported in the literature with analyzes performed on samples of milk and nut derivatives, there are few impedimetric devices [60–62] found so far. Among these works, the work of Chiriacò et al. [63] can be highlighted, who developed a lab-on-chip platform for detecting gliadin (a protein present in gluten) in beer and wheat samples. The immunochip had a detection limit about 20 times lower than the world limit for a food to be considered gluten-free. Although little explored, these systems tend to have a wider linear range, greater sensitivity, and lower detection limits than those using other electrochemical techniques [60].

2.2 Environmental Analysis

Increasingly, living beings (including humans) are being exposed to compounds that can cause risks to their health and consequently lead to an environmental imbalance. Substances such as pesticides, hormones, and drugs are commonly used by man and discarded in nature, becoming pollutants and potentially causing irreversible damage to certain ecosystems. Pollution can directly affect humans by compromising natural resources, leading to soil infertility, scarcity of drinking water and food, and, in some cases, the death of species essential to the development of the resources of that ecosystem [64]. Additionally, several diseases can be linked to exposure to pollution. The presence of harmful substances (e.g., pesticides) discarded in the soil or aquatic bodies can lead to intoxication and, depending on the compound, oncogenesis [65]. On the other hand, air pollution is related to lower respiratory tract infections, preterm births, and pulmonary and cardiovascular diseases, which are the leading causes of death worldwide [66].

Polluting compounds are present in matrices such as water, soil, and air, causing damage to the health of all forms of life. The detection and quantification of these species is an essential tool to assess the environmental condition of a given area, which is important for the elaboration of public policies to avoid future environmental imbalances. In this sense, impedimetric immunosensors for detection in environmental samples (water, soil, and air) can bring advantages such as reduced sensor preparation time and minimal pre-treatment, enabling in situ analysis even in remote locations. Furthermore, it would be ideal to use environmental analysis methods with low consumption of reagents, generating as little waste as possible. Electrochemical devices, which in general are or can be adapted to be miniaturized, are a greener alternative to traditional methods.

Domestic effluents are generated daily in our activities. Sanitary sewers, septic tanks, and grease traps contain organic compounds and microorganisms that are discarded in nature. These effluents usually need treatment before final disposal; however, some compounds may persist after this treatment. For example, antibiotics are widely used in humans and animals and are later excreted in feces and urine. Therefore, they are found at trace level in environmental samples, which is a problem due to the increasing resistance of bacteria to these drugs [67]. Impedimetric immunosensors for detecting antibiotics in environmental samples are rare, but there are several non-biological electrochemical sensors in the literature [68–71]. We can highlight the impedimetric immunosensor developed by Lamarca et al. [72], which was used to determination of ciprofloxacin in wastewater samples. This immunosensor showed high sensitivity and good recovery rate, in addition to detection time (2 min) and detection limit (7.5 pmol L^{-1}) much lower than values obtained by other electrochemical techniques for the detection of this antibiotic.

Although human daily activities involve the disposal of substances, industrial, mining, and agricultural activities are the main responsible for the disposal of toxic compounds. In general, waste generated by mining processes involves inorganic compounds, especially metals. The electrochemical detection of metal ions is widely

discussed in the literature, mainly by voltammetric techniques. As sensors (especially chemically modified ones) are capable of performing this detection, there is no justification for developing immunosensors for detecting metal ions. Industries are responsible for the emission of various gases and chemicals, many of which can cause serious ecological imbalances. Impedimetric immunosensors to determine the presence and concentration of various industrial residues and their respective by-products have been widely developed. Even tap water samples may contain several compounds from the industry at the trace level, especially those that are more persistent in the treatment process. For example, dyes [73] and some drugs [74] are known to be persistent in the usual water treatment and can be present in drinking water, coming into contact with humans, animals, and plants even far from the place where it was discarded [75, 76].

In general, water samples (river, tap, rain, surface, or groundwater) undergo at least the extraction process. It should be noted, however, that most methods involve the use of chromatography [77]. In the case of electrochemical immunosensors, it is possible to carry out the analysis without this process [78]. It is common, however, that the water sample is diluted in buffer, to eliminate the effects of the pH variation. Dilution varies depending on sample conditions and the detection strategy used. For example, more polluted water samples tend to have a greater matrix effect, so they should be more diluted. Also, cross-reactions can occur depending on the choice of the biorecognition element. Thus, if a sensor reacts with a certain interference present in the sample, the dilution must be greater to minimize its presence.

In addition, for water to be considered potable, certain physical, chemical, and biological standards must be followed. Thus, besides possible chemical contamination, water samples can also be evaluated for biological contamination. In countries where treated water is not easily accessible, pathogens (mostly bacteria) present in drinking water can cause serious damage to health. Considered one of the most dangerous bacteria, *Escherichia coli* immunodetection is widely reported in the literature, including EIS-based sensors [79–84]. These devices can have a total construction and analysis time close to 6 h [84], which can be considered an advantage over traditional culture methods.

Agricultural pesticides are considered the most toxic and persistent pollutants for the environment, and the detection of these compounds is widely discussed in the literature. However, impedimetric immunosensors whose application is performed in environmental samples are rare. Here, the detection of carbofuran in water and soil samples can be highlighted [50]. Carbofuran is an insecticide, termite, acaricide, and pesticide considered highly toxic to human and animal health. In addition, its use reduces the quality of the soil and easily contaminates aquatic environments [85]. The water sample reported in this work was only fortified with the pesticide standard, while the soil sample had to undergo an extraction process with acetone, followed by rotary evaporation.

Soil analyzes performed by traditional methods require the sample to go through the extraction process. Generally, the extraction of pesticides and other organic compounds is performed through the difference between their properties (solubility, polarity, volatility, and molecular weight) and those of the remaining components

of the matrix [86]. Although most of the extraction methods require a large amount of sample and consume a high volume of solvent, microextraction is standing out for generating less waste and thus making it greener [86, 87]. With the increasing demand for more environmentally friendly alternatives, there are automated microextraction technologies on the market today for simultaneous sampling, concentration, and cleanup [88]. Due to its high complexity, the soil is too complex to eliminate pre-treatment in analysis by label-free devices. Thus, impedimetric immunosensors are still rarely applied to soil samples.

Atmospheric pollutants can be gaseous compounds (e.g., NOx, CO), particulate matter (e.g., PM_{10}, $PM_{2.5}$), persistent organic pollutants (e.g., organochlorines, polycyclic aromatic hydrocarbons), and heavy metals (e.g., mercury, lead) [89]. These are used to determine the air quality of a given region and consequently to verify if it is within the standards defined by the legislation. Its detection is important not only to identify areas of high health risk but also to assess whether pollution from this area can reach neighboring or even remote locations, thus preventing this from happening [90]. Despite its importance, articles that use electrochemical sensors for gas detection are rare. No articles have been found so far that portray the use of EIS for this purpose. Part of this is due to the complex sample preparation required, which, like soil samples, must at least go through the extraction process. In some cases, it is necessary to carry out a pre-concentration of the analyte to guarantee its detectability. Also, sampling is a complex issue when talking about air. It must be considered that each region is different in terms of emission source and weather conditions so that the sample characteristics (particle size, composition, and concentration) vary according to the sampled area and the time of year [91].

2.3 Clinical Analysis

Clinical diagnoses are the goal of the development of most immunosensors. The identification of a disease or cause of infection can be performed using molecular tests such as polymerase chain reaction (PCR) or immunoassays as enzyme-linked immunosorbent assay (ELISA). While both are sensitive and accurate, they are also time-consuming and expensive as they require specialized personnel and centralized laboratories. Although there are currently numerous works reporting the development of point-of-care (POC) methods, clinical analyzes require high sensitivity and specificity, which is a challenge considering the complexity of biological samples. Thus, new biosensors and bioassays are widely found in the literature due to the specific binding between the analyte and the bioreceptor, leading to greater accuracy compared to non-biological devices [92–95].

Devices such as immunosensors can be used for clinical diagnoses through monitoring of biomarkers, which are molecules of biological importance whose activity is directly related to specific processes at the cellular level. Any protein whose concentration can be monitored for diagnosis is considered a biomarker [96, 97]. Antibodies can even be biomarkers, so their monitoring can be used to detect the presence or

stage of certain infections. Thus, immunodevices can be used in two different ways: immobilizing the antigen to detect the antibody or immobilizing the antibody to detect an antigen [98].

The detection of antibodies is particularly important to monitor the immune response developed by vaccines. Vaccines are known to stimulate the production of antibodies so that the body is prepared to fight the disease. Antibody tests are essential to assess the amount of antibodies produced and, consequently, the expected efficacy of the vaccine [99]. In addition, it is possible to estimate how long the immunity generated by the vaccine lasts, thus predicting the need for booster doses [99]. Studies indicate that vaccinated people have more antibodies than unvaccinated people, increasing protection against serious infections and death [100, 101]. There are also antibody tests to detect whether a person has had contact with a disease—so-called rapid tests. Rapid tests to detect antibodies are currently available on the market for several diseases [102–105]. Furthermore, depending on the type of antibody targeted, it can indicate whether the disease is in the acute (active) phase or if there has been a previous infection. In general, IgG tests are widely used to detect the previous infection and IgM tests are used to identify infections in the first few days [106]. Although commercially available tests are mostly colorimetric, electrochemical immunosensors are being developed using antibodies as targets.

Tests for antibody detection must be applied to blood samples, usually after the process of separating its components. Thus, it is common for serological diagnoses to be performed in plasma or serum, depending on the type of antibody and the protein used as capture antigen. Blood plasma separation is performed by centrifugation with an anticoagulant to remove other blood components. Compared to collecting serum, obtaining plasma is faster, has more protein, and produces a larger final sample volume. However, the anticoagulant to be used in sample preparation must be carefully evaluated to avoid interference with protein binding [107–109]. Although antibodies are present in plasma, their concentration is generally low, which limits the application of this type of sample to very sensitive methods. When using an immunosensor to detect antibodies in plasma, the sensitivity tends to be slightly lower than using buffer due to a large number of interferers. Despite this, the use of the EIS technique makes it possible to achieve greater sensitivity than other techniques, also presenting greater simplicity and speed of analysis [110].

Despite the lower number of different proteins, serum samples are the most common in serological tests. This is due to the similarity with whole blood, which contains practically the same proteins (minus those involved in clotting). In addition, these proteins show greater stability than those present in plasma [108]. Serum separation can be performed using two strategies: spontaneous when the blood sample is left to rest for the clot to form; and mechanical, which involves centrifuging the sample before aspiration using a Pasteur or automatic pipette. Most of the time, both processes are carried out to obtain the largest amount of sample possible. Thus, the blood sample can be kept at rest for a few minutes before being centrifuged. Spontaneous clotting time may vary, as may centrifuge rotation and time [111, 112]. Electrochemical sensors do not require extraction of analytes from the serum sample, as standard methods do. Due to the high sensitivity of impedimetric immunosensors,

detection of antibodies in serum usually requires dilution of this sample in buffer (usually PBS) [111, 113, 114].

In addition to antibody detection, plasma and serum samples can be used for protein biomarkers detection through immune complex formation. With often similar symptoms, the identification of the pathogen-causing disease is an issue that requires care. It is common for some viruses from the same family, for example, to present the same symptoms, as is the case with flaviviruses (dengue, zika, and chikungunya). Antibodies produced by infections caused by such viruses can easily cross-react, compromising the diagnosis. Thus, only a molecular test or detection of a specific biomarker allows for an accurate diagnosis. Present in all flaviviruses, the NS1 protein is expressed in large amounts by all flaviviruses and can be used as a biomarker as it can be detected one day after contamination. Although identification of the type of flavivirus is difficult due to the similarity of the NS1 proteins, the use of a specific antibody can be used to define which virus causes it [115, 116]. Impedimetric immunosensors for the diagnosis of flaviviruses (especially dengue) through the detection of NS1 have been developed. In this case, the linear ranges must be wide so that detection on real samples can be performed. The most common sample is acute-phase serum, which presents values in the range of ug mL^{-1}. Obtaining detection limits generally in the range of ng mL^{-1} indicates the possibility of using these sensors for NS1 detection with high sensitivity [117–119].

Selectivity tests for clinical diagnoses are usually performed considering common elements in the sample used. These compounds can interfere with the analysis, especially those present in greater amounts in the sample. For example, in plasma samples, albumin can be an interferer [109]. Considering the high cross-reactivity, in the case of the NS1 protein, tests with other flaviviruses are also performed [120, 121]. When this study is carried out in the development of electrochemical immunosensors, it is common that there is low cross-reactivity between the different flaviviruses. It is also important to note that there are cases where there is co-infection so that a positive result for two different flaviviruses can occur without necessarily being a wrong result. Thus, it is still a challenge to identify similar viruses in tests other than the standard ones.

Along with the difficulty of identifying similar viruses, there are cases in which it is necessary to differentiate between bacterial and viral infections so that the treatment is correctly oriented [116, 122–124]. C-reactive protein (CRP) and interleukins can be used to differentiate the type of pathogen, as they are overexpressed in the case of bacterial infections [123, 125, 126]. Besides, they can be used as biomarkers for cardiovascular disease and cancer, respectively. The application of impedimetric immunosensors for the detection of these biomarkers in serum [127, 128] reports detection limits much lower than those found by other methods. In addition, they have high recovery rates, indicating the sensor's accuracy and reliability for application in routine analysis. This is especially important considering the label-free strategy, without any amplification of the analytical signal.

In addition to the determination of diseases caused by pathogens, immunosensors have been developed to diagnose different types of cancer. To date, most existing routine procedures are invasive and time-consuming (e.g., histopathology, biopsy).

Biomarker detection allows the diagnosis to be performed in a less invasive way, with reduced cost and high sensitivity. Furthermore, some tests for the detection of cancer biomarkers are currently being used in routine analyses [129, 130]. For example, the detection of prostate-specific antigen (PSA) in the blood is used to diagnose prostate cancer. However, although PSA tests are sensitive, the rate in the body naturally increases with age, so it is recommended that it be performed in addition to a digital rectal exam [131–133].

As with other diseases, most impediment devices for detecting cancer biomarkers are applied to serum samples. However, other samples can be used, such as urine (real or synthetic). Urine can be collected in large quantities and has a smaller number of possible interferents than blood-derived samples. Besides, it is common for drugs or metabolites to be found in high concentrations, so urine is also used in toxicology tests [134]. Furthermore, the use of urine makes the exam non-invasive and can be used mainly in the case of bladder cancer, in addition to the cytological exam. Synthetic urine (prepared according to the protocol published by Brooks and Keevil [135]) is used primarily because it does not involve collecting material from individuals and therefore does not need to be approved by the Ethics Committee. In the case of real urine, it was reported by Shaikh et al. [136] that the samples were placed in a water bath at 37 °C and centrifuged. Thus, the supernatant was obtained, which was used in the analyses. As with serum samples, impedimetric analysis of biomarkers in urine does not suffer significant interference from other proteins, which indicates the selectivity of the devices [136, 137].

2.3.1 SARS-CoV-2

With the SARS-CoV-2 pandemic, the development of new, faster, and cheaper diagnostic methods has become a worldwide goal. In general, tests on samples of nasal secretions are used in PCR analysis, making it possible to detect the presence of the virus even in asymptomatic individuals. Articles reporting impedimetric immunosensors to detect SARS-CoV-2 antigens can be found in the literature, including using artificial nasal secretion samples. This artificial sample is easily prepared with the addition of antibodies (mainly IgG) and inorganic salts in an aqueous medium [138, 139]. In the case of detection by PCR, it is necessary to go through a step of RNA/DNA extraction and purification. Most electrochemical biosensors, however, do not require the sample to be extracted or purified, so it is just diluted in buffer [140]. In all cases, the sample must be inactivated so that there is no risk of contamination during analysis. Sample inactivation can be employing radiation, thermal process, or addition of chemical agents. The best process for inactivating a sample must be evaluated on a case-by-case basis, depending mainly on laboratory conditions and availability. Furthermore, inactivation must be carried out not only when there is a suspicion of a virus, but also of fungi, bacteria, and other microorganisms that may be transmissible [140, 141].

The collection of nasal or nasopharyngeal samples is uncomfortable, which may discourage patients from performing the test. Thus, the search for less invasive and

equally efficient samples and collection methods has been the subject of research. The detection of viral antigens [142] and specific antibodies for SARS-CoV-2 can be performed in blood or serum samples, and there are even commercially available rapid colorimetric tests for the detection of them [143, 144]. Antibody tests, in particular, are accurate, and, as different types of antibodies have different immune windows, it is possible to obtain information about the time of infection. For example, a positive IgM/IgG negative test indicates that the infection is in the acute phase, while a negative IgM/IgG positive test indicates that the person has had contact with the virus, but the acute phase has passed [145]. Impedimetric devices for detecting antibodies are also being developed. Furthermore, tests for quantification of these antibodies present limits in the range of ng mL^{-1}, similar to other electrochemical sensors for virus antibodies detection [146, 147].

In addition to nasal and serum samples, saliva can also be used to detect the presence of the virus. One of the biggest challenges in saliva analysis is that sensors need to have high sensitivity to be able to detect the presence of the analyte at very low concentrations. In addition, a person's saliva can contain different compounds depending on their habits. Thus, the detection of a given analyte must be done by very specific devices, as the chance of a cross-reaction with different compounds is high. In this sense, the collection is very important and must be standardized so that the results are reliable. In general, the individual is asked not to have eaten or performed oral hygiene for at least 2 h before collection. However, this time may vary according to the method and the antigen to be detected. In addition, some methods may require the patient to perform a warm water rinse immediately before collection. This is to remove possible impurities that are still in the mouth and stimulate the production of saliva. Between the collection and the analysis, it is also recommended that a stabilization buffer be added to the saliva so that there is no damage to the sample during the transport and storage process [148, 149].

Saliva samples do not need to undergo an extraction process for detection by impedimetric immunosensors. Thus, only centrifugation is performed to collect the supernatant and discard the precipitate, to obtain the saliva present in the collection material and eliminate suspended materials present in the sample. These devices have low detection limits, especially for the spike proteins (S protein), found on the surface of the virus, and nucleocapsid (N protein) found in its nucleus. Furthermore, detection can be performed in less than 1 h, making the sensors suitable for use in analyzes that require high analytical frequency [150, 151].

2.3.2 Wearable Devices

The integration of new technologies from different areas enables the development of more advanced sensors. Progress in the development of new biocompatible materials, flexible electronics, and near-field communication technology makes it possible to manufacture wearable sensors for health monitoring. These devices are especially interesting to assess biomarker levels continuously and in real time, without the individual having to leave the house. In addition to making exams more accessible

to the patient, this can help reduce the cost to health systems. Commercially, some wearable sensors can be found. Most aim to monitor parameters related to daily activities, such as the number of steps, amount of calories expended, heart rate, maximum oxygen consumption, sleep quality, and physical exercise. Biomarkers such as potassium, sodium, glucose, and lactic acid are also of interest for detection, mostly on sweat [152–154].

Sweat is a sample rich in electrolytes and metabolites, and as it is secreted by the body, it can be collected non-invasively. The biggest challenges in detecting biomarkers in sweat are (1) the high possibility of contamination due to exposure to being secreted and (2) the small amount of sample collected [154]. In this sense, the use of wearable immunosensors can circumvent these problems, providing specific and sensitive results with miniaturized platforms. For the detection of the biomarkers, an ideal wearable sensor should be mechanically similar to the skin. This is because there needs to be movement stability, that is, that the sensor is not disconnected or generates signal noise as the individual moves. Therefore, flexible and resistant materials are preferable for its development. In addition, the response is transmitted quickly, preferably in real time. Depending on the purpose of the analysis, monitoring may also be required to be continuous, so the sensor must be programmed to transmit the results at the desired frequency. For example, if the wearable sensor is to monitor a biomarker every hour, it must be optimized to transmit the response obtained over 60 min. For this, the sensors must also have a power system, which can be by storage (e.g., super capacitors and batteries) or harvesting (e.g., thermoelectric and photovoltaic). Furthermore, the data transmission system must be carefully evaluated on a case-by-case basis, so that the results are not lost with the connection [155–158].

Wearable impedimetric immunosensors can be highly precise and accurate, showing no significant interference in the presence of analyte-like compounds in the sample. For example, a $Ti_3C_2T_x$ MXene-based wearable patch for cortisol detection showed no significant variation in analytical response in the presence of other steroid hormones. In addition, the authors obtained relative standard deviations (RSD) of less than 3% in the fortified sweat analyses [159]. Furthermore, these devices can present results similar to those obtained by ELISA, which indicates a good correlation between the developed sensor and a gold standard technique of analysis [160, 161]. To date, there are few wearable impedimetric immunosensors reported in the literature. However, with the advancement of technologies, it is expected that the number of publications will increase in the coming years [155].

3 Trends in the Validation of Impedimetric Immunosensors

For a new analytical method or device to be used in routine analyses, it is necessary to ensure that its results are statistically reliable, thus showing its effectiveness. This performance evaluation, called *validation*, intends to ensure the proximity between the experimental result and the real result, attesting to its applicability. Validation is performed using parameters indicative of analytical performance, which depend on

the particularities of each system, the proposed objective, available resources, and the objective of the analysis.

Devices for qualitative analyzes (yes or no) in general must evaluate at least the parameters of precision, accuracy, selectivity/specificity, and robustness. On the other hand, the quantitative and semi-quantitative ones must also evaluate the working concentration range, linearity, the limits of detection (LOD), and quantification (LOQ).

3.1 Current Scenario in the Validation of Immunosensors

Recently, a trend in the development of new electrochemical immunosensors has been observed in the literature, with desirable characteristics such as better sensitivity and lower detection limits, aiming to obtain devices that facilitate their application in different areas of society [162, 163]. This trend is confirmed by the numerous published reviews that focus on specific areas such as the development and characteristics of immunosensors applied to the analysis of mycotoxins in foods, the analysis of pesticide residues in food and environmental matrices, and immunosensors for clinical analyzes for the prevention and detection of heart diseases, cancer, diabetes, arteriosclerosis, and infections caused by different types of pathogens such as bacteria and viruses [4, 115, 162–165].

The introduction of nanomaterials in the development of immunosensors has contributed to enhancing the sensitivity and detectability characteristics described above and demonstrates the potential for the application of these devices in routine analysis. However, what can be seen in the numerous articles published on this topic is a greater emphasis on the characterization and optimization of immunosensors and less attention to their analytical performance through very detailed in-house validation studies or interlaboratory validation [4, 162–165]. Given this, it can be said that the greatest challenge of the current scenario of immunosensor development, for their industrial commercialization, and application in routine analysis, is to carry out robust validation studies that make use of real samples and that detail the validation protocol adopted to confirm the validity of the immunosensor in practical applications. The transfer of methods developed in research and development laboratories to industrial, quality control, and diagnostic analysis laboratories is a current need that must be considered so that new devices using immunosensors can be applied to improve society's quality of life.

Clinical, food, and environmental monitoring laboratories are normally regulated by quality assurance systems (ISO standards), which require that standardized analytical methods by accreditation bodies or that have been validated according to validation guides such as ISO 17025, AOAC, EPA, USEPA, FDA, ICH, NATA, i.g., to be adopted in their routine analysis [166]. It is noted that despite the numerous efforts of researchers to develop new immunosensors with applications in different areas, there is a need to demonstrate the reliability and consistency of the results obtained

by them through robust studies of analytical validation for their later application in routine analysis.

It is recognized worldwide that new analytical methods or modifications of existing analytical methods need to have their performance verified by a systematic study involving different parameters, graphic and statistical tests, and acceptance criteria to prove their suitability for the intended use and demonstrate the reliability and consistency of the analytical results [167, 168]. This investigation process is known as *validation*. The validation process is essential so that analytical methods can be applied to real samples in routine analyzes by industrial or quality control laboratories, as well as being adopted as standard methods by inspection bodies. The impact on society of unreliable analytical results can be disastrous especially in the diagnosis of diseases, environmental monitoring or quality assurance, and food safety, causing damage to the industrial sector and society due to decision-making based on methods that have not been properly validated [167–170].

Analytical validation of method or procedure can be performed at different levels:

(1) *Characterization of analytical performance* for standardized methods that is analyzed in laboratories other than those in which they were validated;
(2) *In-house validation* in which validation parameters and acceptance criteria are evaluated in a single laboratory for a developed method or for a standard method used outside the scope in which it was developed;
(3) *Full validation* in which, after carrying out the *in-house validation*, an inter-laboratory study is carried out to determine the reproducibility of the method and its performance in different laboratories.

In research and development laboratories, in-house validation is usually adopted and in accreditation bodies, full validation procedures are used for the standardization of official methods [171]. It is evident from the works reported in the literature that immunosensors are currently developed in research and development laboratories. Given this, this chapter will describe in detail the validation parameters normally adopted for carrying out an in-house validation study and how they are evaluated in the literature for different electrochemical immunosensors.

It is noteworthy to observe that most of the published works considering the development of new immunosensors only assess their analytical performance by presenting some characteristics or validation parameters such as selectivity/specificity, linear range, detection limit, and sensitivity. Validation parameters such as precision and accuracy are usually evaluated separately from the analytical performance study in the application of immunosensors in real samples [4, 27, 162–165, 170–180]. There is also no detail, in most of the works, of the methodological aspects adopted to obtain each of the evaluated parameters and acceptance criteria, as well as the software used to perform the calculations. Besides, only for the detection limit and sensitivity parameters, a mention is made of the adopted planning and calculation method [4, 27, 162–165, 172–180]. These issues make it difficult to transfer the analytical method that makes use of the immunosensor to other laboratories as well as to practical applications.

To carry out robust in-house validation studies, different parameters must be evaluated, such as selectivity/specificity, linearity, sensitivity, detection and quantification limits, precision, accuracy, and robustness through a systematic study involving statistical tools and criteria of acceptance [171]. Various validation guides can be found for different areas as described above.

Due to the considerations made so far, in this chapter, the main validation parameters will be described in detail, as well as the form of evaluation of these in studies reported in the literature involving immunosensors. In addition, a critical assessment of future perspectives in the validation process of these devices will be presented.

(a) *Selectivity/Specificity*

It is observed that the parameters "*specificity*" and "*selectivity*" are used interchangeably in published articles on immunosensors. Specificity refers to the analysis of a single analyte when the method is free of interferents and determines only the compound of interest [181]. Therefore, some analyzes involving enzyme or immunochemical assays can be considered specific. Selectivity, in turn, refers to the analysis of different compounds to the extent that a particular analyte or different analytes can be determined in a complex sample without interference from other components present. In other words, selectivity is used to discriminate between the analyte of interest and other components of the sample, while specificity is the ability to produce signals to effectively identify the analyte [166].

In this sense, attention should be drawn to the need for researchers involved in the validation of these devices to emphasize the characteristic of immunosensors concerning their specific character or not for the analyte of interest, and when it is not possible to prove the specificity of the immunosensor, the most correct term to use is "*selectivity*". The specificity/selectivity evaluation studies of immunosensors are performed with the addition of possible interferents in standard analyte solutions, adopting a univariate strategy in which different interferents are evaluated about the analyte of interest. In some works, studies of standard addition of the analyte in real samples are described to verify the existence of a matrix effect to check the selectivity/specificity of the immunosensor [4, 27, 162–165, 172–180].

(b) *Linearity*

The linearity parameter refers to the ability of an analytical method to obtain analytical responses directly proportional to the concentration of an analyte in a sample. This proportionality relationship is obtained through a calibration function established by an analytical calibration curve [181]. Whenever possible, an attempt is made to establish a linear relationship (simpler calibration model) between the analytical signal and the concentration of the analyte of interest. However, it should be noted that it is not always possible to establish a linear relationship and that other calibration models can be adopted, since the quality of the data about the concentration of the analyte in the sample is crucial for a routine application [182].

In published works on immunosensors, it is observed that the methodological aspects of building the analytical curve (number of standards, concentration of standards, and number of replicates for each point on the curve), the evaluation of the

calibration function (linear, quadratic models, etc.), and statistical tools for analyzing the models are neglected and most of the time they are not presented. Furthermore, there is a tendency to adopt linear models for the relationship between the analytical signal and the concentration of the compound of interest. As acceptance criteria, in most of the studies reported, the coefficient of determination (R^2) is used and in some isolated cases the correlation coefficient (r) as an acceptance criterion of the immunosensor linearity [4, 27, 162–165, 172–180]. These criteria, despite numerous criticisms regarding their use, are still adopted by some validation guidelines [166]. There is a lot of controversy in the literature on the use of these parameters to check linearity.

The correlation coefficient (r) describes the presence of a linear relationship between the two variables analyzed, and the degree of association should be positive or negative. Conversely, the coefficient of determination (R^2) shows the type of association and the proportion of variance explained by the model adopted (linear or polynomial). In neither case is the adequacy of the calibration model evaluated and therefore these parameters cannot be used to evaluate linearity [166, 182]. However, there is a recent, still timid, tendency of some researchers to describe linearity in more detail through the application of linear regression methods and more robust ways of evaluating linearity [183, 184]. It is therefore suggested that researchers involved in the development of immunosensors adopt simple or weighted linear regression methods and model evaluation criteria such as analysis of data homoscedasticity, calculation of regression analysis estimates (F-tests, residual standard deviation) to confirm the linearity of these devices since it is recognized in the literature that these parameters confer greater reliability in choosing the calibration model to be adopted [166, 182].

(c) *Limits of Detection and Quantification*

The limit of detection (LOD) refers to the lowest concentration of the analyte that can be detected, but not necessarily quantified, under the established experimental conditions, while the limit of quantification (LOQ) refers to the smallest amount of the analyte in a sample which can be determined with acceptable precision and accuracy under the established experimental conditions. Different methods for determining these limits can be found in the method validation guidelines, such as those based on blank standard deviations, on the signal/noise ratio, and on the analytical curve [181].

It can be seen in published works on immunosensors that there is a tendency to use the signal/noise ratio method and the method based on standard deviations of blank to determine the detection limit. Few studies make use of the calibration curve method. However, it is important to emphasize that all published works usually present comparisons of the detection limits of the developed immunosensor with those reported in the literature [4, 27, 162–165, 172–180]. The detection limits values may vary depending on the calculation method adopted. Therefore, detection limits comparisons should initially consider how this parameter was obtained.

Most of the studies reported for immunosensors do not present the limits of quantification. This parameter is important for the reliable determination of low analyte

concentrations in the sample of interest and should be included in the immunosensor validation study.

(d) *Precision*

Precision refers to the proximity between the results obtained employing tests with samples prepared as described in the analytical method to be validated. It is normally expressed in relative standard deviations (RSD (%)) and can be evaluated at three levels: (1) repeatability, (2) intermediate precision, and (3) reproducibility. The first two levels can be evaluated in in-house validation studies, while the last one can only be determined when a full validation study is applied [171, 181].

In terms of precision, in the evaluation of immunosensors, different ways of evaluating this parameter are presented. In some studies, precision is evaluated by analyzing the analyte in a standard solution on 3 to 6 immunosensors to demonstrate that the device construction is reproducible and terms such as "inter-assay precision" or "intra-assay precision" are used. In other studies, immunosensor precision is evaluated by the relative standard deviations of recovery tests on real samples [4, 27, 162–165, 172–180]. Few studies report the analysis of intermediate precision in which the analyte determined by the immunosensor is evaluated under different conditions (days, analysts, and equipment) [182, 184]. Another observation is the "erroneous" attribution of reproducibility to the immunosensor, even when it was only evaluated internally in the laboratory where it was developed [4, 27, 162–165, 172–180]

Thus, it is suggested to avoid the term "reproducibility" to attribute precision to immunosensors evaluated in a single laboratory, since this estimate can only be obtained through interlaboratory trials [171]. Another important issue to be highlighted is that the evaluation of different levels of precision in real samples will attribute greater reliability to the analytical data obtained by the immunosensors and will facilitate their transfer to practical applications.

(e) *Accuracy*

Accuracy refers to the degree of agreement between the individual results of the method under study concerning a value accepted as true [181]. This parameter can be determined in different ways: (1) using certified reference materials; (2) by comparing the developed method with a standard reference method and (3) by recovery tests. Of the three ways mentioned, whenever possible, the first or second should be adopted [185]. Recovery assays can provide biased estimates of accuracy if the added analyte behaves differently from the analyte present in the sample due to dissimilarities in its chemical form and reactivity [166].

For the evaluation of immunosensors, recovery assays predominate as a way of evaluating the accuracy, although some works report the comparison with standard methods such as ELISA, PCR, and HPLC [175–177]. However, in most published

works, recovery tests are adopted not to express accuracy but to demonstrate applicability in real samples of the immunosensor. Reliable accuracy estimates are important for transferring the methodology using immunosensors to practical applications, especially in clinical trials where an incorrect diagnosis can lead to serious consequences for the patient's health.

4 Conclusions and Future Perspectives

It is easily verified in the literature that immunosensors have a wide potential of applications in different areas such as clinical, environmental, and food analysis. Every year a greater number of immunosensors are being developed, but on the other hand, their practical application in routine laboratories is still shy. This scenario can be changed by carrying out robust in-house validation studies in which different parameters are evaluated based on guidelines for the validation of specific areas. This will provide greater reliability and consistency to the analytical data obtained by immunosensors, which will facilitate their transfer to routine analysis laboratories. For this to occur, researchers should be encouraged to carry out in-house validation studies of developed immunosensors.

Additionally, impedimetric methods are fast and robust alternatives for the routine analysis in several matrices with studies related to the development of new materials and analysis devices widely reported in the literature. To complement these studies, routine analytical applications need to be validated to ensure data quality and reliability, and several validation guidelines can be used for this purpose, which makes an important contribution to the field of electroanalysis.

Acknowledgements The authors are grateful to CNPq, CAPES, and Fundação Araucária for their financial support.

References

1. He S, Yuan Y, Nag A et al (2020) A review on the use of impedimetric sensors for the inspection of food quality. Int J Environ Res Public Health 17:1–30. https://doi.org/10.3390/ijerph17145220
2. Brosel-Oliu S, Abramova N, Uria N, Bratov A (2019) Impedimetric transducers based on interdigitated electrode arrays for bacterial detection—a review. Anal Chim Acta 1088:1–19. https://doi.org/10.1016/j.aca.2019.09.026
3. Zhang H, Miller BL (2019) Immunosensor-based label-free and multiplex detection of influenza viruses: state of the art. Biosens Bioelectron 141:. https://doi.org/10.1016/j.bios.2019.111476
4. Leva-Bueno J, Peyman SA, Millner PA (2020) A review on impedimetric immunosensors for pathogen and biomarker detection. Med Microbiol Immunol 209:343–362. https://doi.org/10.1007/s00430-020-00668-0

5. Higson SPJ (2009) Introdução aos biossensores. Química Analítica, 1st edn. McGraw-Hill, São Paulo, pp 392–399
6. Lim SA, Ahmed MU (2019) CHAPTER 1. Introduction to immunosensors. pp 1–20
7. Karunakaran C, Pandiaraj M, Santharaman P (2015) Immunosensors. Elsevier Inc.
8. Aydin M, Aydin EB, Sezgintürk MK (2021) Advances in immunosensor technology. Adv Clin Chem 102:1–62. https://doi.org/10.1016/bs.acc.2020.08.001
9. Cho IH, Lee J, Kim J et al (2018) Current technologies of electrochemical immunosensors: perspective on signal amplification. Sensors (Switzerland) 18:1–18. https://doi.org/10.3390/s18010207
10. Piro B, Reisberg S (2017) Recent advances in electrochemical immunosensors. Sensors 17:794–857. https://doi.org/10.3390/s17040794
11. Aydin S (2015) A short history, principles, and types of ELISA, and our laboratory experience with peptide/protein analyses using ELISA. Peptides 72:4–15. https://doi.org/10.1016/j.peptides.2015.04.012
12. Biagini RE, Smith JP, Sammons DL et al (2007) Analytical performance criteria the use of immunochemical and biosensor methods for occupational and environmental monitoring. Part I: Introduction to immunoassays. J Occup Environ Hyg 5:D25–D32. https://doi.org/10.1080/15459620701798182
13. Espina V, Woodhouse EC, Wulfkuhle J et al (2004) Protein microarray detection strategies: focus on direct detection technologies. J Immunol Methods 290:121–133. https://doi.org/10.1016/j.jim.2004.04.013
14. Nellaiappan S, Mandali PK, Prabakaran A, Krishnan UM (2021) Electrochemical immunosensors for quantification of procalcitonin: Progress and prospects. Chemosensors 9:1–16. https://doi.org/10.3390/chemosensors9070182
15. Malvano F, Pilloton R, Albanese D (2020) Label-free impedimetric biosensors for the control of food safety–a review. Int J Environ Anal Chem 100:468–491. https://doi.org/10.1080/03067319.2019.1667096
16. Vogiazi V, De La Cruz A, Mishra S et al (2019) A Comprehensive review: development of electrochemical biosensors for detection of cyanotoxins in freshwater. ACS Sensors 4:1151–1173. https://doi.org/10.1021/acssensors.9b00376
17. Prodromidis MI (2010) Impedimetric immunosensors—a review. Electrochim Acta 55:4227–4233. https://doi.org/10.1016/j.electacta.2009.01.081
18. Strong ME, Richards JR, Torres M et al (2021) Faradaic electrochemical impedance spectroscopy for enhanced analyte detection in diagnostics. Biosens Bioelectron 177:112949. https://doi.org/10.1016/j.bios.2020.112949
19. Randviir EP, Banks CE (2013) Electrochemical impedance spectroscopy: an overview of bioanalytical applications. Anal Methods 5:1098. https://doi.org/10.1039/c3ay26476a
20. Ciucci F (2019) Modeling electrochemical impedance spectroscopy. Curr Opin Electrochem 13:132–139. https://doi.org/10.1016/j.coelec.2018.12.003
21. Lasia A (2014) Electrochemical impedance spectroscopy and its applications. Springer, Nova Iorque
22. Orazem ME, Tribollet B (2008) Electrochemical impedance spectroscopy. John Wiley & Sons Inc., Hoboken, NJ, USA
23. Basic of Electrochemical Impedance Spectroscopy. Gamry Instruments
24. Metrohm (2007) Application Area: Fundamental Electrochemical Impedance Spectroscopy (EIS) Part 1—Basic Principles. Metrohm autolab 1–3
25. Macdonald DD (2006) Reflections on the history of electrochemical impedance spectroscopy. Electrochim Acta 51:1376–1388. https://doi.org/10.1016/j.electacta.2005.02.107
26. Saxena R, Srivastava S (2019) An insight into impedimetric immunosensor and its electrical equivalent circuit. Sensors Actuators B Chem 297:126780. https://doi.org/10.1016/j.snb.2019.126780
27. Díaz-Fernández A, Bernalte E, Fernández-Ramos C et al (2022) An impedimetric immunosensor for the selective detection of CD34+ T-cells in human serum. Sensors Actuators B Chem 356:131306. https://doi.org/10.1016/j.snb.2021.131306

28. Yildirim G, Aras GH, Banyhussan QS et al (2015) Estimating the self-healing capability of cementitious composites through non-destructive electrical-based monitoring. NDT E Int 76:26–37. https://doi.org/10.1016/j.ndteint.2015.08.005
29. Yoshida H, Imafuku Y, Nagai T (2004) Matrix effects in clinical immunoassays and the effect of preheating and cooling analytical samples. Clin Chem Lab Med 42. https://doi.org/10.1515/CCLM.2004.010
30. Mallat E, Barceló D, Barzen C et al (2001) Immunosensors for pesticide determination in natural waters. TrAC Trends Anal Chem 20:124–132. https://doi.org/10.1016/S0165-9936(00)00082-0
31. Nerín C, Aznar M, Carrizo D (2016) Food contamination during food process. Trends Food Sci Technol 48:63–68. https://doi.org/10.1016/j.tifs.2015.12.004
32. Ramos L (2020) Basics and advances in sampling and sample preparation. Elsevier Inc., Second Edi
33. Mehlhorn H (2015) Food-borne disease burden epidemiology reference group. Encycl Parasitol 1–1. https://doi.org/10.1007/978-3-642-27769-6_3884-1
34. Farahi RH, Passian A, Tetard L, Thundat T (2012) Critical issues in sensor science to aid food and water safety. ACS Nano 6:4548–4556. https://doi.org/10.1021/nn204999j
35. Kumar S, Balakrishna K, Batra H (2008) Enrichment-ELISA for detection of Salmonella typhi from food and water samples. Biomed Environ Sci 21:137–143. https://doi.org/10.1016/S0895-3988(08)60019-7
36. Salam F, Tothill IE (2009) Detection of *Salmonella typhimurium* using an electrochemical immunosensor. Biosens Bioelectron 24:2630–2636. https://doi.org/10.1016/j.bios.2009.01.025
37. Mutreja R, Jariyal M, Pathania P et al (2016) Novel surface antigen based impedimetric immunosensor for detection of *Salmonella typhimurium* in water and juice samples. Biosens Bioelectron 85:707–713. https://doi.org/10.1016/j.bios.2016.05.079
38. Ehuwa O, Jaiswal AK, Jaiswal S (2021) Salmonella, food safety and food handling practices. Foods 10:1–16. https://doi.org/10.3390/foods10050907
39. Riu J, Giussani B (2020) Electrochemical biosensors for the detection of pathogenic bacteria in food. TrAC—Trends Anal Chem 126:115863. https://doi.org/10.1016/j.trac.2020.115863
40. Malvano F, Pilloton R, Albanese D (2018) Sensitive detection of *Escherichia coli* O157:H7 in food products by impedimetric immunosensors. Sensors (Switzerland) 18:1–11. https://doi.org/10.3390/s18072168
41. Primiceri E, Chiriacò MS, de Feo F et al (2016) A multipurpose biochip for food pathogen detection. Anal Methods 8:3055–3060. https://doi.org/10.1039/C5AY03295D
42. Jasim I, Shen Z, Mlaji Z et al (2019) An impedance biosensor for simultaneous detection of low concentration of Salmonella serogroups in poultry and fresh produce samples. Biosens Bioelectron 126:292–300. https://doi.org/10.1016/j.bios.2018.10.065
43. Liu J, Jasim I, Shen Z et al (2019) A microfluidic based biosensor for rapid detection of Salmonella in food products. PLoS One 14:e0216873. https://doi.org/10.1371/journal.pone.0216873
44. Bhavadharini B, Kavimughil M, Malini B et al (2022) Recent advances in biosensors for detection of chemical contaminants in food—a review. Food Anal Methods. https://doi.org/10.1007/s12161-021-02213-y
45. Rather IA, Koh WY, Paek WK, Lim J (2017) The Sources of Chemical Contaminants in Food and Their Health Implications. Front Pharmacol 8. https://doi.org/10.3389/fphar.2017.00830
46. García-Valcárcel AI, Tadeo JL (2009) A combination of ultrasonic assisted extraction with LC–MS/MS for the determination of organophosphorus pesticides in sludge. Anal Chim Acta 641:117–123. https://doi.org/10.1016/j.aca.2009.03.046
47. Vidal JC, Bonel L, Ezquerra A et al (2013) Electrochemical affinity biosensors for detection of mycotoxins: a review. Biosens Bioelectron 49:146–158. https://doi.org/10.1016/j.bios.2013.05.008
48. Riberi WI, Zon MA, Fernández H, Arévalo FJ (2020) Impedimetric immunosensor to determine patulin in apple juices using a glassy carbon electrode modified with graphene oxide. Microchem J 158:105192. https://doi.org/10.1016/j.microc.2020.105192

49. Rocha GS, Silva MKL, Cesarino I (2020) Reduced graphene oxide-based impedimetric immunosensor for detection of enterotoxin a in milk samples. Materials (Basel) 13:1751. https://doi.org/10.3390/ma13071751
50. Liu L, Xu D, Hu Y et al (2015) Construction of an impedimetric immunosensor for label-free detecting carbofuran residual in agricultural and environmental samples. Food Control 53:72–80. https://doi.org/10.1016/j.foodcont.2015.01.009
51. Cao Y, Sun X, Guo Y et al (2015) An electrochemical immunosensor based on interdigitated array microelectrode for the detection of chlorpyrifos. Bioprocess Biosyst Eng 38:307–313. https://doi.org/10.1007/s00449-014-1269-3
52. Ermolaeva T, Farafonova O, Karaseva N (2019) Possibilities and prospects of immunosensors for a highly sensitive pesticide detection in vegetables and fruits: a review. Food Anal Methods 12:2785–2801. https://doi.org/10.1007/s12161-019-01630-4
53. Hou L, Zhang X, Kong M et al (2020) A competitive immunoassay for electrochemical impedimetric determination of chlorpyrifos using a nanogold-modified glassy carbon electrode based on enzymatic biocatalytic precipitation. Microchim Acta 187:204. https://doi.org/10.1007/s00604-020-4175-1
54. Malvano F, Albanese D, Pilloton R, Di M (2016) A highly sensitive impedimetric label free immunosensor for Ochratoxin measurement in cocoa beans. Food Chem 212:688–694. https://doi.org/10.1016/j.foodchem.2016.06.034
55. Mehta J, Vinayak P, Tuteja SK et al (2016) Graphene modified screen printed immunosensor for highly sensitive detection of parathion. Biosens Bioelectron 83:339–346. https://doi.org/10.1016/j.bios.2016.04.058
56. Hosu O, Selvolini G, Marrazza G (2018) Recent advances of immunosensors for detecting food allergens. Curr Opin Electrochem 10:149–156. https://doi.org/10.1016/j.coelec.2018.05.022
57. Aquino A, Conte-Junior CA (2020) A systematic review of food allergy: nanobiosensor and food allergen detection. Biosensors 10:194. https://doi.org/10.3390/bios10120194
58. Freitas M, Nouws HPA, Delerue-Matos C (2021) Voltammetric immunosensor to track a major peanut allergen (Ara h 1) in food products employing quantum dot labels. Biosensors 11:426. https://doi.org/10.3390/bios11110426
59. Benedé S, Ruiz-Valdepeñas Montiel V, Povedano E et al (2018) Fast amperometric immunoplatform for ovomucoid traces determination in fresh and baked foods. Sensors Actuators B Chem 265:421–428. https://doi.org/10.1016/j.snb.2018.03.075
60. Liu H, Malhotra R, Peczuh MW, Rusling JF (2010) Electrochemical immunosensors for antibodies to peanut allergen ara h2 using gold nanoparticle−peptide films. Anal Chem 82:5865–5871. https://doi.org/10.1021/ac101110q
61. Huang Y, Bell MC, Suni II (2008) Impedance biosensor for peanut protein ara h 1. Anal Chem 80:9157–9161. https://doi.org/10.1021/ac801048g
62. Singh R, Sharma PP, Baltus RE, Suni II (2010) Nanopore immunosensor for peanut protein Ara h1. Sensors Actuators B Chem 145:98–103. https://doi.org/10.1016/j.snb.2009.11.039
63. Chiriacò MS, De Feo F, Primiceri E et al (2015) Portable gliadin-immunochip for contamination control on the food production chain. Talanta 142:57–63. https://doi.org/10.1016/j.talanta.2015.04.040
64. Ukaogo PO, Ewuzie U, Onwuka C V. (2020) Environmental pollution: causes, effects, and the remedies. INC
65. Baines C, Lerebours A, Thomas F et al (2021) Linking pollution and cancer in aquatic environments: a review. Environ Int 149:106391. https://doi.org/10.1016/j.envint.2021.106391
66. World Health Organization (WHO) (2020) Global leprosy (Hansen disease) update, 2020: impact of COVID-19 on global leprosy control. Wkly Epidemiol Rec 96:421–444
67. Sengupta S, Chattopadhyay MK, Grossart H-P (2013) The multifaceted roles of antibiotics and antibiotic resistance in nature. Front Microbiol 4:. https://doi.org/10.3389/fmicb.2013.00047
68. Joshi A, Kim K-H (2020) Recent advances in nanomaterial-based electrochemical detection of antibiotics: challenges and future perspectives. Biosens Bioelectron 153:112046. https://doi.org/10.1016/j.bios.2020.112046

69. Alsaiari NS, Katubi KMM, Alzahrani FM et al (2021) The application of nanomaterials for the electrochemical detection of antibiotics: a review. Micromachines 12:308. https://doi.org/10.3390/mi12030308
70. Tran TTT, Do MN, Dang TNH et al (2022) A state-of-the-art review on graphene-based nanomaterials to determine antibiotics by electrochemical techniques. Environ Res 208:112744. https://doi.org/10.1016/j.envres.2022.112744
71. Wang Q, Xue Q, Chen T et al (2021) Recent advances in electrochemical sensors for antibiotics and their applications. Chinese Chem Lett 32:609–619. https://doi.org/10.1016/j.cclet.2020.10.025
72. Lamarca RS, De FRAD, Zanoni MVB et al (2020) Simple, fast and environmentally friendly method to determine ciprofloxacin in wastewater samples based on an impedimetric immunosensor. RSC Adv 10:1838–1847. https://doi.org/10.1039/c9ra09083e
73. Rocha CG, Ferreira AAP, Yamanaka H (2016) Label-free impedimetric immunosensor for detection of the textile azo dye Disperse Red 1 in treated water. Sensors Actuators B Chem 236:52–59. https://doi.org/10.1016/j.snb.2016.05.040
74. Giroud F, Gorgy K, Gondran C et al (2009) Impedimetric immunosensor based on a polypyrrole−antibiotic model film for the label-free picomolar detection of ciprofloxacin. Anal Chem 81:8405–8409. https://doi.org/10.1021/ac901290m
75. Waghmode TR, Kurade MB, Sapkal RT et al (2019) Sequential photocatalysis and biological treatment for the enhanced degradation of the persistent azo dye methyl red. J Hazard Mater 371:115–122. https://doi.org/10.1016/j.jhazmat.2019.03.004
76. Su H-C, Liu Y-S, Pan C-G et al (2018) Persistence of antibiotic resistance genes and bacterial community changes in drinking water treatment system: from drinking water source to tap water. Sci Total Environ 616–617:453–461. https://doi.org/10.1016/j.scitotenv.2017.10.318
77. Ribeiro C, Ribeiro AR, Maia AS et al (2014) New trends in sample preparation techniques for environmental analysis. Crit Rev Anal Chem 44:142–185. https://doi.org/10.1080/10408347.2013.833850
78. Fingas M (2016) Water analysis|oil pollution☆. In: Reference module in chemistry, molecular sciences and chemical engineering. Elsevier
79. Barreiros dos Santos M, Agusil JP, Prieto-Simón B et al (2013) Highly sensitive detection of pathogen *Escherichia coli* O157:H7 by electrochemical impedance spectroscopy. Biosens Bioelectron 45:174–180. https://doi.org/10.1016/j.bios.2013.01.009
80. Malvano F, Pilloton R, Albanese D (2018) Sensitive detection of *escherichia coli* O157:H7 in food products by impedimetric immunosensors. Sensors 18:2168. https://doi.org/10.3390/s18072168
81. Wan J, Ai J, Zhang Y et al (2016) Signal-off impedimetric immunosensor for the detection of *Escherichia coli* O157:H7. Sci Rep 6:19806. https://doi.org/10.1038/srep19806
82. Lin D, Pillai RG, Lee WE, Jemere AB (2019) An impedimetric biosensor for *E. coli* O157:H7 based on the use of self-assembled gold nanoparticles and protein G. Microchim Acta 186:169. https://doi.org/10.1007/s00604-019-3282-3
83. Chowdhury AD, De A, Chaudhuri CR et al (2012) Label free polyaniline based impedimetric biosensor for detection of *E. coli* O157:H7 Bacteria. Sensors Actuators B Chem 171–172:916–923. https://doi.org/10.1016/j.snb.2012.06.004
84. Cimafonte M, Fulgione A, Gaglione R et al (2020) Screen printed based impedimetric immunosensor for rapid detection of *Escherichia coli* in drinking water. Sensors (Switzerland) 20:1–17. https://doi.org/10.3390/s20010274
85. Mishra S, Zhang W, Lin Z et al (2020) Carbofuran toxicity and its microbial degradation in contaminated environments. Chemosphere 259:127419. https://doi.org/10.1016/j.chemosphere.2020.127419
86. Tadeo JL, Pérez RA, Albero B et al (2012) Review of sample preparation techniques for the analysis of pesticide residues in soil. J AOAC Int 95:1258–1271. https://doi.org/10.5740/jaoacint.SGE_Tadeo
87. de Toffoli AL, Maciel EVS, Fumes BH, Lanças FM (2018) The role of graphene-based sorbents in modern sample preparation techniques. J Sep Sci 41:288–302. https://doi.org/10.1002/jssc.201700870

88. Dugheri S, Mucci N, Cappelli G et al (2022) Advanced solid-phase microextraction techniques and related automation: a review of commercially available technologies. J Anal Methods Chem 2022:1–15. https://doi.org/10.1155/2022/8690569
89. Fino A (2019) Air Quality Legislation. In: Encyclopedia of Environmental Health. Elsevier, pp 61–70
90. Ashmore M (2013) Air pollution. In: Encyclopedia of biodiversity. Elsevier, pp 136–147
91. Galvão ES, Santos JM, Lima AT et al (2018) Trends in analytical techniques applied to particulate matter characterization: A critical review of fundaments and applications. Chemosphere 199:546–568. https://doi.org/10.1016/j.chemosphere.2018.02.034
92. Ranjan P, Parihar A, Jain S et al (2020) Biosensor-based diagnostic approaches for various cellular biomarkers of breast cancer: a comprehensive review. Anal Biochem 610:113996. https://doi.org/10.1016/j.ab.2020.113996
93. Kumar S, Tripathy S, Jyoti A, Singh SG (2019) Recent advances in biosensors for diagnosis and detection of sepsis: a comprehensive review. Biosens Bioelectron 124–125:205–215. https://doi.org/10.1016/j.bios.2018.10.034
94. Haleem A, Javaid M, Singh RP et al (2021) Biosensors applications in medical field: a brief review. Sensors Int 2:100100. https://doi.org/10.1016/j.sintl.2021.100100
95. Zumpano R, Polli F, D'Agostino C et al (2021) Nanostructure-based electrochemical immunosensors as diagnostic tools. Electrochem 2:10–28. https://doi.org/10.3390/electrochem2010002
96. Califf RM (2018) Biomarker definitions and their applications. Exp Biol Med 243:213–221. https://doi.org/10.1177/1535370217750088
97. Huss R (2014) Biomarkers. In: Atala; A, Allickson J (eds) Translational regenerative medicine, 1st Editio. Elsevier Inc., pp 235–241
98. Redegeld F, Hermann K, Ollert M, Ring J (2019) Antibody detection. Nijkamp Parnham's Princ Immunopharmacol 233–241. https://doi.org/10.1007/978-3-030-10811-3_14
99. Israel A, Shenhar Y, Green I, et al (2021) Large-scale study of antibody titer decay following BNT162b2 mRNA vaccine or SARS-CoV-2 infection. medRxiv Prepr Serv Heal Sci 1–15. https://doi.org/10.1101/2021.08.19.21262111
100. Roerink F, Morgan CL, Knetter SM et al (2018) A novel inactivated vaccine against Lawsonia intracellularis induces rapid induction of humoral immunity, reduction of bacterial shedding and provides robust gut barrier function. Vaccine 36:1500–1508. https://doi.org/10.1016/j.vaccine.2017.12.049
101. Mboumba Bouassa R-S, Péré H, Gubavu C et al (2020) Serum and cervicovaginal IgG immune responses against α7 and α9 HPV in non-vaccinated women at risk for cervical cancer: implication for catch-up prophylactic HPV vaccination. PLoS ONE 15:e0233084. https://doi.org/10.1371/journal.pone.0233084
102. Low SL, Leo YS, Lai YL et al (2021) Evaluation of eight commercial Zika virus IgM and IgG serology assays for diagnostics and research. PLoS One 16:1–15. https://doi.org/10.1371/journal.pone.0244601
103. Vollmer T, Diekmann J, Eberhardt M et al (2016) Monitoring of anti-hepatitis E virus antibody seroconversion in asymptomatically infected blood donors: Systematic comparison of nine commercial anti-HEV IgM and IgG assays. Viruses 8:1–15. https://doi.org/10.3390/v8080232
104. Chien YW, Liu ZH, Tseng FC et al (2018) Prolonged persistence of IgM against dengue virus detected by commonly used commercial assays. BMC Infect Dis 18:1–7. https://doi.org/10.1186/s12879-018-3058-0
105. Yüce M, Filiztekin E, Özkaya KG (2021) COVID-19 diagnosis —a review of current methods. Biosens Bioelectron 172. https://doi.org/10.1016/j.bios.2020.112752
106. Andrey DO, Cohen P, Meyer B et al (2020) Head-to-head accuracy comparison of three commercial COVID-19 IgM/IgG serology rapid tests. J Clin Med 9:2369. https://doi.org/10.3390/jcm9082369
107. Mao X, Huang TJ, Ho C-M (2010) The lab-on-a-chip approach for molecular diagnostics. In: Molecular diagnostics. Elsevier, pp 21–34

108. Guthrie JW (2012) General considerations when dealing with biological fluid samples. In: Comprehensive sampling and sample preparation. Elsevier, pp 1–19
109. Engelking LR (2015) Protein structure. In: Textbook of veterinary physiological chemistry. Elsevier, pp 18–25
110. Palomar Q, Gondran C, Marks R et al (2018) Impedimetric quantification of anti-dengue antibodies using functional carbon nanotube deposits validated with blood plasma assays. Electrochim Acta 274:84–90. https://doi.org/10.1016/j.electacta.2018.04.099
111. Alshammari TM, Al-Hassan AA, Hadda TB, Aljofan M (2015) Comparison of different serum sample extraction methods and their suitability for mass spectrometry analysis. Saudi Pharm J 23:689–697. https://doi.org/10.1016/j.jsps.2015.01.023
112. Mosca T, Forte WCN (2016) Comparative efficiency and impact on the activity of blood neutrophils isolated by percoll, ficoll and spontaneous sedimentation methods. Immunol Invest 45:29–37. https://doi.org/10.3109/08820139.2015.1085393
113. Do Egito EMN, Silva-Júnior AG, Lucena RPS et al (2022) Electrochemical platform for anti-cardiolipin antibody detection in human syphilitic serum. Curr Res Biotechnol 4:58–65. https://doi.org/10.1016/j.crbiot.2022.01.001
114. Chinnadayyala SR, Park J, Abbasi MA, Cho S (2019) Label-free electrochemical impedimetric immunosensor for sensitive detection of IgM rheumatoid factor in human serum. Biosens Bioelectron 143:111642. https://doi.org/10.1016/j.bios.2019.111642
115. Goud KY, Reddy KK, Khorshed A et al (2021) Electrochemical diagnostics of infectious viral diseases: trends and challenges. Biosens Bioelectron 180:113112. https://doi.org/10.1016/j.bios.2021.113112
116. Muller DA, Young PR (2013) The flavivirus NS1 protein: Molecular and structural biology, immunology, role inpathogenesis and application asadiagnostic biomarker. Antiviral Res 98:192–208. https://doi.org/10.1016/j.antiviral.2013.03.008
117. Pothapregada S (2016) Is reactive dengue NS1antigen test a warning call for hospital admissions? J Clin DIAGNOSTIC Res. https://doi.org/10.7860/JCDR/2016/16178.7636
118. Ojha RP, Singh P, Azad UP, Prakash R (2022) Impedimetric immunosensor for the NS1 dengue biomarker based on the gold nanorod decorated graphitic carbon nitride modified electrode. Electrochim Acta 411:140069. https://doi.org/10.1016/j.electacta.2022.140069
119. Nawaz MH, Hayat A, Catanante G et al (2018) Development of a portable and disposable NS1 based electrochemical immunosensor for early diagnosis of dengue virus. Anal Chim Acta 1026:1–7. https://doi.org/10.1016/j.aca.2018.04.032
120. Mendonça PD, Santos LKB, Foguel MV et al (2021) NS1 glycoprotein detection in serum and urine as an electrochemical screening immunosensor for dengue and Zika virus. Anal Bioanal Chem 413:4873–4885. https://doi.org/10.1007/s00216-021-03449-7
121. Luna DMN, Avelino KYPS, Cordeiro MT et al (2015) Electrochemical immunosensor for dengue virus serotypes based on 4-mercaptobenzoic acid modified gold nanoparticles on self-assembled cysteine monolayers. Sensors Actuators B Chem 220:565–572. https://doi.org/10.1016/j.snb.2015.05.067
122. Riedel S (2019) Predicting bacterial versus viral infection, or none of the above: current and future prospects of biomarkers. Clin Lab Med 39:453–472. https://doi.org/10.1016/j.cll.2019.05.011
123. Qureshi A, Niazi JH (2020) Biosensors for detecting viral and bacterial infections using host biomarkers: a review. Analyst 145:7825–7848. https://doi.org/10.1039/d0an00896f
124. Ooi JSG, Lok SM (2021) How NS1 antibodies prevent severe flavivirus disease. Trends Biochem Sci 46:519–521. https://doi.org/10.1016/j.tibs.2021.03.005
125. Yusa T, Tateda K, Ohara A, Miyazaki S (2017) New possible biomarkers for diagnosis of infections and diagnostic distinction between bacterial and viral infections in children. J Infect Chemother 23:96–100. https://doi.org/10.1016/j.jiac.2016.11.002
126. Tarkkinen P, Palenius T, Lövgren T (2002) Ultrarapid, ultrasensitive one-step kinetic immunoassay for C-reactive protein (CRP) in whole blood samples: Measurement of the entire CRP concentration range with a single sample dilution. Clin Chem 48:269–277. https://doi.org/10.1093/clinchem/48.2.269

127. Kanyong P, Catli C, Davis JJ (2020) Ultrasensitive impedimetric immunosensor for the detection of C-reactive protein in blood at surface-initiated-reversible addition-fragmentation chain transfer generated poly(2-hydroxyethyl methacrylate) brushes. Anal Chem 92:4707–4710. https://doi.org/10.1021/acs.analchem.9b05030
128. Aydın EB (2020) Highly sensitive impedimetric immunosensor for determination of interleukin 6 as a cancer biomarker by using conjugated polymer containing epoxy side groups modified disposable ITO electrode. Talanta 215:120909. https://doi.org/10.1016/j.talanta.2020.120909
129. Griesinger F, Eberhardt W, Nusch A et al (2021) Biomarker testing in non-small cell lung cancer in routine care: Analysis of the first 3717 patients in the German prospective, observational, nation-wide CRISP Registry (AIO-TRK-0315). Lung Cancer 152:174–184. https://doi.org/10.1016/j.lungcan.2020.10.012
130. Echle A, Rindtorff NT, Brinker TJ et al (2021) Deep learning in cancer pathology: a new generation of clinical biomarkers. Br J Cancer 124:686–696. https://doi.org/10.1038/s41416-020-01122-x
131. Gilbert R, Tilling K, Martin RM et al (2018) Developing new age-specific prostate-specific antigen thresholds for testing for prostate cancer. Cancer Causes Control 29:383–388. https://doi.org/10.1007/s10552-018-1014-3
132. Soronen V, Talala K, Raitanen J et al (2021) Digital rectal examination in prostate cancer screening at PSA level 3.0-3.9 ng/ml: long-term results from a randomized trial. Scand J Urol 55:348–353. https://doi.org/10.1080/21681805.2021.1966095
133. Smith RA, Andrews KS, Brooks D et al (2018) Cancer screening in the United States, 2018: a review of current American cancer society guidelines and current issues in cancer screening. CA Cancer J Clin 68:297–316. https://doi.org/10.3322/caac.21446
134. Bordin DCM, Monedeiro FF da SS, Campos EG de, et al (2015) Técnicas de preparo de amostras biológicas com interesse forense. Sci Chromatogr 7:125–143. https://doi.org/10.4322/sc.2015.022
135. Brooks T, Keevil CW (1997) A simple artificial urine for the growth of urinary pathogens. Lett Appl Microbiol 24:203–206. https://doi.org/10.1046/j.1472-765X.1997.00378.x
136. Shaikh MO, Huang T-C, Wu T-F, Chuang C-H (2020) Label free impedimetric immunosensor for effective bladder Cancer detection in clinical urine samples. Biomed Microdevices 22:45. https://doi.org/10.1007/s10544-020-00501-8
137. Karami P, Bagheri H, Johari-Ahar M et al (2019) Dual-modality impedimetric immunosensor for early detection of prostate-specific antigen and myoglobin markers based on antibody-molecularly imprinted polymer. Talanta 202:111–122. https://doi.org/10.1016/j.talanta.2019.04.061
138. Aydın EB, Aydın M, Sezgintürk MK (2021) Highly selective and sensitive sandwich immunosensor platform modified with MUA-capped GNPs for detection of spike receptor binding domain protein: a precious marker of COVID 19 infection. Sensors Actuators B Chem 345:130355. https://doi.org/10.1016/j.snb.2021.130355
139. Aydın EB, Aydın M, Sezgintürk MK (2021) New impedimetric sandwich immunosensor for ultrasensitive and highly specific detection of spike receptor binding domain protein of SARS-CoV-2. ACS Biomater Sci Eng 7:3874–3885. https://doi.org/10.1021/acsbiomaterials.1c00580
140. Ben-Ami R, Klochendler A, Seidel M et al (2020) Large-scale implementation of pooled RNA extraction and RT-PCR for SARS-CoV-2 detection. Clin Microbiol Infect 26:1248–1253. https://doi.org/10.1016/j.cmi.2020.06.009
141. Rodriguez-Granger J, Mendiola JC, Martínez LA (2018) Identification of mycobacteria by matrix-assisted laser desorption ionization–time-of-flight mass spectrometry. In: The use of mass spectrometry technology (MALDI-TOF) in clinical microbiology. Elsevier, pp 181–195
142. Muñoz J, Pumera M (2021) 3D-Printed COVID-19 immunosensors with electronic readout. Chem Eng J 425:131433. https://doi.org/10.1016/j.cej.2021.131433
143. Meyer B, Torriani G, Yerly S et al (2020) Validation of a commercially available SARS-CoV-2 serological immunoassay. Clin Microbiol Infect 26:1386–1394. https://doi.org/10.1016/j.cmi.2020.06.024

144. Mak GC, Cheng PK, Lau SS et al (2020) Evaluation of rapid antigen test for detection of SARS-CoV-2 virus. J Clin Virol 129:104500. https://doi.org/10.1016/j.jcv.2020.104500
145. Liu G, Rusling JF (2021) COVID-19 antibody tests and their limitations. ACS Sensors 6:593–612. https://doi.org/10.1021/acssensors.0c02621
146. Hryniewicz BM, Volpe J, Bach-Toledo L et al (2022) Development of polypyrrole (nano)structures decorated with gold nanoparticles toward immunosensing for COVID-19 serological diagnosis. Mater Today Chem 24:100817. https://doi.org/10.1016/j.mtchem.2022.100817
147. Lorenzen AL, dos Santos AM, dos Santos LP et al (2022) PEDOT-AuNPs-based impedimetric immunosensor for the detection of SARS-CoV-2 antibodies. Electrochim Acta 404:139757. https://doi.org/10.1016/j.electacta.2021.139757
148. Czumbel LM, Kiss S, Farkas N, et al (2020) Saliva as a candidate for COVID-19 diagnostic testing: a meta-analysis. Front Med 7. https://doi.org/10.3389/fmed.2020.00465
149. Duś-Ilnicka I, Krala E, Cholewińska P, Radwan-Oczko M (2021) The use of saliva as a biosample in the light of COVID-19. Diagnostics 11:1769. https://doi.org/10.3390/diagnostics11101769
150. Zaccariotto GC, Silva MKL, Rocha GS, Cesarino I (2021) A novel method for the detection of SARS-CoV-2 based on graphene-impedimetric immunosensor. Materials (Basel) 14:4230. https://doi.org/10.3390/ma14154230
151. Brazaca LC, Imamura AH, Gomes NO et al (2022) Electrochemical immunosensors using electrodeposited gold nanostructures for detecting the S proteins from SARS-CoV and SARS-CoV-2. Anal Bioanal Chem. https://doi.org/10.1007/s00216-022-03956-1
152. Seshadri DR, Li RT, Voos JE, et al (2019) Wearable sensors for monitoring the physiological and biochemical profile of the athlete. npj Digit Med 2:72. https://doi.org/10.1038/s41746-019-0150-9
153. Majumder S, Mondal T, Deen M (2017) Wearable sensors for remote health monitoring. Sensors 17:130. https://doi.org/10.3390/s17010130
154. Cheng S, Gu Z, Zhou L, et al (2021) Recent progress in intelligent wearable sensors for health monitoring and wound healing based on biofluids. Front Bioeng Biotechnol 9. https://doi.org/10.3389/fbioe.2021.765987
155. Tu J, Torrente-Rodríguez RM, Wang M, Gao W (2020) The era of digital health: a review of portable and wearable affinity biosensors. Adv Funct Mater 30:1906713. https://doi.org/10.1002/adfm.201906713
156. Takaloo S, Moghimi Zand M (2021) Wearable electrochemical flexible biosensors: with the focus on affinity biosensors. Sens Bio-Sensing Res 32:100403. https://doi.org/10.1016/j.sbsr.2021.100403
157. Gao W, Emaminejad S, Nyein HYY et al (2016) Fully integrated wearable sensor arrays for multiplexed in situ perspiration analysis. Nature 529:509–514. https://doi.org/10.1038/nature16521
158. Yi F, Ren H, Shan J et al (2018) Wearable energy sources based on 2D materials. Chem Soc Rev 47:3152–3188. https://doi.org/10.1039/C7CS00849J
159. Nah JS, Barman SC, Zahed MA et al (2021) A wearable microfluidics-integrated impedimetric immunosensor based on Ti3C2T MXene incorporated laser-burned graphene for noninvasive sweat cortisol detection. Sensors Actuators B Chem 329:129206. https://doi.org/10.1016/j.snb.2020.129206
160. Huynh VL, Trung TQ, Meeseepong M et al (2020) Hollow microfibers of elastomeric nanocomposites for fully stretchable and highly sensitive microfluidic immunobiosensor patch. Adv Funct Mater 30:1–12. https://doi.org/10.1002/adfm.202004684
161. Lee HB, Meeseepong M, Trung TQ et al (2020) A wearable lab-on-a-patch platform with stretchable nanostructured biosensor for non-invasive immunodetection of biomarker in sweat. Biosens Bioelectron 156:112133. https://doi.org/10.1016/j.bios.2020.112133
162. Justino CIL, Duarte AC, Rocha-Santos TAP (2016) Critical overview on the application of sensors and biosensors for clinical analysis. TrAC Trends Anal Chem 85:36–60. https://doi.org/10.1016/j.trac.2016.04.004

163. Shao Y, Zhou H, Wu Q et al (2021) Recent advances in enzyme-enhanced immunosensors. Biotechnol Adv 53:107867. https://doi.org/10.1016/j.biotechadv.2021.107867
164. Kumar V, Vaid K, Bansal SA, Kim K-H (2020) Nanomaterial-based immunosensors for ultrasensitive detection of pesticides/herbicides: Current status and perspectives. Biosens Bioelectron 165:112382. https://doi.org/10.1016/j.bios.2020.112382
165. Jia M, Liao X, Fang L et al (2021) Recent advances on immunosensors for mycotoxins in foods and other commodities. TrAC Trends Anal Chem 136:116193. https://doi.org/10.1016/j.trac.2021.116193
166. Raposo F, Ibelli-Bianco C (2020) Performance parameters for analytical method validation: Controversies and discrepancies among numerous guidelines. TrAC Trends Anal Chem 129:115913. https://doi.org/10.1016/j.trac.2020.115913
167. Patil ST, Ahirrao RA, Pawar SP (2017) A short review on method validation. J Pharm Biosci 5:30. https://doi.org/10.31555/jpbs/2017/5/4/30-37
168. Soriano ML, Zougagh M, Ríos Á, Valcárcel M (2019) Analytical reliability of simple, rapid, minuturizated, direct analytical processes: a call to arms. TrAC Trends Anal Chem 114:98–107. https://doi.org/10.1016/j.trac.2019.03.005
169. Wu AHB (2015) Analytical validation of novel cardiac biomarkers used in clinical trials. Am Heart J 169:674–683. https://doi.org/10.1016/j.ahj.2015.01.016
170. Masucci GV, Cesano A, Hawtin R et al (2016) Validation of biomarkers to predict response to immunotherapy in cancer: volume I—pre-analytical and analytical validation. J Immunother Cancer 4:76. https://doi.org/10.1186/s40425-016-0178-1
171. Thompson M, Ellison SLR, Wood R (2002) Harmonized guidelines for single-laboratory validation of methods of analysis (IUPAC Technical Report). Pure Appl Chem 74:835–855. https://doi.org/10.1351/pac200274050835
172. Zhu L, Dong X-X, Gao C-B et al (2022) Development of a highly sensitive and selective electrochemical immunosensor for controlling of rhodamine B abuse in food samples. Food Control 133:108662. https://doi.org/10.1016/j.foodcont.2021.108662
173. Mehmandoust M, Gumus ZP, Soylak M, Erk N (2022) Electrochemical immunosensor for rapid and highly sensitive detection of SARS-CoV-2 antigen in the nasal sample. Talanta 240:123211. https://doi.org/10.1016/j.talanta.2022.123211
174. Antunes J, Justino C, da Costa JP et al (2018) Graphene immunosensors for okadaic acid detection in seawater. Microchem J 138:465–471. https://doi.org/10.1016/j.microc.2018.01.041
175. Teengam P, Siangproh W, Tontisirin S et al (2021) NFC-enabling smartphone-based portable amperometric immunosensor for hepatitis B virus detection. Sensors Actuators B Chem 326:128825. https://doi.org/10.1016/j.snb.2020.128825
176. Aymard C, Kanso H, Serrano MJ et al (2022) Development of a new dual electrochemical immunosensor for a rapid and sensitive detection of enrofloxacin in meat samples. Food Chem 370:131016. https://doi.org/10.1016/j.foodchem.2021.131016
177. Zhang M, Mei L, Zhang L et al (2021) Ti3C2 MXene anchors CuAu-LDH multifunctional two-dimensional nanomaterials for dual-mode detection of CEA in electrochemical immunosensors. Bioelectrochemistry 142:107943. https://doi.org/10.1016/j.bioelechem.2021.107943
178. Kalyani T, Sangili A, Nanda A et al (2021) Bio-nanocomposite based highly sensitive and label-free electrochemical immunosensor for endometriosis diagnostics application. Bioelectrochemistry 139:107740. https://doi.org/10.1016/j.bioelechem.2021.107740
179. Anusha T, Bhavani KS, Shanmukha Kumar JV et al (2022) Fabrication of electrochemical immunosensor based on GCN-β-CD/Au nanocomposite for the monitoring of vitamin D deficiency. Bioelectrochemistry 143:107935. https://doi.org/10.1016/j.bioelechem.2021.107935
180. Lu L, Gunasekaran S (2019) Dual-channel ITO-microfluidic electrochemical immunosensor for simultaneous detection of two mycotoxins. Talanta 194:709–716. https://doi.org/10.1016/j.talanta.2018.10.091

181. BRASIL, RDC Nº 166, DE 24 DE JULHO DE 2017, Brasília, DOU nº141, de 25 de julho de 2017. Dispõe sobre a validação de métodos analíticos e dá outras providências
182. Raposo F (2016) Evaluation of analytical calibration based on least-squares linear regression for instrumental techniques: a tutorial review. TrAC Trends Anal Chem 77:167–185. https://doi.org/10.1016/j.trac.2015.12.006
183. Medetalibeyoglu H, Beytur M, Akyıldırım O et al (2020) Validated electrochemical immunosensor for ultra-sensitive procalcitonin detection: Carbon electrode modified with gold nanoparticles functionalized sulfur doped MXene as sensor platform and carboxylated graphitic carbon nitride as signal amplification. Sensors Actuators B Chem 319:128195. https://doi.org/10.1016/j.snb.2020.128195
184. de Almeida SV, Cancino-Bernardi J, de Andrade JK et al (2020) Cancer immunosensor based on apo and holo transferrin binding. Microchim Acta 187:438. https://doi.org/10.1007/s00604-020-04420-6
185. Araujo P (2009) Key aspects of analytical method validation and linearity evaluation. J Chromatogr B Anal Technol Biomed Life Sci 877:2224–2234. https://doi.org/10.1016/j.jchromb.2008.09.030

Plasmonics in Bioanalysis: SPR, SERS, and Nanozymes

Heloise R. de Barros, Vítor M. Miguel, Rafael N. P. Colombo, Rafael T. P. da Silva, and Susana I. Cordoba de Torresi

Equal contribution from all authors.

Abstract In its complexity, light-matter interaction has a proven value for many scientific fields, such as quantum mechanics, material sciences and spectroscopy. In recent decades, bioanalytical tools have been developed, taking advantage of this knowledge. Sensing techniques such as the ones depending on (bio) catalytic reactions could be improved in terms of sensitivity and limits of detection and quantification with light stimuli. Others, such as surface plasmon resonance (SPR), could only thrive after the unraveling of some light-matter interaction particularities. In addition, the consolidation of nanoscience, including the capability to synthesize nanoparticles with enzyme-like activity and selectivity (nanozymes), led to a new perspective on the practical advantages of designed materials with optical attributes deriving from subwavelength-scaled particles. A set of techniques could benefit from this phenomenon. Examples are Surface-Enhanced Raman Spectroscopy (SERS), derived from the Raman effect, and Localized Surface Plasmon Resonance (LSPR), derived from SPR. This chapter is an overview of light-matter interaction from the perspective of bioanalytical tools, highlighting the state of the art of plasmonic-based electrochemical and electroanalytical methods, taking advantage of designed nanoparticles with controlled size, geometry and composition.

H. R. de Barros · V. M. Miguel · R. T. P. da Silva · S. I. C. de Torresi (✉)
Instituto de Química, Universidade de São Paulo, São Paulo, Brazil
e-mail: storresi@iq.usp.br

H. R. de Barros
e-mail: barroshr@usp.br

V. M. Miguel
e-mail: vitor.miguel@usp.br

R. T. P. da Silva
e-mail: rafael.trivella.silva@usp.br

R. N. P. Colombo
Instituto de Química de São Carlos, Universidade de São Paulo, São Paulo, Brazil
e-mail: rafael.colombo@usp.br

F. N. Crespilho (ed.), *Advances in Bioelectrochemistry Volume 5*,
https://doi.org/10.1007/978-3-031-10832-7_2

Keywords Bioanalytical methods · Electroanalytical methods · LSPR · Nanozymes · Plasmonics · SERS · SPR

1 Part I. Localized Surface Plasmon Resonance

1.1 Introduction

Plasmonic nanoparticles (PNPs) are a class of nanomaterials with unique properties under incident electromagnetic radiation. Such remarkable properties arise from the interaction of PNPs with light at specific wavelengths, which generates the collective oscillation of the free electrons on the surface of the NP. As a result, the so-called localized surface plasmon resonance (LSPR) takes place. Figure 1 illustrates the phenomenon of LSPR excitation, representing the collective oscillation of the free electron on the surface of spherical NPs upon light irradiation. This phenomenon leads to an intensive absorption signal in a wide range of the ultraviolet, visible, and NIR regions of the electromagnetic spectrum.

The features of the LSPR leverage distinguished physical effects on the PNPs and surroundings. As examples, the optical near-field enhancement, heat generation, and the formation of hot charges [2]. The near-field enhancement is the most commonly studied outcome of LSPR and has been widely explored for surface-enhanced Raman spectroscopy (SERS) in the last few decades, a topic that is going to be deepened further in this chapter. For a system to be an optimized SERS substrate, usually highly uniformly sized and spatially distributed metallic nanoparticles are desired [3]. The near-field enhancement at the nanoparticle resonance frequency arises due to mainly two contributions: (i) the dipolar field formed around the particles alongside the plasmons; (ii) the lightning rod effect, i.e., the strong electric potential gradient formed due to the curvature of a metallic interface [4, 5]. In addition, PNPs are able to generate local heat upon resonant frequency stimulation due to Joule's

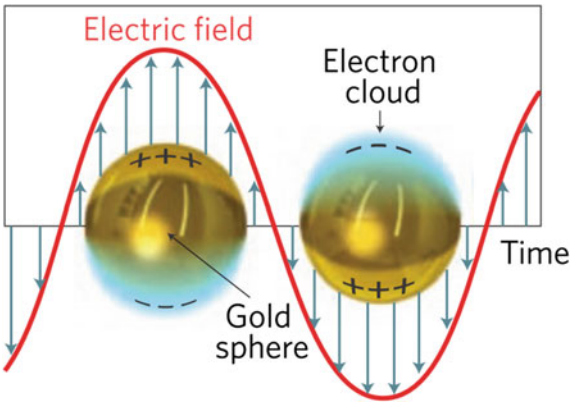

Fig. 1 Schematic illustration of the collective oscillation of free electrons on Au nanospheres upon excitation of the incoming specific light irradiation. The collective oscillation of the free electrons generates the LSPR signal in the electromagnetic spectrum. Adapted with permission from [1]

effect (also called Ohmic heating). Heat production during LSPR excitation emerges through the fast excitation of electrons and their energy loss caused by relaxation processes as electron–phonon coupling, transferring energy from the electrons to the lattice phonons, and in sequence, to the surrounding matter as fast phonon–phonon couplings are achieved [6]. Photothermal therapy is currently the main application that benefits from this outcome, although the field of catalysis has been exploring this effect to improve catalysts performance through thermodynamics [7, 8]. However, powerful, a less explored, and comprehended phenomenon that has brought attention only over the last few years are the generation of hot electrons and hot holes as charge carriers upon LSPR resonance-matching wavelengths. This effect is liable whenever the electrons in collective oscillation overcome the energy from the Fermi level of a determined structure. Its applications mainly concern catalysis and sensing through the charge transfer and redox processes [2, 9]. Nowadays, the attempt to disentangle the contributions from these three main outcomes of LSPR excitation has been challenging the researcher in this field [10–12]. In this task, spectroscopic and theoretical models are the greatest allies, although there is still plenty of room for discoveries that seem to be quite particular in each study system.

1.2 Localized Surface Plasmon Resonance: Practical View

These effects are very sensitive to molecules adsorbed on the PNP surface, which can deliver energy to the attached or surrounding molecules. These properties are especially explored for different kinds of catalysis, such as photo, electro and biocatalysis, and sensors as they foster strongly enhanced energy efficiency around the NPs surface [13–16]. Therefore, LSPR can be used as a fine tool since the techniques relying on it grant high-spatial resolution, as small as the plasmonic structure size, and high specificity enhance the design of very precise applications, with the added benefit of being remotely controllable by light.

Moreover, the physical effects of the LSPR excitation can be tuned by the different characteristics of PNPs, such as their size, morphology, architecture, composition, surface functionalization, and surrounding environment, among many others. This is described by Mie's theory, which *elucidates* the optical properties of spherical particles through the function of the particle's cross-section and the dielectric constant of its composition and the surrounding medium [17]. The derived functions that describe rod-like nanoparticles were developed over Mie's theory by Gans and El-Sayed [18, 19]. The scattering cross section of particles smaller than the incident light wavelength requires a few corrections and comprises a composition of multiple effects as electric and magnetic dipoles and quadrupoles. For metallic particles, electric dipoles dominate in the visible range, while for other materials, a different composition of these can be seen. These several kinds of intrinsic features of the PNPs induce changes in the LSPR profile due to the impact on the optical confinement, charge distribution, and energy dissipation of the entities. Among the commonplace trends, an increase in particles' size often implies a redshift of the electric dipole

band and the appearance of electric quadrupole bands, which in practice results in two bands instead of just one. For nanostars, it is found that the tip-angle is the factor that affects LSPR maximum band peak, as an increase in tip-angle promotes a blueshift of the peak [20]. It is also reported that nanostars produce a different spectral behavior depending on the excitation source wavelength. [21]. That way, the LSPR response relies on the PNP's characteristics to provide enhanced efficiency and performance [22–25].

For example, theoretical simulations show the differences in the plasmonic-driven field enhancement by changing the morphology of Au for nanospheres, nanorods, and nanostars, as shown in Fig. 2A. It is noticeable the stronger plasmonic-driven field enhancement on the rounding edges of the particles, which leverages a special concentration of energy into the tips of the spikes on nanostars [26]. The theoretical enhancement factors calculated for each Au morphology confirm the prominence of Au nanostars compared to gold nanospheres and nanorods (Fig. 2B, left). As a result of this increased field concentration on their tips, Au nanostars showed substantially higher efficiency at the Au-TiO_2 nanocomposites platform for their photocatalytic performance to photodegradation of rhodamine B (RhB) when compared to nanospheres and nanorods (Fig. 2B, right) [23]. Therefore, the different morphologies of the PNPs triggered singular performances to the analyte molecules that reached out the surface of the Au PNPs toward the photocatalytic reaction assessed in this study. This effect has also been explored for other areas beyond the field of nanocatalysis [27, 28], such as plasmonic biocatalysis [29, 30] and electrocatalysis [31–33].

In addition, there are many other distinct physicochemical properties of the PNPs (such as electrical, magnetic, optical, and thermal) together with the small size leading to higher spatial resolution capabilities, their reactivity, and favorable surface for biomolecules binding (directly on their surface or by surface functionalization), which further enhance the possibilities of attainable applications. Therefore, combined with their plasmonic properties, these PNPs provide room for the design of innovative tools in a single platform and exclusive reactions. As an example, it is possible to merge the singular features of PNPs and electrochemical properties.

1.3 Electrochemical Surface Plasmon Resonance

Combining electrochemistry with the distinct optical characteristics of PNPs gives a step forward for a new field of study: the electrochemical surface plasmon resonance (ESPR). The use of electrochemical techniques with PNPs allows to find out new insights toward distinguishing plasmonic properties and their physical effects, paving the way for advances in cutting-edge applications [34]. Particularly, this technology has been showing interesting results for biomolecules and molecules recognition as a powerful electrochemical instrument for bio and analytical sensing [35].

The ESPR technique works as electro-optical biosensing, i.e., detecting electrochemical processes that occur through the LSPR properties of the PNPs [36, 37]. Under light irradiation, these electrochemical processes can also be enhanced by

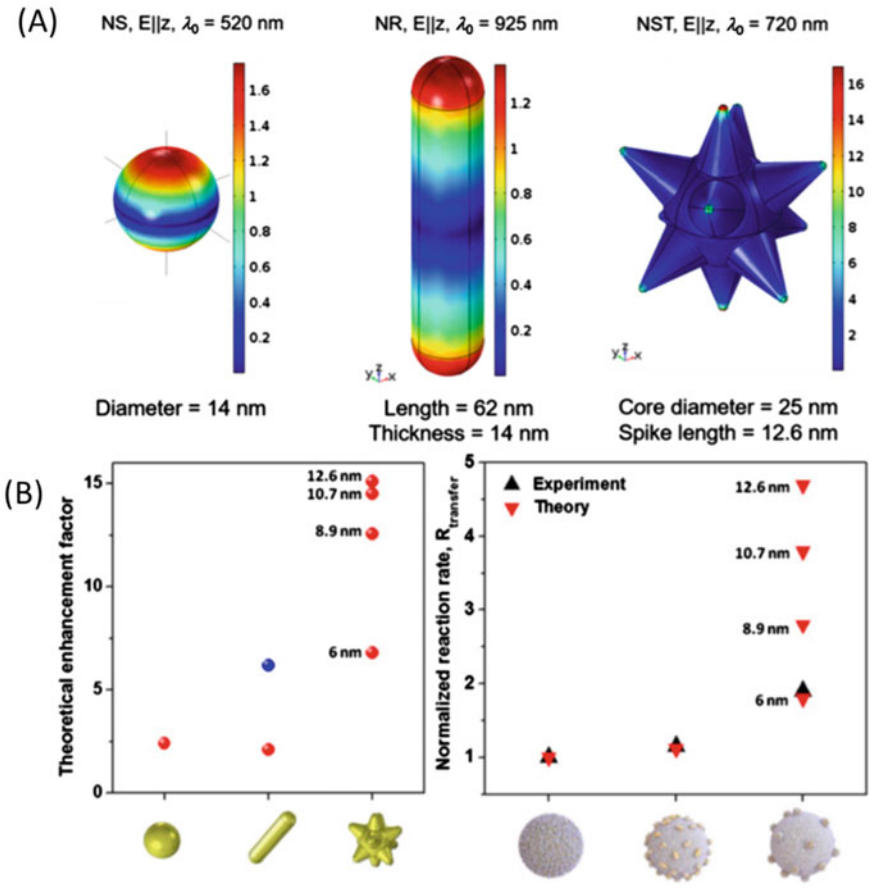

Fig. 2 Theoretical simulations were performed to assess the plasmonic-driven field enhancement of the PNPs Au nanospheres, nanorods, and nanostars upon electromagnetic field irradiation (plasmon-peak wavelengths). Representation of the normal-to-surface field maps (**A**). Left: Theoretical enhancement factors obtained from the calculations. In the case of the Au nanorods, the computed values are represented for a particle when it is parallel (blue point) and longitudinal (red point) to the incoming field. Right: Normalized reaction rates from the photocatalysis of rhodamine B (RhB) by the platform of Au nanostructures attached to the Au-TiO_2 nanocomposites, obtained from experimental (black points) and theoretical (red points) analysis (**B**). Adapted with permission from [23]

the generation of surface plasmons [32]. That way, the electrode surface acts simultaneously as the source for SPR excitation and an electrochemical detector, which provides information about both electrochemical and optical properties of PNPs composites and target molecules. Figure 3 shows a representative illustration of the typical electrochemical cell for ESPR analysis.

Pioneer studies by Lofas made use of thin Au films covered by a dextran layer using SPR properties for bioanalytical applications. In this case, the evanescent

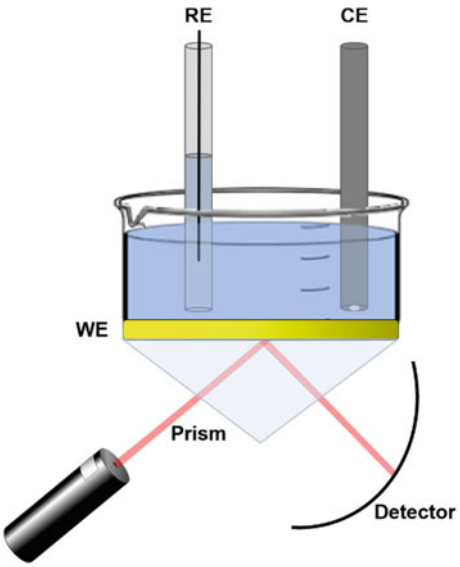

Fig. 3 Illustrative representation of an electrochemical cell for ESPR analysis. The light source reaches out the electrode surface where the PNPs are attached. Upon light irradiation, the light-enhanced electrochemical process is evidenced, and the ESPR takes place

electric field generated on the surface of the metal, i.e., the electromagnetic field spatially localized in the vicinal dielectric which faces an exponential decrease with the perpendicular distance can improve the bioanalytical analysis through covalently bounded biomolecules [38].

1.4 Conclusions

Therefore, ESPR is a powerful tool to promote enhanced analytical detectors for molecules and biomolecules merging plasmonic features, their outcomes, and electrochemical properties. This technology has been explored in heterogeneous catalysis, electrocatalysis, nanocatalysis, sensors, biodetectors, among others. Through such technology, we can expand our knowledge about the physicochemical effects in the plasmonic field. Moreover, these findings provide new information to create lab-on-chip devices, non-invasive analysis in real-time, providing cutting-edge technologies for target diagnosis of diseases, to cite few possibilities. Finally, this combination of features (different LSPR features and PNPs characteristics together with the electrochemical properties) can leverage plenty of new properties and possibilities by tuning each of the NP and light wavelength characteristics in electrochemical devices.

2 Part II. Surface Plasmon Resonance Sensing

2.1 Introduction

Surface plasmon resonance (SPR) sensing is a relatively new technique that has aroused a lot of interest and has been studied and developed in the last 30 years [39, 40]. It is based mainly on sensitive changes in optical properties of metal films (usually Au or Ag) that occur when a target analyte binds at the metal surface, providing high sensitivity by a simple and versatile methodology [41].

Over the years, SPR has been used for different applications, such as medicine, food, gas-phase chemistry, environment, and electrochemical measurements, being a powerful tool for characterization of chemical processes and sensing [42–44]. SPR sensing has become a very important and widely used tool for label-free biomolecular interaction analysis, presenting a low limit of detection (LOD). The LOD for aqueous buffer and complex sample medium can reach values lower than 1 fg mL^{-1} [45, 46] and 20 ng mL^{-1} [47], respectively, which when compared to other techniques, such as UV spectroscopy (1 μg mL^{-1}) [48], ELISA (0.114 ng mL^{-1}) [49], and HPLC (0.04 μg mL^{-1}) [50], evidences the extremely low concentrations that can be measured with this technique.

The excitation of surface plasmons in SPR sensing is most commonly generated by an attenuated total reflection (ATR) of p-polarized (with an electric field parallel to the plane of incidence) incident light between a high-refractive-index medium and a low-refractive-index medium [51, 52]. Depending on the angle at which a light beam reaches the interface of the two mediums, the light may be partly reflected away and refracted to the low-refractive-index medium. ATR occurs when the angle is higher than the critical angle, which leads to the total refraction of light from the normal of the surface and therefore from the interface [53]. If a plasmonic metal layer is coated on a surface between these two media, the incidence of light can induce the generation of surface plasmons on the film. This phenomenon takes place when the wave vector of incident light (k) matches the wavelength of surface plasmons, causing electrons to oscillate in resonance [54]. Since the surface plasmon waves are generated in the metal surface and its wave vector (k_{sp}) propagates parallel to the surface, the parallel component of incident light (k_s) needs to match k_{sp} in magnitude for the SPR to occur, as shown in Fig. 4. Both wave vectors are expressed as follows in Eqs. 1 and 2 [53, 55, 56]:

$$k_s = \frac{2\pi}{\lambda}\eta_p \sin\vartheta = \frac{2\pi}{\lambda}\sqrt{\varepsilon_p}\sin\vartheta \tag{1}$$

$$k_{sp} = \frac{2\pi}{\lambda}\sqrt{\frac{\varepsilon_m \varepsilon_d}{\varepsilon_m + \varepsilon_d}} \tag{2}$$

where ε_m, ε_d, and ε_p are the complex dielectric constants of the metal, the surrounding dielectrics, and the material, respectively, η_p is the refractive index of the dense

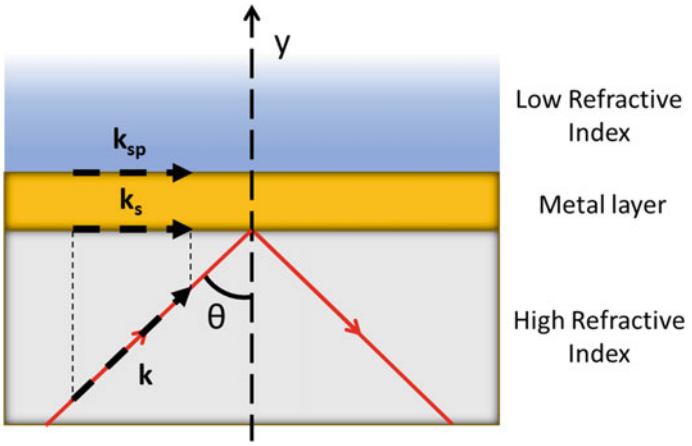

Fig. 4 Schematic representation of a p-polarized light focusing through a high-refractive index into a plasmonic metal covered low-refractive index. Here, the parallel component of the incident light (k_s) matches the wave vector of surface plasmons (k_{sp}) at the given angle, permitting the excitation of SPR

medium, θ and λ are the incidence angle and wavelength of the light. When k_s is equal to k_{sp}, part of the incident light is absorbed into the film generating surface plasmons, and a lower intensity of light is reflected away [56]. The amount of light that is lost in the metallic film depends on both light incidence, and the angle where the generation of surface plasmons is higher and the intensity of reflected light is lower is denominated SPR angle (θ_{SPR}) and can be determined from Eqs. 1 and 2 as shown in Eq. 3 [53]:

$$k_s = k_{sp} \rightarrow \theta_{SPR} = \sin^{-1}\sqrt{\frac{\varepsilon_m \varepsilon_d}{\varepsilon_p(\varepsilon_m + \varepsilon_d)}} \tag{3}$$

As the surface plasmon waves generated can propagate faster than the incident optical wave in the dielectric medium, it is not possible to excite surface plasmons by a direct irradiation of a focused optical wave on the metal-dielectric interface [57]. For the excitation to occur, the propagation constant of the incident optical waves needs to be enhanced to match that of surface plasmons. The most commonly used method is by prism coupling, where a prism with a high-refractive index is used before the plasmonic metal film, as described by Kretschmann [52, 56]. The optical light travels through the prism and is totally reflected at its base, generating in the process an evanescent wave that propagates along with the interface with the metal film. The propagation constant of the wave can, in this case, be adjusted both with the angle or the wavelength, as described in Eq. 1, to match that of surface plasmons, and a photodetector measures the reflected light [55].

The θ or the λ is varied and when the SPR occurs, the reflectance observed in the photodetector decreases reaching the lowest at a specific point θ' or λ'. If an analyte

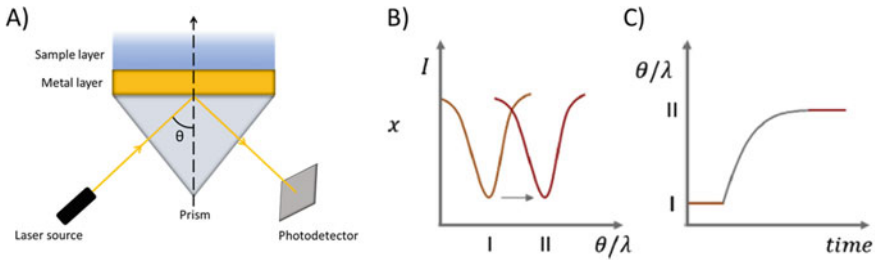

Fig. 5 Schematic of Kretschmann configuration for SPR analysis (**A**). Reflectance response upon variation of θ or λ and the changes of θ or λ necessary for SPR with deposition of the analyte (**B**). Real-time monitoring of θ or λ necessary for SPR upon deposition of the analyte (**C**)

is deposited on the surface of the metal film, the θ' or λ' is shifted, and this shift can be monitored as it is directly proportional and sensitive to the amount of analyte deposited, which is the detection principle of SPR sensing [52, 58]. By monitoring the variation of θ' or λ' over time, it is also possible to obtain data about the kinetics of the deposition process and obtain real-time monitoring of the procedure or reaction (Fig. 5) [59, 60].

2.2 SPR Sensing Applications

Since the detection in SPR sensing is based on the deposition of molecules on the surface of the plasmonic metal film, the selectivity is often a problem in complex systems as a response can be affected by any substances that come in contact with the metal layer [61, 62]. To overcome this issue, principally in biosensing applications, bioreceptors could be immobilized on a metal surface to bind selectively to target molecules [63]. An interesting alternative is the deposition of molecularly imprinted polymers (MIP) on the SPR surface [64], where the target analyte is used to form a mold that is later used to bind to the same analyte selectively.

Yuan et al. [65] developed an SPR sensor for heparin using a polydiallyldimethylammonium (PDDA)-modified Au film as a sensing platform. In a mixture of Au NPs and heparin added on to the positively charged modified film, heparin is preferentially deposited as it interacts stronger with PDDA than the Au NPs (Fig. 6). Through the difference in SPR shift between the Au NPs and heparin, it was possible to achieve a selective sensor with a LOD of 0.026 ng mL^{-1}. The Au NPs also contributed to covering the surface of the sensor in the absence of heparin, preventing the deposition of unwanted molecules.

Modification of the SPR platform with plasmonic nanoparticles to enhance sensing capabilities was also investigated, coupling SPR with LSPR effects and generating an enhanced response. Xia et al. studied a multilayer SPR sensing platform for immunoglobulin G (IgG) where the Au film was modified with Au NPs [66]. To selectively sense IgG, the film was modified with a graphene oxide layer in which

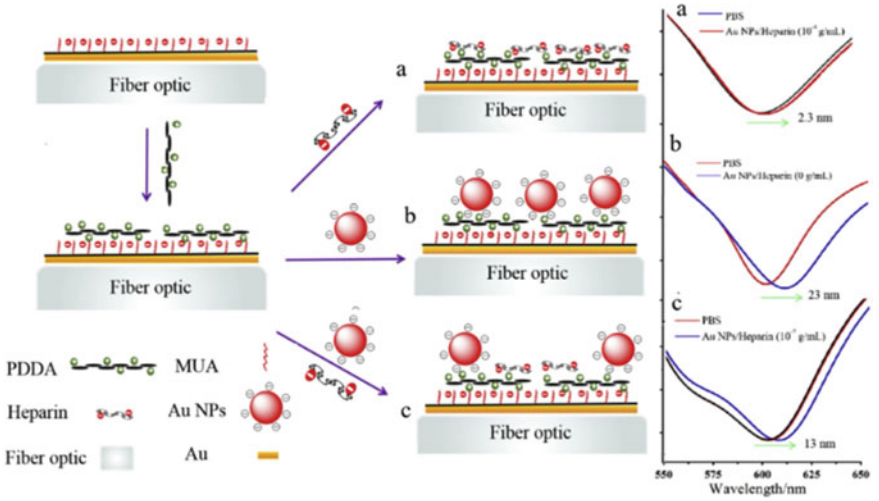

Fig. 6 Schematic representation of PDDA modified SPR sensor for competitive heparin sensing. The modification with PDDA causes a small shift in the SPR peak (**a**). The shift reaches a maximum when only Au NPs are present (**b**), and when heparin is added, it interacts preferentially with the surface, decreasing the shift observed (**c**). Reprinted with permission from [65]

a layer of an IgG antibody was deposited. Distinct morphologies of Au NPs were tested. Interestingly, Au nanorods presented a better response than Au nanospheres, mainly due to its stronger longitudinal LSPR mode. This difference influenced the LOD of the sensor, where the nanospheres presented LOD of 10 ng ml^{-1} and the nanorods of 4.6 ng ml^{-1}.

2.3 Electrochemical SPR Sensors

As SPR sensing presents relatively simple instrumentation and methodology, it can be easily integrated with other techniques, such as mass spectroscopy [67] and electrochemistry [68–70]. In electrochemical applications, small variations in electrostatic fields are measured at the electrode surfaces that, whenever integrated with SPR, are used to study the interaction between electrical energy and chemical changes on the system [71].

Electrochemical surface plasmon resonance (ESPR) involves a three-electrode assembly. The plasmonic metal film can be used as a working electrode and the counter electrode, usually a Pt wire, is placed on the electrolyte to close the circuit. Electrochemical methods are possibly used for the characterization of redox systems by the measurement of current with the variation of the potential applied (by cyclic voltammetry for example) [72, 73]. The variation of the potential might lead to variations in the SPR response of the system as some redox reactions only occur at specific

potentials. Among the possible applications, ESPR is a powerful methodology for studying enzymatic processes, anodic stripping, potential-controlled absorptions, charge transfer reactions, and surface characterizations [74–77]. Figure 3 depicts a schematic representation of the ESPR apparatus and analysis.

Baba et al. [69] developed an ESPR-based glucose sensor in which electrically conducting polymers, poly[*N,N*-dimethylethyl-3-(1*H*-pyrrol-1-yl)propane-1-ammonium chloride] (PPy-Q), and poly(3, 4-ethylenedioxythiophene) (PEDOT), were deposited on the surface of an Au film by a layer-by-layer technique with the deposition of glucose oxidase (GOx) enzyme on the upmost layers (Fig. 7). As the polymers used were able to be doped or undoped by anions in solution, SPR could be used to determine some parameters during the oxidation of glucose under 0.3 $V_{Ag/AgCl}$, as the variations of refractive index, the thickness of absorbed glucose, film thickness, and the dielectric constant of PPy/GOx layer all generate a change in reflectivity during the addition of glucose. A simultaneous determination of glucose was also performed through current and reflectivity through additions of 10 mM of glucose under 0.3 $V_{Ag/AgCl}$, showing that in both cases, it was possible to sense the analyte although the SPR method showed a more sensitive result.

Lu and co-workers [78] applied electrochemical impedance spectroscopy technique coupled with SPR as a source of studying the molecular binding of IgG on the electrode as a model system. By the simultaneous measurements of the SPR angle and admittance density over the time under 0.12 V bias, it was possible to determine and follow the kinetics of protein association and dissociation processes, using concentrations as low as 33 nM. It was observed that the two measurements are equivalent if double layer charging dominates the impedance, but SPR is more sensitive to complementary information regarding changes in bulk refractive index and nonspecific adsorption.

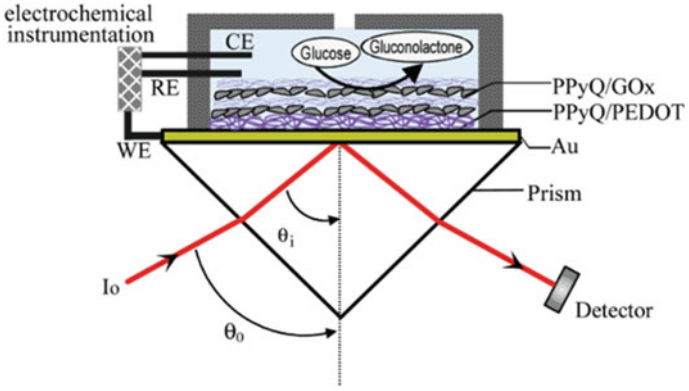

Fig. 7 Schematic representation of the electrochemical cell used for the ESPR sensing of glucose. The Au electrode is covered with a film of PPy-Q/PEDOT and PPy-Q/Gox for the selective detection of glucose both by electrochemical and optical methods. Reprinted with permission from [69]

Another application of ESPR to a sensing platform was performed recently by Ribeiro et al. [70], where the SPR approach was employed for real-time monitoring and sensing, and a square wave voltammetry (SWV) was used as a more sensitive sensing technique for the quantification of the carbohydrate antigen 15–3 (CA 15–3). As a sensing platform, an anti-CA 15–3 antibody was immobilized on the surface of the Au film through covalent bonds. The analysis was performed as described in Fig. 8A, where the θ_{SPR} was monitored over time during the initial association, then through a washing step to remove unbounded material. After the dissociation step, a solution of ferro/ferricyanide is added, and the SWV is performed generating a current response proportional to the antigen's concentration, and finally, the sensor is regenerated with a 0.1 M Gly-HCl (pH 2.0) solution.

On the quantification steps, the concentration of CA 15–3 was varied from 0.1 to 500 U mL^{-1} and measured through the variation on θ_{SPR} (Fig. 8B) and the oxidation current obtained on the SWV procedure (Fig. 8C). The sensitivity obtained through the SWV step was much superior to the SPR step, and the LOD was much lower (0.1

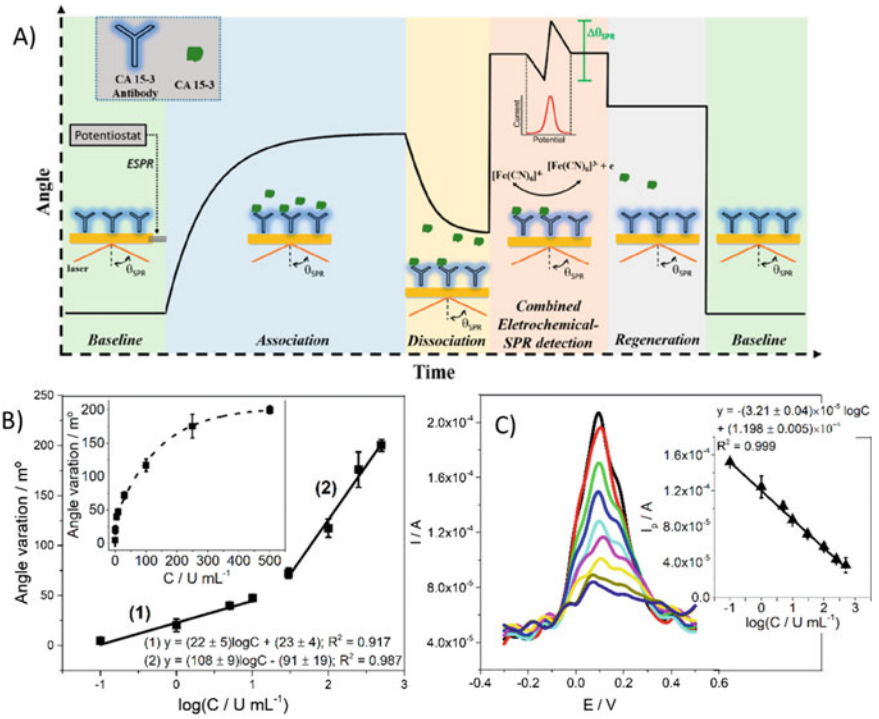

Fig. 8 Schematic representation of the ESPR method used by Ribeiro et al. for the quantification of CA 15–3 (**A**). Analytical curves obtained from the SPR angle variation (**B**) and current from SWV measurements (**C**). Reprinted with permission from [70]

compared with 21.0 U mL^{-1} from SPR). In this case, the ability of real-time monitoring of SPR coupled with the high sensitivity and selectivity of electrochemical methods generate a powerful platform for antigen analysis and measurement.

2.4 Conclusion

In general, ESPR represents a powerful technique for the characterization of chemical and electrochemical processes, real-time analysis and monitoring, and sensitive quantification of target molecules. Its application brings important improvements to health diagnosis, as new developments incorporate higher sensitivities and better selectivity, since it represents a general drawback of SPR sensing and can be overcome by the variety of possible electrochemical methods as has been described in this chapter. SPR sensing techniques also bring much attention to their simplicity and for being able to be applied for the construction of a wide range of label-free biosensing platforms, which when compared with other techniques represent a simpler and cheaper alternative, only requiring a prior modification of the platform for a viable application. Another very interesting advantage of ESPR sensing is that the sensing substrate can be easily modified to change the strategy used depending on the target molecule. Taking into consideration all the advantages discussed, coupling SPR sensing with electrochemical sensing shows a very promising and sensitive platform for biological processes and quantifications.

3 Part III. SERS and Coupled Techniques as Tools for Bioanalysis

3.1 Introduction

When describing aspects of surface-enhanced Raman spectroscopy (SERS), it is virtually impossible to avoid any presentation of the Raman effect and how it brings peculiarities compared to other common spectroscopic characterization techniques, especially fluorescence spectroscopy and infrared spectroscopy (IR).

Raman effect consists of the inelastic light scattering by molecules, whose energies comprise information regarding vibrational modes of ensembles of atoms constituents of the studied molecule, with a prelusive study of sunlight beams in liquid benzene dating ca. 1930 [79]. Compared to other techniques, Raman allows a broad spectral window from as low as a few cm^{-1} to more than 4000 cm^{-1}, high-spectral resolution, and low-bleaching effects compared to fluorescence measurements.

As water is very weakly active to Raman scattering in contrast to IR, it becomes viable to run Raman measurements in aqueous solutions. Additionally, the technique

is easily and commonly coupled to microscopes, allowing for the localized interrogation of micrometric regions of each sample and enabling the confection of chemical maps.

A good analysis in the context of Raman spectroscopy is challenged, however, by the small scattering cross section (as ca. 10^{-30} cm^2 sr^{-1}), which is 8–16 orders of magnitude smaller compared to the ones achieved by IR and fluorescence spectroscopies. This is a major disadvantage even for the very particular—and Raman active—group of fluorescent dyes in resonance mode. This means that, in the event, an incident photon energy matches the energy needed for an electronic transition, structural changes in the molecule will occur, largely increase its polarizability, and therefore, Raman scattering [80]. Hence, an enhancement of the scattering process is needed for most practical applications, and in this context, surface-enhanced Raman spectroscopy (SERS) was developed and is now commonplace for chemical analysis.

SERS effect was explored originally, yet unintentionally, by Fleischmann in 1974 [81] with spectroscopic measurements of pyridine adsorbed onto electrochemically roughened Ag electrodes. Subsequently, the effect was better described by Van Duyne [82], Creighton [83], and Moskovits [84] in 1977 and 1978, studying amines and pyridine adsorbed onto Ag electrodes. These last authors implied that the origin of such an effect could be strongly connected to plasmonic excitations arising from the metal onto the molecules adsorbed in close proximity. Consequently, signaling that the enhancement is strongly dependent on the distance between the metal surface and adsorbed molecules, which makes this a useful tool for surface probing.

The story of SERS development in the last 50 years is rich and full of interesting details. Nonetheless, some of the findings must be at least mentioned as: (i) the most accepted mechanism now being a combination of the electromagnetic field enhancement and chemical charge-transfer processes, (ii) discussions evidencing enhancements up to a theoretical 10^{10} factor, and (iii) the fruitful road of metallic nanoparticles design for numerous hot-spots regions.

It is worth emphasizing that SERS is not at all limited to metals, as examples in oxides and graphene are often reported [85, 86]. Besides, the applications to chemical analysis either standalone in the so-called intrinsic mode or by tagging desired analytes with molecular reporters with high-Raman cross section as fluorescent dyes, in the called extrinsic mode. Some of these will be further discussed here, yet we kindly provide readers with some selected comprehensive and detailed resources [20, 79, 87, 88].

3.2 Designing SERS-Active Substrates

Since the performance of SERS-active platforms strongly depends on the chosen materials, as well as the geometry and spatial disposition of the employed nanoparticles, the design of platforms for a larger electromagnetic field enhancement is naturally linked to nanotechnology. It has become a field of study itself including,

for example, expansion of applications to *operando* mode or the exploration of plasmonics in the UV region [89]. Table 1 summarizes some of the plentiful methods for the confection of SERS-active platforms, with a brief description of some advantages and challenges of each.

Table 1 A brief selection of commonplace methods for the confection of SERS-active platforms, with enlisted advantages and challenges

Method	Description	Advantages	Challenges	References
Colloidal NPs	NPs are dispersed in a colloidal regime to form aggregates with high-hotspot regions densities	Plentiful hotspot regions result in high-scattering enhancement, especially with designed anisotropic nanoparticles, such as nanostars	Aggregation, sedimentation, and aging of the nanoparticles	[90]
Self-assembled monolayers of NPs	NPs self-organized to a stable disposition at a certain interface, leading to a SERS-active film, transferrable to solid surfaces	Straightforward preparation, maximization of hot-spots per unit area, versatility of the NP layer in the interface, and viability to liquid–liquid or liquid–air operation	Stabilization of the active layer with high enhancement, usually multilayers are required	Liquid-liquid [91, 92] Liquid-air [93]
Sphere-segment void (SSV) templates	Platforms are produced by direct electrodeposition of a metal through a monolayer of densely packed polymeric spheres	Tunable electromagnetic field enhancement, reproducibility	Multiple steps are required to form good-quality monolayers of close-packed spheres and determination of deposition layer height/charge	[94]
SHINERS	Metallic NP core coated with silica or alumina shell represents the SERS-active component, being spread onto the substrate with molecules to be probed	Reproducible, chemically stable, high enhancements, viable to biologic material probing	Studies down to monolayer resolution are viable, yet a higher spatial resolution is troublesome	[95]

(continued)

Table 1 (continued)

Method	Description	Advantages	Challenges	References
Spin-coated templates	In most approaches, a dispersion of NPs is spread to a substrate attached to a holder; the system is rotated, and liquid phase excess is eliminated, producing a thin film	Usually very fast and scalable; can be applied to flexible, transparent, and low-cost substrates	Reproducibility issues are common; hydrodynamic effects can cause radial distortion and variations from center to the edge (e.g., capillary waves and thickness gradients)	[96]
Breath-figure method (BFM)	This method consists of producing a template through quick evaporation of a volatile solution comprising a polymer or NPs; as temperature drops, water droplets from air condensate and a porous layer is formed, used as is or for further steps	Versatile process to form templates, low-cost and, if coupled to a spinner, very fast	Can suffer reproducibility issues, dependent on relative humidity	[97, 98]
E-beam lithography	Involves scanning a high-energy beam of electrons through a substrate, selectively removing material with precise spatial control	Very high-spatial precision, reproducibility, and versatility to produce complex geometrical shapes, which grants predictability through modeling	Expensive, time-consuming, can require unwieldy etching and lift-off steps	[99]
Aluminum anodization	The aluminum material is electrochemically anodized and chemically etched to produce a porous membrane in the nanometric diameter range, serving as a template for further processes	Reproducible, low-cost, tunable pore diameter, and layer depth.	Time-consuming with multiple steps and cumbersome chemicals involved	[100]

(continued)

Table 1 (continued)

Method	Description	Advantages	Challenges	References
Metal electrodeposition	Direct electrodeposition is performed onto conducting substrates by applying either a potential or current	High efficiency and reproducibility; a multitude of metallic species can be reduced at the surface with control of geometry and morphology	Only compatible with conducting or semi-conducting substrates	[101, 102]

For a method to develop a SERS-active platform, it is worth considering the requirements for the platform and sensing conditions, the cost of equipment and materials, the time required to produce, and the reproducibility and reliability of the methods. This often leads to a balance between bottom-up and top-down approaches, with multiple successful ideas in both.

3.3 Quantitative Aspects: Enhancement Factors and Chemometrics

Enhancement Factors: SERS brings at its core the intention of enhancing Raman scattering. This means that a SERS-active platform is regarded as superior the better it performs such a role. To compare different approaches, the so-called enhancement factor (EF) is often employed and refers to the mathematical ratio of the signal intensity per molecule of the SERS system against the Raman analog (i.e., non-SERS), as shown in Eq. 4. Here, I refers to the scattering intensity, N is the number of molecules involved in the process, and when it comes to the comparison of the cross-section enhancement—therefore in a single-molecule fashion -, $d\sigma/d\Omega$ refers to the differential Raman cross section.

$$\mathrm{EF} = \frac{\frac{I_{\mathrm{SERS}}}{N_{\mathrm{SERS}}}}{\frac{I_{\mathrm{Raman}}}{N_{\mathrm{Raman}}}}; \quad \mathrm{EF}_{\text{single molecule}} = \frac{\frac{d\sigma_{\mathrm{SERS}}}{d\Omega_{\mathrm{SERS}}}}{\frac{d\sigma_{\mathrm{Raman}}}{d\Omega_{\mathrm{Raman}}}} \tag{4}$$

Despite being conceptually simple, this estimation is not trivial, and distortions are widespread in the literature. They can lead to unrealistic EF values, without physical meaning and not rarely beyond the expected theoretical limit of ca. 10^{10}. This can be estimated by an enhancement in excitation ($\left|E^2(\omega)\right|/\left|E_0^2(\omega)\right| \approx 10^5$) coupled to an emission enhancement of similar order, generating the often described as '$\left|E^4\right|$ enhancement'. One might notice that (i) the chemical enhancement, except in specific cases, will not contribute much to the overall enhancement, and (ii) a 10^{10}

enhancement is too optimistic for most SERS platforms. Frequent errors include the choice of Raman comparison sample, calculation of the number of molecules in each case, laser penetration depth, cross-section values, the area or volume being interrogated by the light source and not accounting for fluorescence suppression.

Another indirect consequence consists of the instituted rally for increasingly high-EF numbers. In practice, the limits of detection often barely change and spectral quality might not suffer significant improvements, as already mentioned in the literature [97]. It is certainly sound to pursue high enhancements shown with practical applications that can solve real-world problems rather than focusing on comparing numbers with sloppy definitions in the literature. Adequate means for EF estimation are available elsewhere, with discussions of overlooked issues [103, 104].

Chemometrics

Incorporation of chemometrics to SERS measurements is still seldom seen in literature, despite recent reports indicating a powerful capability toward quantitative measurements and improved limit of detection. It is worth noticing how spectral richness is beneficial to allow greater possibilities of deconvolutions and peak comparisons for these approaches. This can be achieved, for example, through designed molecular tags and the usage of multiple distinct metallic NPs or laser sources [105, 106].

For example, Brolo and co-workers employed an Au NP-onto-coverslips approach to explore SERS detection of antibiotics at ultralow concentration [107]. Instead of relying on scattering intensity, the occurrence of a scattering event in a hotspot was considered itself as the ‘count’, generating digital maps and quantitative data as the number of molecules aided through non-negative matrix factorization (NMF).

Chemometrics was also employed to study cancer single-cells among a pool of cells flowing through a microfluidic channel in a creative approach by Moskovits and colleagues [108]. The authors employed a Ag NP dimer coupled to a Raman-active tag linked to an affinity biomolecule such that, within a set of spectra with a complex composition of convoluted bands. They successfully applied principal component analysis (PCA) to assess three principal components and describe which peaks compose each PC. Therefore, which one decorously discriminates between cancerous and non-cancerous cells. Classical least squares (CLS) were also explored, granting the additional data of the numerical contribution of each tagged receptor to the overall obtained spectrum.

Other examples in the literature include the usage of partial least squares (PLS) [109], k-nearest neighbor (KNN) and support vector machine (SVM) [110], machine learning [111], and neural networks [112].

3.4 Applications

Applications of SERS are now expected to achieve much more than a bare characterization of vibrational modes, exploring the capabilities of the technique, and hyphenating with other tools, especially electrochemistry.

When it comes to bioanalysis, a plethora of biochemical compounds can be interrogated, and the Raman profile can provide information regarding conformation, enzyme mechanisms [113], presence/absence of biomarkers, discrimination of specific cells within a culture, address neurotransmitters, antibodies, toxins, and even to confer a barcode tag to multiple different analytes [88].

Bartlett and co-workers, inspired by the context of pathogen-specific DNA biodetection, explored the association of electrochemistry with SERS [114]. In the work, electrochemistry was used too drive the melting of hybridized DNA amplicons with a single nucleotide polymorphism, while the labeled complementary single-stranded DNA (ssDNA) provided an intense SERS signal as the chains were attached to Au-coated SSV templates. By relating the decrease of the SERS signal to the applied electrochemical potential, causing the melting of the hybridized pair, *Y. pestis* and *Y. pseudotuberculosis* were successfully discriminated.

The idea of creating a library of compounds and biological elements encoded by their physical and chemical properties, composition, action, and affinity to other elements is central to areas, such as drug development. In this context, it can lead to a faster screening of promising approaches toward viable pharmacological options. When it comes to SERS, the concept of barcoding for high-throughput bioanalysis was developed [115], where beads are functionalized with SERS-tags and peptides. In this approach, each main peak of each tag corresponds to a single bar within a barcode chart, and the combination of these tags and their affinity toward specific proteins could theoretically generate more than one million distinct barcodes through spectral deconvolution. With a similar rationale, Pezzotti and co-workers studied the deconvolution of bands of SARS-CoV-2 variants and were able to engender barcodes to multiple variants as Raman peaks shifted due to differences in S-containing amino acids, interface pH, RNA bases, and the secondary structure (Fig. 9) [116].

Associations of SERS to lateral flow immunoassays (LFIAs) are also becoming more frequent [117–120]. This is given their advantages as faster process time compared to RT-PCR and mass spectroscopy, price compared to RT-LAMP and ELISA, and increased shelf-life compared to pure electrochemical bioassays. In SERS-LFIA bioanalysis, as in Fig. 10, the Raman enhancing element is usually a metallic NP or silica beads coated with NPs, functionalized with specific proteins (here, SARS-CoV-2 S-protein). They ought to interact with the analyte (as IgM and IgG, in this example) and concentrate on the conjugate pad of the test-strip. As the test sample is added and flows through the strip, the analyte, if present, is captured by the respective antibodies in the test lines and the conjugation to the SERS-tags confers detection through the Raman peaks.

Active use of electrochemical methods with SERS can be addressed either as complementary techniques or to acquire information *in tandem* (EC-SERS). The

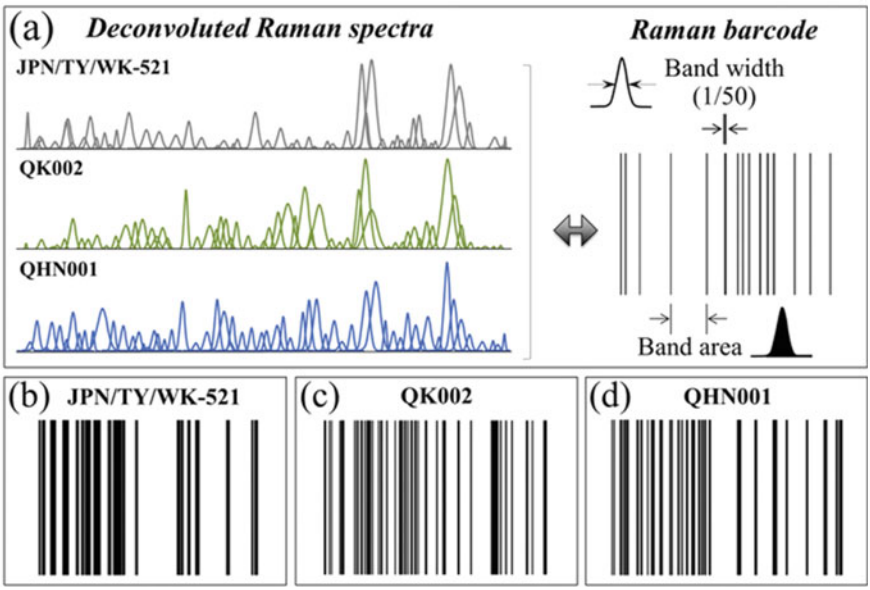

Fig. 9 Summarized process of 'barcoding' SARS-CoV-2 variants through Raman spectral deconvolution. Spectra are obtained for each variant, bands are deconvoluted according to their ascribed composition, the presence of certain peaks leading to a bar whose width relates to the band width. From ref [116] with permission of the publisher

importance of EC-SERS can be exemplified by the case of Ag, with a positively charged surface at the open circuit potential (OCP). Naturally, by changing the potential of the surface relative to a reference electrode, the interface becomes either less or even more charged, with clear effects on the adsorption affinity of molecules to the metal and consequently, the intensity of Raman peaks acquired. This was exemplified by Bindesri et al., collecting Raman spectra during potential steps in a conducting cloth loaded with Ag NPs and levofloxacin as a model drug [121]. Another example consists of changing the charge and morphological characteristics of a SERS-active surface via electrochemical potential sweeps and exploring the consequences in the acquired Raman data. In that case, distinct profiles are commonly seen, as explored by EC-SERS and EC-SOERS, another Raman enhancement specific to the oxidized metal state [122].

3.5 Tip-Enhanced Raman Spectroscopy (TERS)

As a last consideration, when it comes to biomolecules, we already discussed the advantages of Raman relative to fluorescence spectroscopy such as the narrow bands, less photobleaching, and label-less nature of the techniques, and how SERS improved

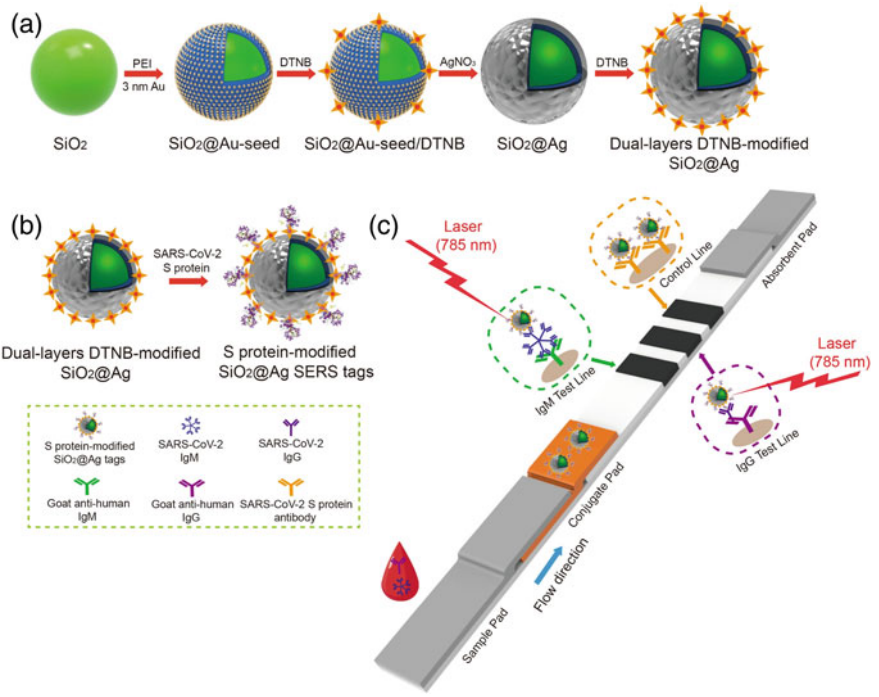

Fig. 10. Schematic of SERS-LFIA bioassays with a SERS-active element as Au NPs (**A**), protein-functionalization of the SERS-tags (**B**), and design of the test-strip, with a sample pad, a SERS-tags loaded conjugation pad, antibody-rich test lines and a control line **C**. The bioconjugation of proteins and respective antibodies allows detection through the Raman peaks. From ref [119] with permission of the publisher

the intrinsically low-Raman cross section. These techniques show extreme importance and usefulness to chemical analysis, yet spatially limited by the diffraction limit of the light, with a consequential optical resolution of many hundreds of nanometers. On the other hand, microscopy techniques such as the scanning probe microscopy (SPM), with ultra-sharp tip probes, provide enough spatial resolution to interrogate atoms of a surface. The combination of SPM and SERS resulted in the elaboration of the tip-enhanced Raman spectroscopy (TERS), amalgamating the remarkably high-spatial resolution of SPM, therefore exploring the sub-wavelength range, with the enhancement of Raman scattering from SERS. For this, TERS tips are manufactured to combine sharpness and a metallic coating or immobilized NPs. The tip is set to sweep or maintain contact to a surface to be probed, and due to the electromagnetic enhancement being strongly dependent on the distance, intense Raman scattering is obtained with information of the nanometric region close to the tip edge only, as schematized in Fig. 11 [123].

With this powerful combination of characterization capabilities, TERS opens a new yet challenging road of opportunities especially for biological applications, with

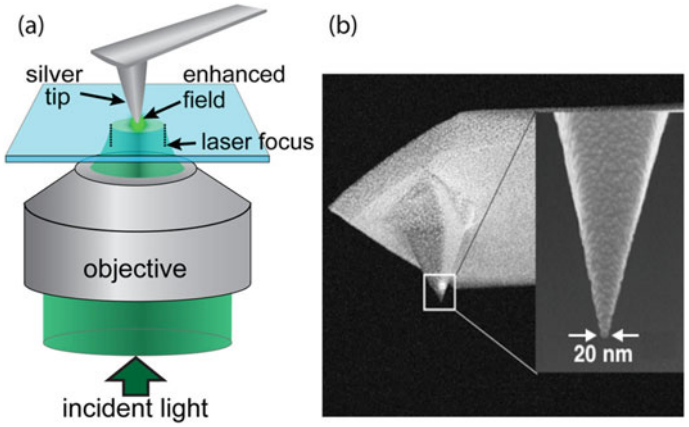

Fig. 11. Scheme of a TERS operation, with a sharp SERS-active tip scanning the sample concomitantly to a focused laser source, promoting the SERS data generation (**a**). Micrograph of a typical TERS tip with a nanometric edge (**b**). From ref. [123] with permission of the publisher

already successful examples of bacteria [124], viruses [125], and isolated whole biomolecules [126, 127].

Wood and co-workers showed the TERS imaging and spectral recording of sub-20 nm hemozoin crystals, an insoluble pigment produced by breakage of hemoglobin by malaria parasite-infected cells, inside the very digestive vacuole of the cell, as indicated by Fig. 12 [128].

Other successful examples include DNA/RNA structural studies, proteins such as β-amyloid, and insulin polymorphs. Once again, electrochemistry can be coupled to an EC-TERS technique, already shown to be capable of providing information on localized electrochemical processes at the nanoscale [129].

Challenges are still abundant to TERS, including tip production, stability, cleanness, data interpretation, and practical/economically viable setups associating UHV-STM-SERS capable of achieving stable single-molecule level investigation.

3.6 Conclusions

The powerfulness of SERS to bioanalysis was certainly long proven, with ubiquitous presence in the literature of the past two decades, while constantly evolving to be considered less of a coadjuvant characterization technique and now a field of study itself. This includes elaborating efficient and stable substrates, recording quantitative data, coupling to other techniques such as EC-SERS or SERS-LFIA and even ingenious and modern approaches to overcome the spatial limitation to study spectroscopic profiles in the nanometer range.

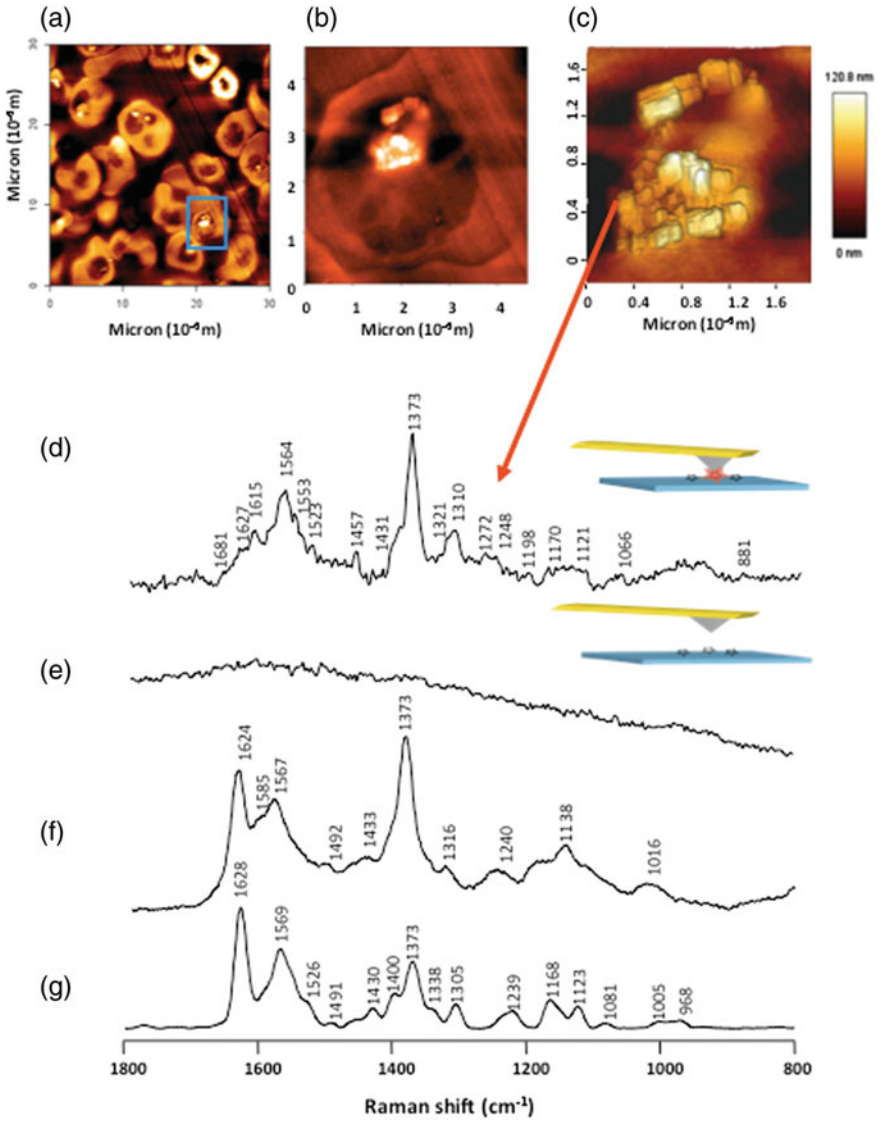

Fig. 12. AFM micrographs of a population of malaria-infected erythrocytes (**a**, **b**, and **c**), with hemozoin crystals (**b**, **c**), TERS spectrum recorded of a hemozoin crystal edge (**d**), control TERS-off spectrum (**e**), control hemozoin SERS, and resonant SERS spectra (**f**, **g**). From ref [128] with permission of the publisher

Considering what has been achieved, the near future will certainly comprise (a) flourishing publication of works employing SERS-active labeled probes for sensing in real samples. These probes require clever functionalization to interact with specific biomolecules, especially considering the context of the SARS-CoV-2 pandemics, which arguably showed that biosensors are needed more than ever, and that bioanalysis is still a field of prolific discoveries and advances; (b) the scalability of SERS-active platforms with enough diversity and lower cost is also still a challenge to be addressed to enable the dissemination of SERS-based sensors; (c) coupling to other techniques should become more common and so will be the innovative usage of statistics for data handling.

In a longer timeframe, new steps to harder and more complex challenges should be seen, including the reproducible recording of spectroscopic information in a single-molecule regime via STM-TERS. The use of in *operando* mode to acquire information on chemical processes occurring in real-time while coupled to other techniques and indeed, new or optimized approaches to *in-vivo* monitoring of biological processes inside cells and throughout tissues, which probably translates as a new class of wet-phase, chemically stable, biocompatible, and versatile SERS-active elements.

4 Part IV. Nanozymes

4.1 Introduction

Enzymes are biocatalysts widely used in various sectors of industry, including food, textile, cosmetics, and the production of biofuels [130]. According to Allied Market Research in March 2020, the enzyme market value was US$ 8.6 billion worth in 2019 and is expected to reach US$ 14.5 billion by 2027. These values already exceed more than 20% of what was previously estimated in 2017, when the world enzyme market was expected to reach US$ 6.8 billion by 2022 [131].

Enzymes are frequently used for industrial, biotechnological, and research applications due to their high selectivity since they are chemo-, regio-, and stereoselective biocatalysts [132]. Moreover, they are low-toxic and environmentally friendly biomolecules and thus, are usually biocompatible. In general, enzymes can catalyze reactions with rate constants up to 17 orders of magnitude higher compared to reactions carried out in their absence [133]. They represent a versatile class of molecules since they are liable for design via gene and protein engineering according to specific demands such as enhancement of desired physical–chemical properties [134].

However, natural enzymes production is limited due to scaling up issues and time-consuming separation and purification steps, which makes them a costly feedstock. Besides, limitations concerning their stability require mild reaction conditions such as temperature, pressure, stirring, pH, and a restricted window of solvents [135–137].

In order to overcome these drawbacks, the development of artificial enzymes has strengthened as a field of study in the 1970s [138]. Classically, biomimetic organic

chemical compounds were designed with a similar structure to enzymes' active site, although with improved physical and chemical robustness [139, 140].

Nevertheless, in the 1990s, biomimetic chemistry of artificial enzymes has expanded its boundaries to the promising field of catalytic nanomaterials, creating the new field of nanozymes by exploring nanomaterials' enzyme-like properties [141–149]. This approximation merged the ease of synthesizing nanomaterials in comparison with complex macromolecules with the more reasonable expenses from their attainment process. In the first moment, mainly fullerene was explored for these applications, although some works with gold, ceria, and rare earth nanomaterials were timidly introduced.

In 2007, Gao and co-workers reported intrinsic peroxidase-like properties in Fe_3O_4 NPs [150]. The authors report that these findings are not unexpected since Fe^{II}/Fe^{III} redox pair in solution is known to catalyze the breakdown of peroxide in Fenton's reagent. Besides, many peroxidases such as horseradish peroxidase (HRP) and cytochrome C comprise iron-containing heme-centers. Alongside the fortification of the field of metallic nanoparticles, this work was considered a turning point in the field of nanomaterials as artificial enzymes.

In the following years, an expressive and emerging number of authors started studying enzyme-like properties of NPs [151, 152]. Among several catalytic outcomes of these nanomaterials, this period elucidated properties concerning their selectivity [153–155], high sensitivity for analytical purposes [156, 157], and low cytotoxicity [158].

Nanozymes performance, as well as most enzymatic kinetic systems, can be approached with Michaelis–Menten model [159, 160]. Therefore, parameters such as substrate specificity (K_M), catalytic rate constant (k_{cat}), catalytic efficiency (k_{cat}/K_M), and maximal reaction velocity (v_{max}). In the case of electrochemical nanozymes, usually maximal reaction current (I_{max}) is used instead [161, 162]. The general Michaelis–Menten model is represented by Eq. 5, where v is the velocity of reaction and $[S]$ is the concentration of a substrate S.

$$v = \frac{V_{max}[S]}{K_M + [S]} \tag{5}$$

The term 'nanozyme' was firstly introduced in 2004 by Manea and co-workers to describe their synthesized Au NPs-based material with ribonuclease-like activity [163]. However, it was only in 2013 that this term was reinforced and extended in a review made by Wei and Wang to every material with enzyme-like properties up to that date [164].

Since then, the number of publications on 'nanozyme' has grown exponentially, as the report generated by the 'Web of Knowledge' shows in Fig. 13.

Alternative and complementary approaches for the definition of 'nanozymes' have been used by other authors, such as Gooding [165, 166]. According to his definition, nanozymes are three-dimensional components that not only mimic the reactions of natural enzymes, but simulate the confined environment with channels that regulate the mass transport and reactant gradients.

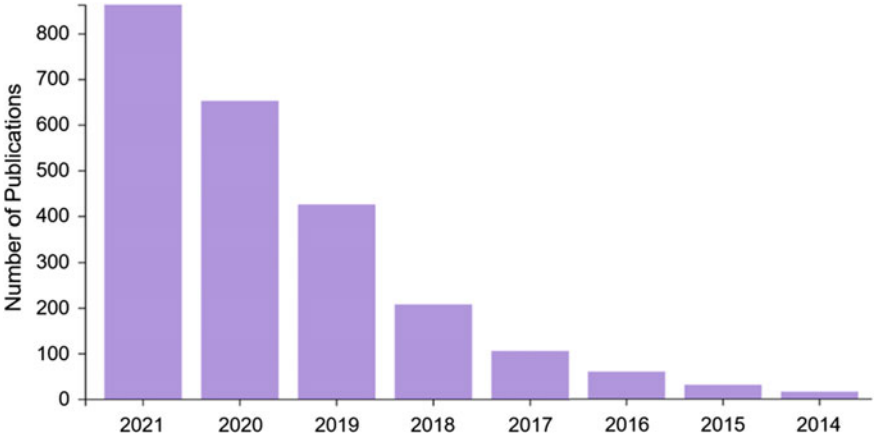

Fig. 13 Number of publications on 'nanozyme' since 2014. This report was generated by the 'Web of Knowledge' in January, 2022

It is noteworthy that, despite the development of this field, there is still a lack of common understanding among the literature concerning the nomenclature and analyzes performed on NPs with enzyme-like properties. While some authors prefer using the classical catalytic approach, those that choose to work with the actual nanozyme approach do not follow the same definitions, standards, and assays.

4.2 Nanozymes Composition: Materials, Size, and Geometry

Besides the promotion of the term 'nanozymes', the work from Wei and Wang highlights the mechanisms, kinetics, and applications of various nanomaterials that mimic natural enzymes [164]. In this review, the authors focus on cerium, iron, and other metal oxide-based nanomaterials, as well as metal-based nanomaterials, such as gold, platinum, and bimetallic structures. A metal-free section of this work is set apart from the carbon-based nanomaterials, such as fullerene, carbon nanotubes, and graphene, including their derivatives. Among the redox enzymes mimicked by these nanozymes, peroxidase, oxidase, catalase, and superoxide dismutase were the major enzymatic classes addressed in this study from 2013.

In 2019, Wu and collaborators published a second part of the review on nanozymes previously elaborated in 2013 [141]. At this time, the review reflected a broader range of nanomaterials developed and explored as nanozymes between 2013 and 2019 in a wider variety of applications. Among the metallic and metallic oxide nanomaterials, copper, vanadium, and molybdenum gained space in the nanozyme scenario mainly for being considered cheaper than noble metals and the ease of synthesis scaling up. Besides, metal–organic-framework (MOF) used as nanozymes has brought attention

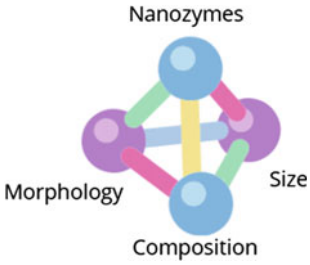

Fig. 14 Relationship and influences of size, morphology, and composition as interdependent parameters in the resultant nanozyme

due to their capability of creating confined spaces with high-surface area and versatile composition.

Furthermore, the review of Wu and collaborators highlights the importance of a rational design of nanozymes regarding their shape, size, and composition as future perspectives in the field. These parameters are interdependent and known for a long time to tune NPs' physical–chemical and catalytic properties in classic catalysis [167]. In an enzyme-mimicking catalytic environment, this is no different. Figure 14 shows a schematic tetrahedron representing the influence of these parameters in a final nanozyme structure, contemplating their interconnections.

The authors claim that high-performance nanozymes with desired properties are liable to be designed if the target application is established, and the structure–activity relationship is deeply investigated at first. Both experimental and computational data may support the design, and in future, artificial intelligence tools could be explored to survey the best candidates.

Examples of references with morphological and compositional variety of nanozymes are summarized in Table 2. The table illustrates an extensive range concerning these two parameters that directly influence physical–chemical properties of the nanozymes. Thus, this reinforces the need of rational designed systems toward an optimized efficiency on application of nanozymes.

4.3 Properties and Applications

Accordingly, as an optical property, LSPR of noble metals nanoparticles is strongly dependent on the tetrahedral pillars (as represented in Fig. 14) in addition to the medium characteristics, as predicted by Mie's theory [233–236]. The high sensitivity of these optical features, including LSPR, makes nanozymes good candidates for sensing purposes.

Although colorimetric sensors based on metallic nanozymes have already been extensively reported, LSPR sensors are less explored. For instance, Au NPs' peroxidase-like activity has been recently used in colorimetric assays for biomedical applications to sense histidine [237], biothiols [238], glucose [239], blood in urine [240], diagnostic of measle virus [241], influenza virus [242, 243], and SARS-CoV-2 [244].

Table 2 Examples of tunable aspects such as morphology and composition of nanozymes

Mimicking enzyme activity	Morphology	Composition	References
Peroxidase	Cubes	Platinum	[168]
	Dots	Carbon	[169, 170]
	Fibers	Vanadia	[171]
	Rods	Vanadia	[171]
	Sheets	Carbon	[172, 173]
		Palladium	[174]
		Vanadia	[171, 175]
	Spheres	Gold	[176–179]
		Iron oxide	[180–183]
		Palladium	[184]
		Platinum	[185, 186]
		Silver	[187, 188]
	Tubes	Carbon	[189]
		Platinum	[190]
	Wires	Vanadia	[191–193]
	Complex structures	MOF	[194–196]
		Multimetallic	[32, 197, 198]
Oxidase	Dots	Copper	[199]
		Platinum	[200, 201]
	Spheres	Molybdenum	[202]
		Gold	[203–206]
		Platinum	[207, 208]
Superoxide dismutase	Cubes	Ceria	[209]
	Dots	Carbon	[210]
	Fullerenes	Carbon	[211]
	Rods	Ceria	[212]
	Sheets	Carbon	[213, 214]
	Spheres	Carbon	[215]
		Ceria	[216–220]
		Melanin	[221]
Hydrolase	Tube	Carbon	[222]
	Sheet	Carbon	[223–225]
	Sphere	Gold	[226–229]
	Complex	MOF	[230–232]

Besides, colorimetric methods were also applied to assess the same peroxidase-like activity of Au nanozymes used to detect copper[237] and mercury [245] ions in biological samples. In environmental samples, for example, the peroxidase-like activity of Au was used to detect methylmercury [246] and organic pesticides [247], whereas platinum nanozymes peroxidase-like activity was used to sense mercury ions [185].

On the other hand, LSPR sensors are designed to detect qualitatively and quantitatively the analyte according to the LSPR shift in the UV–Vis spectrum. Concerning the LSPR sensors, the records are scarcer in comparison with colorimetric probes.

In 2011, Au NPs with glucose oxidase-like properties were used as plasmonic sensors of DNA hybridization owing to the size enlargement of the nanoparticle [248]. In 2021, bimetallic nanozymes of Au-Pt were designed to sense Ag^+ ions in water samples. The LSPR sensor was built in order to detect the reduction of Ag^+ ions on the surface of Au-Pt nanozymes, which ended up with a blueshift of the LSPR maximum [249].

External stimuli of nanozymes with LSPR-matching wavelength sources are capable of promoting enhanced catalytic activities toward an analyte or reactant. Plasmonic nanozyme-based sensors stimulated with the wavelength of the nanoparticle's LSPR maximum have been developed with Au-Pt bimetallic nanomaterials toward hydrogen peroxide in a peroxidase-like fashion with the exposition to near-infrared (NIR) [250]. In another study, Au NPs supported on copper-based MOFs were stimulated with LSPR-matching light, which led to a 1.6-fold improvement in the reaction kinetics of peroxidase and presented antibacterial and wound healing properties [251].

Electrochemical approaches to plasmon-driven catalytic reactions with nanozymes are even rarer in the literature. In electrochemical reactions, metallic nanoparticles have been used as oxidases toward alcohol [252–254] and water [255], as well as reductases toward oxygen [256, 257] and carbon dioxide [258]. In all the previously mentioned examples, LSPR-matching wavelength sources were used to enhance their catalytic activity toward the product formation.

Concerning the direct use of nanozymes as LSPR-enhanced electrochemical sensors, glucose oxidase was mimicked by Au NPs in an electrooxidation system stimulated by light for glucose sensing [259]. The authors found a sixfold enhancement in the sensor sensitivity upon excitation with a LSPR-matching light source.

In 2018, Wang and collaborators synthesized Au/NiAu multilayered nanowire arrays as non-enzymatic glucose sensors [260]. Whenever they were stimulated with LSPR-matching wavelengths, their sensitivity was enhanced by twofold in comparison with the dark conditions.

Au-Pt nanoframes loaded on hexagonal boron nitride exhibited enhanced sensing parameters toward glucose upon NIR stimulus [261]. Glucose was monitored in human tears through electrooxidation, and an enhancement of up to 1.6-fold was achieved under illumination with NIR wavelength.

Concerning the peroxidase-like activity of nanozymes in electrochemical systems, hydrogen peroxide and glucose were detected by nanozymes composed of AuNi

nanodendrite arrays upon visible light exposition [262]. After external light stimulus, glucose detection presented a 3.3-fold enhancement in comparison with dark conditions, whereas hydrogen peroxide presented a 1.5-fold increase.

Au nanorods sensors exhibited a 2–fourfold increase in sensitivity toward hydrogen peroxide whenever irradiated with light [263]. The produced sensor was then used to detect cancer cells with a trace detection of hydrogen peroxide released from cervical cancer cells (HeLa).

Da Silva et al. synthesized AgAu hollow nanoshells supported on graphene oxide (AgAu/GO) and silica submicrospheres ($AgAu/SiO_2$) as sensors for hydrogen peroxide through its reduction reaction [32]. These materials had distinct metallic percentage composition, and thus, their LSPR was apart from each other. After a systematic study concerning the exposition toward different wavelengths, the authors found out that the materials exhibited their best performance toward hydrogen peroxide sensing only once they were irradiated with the external stimuli that matched their LSPR maximum. This happened upon red light toward $AgAu/SiO_2$ and both violet and green lights toward AgAu/GO. When a non-LSPR-matching light was used, practically no improvement was observed, as indicated in Fig. 15. In this work, the improvement in performance was analyzed and stated through parameters such as the sensibility slope, maximum current (I_{max}), and Michaelis–Menten apparent constant $\left(K_M^{app}\right)$.

Miguel et al. developed a peroxidase-like system with MnO_2 nanowires decorated with Au NPs for the electrooxidation of hydrogen peroxide [264]. The increase in the sensor sensitivity upon LSPR-matching laser stimulus was 1.16-fold, which was attributed to a better charge separation by the plasmonic generated hot electrons and the hot holes in the oxide used as support.

4.4 Conclusions

The immense variety of nanozymes-containing systems is reflected in the diversity of optical properties of the metallic nanoparticles. The fine shift in the LSPR makes outstandingly sensitive sensors with or without the aid of electrochemical approaches. In addition, LSPR-stimulus through an external source is a powerful tool of catalytic enhancement, mainly due to hot electron transfer mechanisms and localized heat.

Some authors working with enzyme-like properties of metallic nanoparticles choose not to describe their systems as ‘nanozymes’ or use their analytic approach based on Michaelis–Menten modeling. Instead, they use the classical catalytic approaches to evaluate the efficiency of the nanocatalysts. Thus, the lack of uniformity in the terminology among these two approaches makes gathering information about LSPR nanozymes a critical challenge to be faced.

The literature concerning non-electrochemical systems of nanozymes for either LSPR optical sensors or plasmon-driven catalysis is extensive. The understanding of these mechanisms has significantly advanced in the last decade, which allowed an expanded variety of applications in real samples.

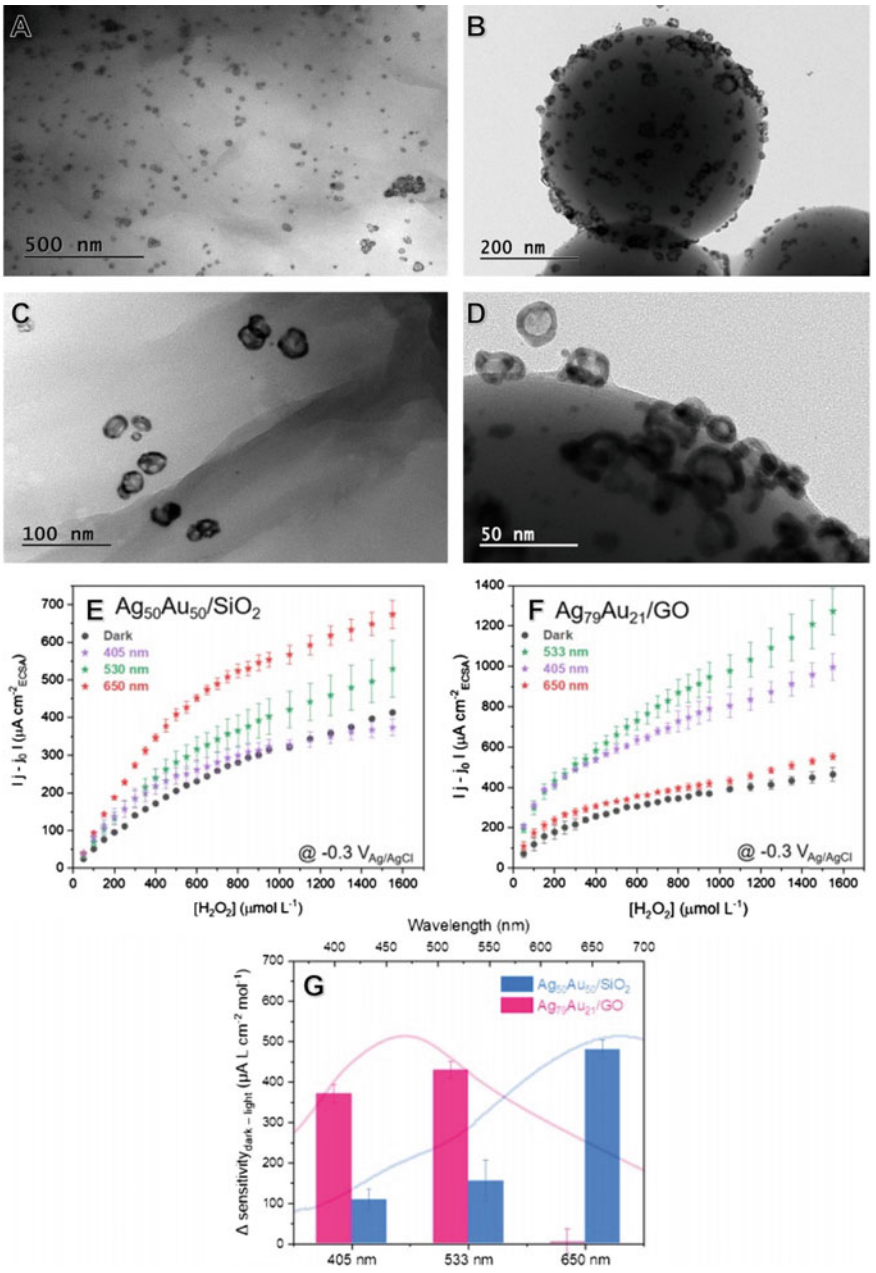

Fig. 15 LSPR stimulated AgAu hollow nanoshells used as nanozymes for hydrogen peroxide sensing. TEM micrographs of $AgAu/SiO_2$ (A,C) and AgAu/GO (B,D). Calibration curves generated by chronoamperometry for $AgAu/SiO_2$ and AgAu/GO in dark and upon different wavelength stimulus (E,F). UV–Vis spectrum of AgAu/GO and $AgAu/SiO_2$ and enhancement in sensitivity found upon each laser stimulus. Reprinted with permission from[32]. Copyright 2022 American Chemical Society

However, despite the recent development of nanozymes as either electrochemical LSPR sensors or electrochemical LSPR-stimulated systems, there is still plenty of room for improvement. The outcomes of LSPR stimuli alongside electrical stimulus are yet to be fully comprehended, and its use in biological applications is at the beginning stagesy [2].

Acknowledgements RTPS is grateful to CAPES (process 88882.328241/2019-01) for the funding. RNPC is grateful to FAPESP (processes 2021/05665-7 and 2018/22214-6) for the funding. VMM is grateful to CNPq (process 141097/2021-3) for the funding. HRB is grateful to FAPESP (process 2019/09668-0), and SICT is grateful to FAPESP (processes 2021/00675-4 and 18/13492-2).

References

1. Juan ML, Righini M, Quidant R (2011) Plasmon nano-optical tweezers. Nat Photonics 5(6):349–356. https://doi.org/10.1038/nphoton.2011.56
2. Baffou G, Quidant R (2014) Nanoplasmonics for chemistry. Chem Soc Rev 43(11):3898. https://doi.org/10.1039/c3cs60364d
3. Yang K, Yao X, Liu B, Ren B (2021) Metallic plasmonic array structures: principles, fabrications, properties, and applications. Adv Mater 33(50):1–21. https://doi.org/10.1002/adma.202007988
4. Maier Sa (2004) Fundamentals and applications plasmonics: fundamentals and applications 677
5. Urbieta M, Barbry M, Zhang Y, Koval P, Sánchez-Portal D, Zabala N, Aizpurua J (2018) Atomic-scale lightning rod effect in plasmonic picocavities: a classical view to a quantum effect. ACS Nano 12(1):585–595. https://doi.org/10.1021/acsnano.7b07401
6. Jain PK (2019) Taking the heat off of plasmonic chemistry. J Phys Chem C 123(40):24347–24351. https://doi.org/10.1021/acs.jpcc.9b08143
7. Yang W, Liang H, Ma S, Wang D, Huang J (2019) Gold nanoparticle based photothermal therapy: development and application for effective cancer treatment. Sustain Mater Technol 22:e00109. https://doi.org/10.1016/j.susmat.2019.e00109
8. Luo S, Ren X, Lin H, Song H, Ye J (2021) Plasmonic photothermal catalysis for solar-to-fuel conversion: current status and prospects. Chem Sci 12(16):5701–5719. https://doi.org/10.1039/d1sc00064k
9. Christopher P, Moskovits M (2017) Hot charge carrier transmission from plasmonic nanostructures. Annu Rev Phys Chem 68(March):379–398. https://doi.org/10.1146/annurev-physchem-052516-044948
10. Zhan C, Liu BW, Huang YF, Hu S, Ren B, Moskovits M, Tian ZQ (2019) Disentangling charge carrier from photothermal effects in plasmonic metal nanostructures. Nat Commun 10(1):1–8. https://doi.org/10.1038/s41467-019-10771-3
11. Zhou L, Swearer DF, Robatjazi H, Alabastri A, Christopher P, Carter EA, Nordlander P, Halas NJ (2019) Response to comment on "quantifying hot carrier and thermal contributions in plasmonic photocatalysis." Science (80-.). *364*(6439):69–72. https://doi.org/10.1126/science.aaw9545
12. Li X, Everitt HO, Liu J (2020) Synergy between thermal and nonthermal effects in plasmonic photocatalysis. Nano Res 13(5):1268–1280. https://doi.org/10.1007/s12274-020-2694-z
13. Rodrigues MP de S, Miguel VM, Germano LD, Córdoba de Torresi SI (2021) Metal oxides as electrocatalysts for water splitting: on plasmon-driven enhanced activity. Electrochem Sci Adv. https://doi.org/10.1002/elsa.202100079

14. Doronin IV, Kalmykov AS, Zyablovsky AA, Andrianov ES, Khlebtsov BN, Melentiev PN, Balykin VI (2022) Resonant concentration-driven control of dye molecule photodegradation via strong optical coupling to plasmonic nanoparticles. Nano Lett 22(1):105–110. https://doi.org/10.1021/acs.nanolett.1c03277
15. Mauriz E, Lechuga LM (2021) Plasmonic biosensors for single-molecule biomedical analysis. Biosensors 11(4). https://doi.org/10.3390/bios11040123
16. Zhang Z, Zhang C, Zheng H, Xu H (2019) Plasmon-driven catalysis on molecules and nanomaterials. Acc Chem Res 52(9):2506–2515. https://doi.org/10.1021/acs.accounts.9b00224
17. Liz-Marzán LM (2004) Nanometals. Mater Today 7(2):26–31. https://doi.org/10.1016/S1369-7021(04)00080-X
18. Gans R (1915) Über die form ultramikroskopischer silberteilchen. Ann Phys 352(10):270–284. https://doi.org/10.1002/andp.19153521006
19. Jain PK, Lee KS, El-Sayed IH, El-Sayed MA (2006) Calculated absorption and scattering properties of gold nanoparticles of different size, shape, and composition: applications in biological imaging and biomedicine. J Phys Chem B 110(14):7238–7248. https://doi.org/10.1021/jp057170o
20. Langer J, de Aberasturi DJ, Aizpurua J, Alvarez-Puebla RA, Auguié B, Baumberg JJ, Bazan GC, Bell SEJ, Boisen A, Brolo AG, Choo J, Cialla-May D, Deckert V, Fabris L, Faulds K, Javier García de Abajo F, Goodacre R, Graham D, Haes AJ, Haynes CL, Huck C, Itoh T, Käll M, Kneipp J, Kotov NA, Kuang H, Le Ru EC, Lee HK. Li JF, Ling XY, Maier SA, Mayerhöfer T, Moskovits M, Murakoshi K, Nam JM, Nie S, Ozaki Y, Pastoriza-Santos I, Perez-Juste J, Popp J, Pucci A, Reich S, Ren B, Schatz GC, Shegai T, Schlücker S, Tay LL, George Thomas K, Tian ZQ, van Duyne RP, Vo-Dinh T, Wang Y, Willets KA, Xu C, Xu H, Xu Y, Yamamoto YS, Zhao B, Liz-Marzán LM (2020) Present and Future of surface-enhanced raman scattering. ACS Nano 14(1):28–117. https://doi.org/10.1021/acsnano.9b04224
21. Hao F, Nehl CL, Hafner JH, Nordlander P (2007) Plasmon resonances of a gold nanostar. Nano Lett 7(3):729–732. https://doi.org/10.1021/nl062969c
22. Saada TN, Pang L, Sravan Kumar K, Dourado AHB, Germano LD, Vicentini ED, Batista APL, de Oliveira-Filho AGS, Dumeignil F, Paul S, Wojcieszak R, Melinte S, Sandu G, Petretto G, Rignanese G-M, Braga AH, Rosado TF, Meziane D, Boukherroub R, de Torresi SIC, da Silva AGM, Szunerits S (2021) The importance of the shape of Cu2O nanocrystals on plasmon-enhanced oxygen evolution reaction in alkaline media. Electrochim Acta 390:138810. https://doi.org/10.1016/j.electacta.2021.138810
23. Sousa-Castillo A, Comesaña-Hermo M, Rodríguez-González B, Pérez-Lorenzo M, Wang Z, Kong XT, Govorov AO, Correa-Duarte MA (2016) Boosting hot electron-driven photocatalysis through anisotropic plasmonic nanoparticles with hot spots in au-tio2 nanoarchitectures. J Phys Chem C 120(21):11690–11699. https://doi.org/10.1021/acs.jpcc.6b02370
24. Kochuveedu ST, Kim DP, Kim DH (2012) Surface-plasmon-induced visible light photocatalytic activity of TiO 2 nanospheres decorated by au nanoparticles with controlled configuration. J Phys Chem C 116(3):2500–2506. https://doi.org/10.1021/jp209520m
25. Murdoch M, Waterhouse GIN, Nadeem MA, Metson JB, Keane MA, Howe RF, Llorca J, Idriss H (2011) The effect of gold loading and particle size on photocatalytic hydrogen production from ethanol over Au/TiO2 nanoparticles. Nat Chem 3(6):489–492. https://doi.org/10.1038/nchem.1048
26. Fabris L (2020) Gold nanostars in biology and medicine: understanding physicochemical properties to broaden applicability. J Phys Chem C. https://doi.org/10.1021/acs.jpcc.0c08460
27. Gellé A, Jin T, De La Garza L, Price GD, Besteiro LV, Moores A (2020) Applications of plasmon-enhanced nanocatalysis to organic transformations. Chem Rev 120(2):986–1041. https://doi.org/10.1021/acs.chemrev.9b00187
28. Quiroz J, Barbosa ECM, Araujo TP, Fiorio JL, Wang Y-C, Zou Y-C, Mou T, Alves TV, de Oliveira DC, Wang B, Haigh SJ, Rossi LM, Camargo PHC (2018) Controlling reaction selectivity over hybrid plasmonic nanocatalysts. Nano Lett 18(11):7289–7297. https://doi.org/10.1021/acs.nanolett.8b03499

29. De Barros HR, García I, Kuttner C, Zeballos N, Camargo PHC, De Torresi SIC, López-Gallego F, Liz-Marzán LM (2021) Mechanistic insights into the light-driven catalysis of an immobilized lipase on plasmonic nanomaterials. ACS Catal 11(1):414–423. https://doi.org/10.1021/acscatal.0c04919
30. De Barros HR, López-Gallego F, Liz-Marzán LM (2021) Light-driven catalytic regulation of enzymes at the interface with plasmonic nanomaterials. Biochemistry 60(13):991–998. https://doi.org/10.1021/acs.biochem.0c00447
31. Rodrigues MP de S, Dourado AHB, Cutolo L de O, Parreira LS, Alves TV, Slater TJA, Haigh SJ, Camargo PHC, Cordoba de Torresi SI (2021) Gold–rhodium nanoflowers for the plasmon-enhanced hydrogen evolution reaction under visible light. ACS Catal 11(21):13543–13555. https://doi.org/10.1021/acscatal.1c02938
32. Da Silva RTP, De Souza Rodrigues MP, Davilla GFB, Da Silva AMRP, Dourado AHB, Córdoba De Torresi SI (2021) AgAu hollow nanoshells on layered graphene oxide and silica submicrospheres as plasmonic nanozymes for light-enhanced electrochemical H2O2 sensing. ACS Appl Nano Mater 4(11):12062–12072. https://doi.org/10.1021/acsanm.1c02611
33. Subramanian P, Meziane D, Wojcieszak R, Dumeignil F, Boukherroub R, Szunerits S (2018) Plasmon-induced electrocatalysis with multi-component nanostructures. Materials (Basel) 12(1):1–12. https://doi.org/10.3390/ma12010043
34. Patskovsky S, Dallaire AM, Meunier M (2016) Electrochemical surface plasmon resonance sensing with absorptive redox mediator film. Sensors Actuators B Chem 222:71–77. https://doi.org/10.1016/j.snb.2015.08.051
35. Blidar A, Feier B, Tertis M, Galatus R, Cristea C (2019) Electrochemical surface plasmon resonance (EC-SPR) Aptasensor for ampicillin detection. Anal Bioanal Chem 411(5):1053–1065. https://doi.org/10.1007/s00216-018-1533-5
36. Jiang X, Cao Z, Tang H, Tan L, Xie Q, Yao S (2008) Electrochemical surface plasmon resonance studies on the deposition of the charge-transfer complex from electrooxidation of o-tolidine and effects of dermatan sulfate. Electrochem commun 10(9):1235–1237. https://doi.org/10.1016/j.elecom.2008.06.012
37. Melo Ferreira DC, Mendes RK, Kubota LT (2013) Electrochemical-surface plasmon resonance: concept and bioanalytical applications. In Nanobioelectrochemistry, Springer Berlin Heidelberg, Berlin, Heidelberg, 127–137. https://doi.org/10.1007/978-3-642-29250-7_7
38. Löfås S, Malmqvist M, Rönnberg I, Stenberg E, Liedberg B, Lundström I (1991) Bioanalysis with surface plasmon resonance. Sensors Actuators B Chem 5(1–4):79–84. https://doi.org/10.1016/0925-4005(91)80224-8
39. Liedberg, B.; Nylander, C.; Lundström, I. Biosensing with Surface Plasmon Resonance - How It All Started. *Biosens. Bioelectron.* **1995**, *10* (8). https://doi.org/10.1016/0956-5663(95)96965-2.
40. Singh P (2016) SPR biosensors: historical perspectives and current challenges. Sensors Actuators B Chem 229:110–130. https://doi.org/10.1016/j.snb.2016.01.118
41. Souto DEP, Volpe J, Gonçalves C de C, Ramos CHI, Kubota LT (2019) A brief review on the strategy of developing SPR-based biosensors for application to the diagnosis of neglected tropical diseases. Talanta 205(July):120122. https://doi.org/10.1016/j.talanta.2019.120122
42. Homola J (2008) Surface plasmon resonance sensors for detection of chemical and biological species. Chem Rev 108(2):462–493. https://doi.org/10.1021/cr068107d
43. Mauriz E, García-Fernández MC, Lechuga LM (2016) Towards the design of universal immunosurfaces for spr-based assays: a review. TrAC - Trends Anal. Chem. 79:191–198. https://doi.org/10.1016/j.trac.2016.02.006
44. Estevez MC, Alvarez M, Lechuga LM (2012) Integrated optical devices for lab-on-a-chip biosensing applications. Laser Photonics Rev 6(4):463–487. https://doi.org/10.1002/lpor.201100025
45. Yuan J, Addo J, Aguilar MI, Wu Y (2009) Surface plasmon resonance assay for chloramphenicol without surface regeneration. Anal Biochem 390(1):97–99. https://doi.org/10.1016/j.ab.2009.04.003

46. Chen S, Liu Y, Yu Q, Peng W (2020) Self-referencing spr biosensing with an ultralow limit-of-detection using long-wavelength excitation. Sensors Actuators B Chem 2021(327):128935. https://doi.org/10.1016/j.snb.2020.128935
47. Grover Shah V, Ray S, Karlsson R, Srivastava S (2015) Calibration-free concentration analysis of protein biomarkers in human serum using surface plasmon resonance. Talanta 144:801–808. https://doi.org/10.1016/j.talanta.2015.06.074
48. Shukla T, Prakash S, Upmanyu N (2019) Simultaneous estimation of thiocolchicoside and ketorolac tromethamine using UV. 96(February):305–310
49. Dong G, Pan Y, Wang Y, Ahmed S, Liu Z, Peng D, Yuan Z (2017) Preparation of a broad-spectrum anti-zearalenone and its primary analogues antibody and its application in an indirect competitive enzyme-linked immunosorbent assay. Food Chem 2018(247):8–15. https://doi.org/10.1016/j.foodchem.2017.12.016
50. Moreno P, Salvadó V (2000) Determination of eight water- and fat-soluble vitamins in multi-vitamin pharmaceutical formulations by high-performance liquid chromatography. J Chromatogr A 870(1–2):207–215. https://doi.org/10.1016/S0021-9673(99)01021-3
51. Otto A (1968) Excitation of nonradiative surface plasma waves in silver by the method of frustrated total reflection. Zeitschrift für Phys 216(4):398–410. https://doi.org/10.1007/BF01391532
52. Kretschmann E, Raether H (1968) Radiative decay of non radiative surface plasmons excited by light. Zeitschrift fur Naturforsch—Sect A J Phys Sci 23(12):2135–2136. https://doi.org/10.1515/zna-1968-1247
53. Miyazaki CM, Shimizu FM, Ferreira M (2017) Surface plasmon resonance (SPR) for sensors and biosensors; Elsevier Inc., https://doi.org/10.1016/B978-0-323-49778-7.00006-0
54. Guo X (2012) Surface plasmon resonance based biosensor technique: a review. J Biophotonics 5(7):483–501. https://doi.org/10.1002/jbio.201200015
55. Qu JH, Dillen A, Saeys W, Lammertyn J, Spasic D (2020) Advancements in SPR biosensing technology: an overview of recent trends in smart layers design, multiplexing concepts, continuous monitoring and in vivo sensing. Anal Chim Acta 1104:10–27. https://doi.org/10.1016/j.aca.2019.12.067
56. Gwon HR, Lee SH (2010) Spectral and angular responses of surface plasmon resonance based on the kretschmann prism configuration. Mater Trans 51(6):1150–1155. https://doi.org/10.2320/matertrans.M2010003
57. Prabowo BA, Purwidyantri A, Liu KC (2018) Surface plasmon resonance optical sensor: a review on light source technology. Biosensors 8(3). https://doi.org/10.3390/bios8030080
58. Hinman SS, McKeating KS, Cheng Q (2018) Surface plasmon resonance: material and interface design for universal accessibility. Anal Chem 90(1):19–39. https://doi.org/10.1021/acs.analchem.7b04251
59. Boozer C, Kim G, Cong S, Guan HW, Londergan T (2006) Looking towards label-free biomolecular interaction analysis in a high-throughput format: a review of new surface plasmon resonance technologies. Curr Opin Biotechnol 17(4):400–405. https://doi.org/10.1016/j.copbio.2006.06.012
60. Homola J, Yee SS, Gauglitz G (1999) Surface plasmon resonance sensors: review. Sensors Actuators B Chem 54(1):3–15. https://doi.org/10.1016/S0925-4005(98)00321-9
61. Caucheteur C, Guo T, Albert J (2015) Review of plasmonic fiber optic biochemical sensors: improving the limit of detection. Anal Bioanal Chem 407(14):3883–3897. https://doi.org/10.1007/s00216-014-8411-6
62. Marinakos SM, Chen S, Chilkoti A (2007) Plasmonic detection of a model analyte in serum by a gold nanorod sensor. Anal Chem 79(14):5278–5283. https://doi.org/10.1021/ac0706527
63. Shynkarenko OV, Kravchenko SA (2015) Surface plasmon resonance sensors: methods of surface functionalization and sensitivity enhancement. Theor Exp Chem 51(5):273–292. https://doi.org/10.1007/s11237-015-9427-5
64. Ahmad OS, Bedwell TS, Esen C, Garcia-Cruz A, Piletsky SA (2019) Molecularly imprinted polymers in electrochemical and optical sensors. Trends Biotechnol 37(3):294–309. https://doi.org/10.1016/j.tibtech.2018.08.009

65. Yuan H, Ji W, Chu S, Liu Q, Guang J, Sun G, Zhang Y, Han X, Masson JF, Peng W (2019) Au nanoparticles as label-free competitive reporters for sensitivity enhanced fiber-optic SPR heparin sensor. Biosens Bioelectron 2020(154):112039. https://doi.org/10.1016/j.bios.2020.112039
66. Xia F, Song H, Zhao Y, Zhao WM, Wang Q, Wang XZ, Wang BT, Dai ZX (2020) Ultra-high sensitivity SPR fiber sensor based on multilayer nanoparticle and au film coupling enhancement. Meas J Int Meas Confed 164:108083. https://doi.org/10.1016/j.measurement.2020.108083
67. Zalewska M, Kochman A, Estève JP, Lopez F, Chaoui K, Susini C, Ozyhar A, Kochman M (2009) Juvenile hormone binding protein traffic—interaction with ATP synthase and lipid transfer proteins. Biochim Biophys Acta—Biomembr 1788(9):1695–1705. https://doi.org/10.1016/j.bbamem.2009.04.022
68. Wang S, Huang X, Shan X, Foley KJ, Tao N (2010) Electrochemical surface plasmon resonance: basic formalism and experimental validation. Anal Chem 82(3):935–941. https://doi.org/10.1021/ac902178f
69. Baba A, Taranekar P, Ponnapati RR, Knoll W, Advincula RC (2010) Electrochemical surface plasmon resonance and waveguide-enhanced glucose biosensing with N-alkylaminated polypyrrole/glucose oxidase multilayers. ACS Appl Mater Interfaces 2(8):2347–2354. https://doi.org/10.1021/am100373v
70. Ribeiro JA, Sales MGF, Pereira CM (2021) Electrochemistry-assisted surface plasmon resonance biosensor for detection of CA 15–3. Anal Chem 93(22):7815–7824. https://doi.org/10.1021/acs.analchem.0c05367
71. Boussaad S, Pean J, Tao NJ (2000) High-resolution multiwavelength surface plasmon resonance spectroscopy for probing conformational and electronic changes in redox proteins. Anal Chem 72(1):222–226. https://doi.org/10.1021/ac990947n
72. Juan-Colás J, Johnson S, Krauss TF (2017) Dual-mode electro-optical techniques for biosensing applications: a review. Sensors (Switzerland) 17(9):1–15. https://doi.org/10.3390/s17092047
73. Sannomiya T, Dermutz H, Hafner C, Vörös J, Dahlin AB (2010) Electrochemistry on a localized surface plasmon resonance sensor. Langmuir 26(10):7619–7626. https://doi.org/10.1021/la9042342
74. Salamifar SE, Lai RY (2014) Application of electrochemical surface plasmon resonance spectroscopy for characterization of electrochemical DNA sensors. Colloids Surfaces B Biointerfaces 122:835–839. https://doi.org/10.1016/j.colsurfb.2014.07.028
75. Chalovich JM, Eisenberg E (1982) Inhibition of actomyosin atpase activity by troponin-tropomyosin without blocking the binding of myosin to actin. J Biol Chem 257(5):2432–2437. https://doi.org/10.1016/s0021-9258(18)34942-1
76. Yao X, Wang J, Zhou F, Wang J, Tao N (2004) Quantification of redox-induced thickness changes of 11- ferrocenylundecanethiol self-assembled monolayers by electrochemical surface plasmon resonance. J Phys Chem B 108(22):7206–7212. https://doi.org/10.1021/jp049651y
77. Huang X, Wang S, Shan X, Chang X, Tao N (2010) Flow-through electrochemical surface plasmon resonance: detection of intermediate reaction products. J Electroanal Chem 649(1–2):37–41. https://doi.org/10.1016/j.jelechem.2009.12.027
78. Lu J, Wang W, Wang S, Shan X, Li J, Tao N (2012) Plasmonic-based electrochemical impedance spectroscopy: application to molecular binding. Anal Chem 84(1):327–333. https://doi.org/10.1021/ac202634h
79. Ding SY, Zhang XM, Ren B, Tian ZQ (2014) Surface-enhanced raman spectroscopy (SERS): general introduction. https://doi.org/10.1002/9780470027318.a9276
80. Meyer SA, Ru ECL, Etchegoin PG (2010) Quantifying resonant raman cross sections with SERS. J Phys Chem A 114(17):5515–5519. https://doi.org/10.1021/jp100669q
81. Fleischmann M, Hendra PJ, McQuillan AJ (1974) Raman spectra of pyridine adsorbed at a silver electrode. Chem Phys Lett 26(2):163–166. https://doi.org/10.1016/0009-2614(74)85388-1

82. Jeanmaire DL, Van Duyne RP (1977) Surface raman spectroelectrochemistry. J Electroanal Chem Interfacial Electrochem 84(1):1–20. https://doi.org/10.1016/S0022-0728(77)80224-6
83. Albrecht MG, Creighton JA (1977) Anomalously intense raman spectra of pyridine at a silver electrode. J Am Chem Soc 99(15):5215–5217. https://doi.org/10.1021/ja00457a071
84. Moskovits M (1978) Surface roughness and the enhanced intensity of raman scattering by molecules adsorbed on metals. J Chem Phys 69(9):4159–4161. https://doi.org/10.1063/1.437095
85. Musumeci A, Gosztola D, Schiller T, Dimitrijevic NM, Mujica V, Martin D, Rajh T (2009) SERS of semiconducting nanoparticles (TiO_2 hybrid composites). J Am Chem Soc 131(17):6040–6041. https://doi.org/10.1021/ja808277u
86. Ling X, Xie L, Fang Y, Xu H, Zhang H, Kong J, Dresselhaus MS, Zhang J, Liu Z (2010) Can graphene be used as a substrate for raman enhancement? Nano Lett 10(2):553–561. https://doi.org/10.1021/nl903414x
87. Fan M, Andrade GFS, Brolo AG (2020) A review on recent advances in the applications of surface-enhanced raman scattering in analytical chemistry. Anal Chim Acta 1097:1–29. https://doi.org/10.1016/j.aca.2019.11.049
88. Bantz KC, Meyer AF, Wittenberg NJ, Im H, Kurtuluş Ö, Lee SH, Lindquist NC, Oh S-H, Haynes CL (2011) Recent progress in SERS biosensing. Phys Chem Chem Phys 13(24):11551. https://doi.org/10.1039/c0cp01841d
89. Cardinal MF, Vander Ende E, Hackler RA, McAnally MO, Stair PC, Schatz GC, Van Duyne RP (2017) Expanding applications of SERS through versatile nanomaterials engineering. Chem Soc Rev. https://doi.org/10.1039/C7CS00207F
90. Girão AV, Pinheiro PC, Ferro M, Trindade T (2017) Tailoring gold and silver colloidal bimetallic nanoalloys towards SERS detection of rhodamine 6G. RSC Adv 7(26):15944–15951. https://doi.org/10.1039/C7RA00685C
91. Jamali SB, Khaskheli MA, Abro MI, Chand R, Rekik N, Affan H, Ikram R (2021) Confirming the SERS enhancement at large mapping area using self-assembly of silver nanocube at liquid-liquid cyclohexane/water interface. J Mol Liq 326:115365. https://doi.org/10.1016/j.molliq.2021.115365
92. Mao M, Zhou B, Tang X, Chen C, Ge M, Li P, Huang X, Yang L, Liu J (2018) Natural deposition strategy for interfacial, self-assembled, large-scale, densely packed, monolayer film with ligand-exchanged gold nanorods for in situ surface-enhanced raman scattering drug detection. Chem A Eur J 24(16):4094–4102. https://doi.org/10.1002/chem.201705700
93. Guo Q, Xu M, Yuan Y, Gu R, Yao J (2016) Self-assembled large-scale monolayer of Au nanoparticles at the air/water interface used as a SERS substrate. Langmuir 32(18):4530–4537. https://doi.org/10.1021/acs.langmuir.5b04393
94. Johnson RP, Mahajan S, Abdelsalam ME, Cole RM, Baumberg JJ, Russell AE, Bartlett PN (2011) SERS from Two-tier sphere segment void substrates. Phys Chem Chem Phys 13(37):16661. https://doi.org/10.1039/c1cp21126a
95. Li JF, Huang YF, Ding Y, Yang ZL, Li SB, Zhou XS, Fan FR, Zhang W, Zhou ZY, Wu DY, Ren B, Wang ZL, Tian ZQ (2010) Shell-isolated nanoparticle-enhanced raman spectroscopy. Nature 464(7287):392–395. https://doi.org/10.1038/nature08907
96. Bai F, Dong J, Qu J, Zhang Z (2021) Construction of flexible, transparent and mechanically robust sers-active substrate with an efficient spin coating method for rapid in-situ target molecules detection. Nanotechnology 32(38):385501. https://doi.org/10.1088/1361-6528/ac09ab
97. Colombo RNP, Moreira RV, de Faria DLA, Córdoba de Torresi SI (2019) Controlling gold electrodeposition on porous polymeric templates produced by the breath-figure method: fabrication of SERS-active surfaces. Chempluschem 84(8). https://doi.org/10.1002/cplu.201900278
98. Yin Z, Zhou Y, Cui P, Liao J, Rafailovich MH, Sun W (2020) Fabrication of ordered bimetallic array with superstructure of gold micro-rings via templated-self-assembly procedure and its SERS application. Chem Commun 56(35):4808–4811. https://doi.org/10.1039/D0CC00942C

99. Wu T, Lin Y-W (2018) Surface-enhanced raman scattering active gold nanoparticle/nanohole arrays fabricated through electron beam lithography. Appl Surf Sci 435:1143–1149. https://doi.org/10.1016/j.apsusc.2017.11.213
100. Hao Q, Huang H, Fan X, Yin Y, Wang J, Li W, Qiu T, Ma L, Chu PK, Schmidt OG (2017) Controlled patterning of plasmonic dimers by using an ultrathin nanoporous alumina membrane as a shadow mask. ACS Appl Mater Interfaces 9(41):36199–36205. https://doi.org/10.1021/acsami.7b11428
101. Chen S, Liu B, Zhang X, Mo Y, Chen F, Shi H, Zhang W, Hu C, Chen J (2018) Electrochemical fabrication of pyramid-shape silver microstructure as effective and reusable SERS substrate. Electrochim Acta 274:242–249. https://doi.org/10.1016/j.electacta.2018.04.120
102. Choi S, Ahn M, Kim J (2013) Highly reproducible surface-enhanced raman scattering-active Au nanostructures prepared by simple electrodeposition: origin of surface-enhanced raman scattering activity and applications as electrochemical substrates. Anal Chim Acta 779:1–7. https://doi.org/10.1016/j.aca.2013.03.058
103. Le Ru EC, Etchegoin PG (2013) Quantifying SERS enhancements. MRS Bull 38(8):631–640. https://doi.org/10.1557/mrs.2013.158
104. Le Ru EC, Blackie E, Meyer M, Etchegoin PG (2007) Surface enhanced raman scattering enhancement factors: a comprehensive study. J Phys Chem C111(37):13794–13803. https://doi.org/10.1021/jp0687908
105. Colombo RNP, Gonçales VR, Gautam S, Tilley R, Gooding JJ, Córdoba de Torresi SI (2020) Spatially localized electrodeposition of multiple metals via light-activated electrochemistry for surface enhanced raman spectroscopy applications. Chem Commun. https://doi.org/10.1039/D0CC01661F
106. Moody AS, Sharma B (2018) Multi-metal, multi-wavelength surface-enhanced raman spectroscopy detection of neurotransmitters. ACS Chem Neurosci 9(6):1380–1387. https://doi.org/10.1021/acschemneuro.8b00020
107. de Albuquerque CDL, Sobral-Filho RG, Poppi RJ, Brolo AG (2018) Digital protocol for chemical analysis at ultralow concentrations by surface-enhanced raman scattering. Anal Chem 90(2):1248–1254. https://doi.org/10.1021/acs.analchem.7b03968
108. Pallaoro A, Hoonejani MR, Braun GB, Meinhart CD, Moskovits M (2015) Rapid identification by surface-enhanced raman spectroscopy of cancer cells at low concentrations flowing in a microfluidic channel. ACS Nano 9(4):4328–4336. https://doi.org/10.1021/acsnano.5b00750
109. Zhu A, Xu Y, Ali S, Ouyang Q, Chen Q (2021) Au@Ag nanoflowers based SERS coupled chemometric algorithms for determination of organochlorine pesticides in milk. LWT 150:111978. https://doi.org/10.1016/j.lwt.2021.111978
110. Pan H, Ahmad W, Jiao T, Zhu A, Ouyang Q, Chen Q (2022) Label-free Au NRs-based SERS coupled with chemometrics for rapid quantitative detection of thiabendazole residues in citrus. Food Chem 375:131681. https://doi.org/10.1016/j.foodchem.2021.131681
111. Zhu X, Liu P, Xue T, Ge Y, Ai S, Sheng Y, Wu R, Xu L, Tang K, Wen Y (2021) A novel graphene-like titanium carbide MXene/Au–Ag nanoshuttles bifunctional nanosensor for electrochemical and SERS intelligent analysis of ultra-trace carbendazim coupled with machine learning. Ceram Int 47(1):173–184. https://doi.org/10.1016/j.ceramint.2020.08.121
112. Skvortsova A, Trelin A, Kriz P, Elashnikov R, Vokata B, Ulbrich P, Pershina A, Svorcik V, Guselnikova O, Lyutakov O (2022) SERS and advanced chemometrics—utilization of siamese neural network for picomolar identification of beta-lactam antibiotics resistance gene fragment. Anal Chim Acta 1192:339373. https://doi.org/10.1016/j.aca.2021.339373
113. Carey P, Pusztai-Carey M (2021) Advances in applying raman spectroscopy to the study of enzyme mechanisms. J Raman Spectrosc 52(12):2550–2556. https://doi.org/10.1002/jrs.6170
114. Papadopoulou E, Goodchild SA, Cleary DW, Weller SA, Gale N, Stubberfield MR, Brown T, Bartlett PN (2015) Using surface-enhanced raman spectroscopy and electrochemically driven melting to discriminate yersinia pestis from Y. Pseudotuberculosis based on single nucleotide polymorphisms within unpurified polymerase chain reaction amplicons. Anal Chem 87(3):1605–1612. https://doi.org/10.1021/ac503063c

115. Kang H, Jeong S, Koh Y, Geun Cha M, Yang JK, Kyeong S, Kim J, Kwak SY, Chang HJ, Lee H, Jeong C, Kim JH, Jun BH, Kim YK, Hong Jeong D, Lee YS (2015) Direct identification of on-bead peptides using surface-enhanced raman spectroscopic barcoding system for high-throughput bioanalysis. Sci Rep 5(January):1–11. https://doi.org/10.1038/srep10144
116. Pezzotti G, Boschetto F, Ohgitani E, Fujita Y, Shin-Ya M, Adachi T, Yamamoto T, Kanamura N, Marin E, Zhu W, Nishimura I, Mazda O (2022) Raman molecular fingerprints of SARS-CoV-2 British variant and the concept of Raman barcode. Adv Sci 9(3):2103287. https://doi.org/10.1002/advs.202103287
117. Jia X, Liu Z, Peng Y, Hou G, Chen W, Xiao R (2021) Automatic and sensitive detection of west nile virus non-structural protein 1 with a portable SERS–LFIA detector. Microchim Acta 188(6):206. https://doi.org/10.1007/s00604-021-04857-3
118. Yadav S, Sadique MA, Ranjan P, Kumar N, Singhal A, Srivastava AK, Khan R (2021) SERS based lateral flow immunoassay for point-of-care detection of SARS-CoV-2 in clinical samples. ACS Appl Bio Mater 4(4):2974–2995. https://doi.org/10.1021/acsabm.1c00102
119. Liu H, Dai E, Xiao R, Zhou Z, Zhang M, Bai Z, Shao Y, Qi K, Tu J, Wang C, Wang S (2021) Development of a SERS-based lateral flow immunoassay for rapid and ultra-sensitive detection of anti-SARS-CoV-2 IgM/IgG in clinical samples. Sensors Actuators B Chem 329:129196. https://doi.org/10.1016/j.snb.2020.129196
120. Xiao R, Lu L, Rong Z, Wang C, Peng Y, Wang F, Wang J, Sun M, Dong J, Wang D, Wang L, Sun N, Wang S (2020) Portable and multiplexed lateral flow immunoassay reader based on SERS for highly sensitive point-of-care testing. Biosens Bioelectron 168:112524. https://doi.org/10.1016/j.bios.2020.112524
121. Bindesri SD, Alhatab DS, Brosseau CL (2018) Development of an electrochemical surface-enhanced Raman spectroscopy (EC-SERS) fabric-based plasmonic sensor for point-of-care diagnostics. Analyst 143(17):4128–4135. https://doi.org/10.1039/C8AN01117F
122. Hernandez S, Perales-Rondon JV, Heras A, Colina A (2020) Electrochemical SERS and SOERS in a single experiment: a new methodology for quantitative analysis. Electrochim Acta 334:135561. https://doi.org/10.1016/j.electacta.2019.135561
123. Verma P (2017) Tip-enhanced Raman spectroscopy: technique and recent advances. Chem Rev 117(9):6447–6466. https://doi.org/10.1021/acs.chemrev.6b00821
124. Neugebauer U, Rösch P, Schmitt M, Popp J, Julien C, Rasmussen A, Budich C, Deckert V (2006) On the way to nanometer-sized information of the bacterial surface by tip-enhanced raman spectroscopy. ChemPhysChem 7(7):1428–1430. https://doi.org/10.1002/cphc.200600173
125. Dou T, Li Z, Zhang J, Evilevitch A, Kurouski D (2020) Nanoscale structural characterization of individual viral particles using atomic force microscopy infrared spectroscopy (AFM-IR) and tip-enhanced raman spectroscopy (TERS). Anal Chem 92(16):11297–11304. https://doi.org/10.1021/acs.analchem.0c01971
126. D'Andrea C, Foti A, Cottat M, Banchelli M, Capitini C, Barreca F, Canale C, de Angelis M, Relini A, Maragò OM, Pini R, Chiti F, Gucciardi PG, Matteini P (2018) Nanoscale discrimination between toxic and nontoxic protein misfolded oligomers with tip-enhanced raman spectroscopy. Small 14(36):1800890. https://doi.org/10.1002/smll.201800890
127. Shao F, Zenobi R (2019) Tip-enhanced Raman spectroscopy: principles, practice, and applications to nanospectroscopic imaging of 2D materials. Anal Bioanal Chem 411(1):37–61. https://doi.org/10.1007/s00216-018-1392-0
128. Wood BR, Bailo E, Khiavi MA, Tilley L, Deed S, Deckert-Gaudig T, McNaughton D, Deckert V (2011) Tip-enhanced Raman scattering (TERS) from hemozoin crystals within a sectioned erythrocyte. Nano Lett 11(5):1868–1873. https://doi.org/10.1021/nl103004n
129. Kurouski D, Mattei M, Van Duyne RP (2015) Probing redox reactions at the nanoscale with electrochemical tip-enhanced raman spectroscopy. Nano Lett 15(12):7956–7962. https://doi.org/10.1021/acs.nanolett.5b04177
130. Kirk O, Borchert TV, Fuglsang CC (2002) Industrial enzyme applications. Current Opinion Biotechnol 345–351. https://doi.org/10.1016/S0958-1669(02)00328-2

131. Binod P, Sindhu R, Madhavan A, Abraham A, Mathew AK, Beevi US, Sukumaran RK, Singh SP, Pandey A (2017) Recent developments in l—glutaminase production and applications—an overview. Bioresour Technol 245:1766–1774. https://doi.org/10.1016/j.biortech.2017.05.059
132. Rodrigues RC, Ortiz C, Berenguer-Murcia Á, Torres R, Fernández-Lafuente R (2013) Modifying enzyme activity and selectivity by immobilization. Chem Soc Rev 42(15):6290–6307. https://doi.org/10.1039/C2CS35231A
133. Lehninger A, Nelson D, Cox M (2008) Lehninger principles of biochemistry. Freeman, W. H
134. Leveson-Gower RB, Mayer C, Roelfes G (2019) The importance of catalytic promiscuity for enzyme design and evolution. Nat Rev Chem 3(12):687–705. https://doi.org/10.1038/s41570-019-0143-x
135. Kumar A, Singh S (2013) Directed evolution: tailoring biocatalysts for industrial applications. Crit Rev Biotechnol 33(4):365–378. https://doi.org/10.3109/07388551.2012.716810
136. Woodley JM (2013) Protein engineering of enzymes for process applications. Curr Opin Chem Biol 17(2):310–316. https://doi.org/10.1016/j.cbpa.2013.03.017
137. Stepankova V, Bidmanova S, Koudelakova T, Prokop Z, Chaloupkova R, Damborsky J (2013) Strategies for stabilization of enzymes in organic solvents. ACS Catal 3(12):2823–2836. https://doi.org/10.1021/cs400684x
138. Breslow R (ed) (2005) Artificial Enzymes, Wiley. https://doi.org/10.1002/3527606645
139. Breslow R (1972) Centenary lecture biomimetic chemistry. Chem Soc Rev 1(4):553. https://doi.org/10.1039/cs9720100553
140. Tabushi I (1984) Design and synthesis of artificial enzymes. Tetrahedron 40(2):269–292. https://doi.org/10.1016/S0040-4020(01)91173-1
141. Wu J, Wang X, Wang Q, Lou Z, Li S, Zhu Y, Qin L, Wei H (2019) Nanomaterials with enzyme-like characteristics (nanozymes): next-generation artificial enzymes (II). Chem Soc Rev 48(4):1004–1076. https://doi.org/10.1039/c8cs00457a
142. Beltrame P, Comotti M, Della Pina C, Rossi M (2006) Aerobic oxidation of glucose: II. Catalysis by colloidal gold. Appl Catal A Gen 297(1):1–7. https://doi.org/10.1016/j.apcata.2005.08.029
143. Ali SS, Hardt JI, Quick KL, Sook Kim-Han J, Erlanger BF, Huang TT, Epstein CJ, Dugan LL (2004) A biologically effective fullerene (C 60) derivative with superoxide dismutase mimetic properties. Free Radic Biol Med 37(8):1191–1202. https://doi.org/10.1016/j.freeradbiomed.2004.07.002
144. Dugan LL, Gabrielsen JK, Yu SP, Lin TS, Choi DW (1996) Buckminsterfullerenol free radical scavengers reduce excitotoxic and apoptotic death of cultured cortical neurons. Neurobiol Dis 3(2):129–135. https://doi.org/10.1006/nbdi.1996.0013
145. Pasquato L, Rancan F, Scrimin P, Mancin F, Frigeri C (2000) N-methylimidazole-functionalized gold nanoparticles as catalysts for cleavage of a carboxylic acid ester. Chem Commun 2(22):2253–2254. https://doi.org/10.1039/b005244m
146. Tarnuzzer RW, Colon J, Patil S, Seal S (2005) Vacancy engineered ceria nanostructures for protection from radiation-induced cellular damage. Nano Lett 5(12):2573–2577. https://doi.org/10.1021/nl052024f
147. Dugan LL, Turetsky DM, Du C, Lobner D, Wheeler M, Almli CR, Shen CK-F, Luh T-Y, Choi DW, Lin T-S (1997) Carboxyfullerenes as neuroprotective agents. Proc Natl Acad Sci 94(17):9434–9439. https://doi.org/10.1073/pnas.94.17.9434
148. Chen J, Patil S, Seal S, McGinnis JF (2006) Rare Earth nanoparticles prevent retinal degeneration induced by intracellular peroxides. Nat Nanotechnol 1(2):142–150. https://doi.org/10.1038/nnano.2006.91
149. Tokuyama H, Yamago S, Nakamura E, Shiraki T, Sugiura Y (1993) Photoinduced biochemical activity of fullerene carboxylic acid. J Am Chem Soc 115(17):7918–7919. https://doi.org/10.1021/ja00070a064
150. Gao L, Zhuang J, Nie L, Zhang J, Zhang Y, Gu N, Wang T, Feng J, Yang D, Perrett S, Yan X (2007) Intrinsic peroxidase-like activity of ferromagnetic nanoparticles. Nat Nanotechnol 2(9):577–583. https://doi.org/10.1038/nnano.2007.260

151. Xie J, Zhang X, Wang H, Zheng H, Huang Y, Xie J (2012) Analytical and environmental applications of nanoparticles as enzyme mimetics. TrAC - Trends Anal. Chem. 39:114–129. https://doi.org/10.1016/j.trac.2012.03.021
152. Na HX, Bo LJ, Shuai H, Tao W, Qi LW, Ke Z, Wei HW, Lu JY, Xuan RH, Qi W, Chun WX (2011) Research progress of nanoparticles as enzyme mimetics. Sci China Physics Mech Astron 54(10):1749–1756. https://doi.org/10.1007/s11433-011-4480-0
153. Zu Y, Ting AL, Gao Z (2011) Visualizing Low-level point mutations: enzyme-like selectivity offered by nanoparticle probes. Small 7(3):306–310. https://doi.org/10.1002/smll.201001774
154. Tseng CW, Chang HY, Chang JY, Huang CC (2012) Detection of mercury ions based on mercury-induced switching of enzyme-like activity of platinum/gold nanoparticles. Nanoscale 4(21):6823–6830. https://doi.org/10.1039/c2nr31716h
155. Lien CW, Chen YC, Chang HT, Huang CC (2013) Logical Regulation of the enzyme-like activity of gold nanoparticles by using heavy metal ions. Nanoscale 5(17):8227–8234. https://doi.org/10.1039/c3nr01836a
156. Long YJ, Li YF, Liu Y, Zheng JJ, Tang J, Huang CZ (2011) Visual observation of the mercury-stimulated peroxidase mimetic activity of gold nanoparticles. Chem Commun 47(43):11939–11941. https://doi.org/10.1039/c1cc14294a
157. Chang Q, Deng K, Zhu L, Jiang G, Yu C, Tang H (2009) Determination of hydrogen peroxide with the aid of peroxidase-like fe 3o4 magnetic nanoparticles as the catalyst. Microchim Acta 165(3–4):299–305. https://doi.org/10.1007/s00604-008-0133-z
158. Chen Z, Yin JJ, Zhou YT, Zhang Y, Song L, Song M, Hu S, Gu N (2012) Dual enzyme-like activities of iron oxide nanoparticles and their implication for diminishing cytotoxicity. ACS Nano 6(5):4001–4012. https://doi.org/10.1021/nn300291r
159. Liang M, Yan X (2019) Nanozymes: from new concepts, mechanisms, and standards to applications. Acc Chem Res 52(8):2190–2200. https://doi.org/10.1021/acs.accounts.9b00140
160. Jiang B, Duan D, Gao L, Zhou M, Fan K, Tang Y, Xi J, Bi Y, Tong Z, Gao GF, Xie N, Tang A, Nie G, Liang M, Yan X (2018) Standardized assays for determining the catalytic activity and kinetics of peroxidase-like nanozymes. Nat Protoc 13(7):1506–1520. https://doi.org/10.1038/s41596-018-0001-1
161. Ramanavičius A, Kaušaite A, Ramanavičiene A (2005) Polypyrrole-coated glucose oxidase nanoparticles for biosensor design. Sensors Actuators B Chem 111–112(SUPPL.):532–539. https://doi.org/10.1016/j.snb.2005.03.038
162. Anusha JR, Raj CJ, Cho BB, Fleming AT, Yu KH, Kim BC (2015) Amperometric glucose biosensor based on glucose oxidase immobilized over chitosan nanoparticles from gladius of uroteuthis duvauceli. Sensors Actuators B Chem 215:536–543. https://doi.org/10.1016/j.snb.2015.03.110
163. Manea F, Houillon FB, Pasquato L, Scrimin P (2004) Nanozymes: gold-nanoparticle-based transphosphorylation catalysts. Angew. Chemie - Int. Ed. 43(45):6165–6169. https://doi.org/10.1002/anie.200460649
164. Wei H, Wang E (2013) nanomaterials with enzyme-like characteristics (nanozymes): next-generation artificial enzymes. Chem Soc Rev 42(14):6060–6093. https://doi.org/10.1039/c3cs35486e
165. Benedetti TM, Andronescu C, Cheong S, Wilde P, Wordsworth J, Kientz M, Tilley RD, Schuhmann W, Gooding JJ (2018) Electrocatalytic nanoparticles that mimic the three-dimensional geometric architecture of enzymes: nanozymes. J Am Chem Soc 140(41):13449–13455. https://doi.org/10.1021/jacs.8b08664
166. Gooding JJ (2019) Can nanozymes have an impact on sensing? ACS Sensors 4(9):2213–2214. https://doi.org/10.1021/acssensors.9b01760
167. Cuenya BR (2010) Synthesis and catalytic properties of metal nanoparticles: size, shape, support, composition, and oxidation state effects. Thin Solid Films 518(12):3127–3150. https://doi.org/10.1016/j.tsf.2010.01.018
168. Ye H, Liu Y, Chhabra A, Lilla E, Xia X (2017) Polyvinylpyrrolidone (PVP)-capped Pt nanocubes with superior peroxidase-like activity. ChemNanoMat 3(1):33–38. https://doi.org/10.1002/cnma.201600268

169. Garg B, Bisht T (2016) Carbon nanodots as peroxidase nanozymes for biosensing. Molecules 21(12):1–16. https://doi.org/10.3390/molecules21121653
170. Yang W, Huang TT, Zhao M, Luo F, Weng W, Wei Q, Lin Z, Chen G (2016) High peroxidase-like activity of iron and nitrogen co-doped carbon dots and its application in immunosorbent assay. Talanta 2017(164):1–6. https://doi.org/10.1016/j.talanta.2016.10.099
171. Tian R, Sun J, Qi Y, Zhang B, Guo S, Zhao M (2017) Influence of VO2 nanoparticle morphology on the colorimetric assay of H2O2 and glucose. Nanomaterials 7(11). https://doi.org/10.3390/nano7110347
172. Qiao F, Wang J, Ai S, Li L (2015) As a new peroxidase mimetics: the synthesis of selenium doped graphitic carbon nitride nanosheets and applications on colorimetric detection of H_2O_2 and xanthine. Sensors Actuators B Chem 216:418–427. https://doi.org/10.1016/j.snb.2015.04.074
173. Dong Y, Li J, Shi L, Guo Z (2015) Iron impurities as the active sites for peroxidase-like catalytic reaction on graphene and its derivatives. ACS Appl Mater Interfaces 7(28):15403–15413. https://doi.org/10.1021/acsami.5b03486
174. Wei J, Chen X, Shi S, Mo S, Zheng N (2015) An investigation of the mimetic enzyme activity of two-dimensional Pd-based nanostructures. Nanoscale 7(45):19018–19026. https://doi.org/10.1039/c5nr05675f
175. Huang L, Zhu W, Zhang W, Chen K, Wang J, Wang R, Yang Q, Hu N, Suo Y, Wang J (2018) Layered vanadium(IV) disulfide nanosheets as a peroxidase-like nanozyme for colorimetric detection of glucose. Microchim Acta 185(1):1–8. https://doi.org/10.1007/s00604-017-2552-1
176. Jiang C, Zhu J, Li Z, Luo J, Wang J, Sun Y (2017) Chitosan-gold nanoparticles as peroxidase mimic and their application in glucose detection in serum. RSC Adv 7(70):44463–44469. https://doi.org/10.1039/c7ra08967h
177. Singh R, Belgamwar R, Dhiman M, Polshettiwar V (2018) Dendritic fibrous nano-silica supported gold nanoparticles as an artificial enzyme. J Mater Chem B 6(11):1600–1604. https://doi.org/10.1039/c8tb00310f
178. Liu Y, Wang C, Cai N, Long S, Yu F (2014) Negatively charged gold nanoparticles as an intrinsic peroxidase mimic and their applications in the oxidation of dopamine. J Mater Sci 49(20):7143–7150. https://doi.org/10.1007/s10853-014-8422-x
179. Han TH, Khan MM, Lee J, Cho MH (2014) Optimization of positively charged gold nanoparticles synthesized using a stainless-steel mesh and its application for colorimetric hydrogen peroxide detection. J Ind Eng Chem 20(4):2003–2009. https://doi.org/10.1016/j.jiec.2013.09.023
180. Pan Y, Li N, Mu J, Zhou R, Xu Y, Cui D, Wang Y, Zhao M (2015) Biogenic magnetic nanoparticles from burkholderia Sp. YN01 exhibiting intrinsic peroxidase-like activity and their applications. Appl Microbiol Biotechnol 99(2):703–715. https://doi.org/10.1007/s00253-014-5938-6
181. Woo MA, Kim MII, Jung JH, Park KS, Seo TS, Park HG (2013) A novel colorimetric immunoassay utilizing the peroxidase mimicking activity of magnetic nanoparticles. Int J Mol Sci 14(5):9999–10014. https://doi.org/10.3390/ijms14059999
182. Can Z, Üzer A, Türkekul K, Erçaı E, Apak R (2015) Determination of triacetone triperoxide with a N, N-Dimethyl-p-phenylenediamine sensor on nafion using Fe3O4 magnetic nanoparticles. Anal Chem 87(19):9589–9594. https://doi.org/10.1021/acs.analchem.5b01775
183. Cheng R, Li GQ, Cheng C, Shi L, Zheng X, Ma Z (2015) Catalytic oxidation of 4-chlorophenol with magnetic Fe3O4 nanoparticles: mechanisms and particle transformation. RSC Adv 5(82):66927–66933. https://doi.org/10.1039/c5ra10433e
184. Liu Y, Purich DL, Wu C, Wu Y, Chen T, Cui C, Zhang L, Cansiz S, Hou W, Wang Y, Yang S, Tan W (2015) Ionic functionalization of hydrophobic colloidal nanoparticles to form ionic nanoparticles with enzymelike properties. J Am Chem Soc 137(47):14952–14958. https://doi.org/10.1021/jacs.5b08533
185. Li W, Chen B, Zhang H, Sun Y, Wang J, Zhang J, Fu Y (2015) BSA-stabilized Pt nanozyme for peroxidase mimetics and its application on colorimetric detection of mercury(II) ions. Biosens Bioelectron 66:251–258. https://doi.org/10.1016/j.bios.2014.11.032

186. He SB, Deng HH, Liu AL, Li GW, Lin XH, Chen W, Xia XH (2014) Synthesis and peroxidase-like activity of salt-resistant platinum nanoparticles by using bovine serum albumin as the scaffold. ChemCatChem 6(6):1543–1548. https://doi.org/10.1002/cctc.201400011
187. Karim MN, Anderson SR, Singh S, Ramanathan R, Bansal V (2018) Nanostructured silver fabric as a free-standing nanozyme for colorimetric detection of glucose in urine. Biosens Bioelectron 110(March):8–15. https://doi.org/10.1016/j.bios.2018.03.025
188. Sloan-Dennison S, Laing S, Shand NC, Graham D, Faulds K (2017) A novel nanozyme assay utilising the catalytic activity of silver nanoparticles and SERRS. Analyst 142(13):2484–2490. https://doi.org/10.1039/c7an00887b
189. Zhang R, He S, Zhang C, Chen W (2015) Three-dimensional Fe- and N-incorporated carbon structures as peroxidase mimics for fluorescence detection of hydrogen peroxide and glucose. J Mater Chem B 3(20):4146–4154. https://doi.org/10.1039/c5tb00413f
190. Cai K, Lv Z, Chen K, Huang L, Wang J, Shao F, Wang Y, Han H (2013) Aqueous synthesis of porous platinum nanotubes at room temperature and their intrinsic peroxidase-like activity. Chem Commun 49(54):6024–6026. https://doi.org/10.1039/c3cc41880d
191. Xie J, Zhang X, Jiang H, Wang S, Liu H, Huang Y (2014) V2O5 nanowires as a robust and efficient peroxidase mimic at high temperature in aqueous media. RSC Adv 4(50):26046–26049. https://doi.org/10.1039/c4ra03118k
192. Vernekar AA, Sinha D, Srivastava S, Paramasivam PU, D'Silva P, Mugesh G (2014) An antioxidant nanozyme that uncovers the cytoprotective potential of vanadia nanowires. Nat Commun 5. https://doi.org/10.1038/ncomms6301
193. Natalio F, André R, Hartog AF, Stoll B, Jochum KP, Wever R, Tremel W (2012) Vanadium pentoxide nanoparticles mimic vanadium haloperoxidases and thwart biofilm formation. Nat Nanotechnol 7(8):530–535. https://doi.org/10.1038/nnano.2012.91
194. Gao C, Zhu H, Chen J, Qiu H (2017) Facile synthesis of enzyme functional metal-organic framework for colorimetric detecting h2o2 and ascorbic acid. Chinese Chem Lett 28(5):1006–1012. https://doi.org/10.1016/j.cclet.2017.02.011
195. Lin T, Qin Y, Huang Y, Yang R, Hou L, Ye F, Zhao S (2018) A label-free fluorescence assay for hydrogen peroxide and glucose based on the bifunctional MIL-53(Fe) nanozyme. Chem Commun 54(14):1762–1765. https://doi.org/10.1039/c7cc09819g
196. Ortiz-Gómez I, Salinas-Castillo A, García AG, Álvarez-Bermejo JA, de Orbe-Payá I, Rodríguez-Diéguez A, Capitán-Vallvey LF (2018) Microfluidic paper-based device for colorimetric determination of glucose based on a metal-organic framework acting as peroxidase mimetic. Microchim. Acta 185(1). https://doi.org/10.1007/s00604-017-2575-7
197. Wan S, Wang Q, Ye H, Kim MJ, Xia X (2018) Pd–Ru bimetallic nanocrystals with a porous structure and their enhanced catalytic properties. Part Part Syst Charact 35(5):1–5. https://doi.org/10.1002/ppsc.201700386
198. Fu XM, Liu ZJ, Cai SX, Zhao YP, Wu DZ, Li CY, Chen JH (2016) Electrochemical aptasensor for the detection of vascular endothelial growth factor (VEGF) based on DNA-templated Ag/Pt bimetallic nanoclusters. Chinese Chem Lett 27(6):920–926. https://doi.org/10.1016/j.cclet.2016.04.014
199. Ren X, Liu J, Ren J, Tang F, Meng X (2015) One-pot synthesis of active copper-containing carbon dots with laccase-like activities. Nanoscale 7(46):19641–19646. https://doi.org/10.1039/c5nr04685h
200. Liu J, Jiang X, Wang L, Hu Z, Wen T, Liu W, Yin J, Chen C, Wu X (2015) Ferroxidase-like activity of Au Nanorod/Pt Nanodot structures and implications for cellular oxidative stress. Nano Res 8(12):4024–4037. https://doi.org/10.1007/s12274-015-0904-x
201. Lee JW, Yoon S, Lo YM, Wu H, Lee SY, Moon B (2015) Intrinsic polyphenol oxidase-like activity of gold@platinum nanoparticles. RSC Adv 5(78):63757–63764. https://doi.org/10.1039/c5ra07636f
202. Ragg R, Natalio F, Tahir MN, Janssen H, Kashyap A, Strand D, Strand S, Tremel W (2014) Molybdenum trioxide nanoparticles with intrinsic sulfite oxidase activity. ACS Nano 8(5):5182–5189. https://doi.org/10.1021/nn501235j

203. Odrozek K, Maresz K, Koreniuk A, Prusik K, Mrowiec-Białoń J (2014) Amine-stabilized small gold nanoparticles supported on AlSBA-15 as effective catalysts for aerobic glucose oxidation. Appl Catal A Gen 475:203–210. https://doi.org/10.1016/j.apcata.2014.01.024
204. Delidovich IV, Moroz BL, Taran OP, Gromov NV, Pyrjaev PA, Prosvirin IP, Bukhtiyarov VI, Parmon VN (2013) Aerobic selective oxidation of glucose to gluconate catalyzed by Au/Al2O3 and Au/C: impact of the mass-transfer processes on the overall kinetics. Chem Eng J 223:921–931. https://doi.org/10.1016/j.cej.2012.11.073
205. Miedziak PJ, Alshammari H, Kondrat SA, Clarke TJ, Davies TE, Morad M, Morgan DJ, Willock DJ, Knight DW, Taylor SH, Hutchings GJ (2014) Base-free glucose oxidation using air with supported gold catalysts. Green Chem 16(6):3132–3141. https://doi.org/10.1039/c4gc00087k
206. Ma C, Xue W, Li J, Xing W, Hao Z (2013) Mesoporous carbon-confined Au catalysts with superior activity for selective oxidation of glucose to gluconic acid. Green Chem 15(4):1035–1041. https://doi.org/10.1039/c3gc36891b
207. Wang Y, He C, Li W, Zhang J, Fu Y (2017) Catalytic performance of oligonucleotide-templated pt nanozyme evaluated by laccase substrates. Catal. Letters 147(8):2144–2152. https://doi.org/10.1007/s10562-017-2106-5
208. Liu Y, Wu H, Chong Y, Wamer WG, Xia Q, Cai L, Nie Z, Fu PP, Yin JJ (2015) Platinum nanoparticles: efficient and stable catechol oxidase mimetics. ACS Appl Mater Interfaces 7(35):19709–19717. https://doi.org/10.1021/acsami.5b05180
209. Fernandez-Garcia S, Jiang L, Tinoco M, Hungria AB, Han J, Blanco G, Calvino JJ, Chen X (2016) Enhanced hydroxyl radical scavenging activity by doping lanthanum in ceria nanocubes. J Phys Chem C 120(3):1891–1901. https://doi.org/10.1021/acs.jpcc.5b09495
210. Xu ZQ, Lan JY, Jin JC, Dong P, Jiang FL, Liu Y (2015) Highly photoluminescent nitrogen-doped carbon nanodots and their protective effects against oxidative stress on cells. ACS Appl Mater Interfaces 7(51):28346–28352. https://doi.org/10.1021/acsami.5b08945
211. Wang Z, Wang S, Lu Z, Gao X (2015) Syntheses, structures and antioxidant activities of fullerenols: knowledge learned at the atomistic level. J Clust Sci 26(2):375–388. https://doi.org/10.1007/s10876-015-0855-0
212. Pulido-Reyes G, Rodea-Palomares I, Das S, Sakthivel TS, Leganes F, Rosal R, Seal S, Fernández-Pinãs F (2015) Untangling the biological effects of cerium oxide nanoparticles: the role of surface valence states. Sci Rep 5:1–14. https://doi.org/10.1038/srep15613
213. Vernekar AA, Mugesh G (2012) Hemin-functionalized reduced graphene oxide nanosheets reveal peroxynitrite reduction and isomerization activity. Chem A EurJ 18(47):15122–15132. https://doi.org/10.1002/chem.201202272
214. Ren X, Meng X, Ren J, Tang F (2016) Graphitic carbon nitride nanosheets with tunable optical properties and their superoxide dismutase mimetic ability. RSC Adv 6(95):92839–92844. https://doi.org/10.1039/c6ra21624b
215. Fan K, Xi J, Fan L, Wang P, Zhu C, Tang Y, Xu X, Liang M, Jiang B, Yan X, Gao L (2018) In vivo guiding nitrogen-doped carbon nanozyme for tumor catalytic therapy. Nat Commun 9(1). https://doi.org/10.1038/s41467-018-03903-8
216. Bhushan B, Gopinath P (2015) Antioxidant nanozyme: a facile synthesis and evaluation of the reactive oxygen species scavenging potential of nanoceria encapsulated albumin nanoparticles. J Mater Chem B 3(24):4843–4852. https://doi.org/10.1039/c5tb00572h
217. Baldim V, Bedioui F, Mignet N, Margaill I, Berret JF (2018) The enzyme-like catalytic activity of cerium oxide nanoparticles and its dependency on Ce3+ surface area concentration. Nanoscale 10(15):6971–6980. https://doi.org/10.1039/c8nr00325d
218. Hijaz M, Das S, Mert I, Gupta A, Al-Wahab Z, Tebbe C, Dar S, Chhina J, Giri S, Munkarah A, Seal S, Rattan R (2016) Folic acid tagged nanoceria as a novel therapeutic agent in ovarian cancer. BMC Cancer 16(1):1–14. https://doi.org/10.1186/s12885-016-2206-4
219. Szymanski CJ, Munusamy P, Mihai C, Xie Y, Hu D, Gilles MK, Tyliszczak T, Thevuthasan S, Baer DR, Orr G (2015) Shifts in oxidation states of cerium oxide nanoparticles detected inside intact hydrated cells and organelles. Biomaterials 62:147–154. https://doi.org/10.1016/j.biomaterials.2015.05.042

220. Yang ZY, Luo SL, Li H, Dong SW, He J, Jiang H, Li R, Yang XC (2014) Alendronate as a robust anchor for ceria nanoparticle surface coating: facile binding and improved biological properties. RSC Adv 4(104):59965–59969. https://doi.org/10.1039/c4ra12007h
221. Liu Y, Ai K, Ji X, Askhatova D, Du R, Lu L, Shi J (2017) Comprehensive insights into the multi-antioxidative mechanisms of melanin nanoparticles and their application to protect brain from injury in ischemic stroke. J Am Chem Soc 139(2):856–862. https://doi.org/10.1021/Jacs.6b11013
222. Zhang Q, He X, Han A, Tu Q, Fang G, Liu J, Wang S, Li H (2016) Artificial hydrolase based on carbon nanotubes conjugated with peptides. Nanoscale 8(38):16851–16856. https://doi.org/10.1039/c6nr05015h
223. Ma X, Zhang L, Xia M, Li S, Zhang X, Zhang Y (2017) Mimicking the active sites of organophosphorus hydrolase on the backbone of graphene oxide to destroy nerve agent simulants. ACS Appl Mater Interfaces 9(25):21089–21093. https://doi.org/10.1021/acsami.7b07770
224. He X, Zhang F, Liu J, Fang G, Wang S (2017) Homogenous graphene oxide-peptide nanofiber hybrid hydrogel as biomimetic polysaccharide hydrolase. Nanoscale 9(45):18066–18074. https://doi.org/10.1039/c7nr06525f
225. Hostert L, Blaskievicz SF, Fonsaca JES, Domingues SH, Zarbin AJG, Orth ES (2017) Imidazole-derived graphene nanocatalysts for organophosphate destruction: powder and thin film heterogeneous reactions. J Catal 356:75–84. https://doi.org/10.1016/j.jcat.2017.10.008
226. Salvio R, Cincotti A (2014) Guanidine based self-assembled monolayers on au nanoparticles as artificial phosphodiesterases. RSC Adv 4(54):28678–28682. https://doi.org/10.1039/c4ra03150d
227. Diez-Castellnou M, Mancin F, Scrimin P (2014) Efficient phosphodiester cleaving nanozymes resulting from multivalency and local medium polarity control. J Am Chem Soc 136(4):1158–1161. https://doi.org/10.1021/ja411969e
228. Yapar S, Oikonomou M, Velders AH, Kubik S (2015) Dipeptide recognition in water mediated by mixed monolayer protected gold nanoparticles. Chem Commun 51(75):14247–14250. https://doi.org/10.1039/c5cc05909g
229. Chen JLY, Pezzato C, Scrimin P, Prins LJ (2016) Chiral nanozymes-gold nanoparticle-based transphosphorylation catalysts capable of enantiomeric discrimination. Chem A Eur J 22(21):7028–7032. https://doi.org/10.1002/chem.201600853
230. Lee DT, Zhao J, Peterson GW, Parsons GN (2017) Catalytic, "MOF-Cloth" formed via directed supramolecular assembly of UiO-66-NH2 crystals on atomic layer deposition-coated textiles for rapid degradation of chemical warfare agent simulants. Chem Mater 29(11):4894–4903. https://doi.org/10.1021/acs.chemmater.7b00949
231. Islamoglu T, Atilgan A, Moon SY, Peterson GW, Decoste JB, Hall M, Hupp JT, Farha OK (2017) Cerium(IV) vs zirconium(IV) based metal-organic frameworks for detoxification of a nerve agent. Chem Mater 29(7):2672–2675. https://doi.org/10.1021/acs.chemmater.6b04835
232. McCarthy DL, Liu J, Dwyer DB, Troiano JL, Boyer SM, Decoste JB, Bernier WE, Jones WE (2017) Electrospun metal-organic framework polymer composites for the catalytic degradation of methyl paraoxon. New J Chem 41(17):8748–8753. https://doi.org/10.1039/c7nj00525c
233. Sui M, Kunwar S, Pandey P, Lee J (2019) Strongly confined localized surface plasmon resonance (LSPR) Bands of Pt, AgPt AgAuPt nanoparticles. Sci Rep 9(1):1–14. https://doi.org/10.1038/s41598-019-53292-1
234. Boote BW, Alves RA thin films of Ag—Au nanoparticles dispersed in TiO 2: influence of composition and microstructure on the LSPR and SERS responses
235. Genç A, Patarroyo J, Sancho-Parramon J, Bastús NG, Puntes V, Arbiol J (2017) Hollow metal nanostructures for enhanced plasmonics: synthesis, local plasmonic properties and applications. Nanophotonics 6(1):193–213. https://doi.org/10.1515/nanoph-2016-0124
236. Mayer KM, Hafner JH (2011) Localized surface plasmon resonance sensors. Chem Rev 111(6):3828–3857. https://doi.org/10.1021/cr100313v

237. Liu Y, Ding D, Zhen Y, Guo R (2017) Amino acid-mediated 'Turn-off/Turn-on' nanozyme activity of gold nanoclusters for sensitive and selective detection of copper ions and histidine. Biosens Bioelectron 92:140–146. https://doi.org/10.1016/j.bios.2017.01.036
238. Sun Y, Wang J, Li W, Zhang J, Zhang Y, Fu Y (2015) DNA-stabilized bimetallic nanozyme and its application on colorimetric assay of biothiols. Biosens Bioelectron 74:1038–1046. https://doi.org/10.1016/j.bios.2015.08.001
239. Cho S, Shin HY, Mil Kim (2017) Nanohybrids consisting of magnetic nanoparticles and gold nanoclusters as effective peroxidase mimics and their application for colorimetric detection of glucose. Biointerphases 12(1):01A401. https://doi.org/10.1116/1.4974198
240. Wu Y, Chen Y, Li Y, Huang J, Yu H, Wang Z (2018) Accelerating peroxidase-like activity of gold nanozymes using purine derivatives and its application for monitoring of occult blood in urine. Sensors Actuators B Chem 270(May):443–451. https://doi.org/10.1016/j.snb.2018.05.057
241. Long L, Liu J, Lu K, Zhang T, Xie Y, Ji Y, Wu X (2018) Highly sensitive and robust peroxidase-like activity of Au-Pt core/shell nanorod-antigen conjugates for measles virus diagnosis. J Nanobiotechnol 16(1):1–10. https://doi.org/10.1186/s12951-018-0371-0
242. Ahmed SR, Kim J, Suzuki T, Lee J, Park EY (2016) Enhanced catalytic activity of gold nanoparticle-carbon nanotube hybrids for influenza virus detection. Biosens Bioelectron 85:503–508. https://doi.org/10.1016/j.bios.2016.05.050
243. Oh S, Kim J, Tran VT, Lee DK, Ahmed SR, Hong JC, Lee J, Park EY, Lee J (2018) Magnetic nanozyme-linked immunosorbent assay for ultrasensitive influenza a virus detection. ACS Appl Mater Interfaces 10(15):12534–12543. https://doi.org/10.1021/acsami.8b02735
244. Fu Z, Zeng W, Cai S, Li H, Ding J, Wang C, Chen Y, Han N, Yang R (2021) Porous Au@Pt nanoparticles with superior peroxidase-like activity for colorimetric detection of spike protein of SARS-CoV-2. J Colloid Interface Sci 604:113–121. https://doi.org/10.1016/j.jcis.2021.06.170
245. Han KN, Choi JS, Kwon J (2017) Gold nanozyme-based paper chip for colorimetric detection of mercury ions. Sci Rep 7(1):1–7. https://doi.org/10.1038/s41598-017-02948-x
246. Xie ZJ, Bao XY, Peng CF (2018) Highly sensitive and selective colorimetric detection of methylmercury based on DNA functionalized gold nanoparticles. Sensors (Switzerland) 18(8). https://doi.org/10.3390/s18082679
247. Weerathunge P, Ramanathan R, Shukla R, Sharma TK, Bansal V (2014) Aptamer-controlled reversible inhibition of gold nanozyme activity for pesticide sensing. Anal Chem 86(24):11937–11941. https://doi.org/10.1021/ac5028726
248. Zheng X, Liu Q, Jing C, Li Y, Li D, Luo W, Wen Y, He Y, Huang Q, Long YT, Fan C (2011) Catalytic gold nanoparticles for nanoplasmonic detection of DNA hybridization. Angew. Chemie - Int. Ed. 50(50):11994–11998. https://doi.org/10.1002/anie.201105121
249. Tian Y, Chen Y, Chen M, Song ZL, Xiong B, Zhang XB (2020) Peroxidase-like Au@Pt Nanozyme as an integrated nanosensor for Ag+ Detection by LSPR spectroscopy. Talanta 2021(221):121627. https://doi.org/10.1016/j.talanta.2020.121627
250. Liu X, Wan Y, Jiang T, Zhang Y, Huang P, Tang L (2020) Plasmon-activated nanozymes with enhanced catalytic activity by near-infrared light irradiation. Chem Commun 56(12):1784–1787. https://doi.org/10.1039/c9cc08223a
251. Liao X, Xu Q, Sun H, Liu W, Chen Y, Xia X-H, Wang C (2022) Plasmonic nanozymes: localized surface plasmonic resonance regulates reaction kinetics and antibacterial performance. J Phys Chem Lett 13(1):312–323. https://doi.org/10.1021/acs.jpclett.1c03804
252. Wang H, Zhao W, Zhao Y, Xu CH, Xu JJ, Chen HY (2020) Real-time tracking the electrochemical synthesis of Au@Metal core-shell nanoparticles toward photo enhanced methanol oxidation. Anal Chem 92(20):14006–14011. https://doi.org/10.1021/acs.analchem.0c02913
253. Pari S, Jha NS, Ganesan TS, Jha SK (2020) Pulse electrodeposited Au-WO3Catalyst from a water-ionic liquid microemulsion for photoaccelerated methanol electrooxidation. J Phys Chem C 124(40):21957–21967. https://doi.org/10.1021/acs.jpcc.0c05656
254. Pang L, Barras A, Mishyn V, Heyte S, Heuson E, Oubaha H, Sandu G, Melinte S, Boukherroub R, Szunerits S (2020) Plasmon-driven electrochemical methanol oxidation on gold nanohole

electrodes. ACS Appl Mater Interfaces 12(45):50426–50432. https://doi.org/10.1021/acsami.0c14436
255. Graf M, Vonbun-Feldbauer GB, Koper MTM (2021) Direct and broadband plasmonic charge transfer to enhance water oxidation on a gold electrode. ACS Nano 15(2):3188–3200. https://doi.org/10.1021/acsnano.0c09776
256. Shi F, He J, Zhang B, Peng J, Ma Y, Chen W, Li F, Qin Y, Liu Y, Shang W, Tao P, Song C, Deng T, Qian X, Ye J, Wu J (2019) Plasmonic-enhanced oxygen reduction reaction of silver/graphene electrocatalysts. Nano Lett 19(2):1371–1378. https://doi.org/10.1021/acs.nanolett.8b05053
257. Saada TN, Marques Da Silva AG, Subramanian P, Pang L, Adnane N, Djafari-Rouhani B, Mishyn V, Meziane D, Melinte S, Sandu G, Dumeignil F, Paul S, Wojcieszak R, Boukherroub R, Szunerits S (2020) Plasmon-enhanced electrocatalytic oxygen reduction in alkaline media on gold nanohole electrodes. J Mater Chem A 8(20):10395–10401. https://doi.org/10.1039/c9ta14174j
258. He LQ, Yang H, Huang JJ, Lu XH, Li GR, Liu XQ, Fang PP, Tong YX (2019) Enhanced catalytic activity of Au core Pd shell Pt cluster trimetallic nanorods for CO_2 reduction. RSC Adv 9(18):10168–10173. https://doi.org/10.1039/c8ra10494h
259. Wang C, Nie XG, Shi Y, Zhou Y, Xu JJ, Xia XH, Chen HY (2017) Direct plasmon-accelerated electrochemical reaction on gold nanoparticles. ACS Nano 11(6):5897–5905. https://doi.org/10.1021/acsnano.7b01637
260. Wang L, Zhu W, Lu W, Qin X, Xu X (2018) Surface plasmon aided high sensitive non-enzymatic glucose sensor using Au/NiAu multilayered nanowire arrays. Biosens Bioelectron 111(1):41–46. https://doi.org/10.1016/j.bios.2018.03.067
261. Tian Y, Cui Q, Xu L, Jiao A, Ma H, Wang C, Zhang M, Wang X, Li S, Chen M (2021) Alloyed AuPt Nanoframes Loaded on H-BN Nanosheets as an Ingenious Ultrasensitive near-Infrared Photoelectrochemical Biosensor for Accurate Monitoring Glucose in Human Tears. Biosens Bioelectron 192(April):113490. https://doi.org/10.1016/j.bios.2021.113490
262. Wang L, Zhu W, Lu W, Shi L, Wang R, Pang R, Cao YY, Wang F, Xu X (2019) One-step electrodeposition of AuNi nanodendrite arrays as photoelectrochemical biosensors for glucose and hydrogen peroxide detection. Biosens Bioelectron 142(1):111577. https://doi.org/10.1016/j.bios.2019.111577
263. Maji SK (2019) Plasmon-enhanced electrochemical biosensing of hydrogen peroxide from cancer cells by gold nanorods. ACS Appl Nano Mater 7162–7169. https://doi.org/10.1021/acsanm.9b01675
264. Miguel, V. M.; Rodrigues, M. P. D. S.; Braga, A. H.; de Torresi, S. I. C. MnO 2 Nanowires Decorated with Au Nanoparticles for Plasmon-Enhanced Electrocatalytic Detection of H 2 O 2. *ACS Appl. Nano Mater.* **2022**, acsanm.2c00218. https://doi.org/10.1021/acsanm.2c00218.

Carbon Nanomaterials in Electrochemical Biodevices

Thiago da Costa Oliveira and Steffane Quaresma Nascimento

Abstract A biosensor is a measuring system that contains a biological receptor unit that is highly selective for target analytes (DNA/RNA, proteins, or simple chemicals like glucose or hydrogen peroxide). Carbon nanomaterials (CNMs) are appealing possibilities for enhancing biosensor sensitivity while maintaining low detection limits due to their ability to immobilize a high number of bioreceptor units in a small space while also acting as a transducer. Furthermore, CNMs can be functionalized and conjugated with organic compounds or metallic nanoparticles; the generation of surface functional groups leads to the formation of nanomaterials with novel capabilities (electrical, physical, chemical, optical, and mechanical). CNMs have been frequently used in biosensor applications due to their fascinating features. Carbon nanotubes (CNTs) and carbon fibers (CFs) are used as scaffolds for biomolecule immobilization at their surfaces, as well as transducers for signal conversion involved in biological analyte recognition. This chapter provides an in-depth examination of the synthesis and functionalization of CNMs, as well as their potential applications in electrochemical devices (based primarily on the detection of current, potential, impedance, or other electrical property).

Keyword Carbon nanotubes · Carbon nanofibers · Nanomaterials functionalization · Biodevices · Electrochemical detection

1 Overview

Carbon atoms have a narrow band gap between their 2s and 2p electronic shells can undergo sp, sp^2, and sp^3 hybridizations. The two most well-known allotropic forms of carbon are diamond (sp^3 hybridization) and graphite (sp^2 hybridization) [1]. Graphite is the most widely used natural material option, with applications in a wide range of large-scale industrial technical problems. Because of the high demand for synthetic graphite in the market, its use has increased significantly in recent years.

T. da Costa Oliveira (✉) · S. Q. Nascimento
São Carlos Institute of Chemistry, University of São Paulo (USP), São Carlos, SP 13560-970, Brazil
e-mail: thiago.oliv.costa@gmail.com

F. N. Crespilho (ed.), *Advances in Bioelectrochemistry Volume 5*,
https://doi.org/10.1007/978-3-031-10832-7_3

Widespread scientific in-depth investigation into graphite has shown that its exclusive integration of physical and chemical features of stacked layers of hexagonal sp^2 carbon arrays. Over the last two decades, graphite has been used as a precursor material to generate a wide range of carbon nanomaterials using enhanced manufacturing processes and nanostructured materials, most notably fullerenes, single- and multi-walled nanotubes, and grapheme [2]. The geometrical structure of nanomaterial particles is the primary criterion for their classification, since nanomaterials have size-dependent physical, chemical, and biological properties. These particles may take the form of tubes, horns, spheres, or ellipsoids. CNTs and carbon nanohorns (CNHs) are tube or horn-shaped particles, respectively; fullerenes contain spherical or ellipsoidal nanoparticles [3]. Due to low toxicity and large-scale demand, CNMs have numerous technical uses in micro and nanoelectronics, gas storage, the fabrication of conductive polymers, composites, paints, textiles, batteries with extended lives, and biosensors [4].

According to their structural dimensions, NMs are divided into four classes (Fig. 1). Zero-dimensional nanomaterials (0D-NMs, i.e., fullerenes, particulate diamonds, and carbon dots) are nanoscale materials in all dimensions. One-dimensional nanoscale materials (1D-NMs, i.e., CNTs, CNFs, and diamond nanorods) have one dimension larger than nanoscale. Thin-sheet materials with nanoscale thickness are commonly referred to as two-dimensional NMs (2D-NMs, i.e., graphene, graphite sheets). Fibrous, powdery, polycrystalline, and multilayer materials are all examples of three-dimensional NMs (3D-NMs), which are made up of various building blocks, such as 0D-, 1D-, and 2D-NMs [5]. 2D hexagonal carbon lattices make up the majority of carbon nanostructures. However, in fact, employing a carbon lattice as a starting material hinders the creation of carbon nanostructures. Graphitic nanostructures are typically made by reorganizing carbon atoms from sources such as graphite, organic gases, or volatile organic compounds, as opposed to graphene nanoplatelets and multilayer carbon nanosheets that can be isolated from naturally occurring graphite, using instrumental techniques. Carbon vapor deposition (CVD), laser ablation, and arc discharge are the most popular methods [6, 7].

Because of their large surface area, CNMs have been widely used in electrochemical biosensors because many detection events can occur simultaneously on their surface and biomolecule attachment is easy. These materials have electrical, photonic, physical, and mechanical qualities that allow them to be used in biosensors [8]. These materials are inexpensive, have a wide voltage range over which the CNM electrode can perform, and have good electrocatalytic activity for a variety of redox systems (chemical and biological). Biosensors' electrochemical performance can be enhanced by altering their structure to modify their electrical, chemical, and structural properties for a given application [9]. CNMs-based surfaces can be easily tailored through various covalent and non-covalent functionalization methods, which improve their electrochemical sensing capabilities. Furthermore, these materials are highly biocompatible. Electrochemical sensors based on CNTs have higher sensitivity, selectivity, fast electron transfer rate, and low detection limits [10, 11].

Doping can have a significant impact on the electronic, mechanical, and conducting properties of CNTs [12]. Furthermore, the different types of CNMs

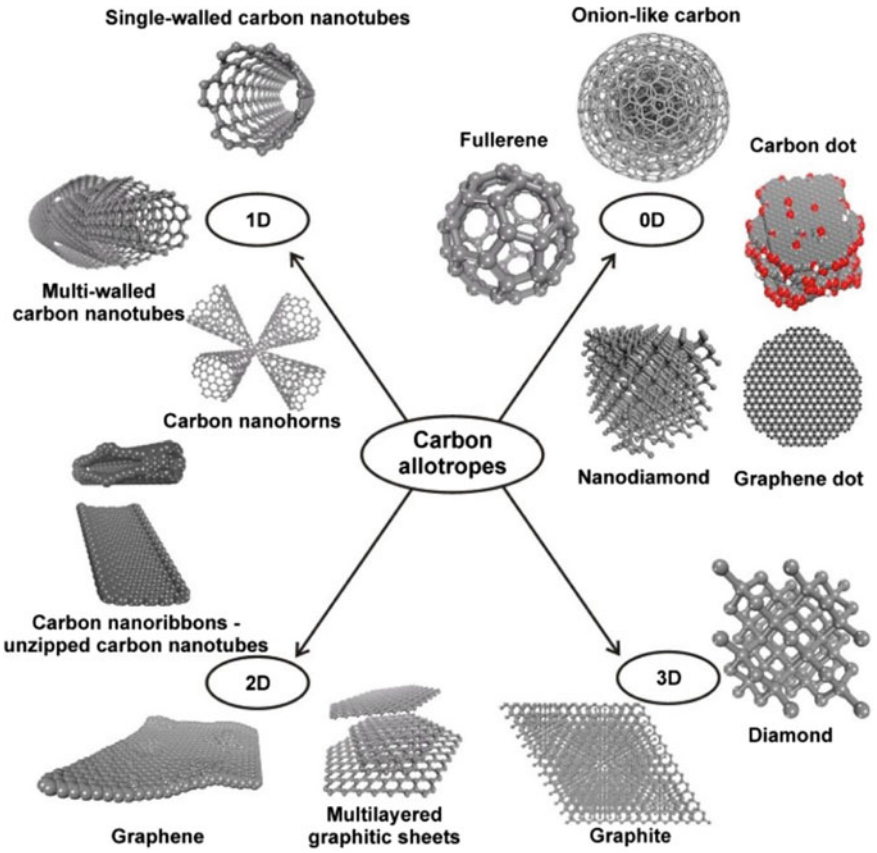

Fig. 1 Carbon nanoallotropes: Carbon dots, nanodiamond, fullerenes, carbon nanotubes, carbon nanohorns, graphene, carbon nanoribbons, and combined superstructures. Reprinted from [5] with permission

have different densities of states. The density of states of the CNMs-based electrode determines the electron transfer capabilities with target molecules. For a faster electron transfer process, the energy of electrons in the electrode should be equivalent to the energy of electrons in the redox reaction. The chance of electrons having enough high energy to transfer to the redox system grows as the density of states increases. The density of states in CNMs varies with structure and can be altered by modulating their atomic bonding patterns. It is also determined by the tube diameter in the case of CNTS. By carefully peeling off CNTs, the density of states can be enhanced. By altering the electronic structure of multi-walled CNTS, controlled oxidation can improve their electrochemical performance [5, 13]. Inorganic particles can be effectively chemically linked to CNMs to modify the electronic structure of each component, resulting in hybrid structures with synergistic electrocatalytic activity [9].

2 Carbon Nanomaterials

Fullerenes, C_{60} molecules of varying sizes (30–3000 carbon atoms), were found in the early 1980s. Fullerenes are closed hollow cages composed of sp^2-hybridized carbon atoms organized in 12 pentagons and a calculable number of hexagons based on the total amount of carbon atoms. A fullerene containing $20 + 2n$ carbon atoms will include n hexagons [5]. The closed shapes of the fullerenes dictate the number of pentagons, which is always 12 in those with perfect structures known as truncated icosahedral (stable carbon nanostructures). As a result, C_{60} and other fullerenes (C_{70}, C_{76}, C_{82}, and C_{84}) can be thought of as a carbon nanoallotrope with hybridization between sp^2 and sp^3 [8]. The carbon atom arrangement is pyramidalized rather than planar, and thus, a "pseudo"-sp^3-bonding component must be present in the essentially sp^2 carbons. C_{60} is succinctly a spherical molecule with an exterior diameter of 0.71 nm and chemical characteristics that are extremely comparable to organic molecules. It is, nonetheless, the smallest carbon nanostructure and a representative 0D carbon nanoallotrope [7]. Because of its ability to avoid the formation of double bonds in the pentagonal rings, the C_{60} molecule is commonly stated to be not superaromatic. There are two types of bond lengths discovered using an X-ray diffraction pattern, one with a length of 1.38 Å connecting C-atoms common to a couple of neighboring hexagons and the other with a length of 1.45 Å connecting C-atoms common to the pentagon-hexagon pair. Nowadays, vaporization of graphite by pyrolysis, radio-frequency-plasma, or arc discharge-plasma processes is widely used for commercial-scale production of fullerenes [14, 15].

Among the many investigations on fullerene, one of the most admirable discoveries is the ability of the C_{60} molecule to acquire from one to six electrons, even though it is already rich in electrons, forming equivalent anions. This is only feasible because the C_{60} molecule's non-binding LUMO molecular orbitals have an extremely low energy level [5]. Fullerenes also have good chemical stability, huge surface area, high mechanical resistance, and the ability to create a superconductor when mixed with alkali metals and can be easily modified with a wide range of functionalized chemicals via structural flaws or the intermediary production of epoxy rings [7]. Furthermore, fullerenes can interact hydrophobically with CNTs and graphene materials. Nevertheless, fullerenes have a high electron exchange capacity and can mediate electron transfer in the construction of various electrochemical sensors and biosensors with electrocatalytic response [15].

Carbon nanotubes (CNTs) are one of the allotropic modifications of carbon that were discovered in 1991 by Japanese scientist Iijima [16]. Using sp^2 hybridization, each carbon atom with three electrons forms trigonally coordinated bonds to three other carbon atoms in CNTs. CNT is made up of one layer of graphene that has been seamlessly rolled into the shape of a hollow tube. Carbon nanotubes are distinguished by rolled graphene sheets stacked in cylindrical/tubular structures with diameters of several nanometers. CNTs can vary in length, diameter, number of layers, and chirality vectors (symmetry of the nulled graphite sheet) [7].

CNTs are classified into two types based on their structures: single-walled carbon nanotubes (SWCNTs) and multi-walled carbon nanotubes (MWCNTs). **SWCNTs** are made by rolling a single layer of graphite (referred to as a graphene layer) into a seamless cylinder (long wrapped graphene sheets). SWCNTs have a length-to-diameter ratio of 1000 or larger, allowing them to be called a nearly one-dimensional structure, as previously stated. The majority of SWCNTs have a diameter of approximately 1–3 nm, (whereas MWCNTs have a diameter of 5–25 nm and a length of approximately 10 nm) [6]. Two separate areas with diverse physical and chemical properties form a SWCNT. The tube's sidewall is the first, and the tube's end cap is the second. The terminating cap is made up of pentagons and hexagons. The well-known C_{60} hemisphere appears to be the smallest cap that fits on to the cylinder of the carbon tube. This cap is well supported by the smallest experimental value of CNT diameter of 0.7 nm [17].

MWCNTs are a cluster of concentric SWCNTs of varied diameters (made of many layers of graphite rolled in on themselves to produce a tube shape). The length and diameter of these structures, as well as their characteristics, differ greatly from those of SWCNTs. MWCNTs have an interlayer distance of about 3.3 Å, which is comparable to the gap between graphene layers in graphite [6]. MWCNTs (double-walled carbon nanotubes, or DWCNTs) are a unique case that must be noted due to their morphology and features that are extremely similar to SWCNTs [18]. The gram-scale synthesis of DWCNTs was first proposed in 2003 by the chemical vapor deposition (CVD) technique, which involves the selective reduction of oxide solid solutions in methane and hydrogen [19].

The single layer of graphene in CNTs can be rolled in a variety of ways. The CNTs are classified as zigzag, armchair, or chiral based on the number of unit vectors in the graphene crystal lattice along two directions in the honeycomb structure, as can be seen in Fig. 2a. The chirality of carbon nanotubes has a significant impact on their properties. SWCNTs' electrical properties are determined by their chirality or hexagon orientation with respect to the tube axis [20]. The chirality of a CNT determines whether it is metallic or semiconducting in nature. The electrochemical properties of SWCNTs are determined by their roll-up vectors (n, m). The SWCNTs are metallic if the roll-up vectors $n - m = 3q$, where q can be any integer/zero. If $n - m = 3q$, the SWCNTs are semi-conductive. If $n = m$, the nanotubes are referred to as armchair. If $m = 0$, they are referred to as zigzag; otherwise, they are referred to as chiral [21]. Furthermore, depending on the diameter of the tubes, SWCNTs can exhibit electrical conductivity or semi-conductive properties. Armchair SWCNTs have higher electrical conductivity than copper, whereas zigzag and chiral SWCNTs have semi-conductive properties that allow them to be used in sensor fabrication [20–23].

When compared to other fibrous materials, CNTs have superior physical properties such as rigidity, strength, and elasticity. They have a higher aspect ratio (length-to-diameter ratio) than other materials. CNTs' high aspect ratios can range from 10^2 to 10^7 [23]. Because of their smaller diameter, SWCNTs have a higher aspect ratio than MWCNTs. In addition, they have high thermal and electrical conductivities when compared to other conductive materials. CNTs have a strength that is

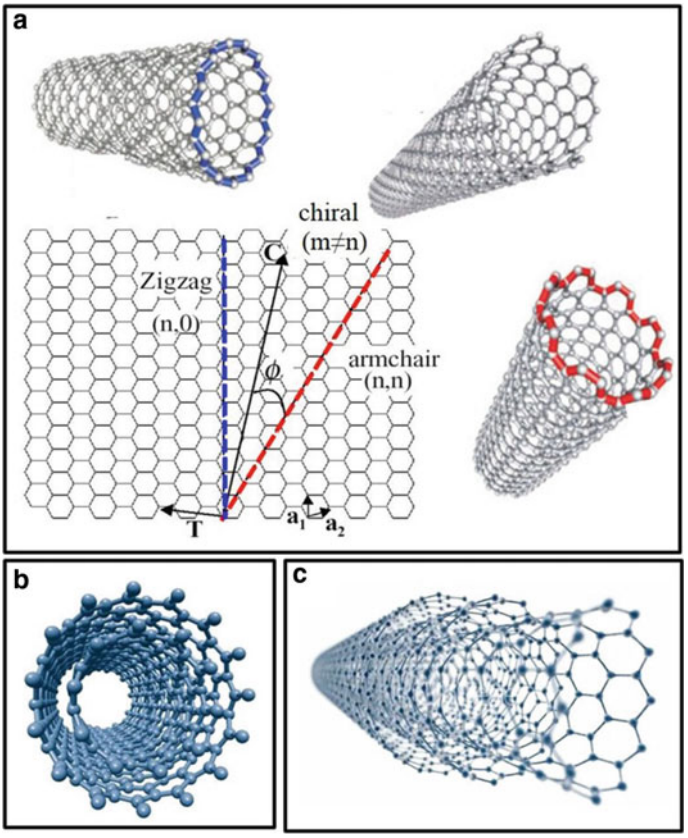

Fig. 2 Structure and models of carbon nanotubes in function of their number of walls. **a** Single-wall carbon nanotubes (SWCNTs) structures in function of their chirality (zigzag, armchair, and chiral); **b** double-walled carbon nanotubes (DWCNTs); and **c** multi-walled carbon nanotubes (MWCNTs) made up of several concentric sheets. Reprinted from [24] with permission

10–100 times that of strong steel at a fraction of the weight [25]. These nanomaterials do have such distinguishing characteristics that make them potential candidates for use in technological fields. Because of their high electron transfer capabilities, carbon nanotubes have been used as an electrode in electrochemical reactions [7, 26]. They can be used in electrochemical sensors because they allow electron transfer in chemical reactions at the electrode interface. CNTs have numerous applications in nano-electro-mechanical systems [4, 27, 28].

3 Synthesis

As aforementioned, carbon nanotubes were discovered in the carbon soot of graphite electrodes during an arc discharge experiment in 1991, using a current of 100 amps to produce fullerenes [16]. However, two researchers at NEC's Fundamental Research Laboratory produced the first macroscopic CNTs in 1992 [29]. The same method was used as in 1991. Because of the high temperatures caused by the discharge, the carbon contained in the negative electrode sublimates during this process. Because carbon nanotubes were discovered using this method, it has become the most widely used method of CNT synthesis.

First, a carbon arc discharge with a suitable catalyst was used to synthesize SWCNTs or MWCNTs with a high yield and greater control over the size of the synthesized nanotubes [6]. The CVD method has resulted in CNTs with smaller diameters, lower yield, but higher quality. The laser ablation method produces a lower yield and a much smaller diameter, but it produces much finer quality. Metallic and semi-conductive carbon nanotubes can be synthesized via selective functionalization, selective destruction via electrical heating, or separation via density gradient ultra-centrifugation [23].

Using transition metal nanoparticle catalysts, CVD was used to produce high-quality SWCNTs and MWCNTs in vertically aligned arrays. They were synthesized on a massive scale using arc discharge and CVD methods (Co-Mo catalysts). The CVD method, which requires simple equipment and mild temperature and pressure conditions, is better suited for large-scale CNT production than the other two methods. Vertically aligned arrays of CNTs were created using metallic and quasi-crystalline substrates. CNTs have been reported to be synthesized by pyrolyzing metal carbonyls in the presence of other hydrocarbons. The presence of transition metals in graphite electrodes has resulted in CNTs with higher product output and reproducibility [5]. Transition metal catalysts and the CVD method have been investigated to obtain high-quality CNTs in vertically aligned arrays. Catalysts are used in the CVD synthesis to grow nanotubes on substrates. Metallic nanoparticles are used as catalysts, and their size is determined by the diameter of the nanotubes to be synthesized (0.5–5 nm for SWCNTs, 8–10 nm for MWCNTs) [7]. Ni, Co, and Fe nanoparticles have been used as nano catalysts in the synthesis of CNTs. The CVD reactors use inert gas methane to produce SWCNTs and ethylene to produce MWCNTs. The substrate is heated to 850–1000 °C for SWCNTs and 550–700 °C for MWCNTs synthesis [6, 23]. Carbon is produced during the thermal decomposition of hydrocarbons and is dissolved in the metal nanocatalyst. When a certain concentration of carbon is reached, a semi-fullerene cap forms, which serves as the fundamental unit for the growth of the nanotube. Carbon is continuously flowed from the hydrocarbon source to the catalyst particle. Finally, CNTs are obtained following a purification process and the removal of catalysts from the tips and surfaces of nanotubes [30]. The final step is being researched so that high-quality synthesized material can be obtained.

When different carbon nanomaterials are purified, often with acid(s) at elevated temperatures and for extended periods of time, changes in the amount of metallic catalyst nanoparticles, surface functionalization of carbon, and overall morphology occur. Spectroscopic studies revealed that changes in the morphology of CNF, for example, were significant depending on their original morphology [31]. Although arc discharge and laser ablation methods produce a large amount of SWCNTs, they have drawbacks as well, such as the need to evaporate C-atoms from solid state sources at very high temperatures (>3000 °C), and the nanotubes bundle together during formation, which limits their applications [32]. The length of a CNT is determined by the time it takes for it to grow. The diameter of synthesized SWCNTs ranges from 0.7 to 3 nm, while MWCNTs range from 10 to 200 nm. Because of their large surface area, CNTs can effectively load various types of drugs on their internal and external surfaces [27].

Graphene nanoribbons (GNR): Thin ribbons of graphene monolayers are a new type of graphene that is gaining a lot of attention in the scientific community. The majority of research on these materials has concentrated on the thin elongated graphene monolayer strips that can be created by "unzipping" CNTs [9, 33]. Graphene nanoribbons are frequently described as a one-dimensional sp^2-hybridized carbon strip of finite dimension with defined edges, with carbon atoms that are not three-coordinated. Graphene nanoribbons are classified into three types based on their edge termination: (i) armchair, (ii) zigzag, (iii), and chiral nanoribbons [34]. Edge reconstruction is possible because the edge carbon atoms are not bound saturated. While the edge pattern of the armchair graphene nanoribbon is stable due to the presence of strong dangling bonds, edge reconstructions are expected at high temperatures for zigzag graphene nanoribbons. Hydrogen saturation is commonly used to stabilize the edge structure [35]. Other edge profiles involving pentagonal and heptagonal carbon rings have been observed; however, such edge reconstructions are extremely rare. Graphene nanoribbons, like graphene, can have bilayered or few-layered configurations; the design is designated a graphitic nanoribbon when more layers of finite graphene strips are placed together [36, 37].

Carbon nanodiamonds (CNDs) are a structural family of nanocarbons that includes fullerens, tubes, onions, and horns. The first nanoscale diamond particles were created in the 1960s by detonating carbon-containing explosives. However, it took nearly three decades after the initial discovery for these nanodiamonds to become more well-known in the scientific world. Only in the late 1990s did nanodiamonds begin to be studied more thoroughly, and they gradually began to find their way into various applications [31]. CNDs are diamondoid-like sp^3 carbon nanoparticles with sizes more than 1–2 nm but less than 20 nm. They are not dispersible, and thus, top-down processes like jet milling or microdiamond abrasion are used to make them. With diameters greater than 20 nm, this form of nanostructure acts as bulk diamonds [9]. Diamondoids, on the other hand, are naturally occurring sp^3 carbon nanostructures with diameters less than 1 nm found in petroleum deposits. The sp^3-hybridized surface-bound carbon atoms of these diamondoids are generally attached to hydrogen or other non-carbon atoms. As a result, they have properties that are more akin to organic molecules than bulk diamonds [31]. As the diameter of

the sp^3 carbon cluster increases, the percentage of carbon atoms at the surface drops, and the diamond feature of the nanoparticles becomes more prominent [38].

Nanodiamonds' size, shape, and quality are determined by the procedures employed to make them. Detonating an explosive mixture of carbon-containing substances such as trinitrotoluene and hexogen is the most well-known method for mass-producing nanodiamonds. Up to 75% of the resulting soot is made up of nanodiamonds with diameters of 4–5 nm and a limited size distribution. Because of their small size and narrow size distribution, they are a popular research topic. They tend to aggregate with each other if not thoroughly cleaned. Furthermore, they are relatively chemically inert while remaining reactive enough to allow functionalization. Another benefit is their large relative surface area, which can be used to effectively attach various compounds. They have high hardness, thermal conductivity, refractive index, coefficient of friction, insulation properties, and high biocompatibility [31, 39].

Carbon nanohorns. Iijima discovered SWNHs in 1999 while researching CNT formation [40]. Nanohorns are tubular/conical structures made of a single graphenic layer. They are typically found in large spherical aggregates with diameters ranging from 80 to 100 nm and resembling dahlia flowers. Individual nanohorns have diameters of 1–2 nm at the tips and 45 nm at the base of the cone. The wall-to-wall distance between SWNHs is approximately 0.4 nm [9]. Other types of SWNH aggregations were observed that resembled the characteristics of buds and seeds. Cones are formed by cutting a wedge from a single graphenic layer and connecting the exposed edges in a seamless manner. They are more easily synthesized than CNTs, on a larger scale, at room temperature without the use of metal catalysts. They can be created through the use of carbon rod arc discharge, laser ablation of pure graphite, and Joule heating. CNHs have a high surface area and good porosity, which can be used to their advantage in the field of biosensing [8].

Carbon dots (CDs) are *quasi-spherical* carbon nanoparticles with diameters of 2–10 nm that have a high oxygen content and composed of various volumetric ratios of graphitic and turbostratic carbon. CDs are typically amorphous and contain mostly sp^3-hybridized carbon [9]. Carbon nanodot, carbon quantum dot, and graphene quantum dot classes are mentioned in addition to CD classes. As a result, graphene quantum dots are frequently used in electrochemical sensors. They have a lateral dimension of about 100 nm and are made up of up to ten single atom layers with a visible graphene lattice [14]. CDs have been proved to be non-toxic in vitro experiments. They were also a promising candidate for biosensor components because of their capacity to operate as an electron donor and receiver. As a result, CDs are the CNM with the most biosensor publications, trailing only graphene and carbon nanotubes. Carbon nanodots are relatively smaller (spherical particles of about 10 nm in diameter). They are typically used in electrochemical sensor assemblies after being functionalized with redox labels or receptors [15].

Carbon nanodots are created utilizing a variety of processes, and there has been a surge of interest in carbon nanomaterials in recent years. Carbon nanodots are typically manufactured utilizing a top-down process based on a laser ablation strategy and treated mixes of graphite powder and cement. This process creates the main structure

of the carbon dots, which will then be treated with oxidative to enrich the surfaces of the carbon dots with reactive oxygen groups [14, 15]. Surface passivation occurs with a range of organic compounds and oligomers that are often incorporated on carbon dots. Because of the multiple advantages of the electrochemical etching strategy, such as abundant conductive carbonaceous substrates (graphite rod), abundant natural resources, and low cost, the electrochemical etching method, a top-down approach, is a viable method to create carbon nanodots [2]. Carbon nanodots' dimensions and chemical compositions can be easily adjusted by adjusting a variety of synthetic parameters such as pH, concentration, electrolyte composition, and electrochemical mode of electrolysis (potentiostatic, galvanostatic, and potential varying techniques, etc.). However, long-term stability, which is one of the most crucial features in a biosensor, is hardly obtained [5].

Carbon black (CB) belongs to the amorphous nanocarbon family, with average diameters ranging from 3 to 100 nm, and has lately been used in biosensing applications, compared to nanocarbons that are notable in biosensor applications [9]. It is a potential nanocarbon for biosensing applications because of its low cost, high analytical sensitivity, experimental simplicity, mobility, and good selectivity. CB has also been claimed to be a feasible alternative to other members of the family, such as graphene and graphene-like structures, fullerenes, and CNTs, and to boost the activity in enzyme biosensors, due to its high conductivity [5, 41]. Particle size, porosity, surface chemical characteristics, aggregate morphology, and surface area define the physical properties of CB, which is made up of sp^2 and sp^3 hybridized carbon atoms. CB is also frequently seen as a loosely bound agglomerates piled on top of one another [15]. This makes it difficult to collect consistent and rigorous data in the production operations of biomolecular applications of CB, such as obtained with graphene and graphene-like structures [7]. In addition, characterization methods for these structures, which are each a few unit cell size, are required.

4 Functionalization of CNMs

CNMs are regarded to be excellent building blocks for manufacturing nanoscale functionalized materials due to their huge surface area and outstanding electrical and mechanical capabilities. In order to develop diverse functionalized CNMs, a wide range of organic and inorganic NMs have been investigated to date. Based on the difference in bonding between CNMs and their functionalized derivatives, these techniques are categorized into two categories: covalent and non-covalent functionalization [2, 42].

Covalent functionalization in CNMs depends on reactions with oxygen-containing groups bonded to the CNMs'-conjugated skeleton. Non-covalent functionalization involves the use of various functional molecules or active species as assembly mediators to functionalize the surface of CNMs through non-covalent interactions [43]. The most straightforward method for chemical functionalization of CNMs is to insert carboxylic acid (–COOH) groups on the surface via an oxidation process that uses

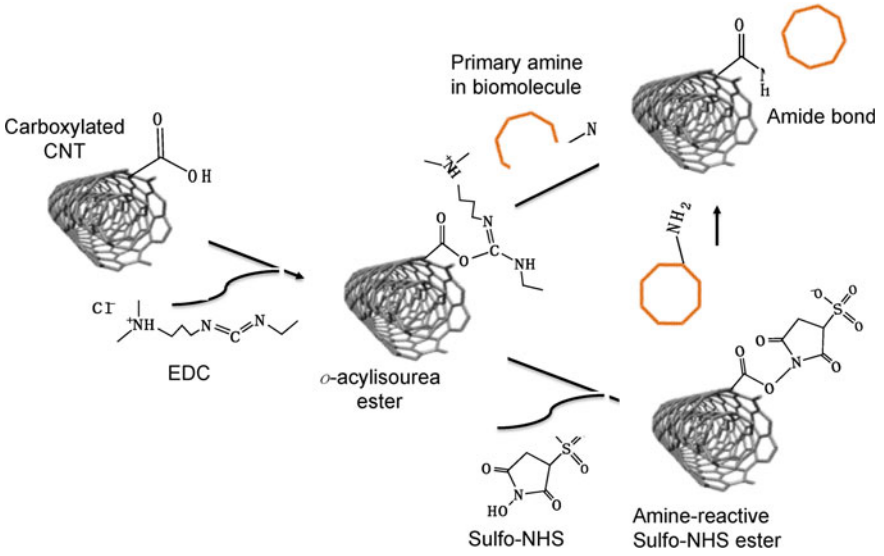

Fig. 3 Reaction scheme for EDC and EDC-NHS-based covalent crosslinking of biomolecule with carbon nanotube. Reprinted from [43] with permission

concentrated acids such as H_2SO_4, HNO_3, HCl, or H_2O_2, or acid mixture [2, 44]. Furthermore, the structure of these carboxylic acids can be used for covalent attachment of organic or inorganic groups, resulting in highly dispersible carbon materials [12]. Carbodiimide compounds (Fig. 3), which can activate carboxyl groups on CNTs for direct reactivity with primary amines in biomolecules, can be used to react carboxylated CNTs with biomolecules. N-ethyl-N'-(3-dimethylaminopropyl) carbodiimide hydrochloride is a common water-soluble carbodiimide (EDC). When EDC combines with carboxyl groups, it forms an intermediate o-acylisourea ester that can be easily displaced by primary amine in the biomolecule [45].

Surface modification of CNMs is critical for biomedical applications. Firstly, most CNMs are insoluble in aqueous solutions. Nonetheless, several biomedical applications of these materials could be understood on the basis of their water solubility and ease of use in a biological system [27]. These materials' solubility can be increased with the right surface modification. Second, the surface treatment can imbue the CNMs with properties that can be used in various applications. The surface treatment is also effective in reducing the toxicity of CNMs [46–48].

The modification of CNMs with metal and metal oxide NPs, with strict control over the size, shape, and crystalline structure, has become critical for nanotechnology applications in many fields such as medicine, catalysis, and electronics [8]. Surface deposition of metals and metal oxides onto CNMs has traditionally been accomplished through a bottom-up approach. Many wet chemistry methods, such as hydrothermal, microwave synthesis, and sol–gel processing, have been developed to date for the synthesis of metal and metal oxide NPs [48]. The role of hydrothermal

synthesis is performed in an autoclave using an aqueous solution reaction. The inner temperature of the autoclave can be raised above the boiling point of water, reaching the pressure of vapor saturation. Hydrothermal synthesis is commonly used for depositing metal and metal oxide NPs on CNMs such as graphene and CNTs, which can be easily obtained by hydrothermally treating peptized precipitates of a metal precursor with water. By controlling the solution composition, reaction temperature, pressure, solvent properties, additives, and aging time, the hydrothermal method can be used to monitor particle size, morphology, crystalline phase, and surface chemistry [8].

5 Application of CNMs in Biosensing

The sensors and biosensors developed are usually evaluated for some parameters that determine their analytical performance, such as sensitivity, selectivity, limit of detection (LOD) and quantification (LOQ), repeatability, and reproducibility, in order to guarantee the quality of the results obtained and to validate the analytical method. Different modifications to the same base electrode can result in sensors with varying specificities for a given analyte. Numerous studies involving electrochemical sensors and biosensors based on graphene, carbon nanotubes, and fullerene have been described in recent literature for the detection of drugs and compounds of clinical interest.

Arvand and Hemmati developed a nanocomposite of graphene quantum dots (GQDs), Fe_3O_4 nanoparticles, and functionalized MWCNT (Fe_3O_4@GQD/*f*–MWCNT) for sensitive detection of progesterone (P4). The estimated LOD and sensitivity were 2.18 nmol L^{-1} and 16.84 μA L μmol^{-1}, respectively. This sensor demonstrated outstanding stability, selectivity, sensitivity, and repeatability, and it could be successfully used to determine P4 in human serum samples and pharmaceutical items with high recoveries and without interference from interfering substances [49].

Sutradhar and Patnaik using thiol-capped gold nanoparticle-based nanocomposite with 3-amino-5-mercapto-1,2,4-triazole as the ligand created a gold nanoparticle-functionalized fullerene (C_{60})-modified vitreous carbon electrode for glucose detection (Fig. 4). The electrocatalytic behavior of the AuNPs@C_{60}/GCE sensor was investigated using cyclic voltammetry (CV) and electrochemical impedance spectroscopy (EIS). The highly stable and low onset potential non-enzymatic sensor exhibited high electrocatalytic activity and effective electron transfer from the electro-catalyst to the substrate electrode in a linear concentration range of 0.025–0.8 mmol L^{-1} and a higher sensitivity response of 1.2 μAμmol^{-1} L cm^{-2} with good reproducibility, long-term stability, free of interference from chlorine and oxygen, and detection limit of 22.0 μmol L^{-1} [50].

By covering and attaching SWNT with conductive polymer, Jin et al. create stretchable and transparent electrochemical sensors based on single-walled carbon nanotubes (SWNTs). Poly-(3,4-ethylenedioxythiophene), PEDOT, was chosen as a

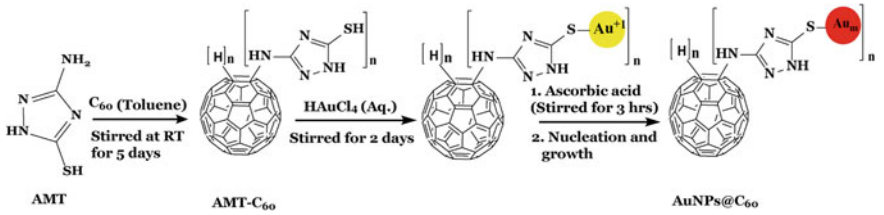

Fig. 4 Schematic representation for synthetic route of AuNPs@C_{60} nanocomposite. Reprinted from [50] with permission

binder for its high conductivity, strong electrochemical activity, and biocompatibility. Additionally, as an excellent conductive coating and binder, it minimizes contact resistance and considerably improves the electrochemical performance of SWNTs films. Furthermore, the optoelectronic and electrochemical sensing performance is exceptionally stable during the stretching and bending processes. Proof-of-concept tests were carried out, which involved recording NO release from mechanically sensitive endothelial cells cultivated on the stretchable sensor, revealing its promising potential in real-time monitoring of mechanically induced biochemical signals from living cells and tissues [51].

The determination of L-Dopa is critical because it is the immediate precursor of dopamine (DA) and is used to treat Parkinson's disease. Because DA does not cross the blood–brain barrier, it cannot be administered orally. Thus, L-Dopa is administered and converted into dopamine by the enzyme dopa-decarboxylase, stimulating dopamine production in the body. Sooraj and colleagues developed a sensor for L-Dopa determination in human urine and pharmaceutical samples by grafting copper nanoparticles with molecular imprinted polymer on MWCNTs (CuNPs/MWCNT-MIPs). The non-covalent interaction between L-Dopa and the functional groups present in the polymer composite sorbent's selective binding sites is primarily responsible for the recognition capacity toward L-Dopa with a detection limit of 7.23 nmol L^{-1}. The electrochemical investigation reveals that the imprinted (CuNPs/MWCNT-MIP) material has adequate selectivity, distinguishing between L-Dopa and structurally related compounds like DA, uric acid (UA), 3,4-dihydroxyphenylacetic acid, and homovanillic acid [52].

Anojčić et al. [53] developed carbonaceous nanomaterial-modified carbon paste electrodes (CPEs) with MWCNTs in their native and functionalized (ox-MWCNT) forms to determine DA. The method demonstrated a linear concentration range of 16.15–192.70 ng mL^{-1}, low detection limit of 4.89 ng mL^{-1}, and a relative standard deviation (RSD) of less than 1.3%, under optimized conditions. Interferences from ascorbic acid were also insignificant. The developed method was successfully applied for DA determination in injection/selected infusion matrix solutions, with the obtained results being in good agreement with the DA content declared by the producer and the method's RSD being less than 1.0% [53].

Upadhyay and Srivastava [54] describe an enantioselective electrochemical sensor that distinguishes atorvastatin isomers for the first time (ATS). The sensor was created

using a glassy carbon electrode (GCE) that had been modified with a functionalized MWCNT containing hydroxypropyl-β-cyclodextrin (HBC). The developed method demonstrated the outstanding benefits of chiral nanocomposite-modified electrodes, such as excellent enantioselectivity, high stereospecificity, and good reproducibility [54].

Zhang and Li [55] used a glassy carbon electrode modified with non-covalent self-assembly of porphyrin-diazocine-porphyrin (PDP) and fullerene (C_{60}), PDP-C_{60}/GCE for DA detection. This process, widely employed for the production of novel functional optoelectronic materials, involves the combination of electron-rich and electron-withdrawing chemical moieties inside a donor–acceptor (D-A) systems. DA electrochemical activity was measured using cyclic voltammetry (CV) and differential pulse voltammetry (DPV). The anodic peak current rose linearly with increasing DA concentration in the 0–200 μmol L^{-1} range, and the detection limit was determined to be 0.015 μmol L^{-1}. Thus, the suggested sensor demonstrated good sensitivity, acceptable selectivity, outstanding repeatability, and stability, indicating that PDP–C_{60}/GCE is a viable electrode material for dopamine analysis in real samples [55].

The examples listed above illustrate some characteristics of biodevices built from modifications and/or combinations of CNMs, such as CNTs, C_{60} and CDs. Next, carbon fibers (CFs), another type of CNM, will be discussed.

6 Carbon Fibers

The electrochemistry of carbon materials has been prominent recently in the scientific community due to properties such as reproducibility, low cost, high sensitivity, and easy handling [56]. Among these materials, carbon fibers (CFs) have drawn attention in 1950s when Bacon produced the first CFs [57]. CFs are long filaments that have 90% by weight of carbon in their composition and exhibit these properties high modulus, compressive and tensile strength, flexibility, and adjustable electrochemical performance that candidates these materials for a range of applications. Aerospace, automobiles, chemicals, transportation, construction, sewage treatment, and other areas are examples [58, 59]. Furthermore, chemical and electrochemical techniques are used to functionalize CFs to promote the production of reactive groups for attaching electrochemically active molecules such as noble metals, metal oxides, polymers, and proteins [60–62]. CFs are used to make electrochemical sensors with high sensitivity and adaptability, as well as energy equipment (supercapacitors and batteries) with high energy/power density, because of this change [63]. Thus, this topic will discuss the characteristics, fabrication methods of fibers, and their applications, focusing on the current progress on biosensors based on CFs. Figure 5 describes the interest and focus of this topic.

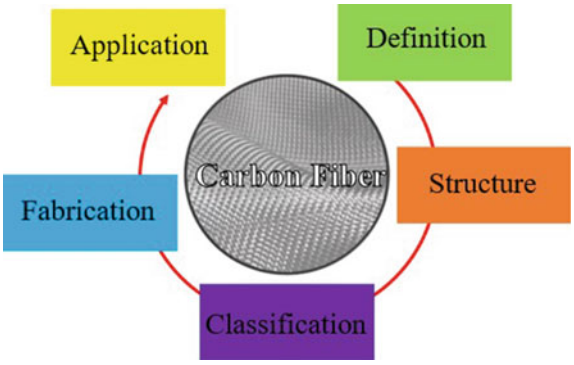

Fig. 5 Description of the interest and focus of this topic

6.1 Structure of Carbon Fibers

CFs can have a crystalline, amorphous, or partially crystalline structure and can be short, long, or continuous. Carbon fiber has an atomic structure comparable to graphite, with a spacing of 3.35 (d, d (002) in the c direction between the planes of the layers. It is composed of layers of carbon atoms arranged in a pattern [64]. Shaped hexagonal (Fig. 6.) It has a high modulus of 0.18–0.35 GPa; however, in a wet environment, its shear strength along the axis is poor [65].

In graphitic microdomains, the fiber structure is made up of sp^2 hybridized carbon atoms organized in a two-dimensional hexagonal structure stacked parallel to each other in a regular pattern bonded by van der Waals forces [65, 66]. The carbon atoms in the graphite layer are covalently linked to this structural configuration due to the

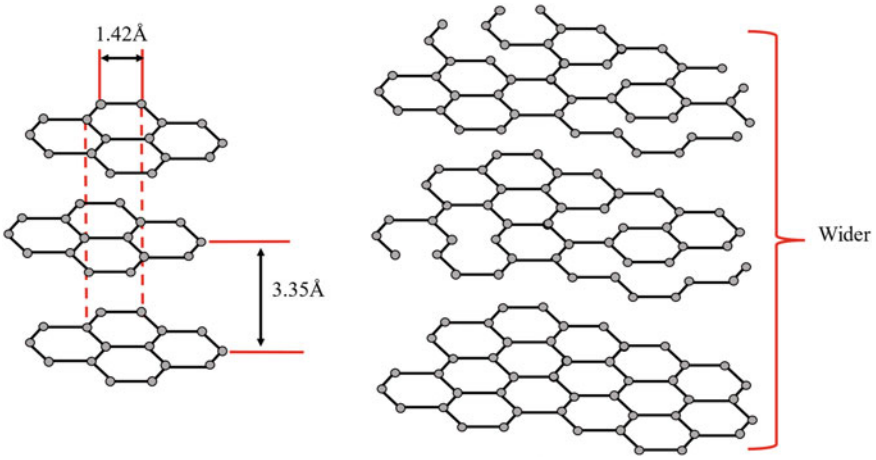

Fig. 6 Structure of carbon fibers in their graphitic form

superposition of the sp^2 orbitals and the delocalization of electrons. This structural configuration is responsible for graphite's high electrical and thermal conductivity [67]. The primary structural unit of most fibers is stacked turbostratic layers [68]. The spacing between the turbostratic layers is greater than the graphitic layers (Fig. 6).

The basic structural unit can split, fold, twist, and connect the other basic structural units in an irregular or random pattern to form microdomains. Carbon fibers have a non-uniform structure as a result [64]. The d spacing was raised to 3.44 because of sp^3 binding and uneven stacking. The fiber production process, which includes precursors and processing conditions, determines the structural unit. Carbon fibers with alternative precursors, such as polyacrylonitrile (PAN), have a turbostratic structure, whereas mesophase pitch and steam-grown carbon fibers have a well-stacked graphitic crystal structure [69]. During graphitization of stabilized PAN-based fibers, the crystalline domain is produced by amalgamation with nearby crystallites or integration of the surrounding disordered carbons. In addition, by rotation and displacement, the layer planes inside the crystalline domain were repositioned. Graphite fibers, on the other hand, nevertheless have enormous turbostratic domains since these configurations occur only locally [70].

6.2 *Fabrication of Carbon Fibers*

The discovery of CFs took place over a century ago. The most frequent precursors utilized in the manufacture of CFs are PAN, pitch, and rayon. In these cases, 90% of CFs made of PAN, and the remaining 10% are made of pitch, rayon, or other materials. Because PAN-based CFs have higher strength, modulus, and voltage, as well as higher throughput [59, 71, 72].

Most of the time, the fiber production process combines chemical and mechanical stages. Three fundamental processes are typical in the case of polymeric precursors, as they are in the case of PAN: spinning, thermostabilization, and carbonization. The graphitization phase is a follow-up to the carbonization process, in which the heat treatment temperature is increased to about 3000 °C [57]. Figure 7 depicts a simple PAN fiber fabrication process.

The initial step is spinning, which can be accomplished in three ways: melt spinning, wet spinning, or dry spinning. The precursor is melted and extruded in the

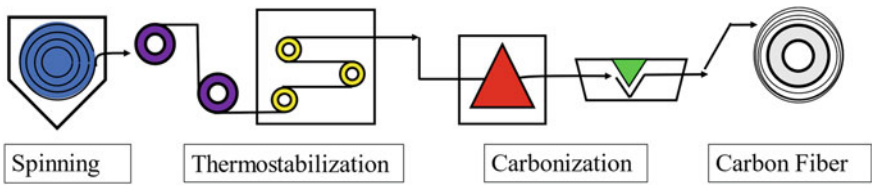

Fig. 7 Illustrative diagram that describes the carbon fiber fabrication process

first step. After the filaments emerge, they cool and solidify into the desired shape [73, 74]. It is the favored approach since it does not require any resources other than the melting of basic materials. In the second scenario, a concentrated precursor solution is extruded through the pores in a coagulation bath. Because the solvent is more soluble in the coagulation fluid than the precursor, the precursor precipitates as a fiber as the solution emerges through the perforations. A concentrated precursor solution is used in the dry spinning process. In a drying chamber, extrude the yarn such that the solvent evaporates, and the precursor crystallizes as a fiber. Dry or wet centrifugation is indicated if the raw material degrades at melting temperature [73, 75].

The extruded material in the spinning process must be heat-treated to improve its glass transition temperature. During the carbonization process, which converts the PAN from thermoplastic to thermoset, this phase is necessary to ensure the material's infusibility. Because it is one of the priciest aspects of the process, optimization studies have been used to reduce the time it takes to stabilize while maintaining the required characteristics [76]. If a thermostabilization procedure is not completed, fiber quality suffers. The procedure must be heated at an acceptable rate such that T_g rises faster than the thermostabilization temperature and the supplied groups oxidize [59].

For organic materials, carbonization and graphitization are similar processes, which differ only in the degree of orientation and crystallization obtained based on temperature. The proposal to carbonize the fiber is to produce flat sheets of graphene, graphene, or hybrid, with high carbon content [57, 65]. During this stage, the majority of the non-carbon components in the fiber are volatilized as methane, hydrogen, cyanide, water, carbon monoxide, carbon dioxide, ammonia, and a range of other gases, enriching the carbon bonds and enhancing the fiber's mechanical, electrical, and thermal characteristics [57, 69].

Precursors with many heteroatoms lose more carbon during gasification, resulting in a fiber with a lot of pores and poor mechanical characteristics. The amount of mass lost at this step differs depending on the precursor. PAN has a density of 55–60%, whereas isotropic pitches have a density of 20–45%, with substantial dimensional contraction [77]. The carbonization stage increases the carbon content, but the graphitization step transforms carbon into graphite, which has a unique structure [70, 78]. At 1500 °C, the maximum tensile strength is achieved. There is a rise in modulus and a decrease in strength above this temperature. A fast carbonization rate causes fiber defects, while slow rates cause a very large loss of heteroatoms [64]. An optimization of the process is recommended.

6.3 Classification of Carbon Fibers

CFs have been classified in three different ways, namely performance, precursor, and commercial availability. Based on performance as CFs, they can be classified into the following groups: ultra-high modulus (UHM), high modulus (HM), intermediate

modulus (IM), standard modulus type (HT), and low modulus type (LM). The UHM and HM CFs are highly graphitized between 2000 and 3000 °C, characterized by a high modulus (>450 GPa) and (>350 GPa), respectively. As type IM CFs have carbon fiber tensile strength greater than (>200 GPa). The HT type is isotropic carbon fibers, which show a random orientation of the crystals and have a modulus less than (<100 GPa). As LM-type CFs have lower tensile strength (>4.5 GPA) [57, 65].

Carbon fibers are created by heating and stretching synthetic fibers (precursor fibers). Processing carbon fibers from diverse precursors needs a variety of circumstances to generate acceptable end products. The fundamental features are the same in both cases. The processing routes for many precursors are comparable on a macro level. Furthermore, carbon fiber precursor materials are crucial because the first precursor materials have a significant impact on the combination of diverse mechanical, physical, and chemical properties and behaviors in carbon fibers [57, 65]. PAN, pitch, Rayan, and cellulose are among the precursors that may be used to classify fibers.

They are categorized as high-performance carbon fibers (HPCF), general-purpose carbon fibers (GPCF), and activated carbon fibers based (ACF) on their commercial availability as fibers. HPFCs are distinguished by their high graphitic carbon content, which gives them mechanical strength. They are primarily utilized in carbon fiber reinforced polymer composites (CFRPs) for the aerospace sector [79]. They have low tensile strength and modulus as type GPCF, but they are inexpensive, thanks to isotropic carbon fibers, which are mostly utilized in the textile sector. Because of their unusual characteristics, including as adsorptive capabilities, ACF-type fibers have recently attracted interest in materials. Because of their nanopore architectures and particular CO_2 affinity of ACF surface, ACFs absorb more CO_2 than well-known adsorbent materials such as MOF-5, zeolite, and active carbon [80]. Figure 8 shows the classification of carbon fibers according to performance, precursor, and commercial availability.

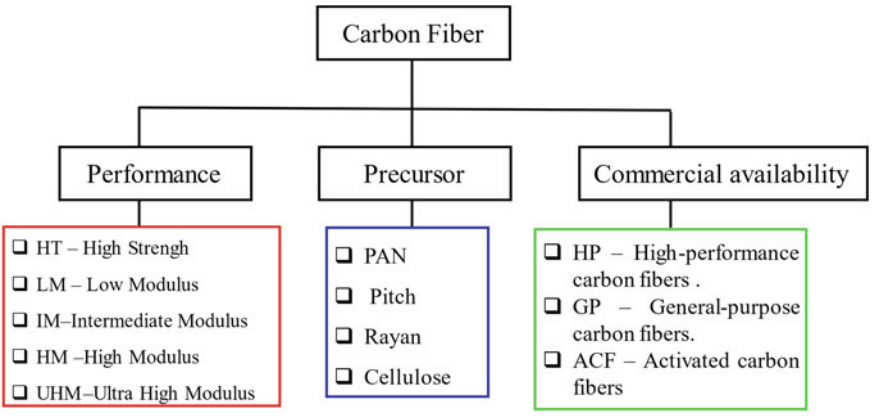

Fig. 8 Classification of carbon fibers

6.4 Application of Carbon Fibers in Biosensing

Because of its superior mechanical properties, high-performance carbon fibers are utilized in aerospace, aeronautics, transportation, sports, compressed gas storage, and civil engineering. Carbon fibers have recently acquired popularity as a foundation material for biodevice manufacturing [65]. Because of the remarkable characteristics of CFs, including as low relative density, high mechanical strength, high conductivity, high temperature resistance, and flexibility, fiber-based electrochemical biosensors have stood out in this context. Thus, the next paragraphs describe the application of carbon fibers in the most diverse electrochemical biodevices.

Although the first analytical application of carbon fibers was made in 1975 by Jennings et al., their interest in electrochemical devices only grew after work carried out in 1979 by Armstrong-James, Ponchon and collaborators [81, 82]. The results found by these researchers showed a remarkable improvement in the quality of voltammetric results due to the unique characteristics of carbon fibers. From these works, the interest in the use of this material in the construction of sensors and biosensors has grown, and it is currently possible to observe a growing increase in the number of publications on the use of carbon fibers in electrochemical measurements. Carbon fiber-based electrochemical biosensors are widely used for the detection of physiological and cancer biomarkers and for wearable electrochemical sensor applications.

The work by Liu Deng and associates, which describes a carbon fiber biosensor modified with Au@Pt nanoparticles for microbial detection, is an example of carbon fiber-based electrochemical biosensors. In this study, the relative suppression of *E. coli* activity is linear and has a LOD of 0.09 mg L^{-1}. The use of carbon fiber modified with NPs Au@Pt and its high conductivity, biocompatibility, and electrocatalytic activity, according to the scientists, improved the microbial biosensor. The microbial biosensor of this material has the potential to be used in environmental monitoring [83].

Human physiological indices and cellular activity components are also monitored using CF-based biosensors. One of the most significant indicators is glucose, and keeping track of it is critical for avoiding health concerns including hypertension, heart disease, and neurological issues. Salazar and colleagues describe the development of a glucose biosensor using a Prussian Blue modified carbon fiber electrode. Carbon fibers and PB film have electrocatalytic characteristics that allow for enzymatic by-product (H_2O_2) identification. Against a variety of physiologically interfering substances, the biosensor showed good glucose selectivity. Furthermore, the biosensor's sensitivity and stability are adequate to monitor multiphase and reversible changes in brain ECF glucose levels throughout physiological tests, demonstrating the biosensor's good characteristics and use in neuroscience [84].

With the 0.132 μmol L^{-1} LOD and rapid reaction time for an AU detection in GE/CFE, Jiao and colleagues developed a simple and cost-effective graphene-modified carbon fiber (GE/CFE) biosensor for uric acid (UA) determination. With a

relative standard deviation of 2.8%, the UA with GE/CFE determination is extremely selective and repeatable [85].

Iost and colleagues also describe the development of a carbon fiber-based biosensor for glucose detection. An electrochemical mediator and glucose oxidase enzyme are used to modify biosensors like carbon fibers. The sensor was shown to detect 30 mg dL^{-1} in a normal and 200 mg dL^{-1} in a diabetic state in vivo. The biosensor has shown promise in terms of potential implanted bioelectronic device applications [86]. The research presented in this issue demonstrates the rising need for electrochemical biodevices made of carbon fibers, as well as their relevance in the scientific community for medical applications.

Yan Zhang and colleagues created a flexible carbon fiber-based biosensor enclosed by gold nanoparticles and adorned with nitrogen-doped carbon nanotube arrays, CF@NCNTAs–AuNPs (Fig. 9), and investigated its practical use in electrochemical detection in situ H_2O_2 produced by live cancer cells. With a LOD of 50 nmol L^{-1}, this biosensor has outstanding electrocatalytic capabilities [87]. An electrochemical H_2O_2 biosensor was also published by Yuan et al. To construct a two-dimensional core–shell structure, carbon sheets doped with VS2@VC@N and decorated with ultra-fine Pd nanoparticles grown vertically in CFs are used. With the 50 nmol L^{-1}

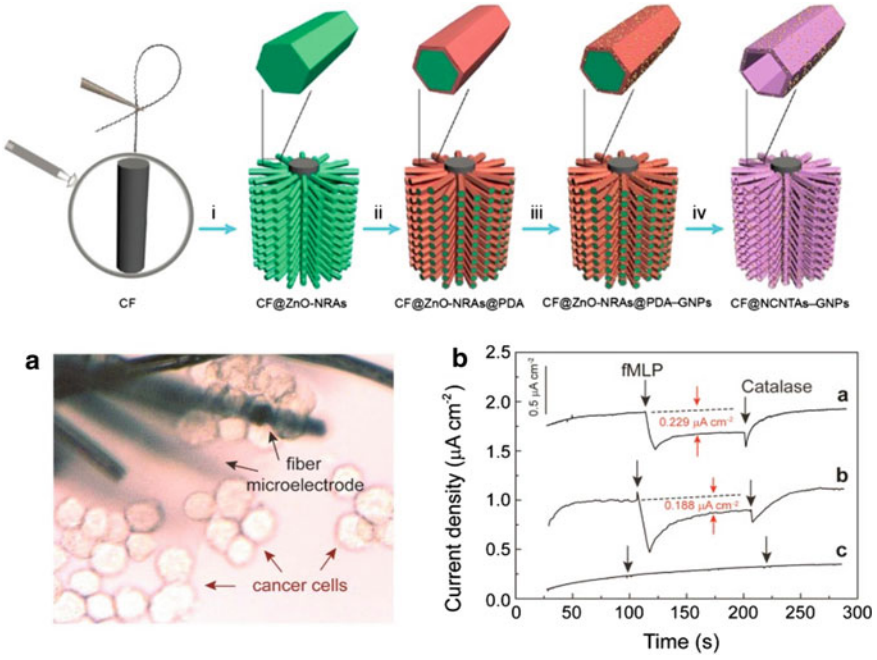

Fig. 9 Manufacturing of the CF@NCNTAs–GNPs nanocomposite is depicted schematically. **a** Digital microscope pictures of the CF@NCNTAs–AuNPs microelectrode, which was placed near the cells using a micromanipulator. **b** Current responses of the CF@NCNTAs–GNPs microelectrode in amperometric mode. Reproduced with the author's permission [87]

LOD, this biosensor exhibited strong electron transfer capability, electrocatalytic activity, stability, and biocompatibility to detect H_2O_2 in live cancer cells and cancer tissue in real time, although the unique rosette-like matrix structure [88].

In addition to traditional carbon fiber-based biosensors, flexible electronic and wearable smart devices have evolved substantially recently. Rather of lowering sensitivity and accuracy, they make the device smaller, more portable, and more intelligent. As a result, these devices have stood out. Vomero and colleagues, for example, describe the development of a flexible biosensor made of carbon fibers that may be implanted in mouse brain tissue. The micromachining technique is used to insert flexible CFS in this study. The whole electrocorticography (ECoG) electrode set is made entirely of single carbon fiber, with no joints or metal linkages. In vitro, the produced super flexible neural biodevice exhibited high electrochemical stability and outstanding mechanical characteristics, and after in vivo implantation, it displays good recording performance [89].

In carbon fiber microelectrodes, Asrat and colleagues demonstrated direct detection of DNA and RNA. And they show that this detection is effective even in complex serum samples, and according to the author, this measurement is not masked due to the properties of the combination of the FSCV technique and CFs. This is the first paper to show that FSCV can co-detect nucleobases when polymerized into DNA or RNA when employed with CFMEs, and it might open the way for future therapeutic, diagnostic, and research applications [90].

7 Concluding Remarks

Carbon nanomaterials (CNMs) pose as a versatile group of nanomaterials that can be used to fabricate or modify biodevices. Such versatility comes from the possibility of creating different functional groups that act as binding sites for different biomolecules or tissues. Carbon nanostructures, which have unique electrical, optical, physical, and chemical properties, have gotten a lot of attention. In recent decades, the number of published works reporting the use of these nanomaterials draws attention due to their range of applications, covering fields of research as varied as energy storage and supercapacitors to nanomedicine. In addition, the compatibility shown by carbon nanomaterials allows the creation of composites that have additional advantages to the original materials, such as higher biocompatibility and dispersibility.

The incorporation of different nanomaterials into the design of electrochemical biosensors has substantially enhanced their detection sensitivity. Alternatively, flexible and wearable point-of-care (POC) electrochemical sensor can be developed to quantify sweat metabolites and secretions in real time. It is thought to be a promising

approach for real-time monitoring of mechanically produced biochemical signals in sensitive cells and tissues during mechano-transduction.

Further Reading

JARIWALA, Deep, et al. Carbon nanomaterials for electronics, optoelectronics, photovoltaics, and sensing. Chemical Society Reviews, v. 42, n. 7, p. 2824–2860, 2013.

ALKIRE, Richard C.; BARTLETT, Philip N.; LIPKOWSKI, Jacek (Ed.). Electrochemistry of Carbon Electrodes. John Wiley & Sons, 2015.

GEORGAKILAS, Vasilios et al. Broad family of carbon nanoallotropes: classification, chemistry, and applications of fullerenes, carbon dots, nanotubes, graphene, nanodiamonds, and combined superstructures. Chemical reviews, v. 115, n. 11, p. 4744–4822, 2015.

SATTLER, Klaus D. (Ed.). Carbon Nanomaterials Sourcebook: Graphene, Fullerenes, Nanotubes, and Nanodiamonds, Volume I. CRC Press, 2016.

YANG, Nianjun. Nanocarbons for electroanalysis. John Wiley & Sons, 2017.

HUI, Yuen Y. et al. (Ed.). Carbon nanomaterials for bioimaging, bioanalysis, and therapy. John Wiley & Sons, 2019.

YANG, Nianjun; ZHAO, Guohua; FOORD, John S. (Ed.). Nanocarbon Electrochemistry. John Wiley & Sons, 2020.

Summary

ACF	Activated Carbon Fibers
AuNPS	Gold Nanoparticles
CB	Carbon Black
CDs	Carbon Dots
CFRPs	Carbon Fiber Reinforced Polymer Composites
CFs	Carbon Fibers
CND	Carbon Nanodiamonds
CNH	Carbon Nanohorns
CNM	Carbon Nanomaterials
CNT	Carbon Nanotubes
CPEs	Carbon Paste Electrodes
CuNPs	Cooper Nanoparticles
CVD	Chemical Vapor Deposition
DA	Dopamine
DNA	Deoxyribonucleic Acid
DWCNTs	Double-Walled Carbon Nanotubes
ECoG	Electrocorticography
EIS	Electrochemical Impedance Spectroscopy
FSCV	Fast-Scan Cyclic Voltammetry
GCE	Glassy Carbon Electrode

GNR	Graphene Nanoribbons
GPCF	General-Purpose Carbon Fibers
GQDs	Graphene Quantum Dots
HBC	Hydroxypropyl-B-Cyclodextrin
HM	High Modulus
HPCF	High-Performance Carbon Fibers
HT	Standard Modulus
IM	Intermediate Modulus
LM	Low Modulus
LOD	Limit Of Detection
LUMO	Lowest Unoccupied Molecular Orbital
MIP	Molecular Imprinted Polymer
MWCNT	Multi-Walled Carbon Nanotubes
NCNTAs	Nitrogen-Doped Carbon Nanotube Arrays
PAN	Polyacrylonitrile
PB	Prussian Blue $Fe_4[Fe(CN)_6]_3$
POC	Point-of-care
RNA	Ribonucleic Acid
RSD	Relative Standard Deviation
SWCNT	Single-Walled Carbon Nanotubes
UA	Uric Acid
UHM	Ultra-High Modulus

References

1. Putz MV (2011) Carbon bonding and structures, 1st edn. Springer Netherlands, Dordrecht
2. Maduraiveeran G, Jin W (2021) Carbon nanomaterials: synthesis, properties and applications in electrochemical sensors and energy conversion systems. Mater Sci Eng B 272:115341. https://doi.org/10.1016/j.mseb.2021.115341
3. Jiang X, Kang Z, Guo X, Zhuang H (2019) Novel carbon materials and composites—synthesis, properties and applications, 1st edn. Wiley
4. Hazra A, Goswami R (2021) Carbon nanomaterial electronics: devices and applications. Springer Singapore, Singapore
5. Georgakilas V, Perman JA, Tucek J, Zboril R (2015) Broad family of carbon nanoallotropes: classification, chemistry, and applications of fullerenes, carbon dots, nanotubes, graphene, nanodiamonds, and combined superstructures. Chem Rev 115:4744–4822. https://doi.org/10.1021/cr500304f
6. Kingston CT, Simard B (2003) Fabrication of carbon nanotubes. Anal Lett 36:3119–3145. https://doi.org/10.1081/AL-120026564
7. Porto LS, Silva DN, de Oliveira AEF, Pereira AC, Borges KB (2020) Carbon nanomaterials: synthesis and applications to development of electrochemical sensors in determination of drugs and compounds of clinical interest. Rev Anal Chem 38:1–16. https://doi.org/10.1515/revac-2019-0017
8. Barhoum A, Shalan AE, El-Hout SI, Ali GAM, Abdelbasir SM, Abu Serea ES, Ibrahim AH, Pal K (2019) A Broad family of carbon nanomaterials: classification, properties, synthesis, and

emerging applications. Handbook of nanofibers. Springer International Publishing, Cham, pp 1–40
9. Kour R, Arya S, Young S, Gupta V, Bandhoria P, Khosla A (2020) Review—recent advances in carbon nanomaterials as electrochemical biosensors. J Electrochem Soc 167:037555. https://doi.org/10.1149/1945-7111/ab6bc4
10. Si Y, Lee HJ (2020) Carbon nanomaterials and metallic nanoparticles- incorporated electrochemical sensors for small metabolites: Detection methodologies and applications. Curr Opin Electrochem 22:234–243. https://doi.org/10.1016/j.coelec.2020.08.007
11. Ehtesabi H (2020) Carbon nanomaterials for salivary-based biosensors: a review. Mater Today Chem 17:100342. https://doi.org/10.1016/j.mtchem.2020.100342
12. Power AC, Gorey B, Chandra S, Chapman J (2018) Carbon nanomaterials and their application to electrochemical sensors: a review. Nanotechnol Rev 7:19–41. https://doi.org/10.1515/ntrev-2017-0160
13. Wong H-SP, Akinwande D (2010) Carbon nanotube and graphene device physics, 1st edn. Cambridge University Press, Cambridge
14. Arnault J-C, Eder D (2021) Synthesis and applications of nanocarbons, 1st edn. Wiley
15. Evtugyn G, Porfireva A, Shamagsumova R, Hianik T (2020) Advances in electrochemical aptasensors based on carbon nanomaterials. Chemosensors 8. https://doi.org/10.3390/chemosensors8040096
16. Iijima S (1991) Helical microtubules of graphitic carbon. Nature 354:56–58. https://doi.org/10.1038/354056a0
17. Wildgoose GG, Banks CE, Leventis HC, Compton RG (2006) Review chemically modified carbon nanotubes for use in electroanalysis. Microchim Acta 214:187–214. https://doi.org/10.1007/s00604-005-0449-x
18. Saito Y, Nakahira T, Uemura S (2003) Growth conditions of double-walled carbon nanotubes in arc discharge. J Phys Chem B 107:931–934. https://doi.org/10.1021/jp021367o
19. Cui H, Eres G, Howe JY, Puretkzy A, Varela M, Geohegan DB, Lowndes DH (2003) Growth behavior of carbon nanotubes on multilayered metal catalyst film in chemical vapor deposition. Chem Phys Lett 374:222–228. https://doi.org/10.1016/S0009-2614(03)00701-2
20. Artyukhov VI, Penev ES, Yakobson BI (2014) Why nanotubes grow chiral. Nat Commun 5.https://doi.org/10.1038/ncomms5892
21. Doi Y, Nakatani A (2016) Structure and stability of discrete breather in zigzag and armchair carbon nanotubes. Lett Mater 6:49–53. https://doi.org/10.22226/2410-3535-2016-1-49-53
22. Wang Q (2004) Effective in-plane stiffness and bending rigidity of armchair and zigzag carbon nanotubes. Int J Solids Struct 41:5451–5461. https://doi.org/10.1016/j.ijsolstr.2004.05.002
23. Endo M, Hayashi T, Ahm Kim Y, Terrones M, Dresselhaus MS (2004) Applications of carbon nanotubes in the twenty-first century. Philos Trans R Soc London Ser A Math Phys Eng Sci 362:2223–2238. https://doi.org/10.1098/rsta.2004.1437
24. Tîlmaciu CM, Morris MC (2015) Carbon nanotube biosensors. Front Chem 3:1–21. https://doi.org/10.3389/fchem.2015.00059
25. Salvetat J-P, Bonard J-M, Thomson NH, Kulik AJ, Forró L, Benoit W, Zuppiroli L (1999) Mechanical properties of carbon nanotubes. Appl Phys A Mater Sci Process 69:255–260. https://doi.org/10.1007/s003390050999
26. Zanin H, May PW, Fermin DJ, Plana D, Vieira SMC, Milne WI, Corat EJ (2014) Porous boron-doped diamond/carbon nanotube electrodes. ACS Appl Mater Interfaces 6:990–995. https://doi.org/10.1021/am4044344
27. Sireesha M, Jagadeesh Babu V, Kranthi Kiran AS, Ramakrishna S (2018) A review on carbon nanotubes in biosensor devices and their applications in medicine. Nanocomposites 4:36–57. https://doi.org/10.1080/20550324.2018.1478765
28. Gergeroglu H, Yildirim S, Ebeoglugil MF (2020) Nano-carbons in biosensor applications: an overview of carbon nanotubes (CNTs) and fullerenes—(C_{60}). SN Appl Sci 2:1–22. https://doi.org/10.1007/s42452-020-2404-1
29. Ebbesen TW, Ajayan PM (1992) Large-scale synthesis of carbon nanotubes. Nature 358:220–222. https://doi.org/10.1038/358220a0

30. Sudha PN, Sangeetha K, Vijayalakshmi K, Barhoum A (2018) Chapter 12—Nanomaterials history, classification, unique properties, production and market. Elsevier
31. Laurila T, Sainio S, Caro MA (2017) Hybrid carbon based nanomaterials for electrochemical detection of biomolecules. Prog Mater Sci 88:499–594. https://doi.org/10.1016/j.pmatsci.2017.04.012
32. Li Y, Maruyama S (2019) Single-walled carbon nanotubes: preparations, properties and applications, 1st edn. Springer Nature Switzerland, Cham, Switzerland
33. Santos H, Chico L, Brey L (2009) Carbon nanoelectronics: unzipping tubes into graphene ribbons. Phys Rev Lett 086801:24–27. https://doi.org/10.1103/PhysRevLett.103.086801
34. Terrones M (2009) Nanotubes unzipped. Nature 458:845–846. https://doi.org/10.1038/458845a
35. Li Y, Liao J, Wang S, Chiang W (2016) Intercalation-assisted longitudinal unzipping of carbon nanotubes for green and scalable synthesis of graphene nanoribbons. Nat Publ Gr 1–12.https://doi.org/10.1038/srep22755
36. Pillai VK (2011) Electrochemical unzipping of multi-walled carbon nanotubes for facile synthesis of high-quality graphene nanoribbons. J Am Chem Soc, 4168–4171. https://doi.org/10.1021/ja1101739
37. Kosynkin DV, Higginbotham AL, Sinitskii A, Lomeda JR, Dimiev A, Price BK, Tour JM (2009) Longitudinal unzipping of carbon nanotubes to form graphene nanoribbons. Nature 458:872–877. https://doi.org/10.1038/nature07872
38. Zhang Y, Rhee KY, Hui D, Park SJ (2018) A critical review of nanodiamond based nanocomposites: synthesis, properties and applications. Compos Part B Eng 143:19–27. https://doi.org/10.1016/j.compositesb.2018.01.028
39. Kazi S (2014) A review article on nanodiamonds discussing their properties and applications. Int J Pharm Sci Invent 3:40–45
40. Iijima S, Yudasaka M, Yamada R, Bandow S, Suenaga K, Kokai F, Takahashi K (1999) Nano-aggregates of single-walled graphitic carbon nano-horns. Chem Phys Lett 309:165–170. https://doi.org/10.1016/S0009-2614(99)00642-9
41. Nelis JLD, Migliorelli D, Jafari S, Generelli S, Lou-Franco J, Salvador JP, Marco MP, Cao C, Elliott CT, Campbell K (2020) The benefits of carbon black, gold and magnetic nanomaterials for point-of-harvest electrochemical quantification of domoic acid. Microchim Acta 187. https://doi.org/10.1007/s00604-020-4150-x
42. Wang J, Lin Y (2008) Functionalized carbon nanotubes and nanofibers for biosensing applications. TrAC 27:619–626. https://doi.org/10.1016/j.trac.2008.05.009
43. Zhou Y, Fang Y, Ramasamy RP (2019) Non-covalent functionalization of carbon nanotubes for electrochemical biosensor development. Sensors (Switzerland) 19.https://doi.org/10.3390/s19020392
44. Georgakilas V, Otyepka M, Bourlinos AB, Chandra V, Kim N, Kemp KC, Hobza P, Zboril R, Kim KS (2012) Functionalization of graphene: covalent and non-covalent approaches. Deriv Appl. https://doi.org/10.1021/cr3000412
45. Liu S (2019) Functionalization of carbon nanomaterials for biomedical applications. C—J Carbon Res 5:72. https://doi.org/10.3390/c5040072
46. Shin SW, Song IH, Um SH (2015) Role of physicochemical properties in nanoparticle toxicity. Nanomaterials, 1351–1365. https://doi.org/10.3390/nano5031351
47. Buzea C, Pacheco II, Robbie K, Buzea C (2016) Nanomaterials and nanoparticles: sources and toxicity. Biointerphases 17. https://doi.org/10.1116/1.2815690
48. Hwang HS, Jeong JW, Kim YA, Chang M (2020) Carbon nanomaterials as versatile platforms for biosensing applications. Micromachines 11:814. https://doi.org/10.3390/mi11090814
49. Arvand M, Hemmati S (2017) Magnetic nanoparticles embedded with graphene quantum dots and multiwalled carbon nanotubes as a sensing platform for electrochemical detection of progesterone. Sens Actuators, B Chem 238:346–356. https://doi.org/10.1016/j.snb.2016.07.066
50. Sutradhar S, Patnaik A (2017) A new fullerene-C60—nanogold composite for non-enzymatic glucose sensing. Sens Actuators B Chem 241:681–689. https://doi.org/10.1016/j.snb.2016.10.111

51. Jin ZH, Liu YL, Chen JJ, Cai SL, Xu JQ, Huang WH (2017) Conductive polymer-coated carbon nanotubes to construct stretchable and transparent electrochemical sensors. Anal Chem 89:2032–2038. https://doi.org/10.1021/acs.analchem.6b04616
52. Sooraj MP, Nair AS, Pillai SC, Hinder SJ, Mathew B (2020) CuNPs decorated molecular imprinted polymer on MWCNT for the electrochemical detection of L-DOPA. Arab J Chem 13:2483–2495. https://doi.org/10.1016/j.arabjc.2018.06.002
53. Anojčić J, Guzsvány V, Kónya Z, Mikov M (2019) Rapid, trace-level direct cathodic voltammetric determination of dopamine by oxidized multiwalled carbon nanotube-modified carbon paste electrode in selected samples of pharmaceutical importance. Ionics (Kiel) 25:6093–6106. https://doi.org/10.1007/s11581-019-03156-5
54. Upadhyay SS, Srivastava AK (2019) Hydroxypropyl β-cyclodextrin cross-linked multiwalled carbon nanotube-based chiral nanocomposite electrochemical sensors for the discrimination of multichiral drug atorvastatin isomers. New J Chem 43:11178–11188. https://doi.org/10.1039/C9NJ02508A
55. Zhang M, Li J (2020) Preparation of porphyrin derivatives and C60 supramolecular assemblies as a sensor for detection of dopamine. Dye Pigment 173:107966. https://doi.org/10.1016/j.dyepig.2019.107966
56. McCreery RL (2008) Advanced carbon electrode materials for molecular electrochemistry. Chem Rev 108:2646–2687. https://doi.org/10.1021/cr068076m
57. Frank E, Steudle LM, Ingildeev D, Spörl JM, Buchmeiser MR (2014) Carbon fibers: precursor systems, processing, structure, and properties. Angew Chemie Int Ed 53:5262–5298. https://doi.org/10.1002/anie.201306129
58. Hiremath N, Mays J, Bhat G (2017) Recent developments in carbon fibers and carbon nanotube-based fibers: a review. Polym Rev 57:339–368. https://doi.org/10.1080/15583724.2016.1169546
59. Choi D, Kil H-S, Lee S (2019) Fabrication of low-cost carbon fibers using economical precursors and advanced processing technologies. Carbon N Y 142:610–649. https://doi.org/10.1016/j.carbon.2018.10.028
60. Szczurek A, Barcikowski M, Leluk K, Babiarczuk B, Kaleta J, Krzak J (2017) Improvement of interaction in a composite structure by using a sol-gel functional coating on carbon fibers. Materials (Basel) 10:990. https://doi.org/10.3390/ma10090990
61. García-Ruíz J, Díaz Lantada A (2017) 3D printed structures filled with carbon fibers and functionalized with mesenchymal stem cell conditioned media as in vitro cell niches for promoting chondrogenesis. Materials (Basel) 11:23. https://doi.org/10.3390/ma11010023
62. Wenrui Z, Fanxing M, Yanan Q, Fei C, Haitao Y, Minwei Z (2020) Fabrication and Specific functionalisation of carbon fibers for advanced flexible biosensors. Front Chem 8.https://doi.org/10.3389/fchem.2020.582490
63. Wang C, Xia K, Wang H, Liang X, Yin Z, Zhang Y (2019) Advanced carbon for flexible and wearable electronics. Adv Mater 31:1801072. https://doi.org/10.1002/adma.201801072
64. Huang X (2009) Fabrication and properties of carbon fibers. Materials (Basel) 2:2369–2403. https://doi.org/10.3390/ma2042369
65. Park S (2018) Carbon fibers, 2nd edn. Springer Singapore, Singapore
66. Joshi K, Arefev MI, Zhigilei LV (2019) Generation and characterization of carbon fiber microstructures by atomistic simulations. Carbon N Y 152:396–408. https://doi.org/10.1016/j.carbon.2019.06.014
67. Conard J (2002) Electronic structure of various forms of solid state carbons. Graphite intercalation compounds. In: New trends in intercalation compounds for energy storage. Springer Netherlands, Dordrecht, pp 39–62
68. Kim M-A, Jang D, Tejima S, Cruz-Silva R, Joh H-I, Kim HC, Lee S, Endo M (2016) Strengthened PAN-based carbon fibers obtained by slow heating rate carbonization. Sci Rep 6:22988. https://doi.org/10.1038/srep22988
69. Newcomb BA (2016) Processing, structure, and properties of carbon fibers. Compos Part A Appl Sci Manuf 91:262–282. https://doi.org/10.1016/j.compositesa.2016.10.018

70. Rahaman MSA, Ismail AF, Mustafa A (2007) A review of heat treatment on polyacrylonitrile fiber. Polym Degrad Stab 92:1421–1432. https://doi.org/10.1016/j.polymdegradstab.2007.03.023
71. Al Aiti M, Jehnichen D, Fischer D, Brünig H, Heinrich G (2018) On the morphology and structure formation of carbon fibers from polymer precursor systems. Prog Mater Sci 98:477–551. https://doi.org/10.1016/j.pmatsci.2018.07.004
72. Saritas O, Sokolov A, Vishnevskiy K (2019) New materials: the case of carbon fibres. In: Meissner D, Gokhberg L, Saritas O (eds) Emerging technologies for economic development, 1 st edn. Springer Nature Switzerland AG 2019, Cham, Switzerland, pp 13–47
73. Nakajima T, Kajiwara K, McIntyre JE (1994) Advanced fiber spinning technology, 1st edn. Elsevier
74. Chen JY (2017) Activated carbon fiber and textiles, 1st edn. Elsevier
75. Beckman I, Lozano C, Freeman E, Riveros G (2021) Fiber selection for reinforced additive manufacturing. Polymers (Basel) 13:2231. https://doi.org/10.3390/polym13142231
76. Baker DA, Rials TG (2013) Recent advances in low-cost carbon fiber manufacture from lignin. J Appl Polym Sci 130:713–728. https://doi.org/10.1002/app.39273
77. Chung DDL (1994) Carbon fiber composites, 1st edn. Elsevier
78. Chen H, Wang S, Zhang X, Zhao Y, Zhang H (2021) A study of chemical structural evolution of thermally altered coal and its effect on graphitization. Fuel 283:119295. https://doi.org/10.1016/j.fuel.2020.119295
79. Altin Karataş M, Gökkaya H (2018) A review on machinability of carbon fiber reinforced polymer (CFRP) and glass fiber reinforced polymer (GFRP) composite materials. Def Technol 14:318–326. https://doi.org/10.1016/j.dt.2018.02.001
80. Chiang Y-C, Juang R-S (2017) Surface modifications of carbonaceous materials for carbon dioxide adsorption: a review. J Taiwan Inst Chem Eng 71:214–234. https://doi.org/10.1016/j.jtice.2016.12.014
81. Ponchon JL, Cespuglio R, Gonon F, Jouvet M, Pujol JF (1979) Normal pulse polarography with carbon fiber electrodes for in vitro and in vivo determination of catecholamines. Anal Chem 51:1483–1486. https://doi.org/10.1021/ac50045a030
82. Armstrong-James M, Millar J (1979) Carbon fibre microelectrodes. J Neurosci Methods 1:279–287. https://doi.org/10.1016/0165-0270(79)90039-6
83. Deng L, Guo S, Zhou M, Liu L, Liu C, Dong S (2010) A silk derived carbon fiber mat modified with Au@Pt urchilike nanoparticles: a new platform as electrochemical microbial biosensor. Biosens Bioelectron 25:2189–2193. https://doi.org/10.1016/j.bios.2010.02.005
84. Salazar P, O'Neill RD, Martín M, Roche R, González-Mora JL (2011) Amperometric glucose microbiosensor based on a Prussian Blue modified carbon fiber electrode for physiological applications. Sensors Actuators B Chem 152:137–143. https://doi.org/10.1016/j.snb.2010.11.056
85. Du J, Yue R, Yao Z, Jiang F, Du Y, Yang P, Wang C (2013) Nonenzymatic uric acid electrochemical sensor based on graphene-modified carbon fiber electrode. Colloids Surf A Physicochem Eng Asp 419:94–99. https://doi.org/10.1016/j.colsurfa.2012.11.060
86. Iost RM, Sales FCPF, Martins MVA, Almeida MC, Crespilho FN (2015) Glucose biochip based on flexible carbon fiber electrodes. In vivo diabetes evaluation in rats. ChemElectroChem 2:518–521. https://doi.org/10.1002/celc.201402339
87. Zhang Y, Xiao J, Sun Y, Wang L, Dong X, Ren J, He W, Xiao F (2018) Flexible nanohybrid microelectrode based on carbon fiber wrapped by gold nanoparticles decorated nitrogen doped carbon nanotube arrays: in situ electrochemical detection in live cancer cells. Biosens Bioelectron 100:453–461. https://doi.org/10.1016/j.bios.2017.09.038
88. Yuan H, Zhao J, Wang Q, Manoj D, Zhao A, Chi K, Ren J, He W, Zhang Y, Sun Y, Xiao F, Wang S (2020) Hierarchical core-shell structure of 2D VS 2 @VC@N-doped carbon sheets decorated by ultrafine Pd nanoparticles: assembled in a 3D rosette-like array on carbon fiber microelectrode for electrochemical sensing. ACS Appl Mater Interfaces 12:15507–15516. https://doi.org/10.1021/acsami.9b21436

89. Vomero M, Gueli C, Zucchini E, Fadiga L, Erhardt JB, Sharma S, Stieglitz T (2020) Flexible bioelectronic devices based on micropatterned monolithic carbon fiber mats. Adv Mater Technol 5:1900713. https://doi.org/10.1002/admt.201900713
90. Asrat TM, Cho W, Liu FA, Shapiro SM, Bracht JR, Zestos AG (2021) Direct detection of DNA and RNA on carbon fiber microelectrodes using fast-scan cyclic voltammetry. ACS Omega 6:6571–6581. https://doi.org/10.1021/acsomega.0c04845

Inorganic Complexes and Metal-Based for Biomarkers Sensors

Caio Lenon Chaves Carvalho, Aurileide Maria Bispo Frazão Soares, Jéssica Randel da Silva Alves, Gleison de Andrade Rodrigues, Nielson José Silva Furtado, Germano Pereira dos Santos, and Janildo Lopes Magalhães

Abstract Modern coordination chemistry is a multidisciplinary and transversal science that makes a bridge between inorganic and bioanalytical chemistry. Due to the possibility of designing coordination complexes with different types of ligands, its application extends to colorimetric, magnetic, and electrochemical biosensors. In this chapter, the applications of inorganic complexes and metal-based biomarkers sensors will be addressed, with focus on the physical and chemical properties. We shall explore some examples of application in electrochemical biosensors, with the aim of improving human health care in clinical diagnosis.

Keywords Inorganic complexes · Metal-base materials · Electrochemistry · Biomarkers · Clinical diagnosis

1 Inorganic Complexes

The theory of the chemistry of coordination compounds was developed from the research of Alfred Werner and Sophus Mads Jörgensen, who observed compounds with characteristics similar to those of double salts, but which had different properties, such as solubility, less species in solution, conductivity, different color, dipole moment, and besides the valence rules were not respected. These compounds are called complexes or coordination compounds [1]. Coordination compounds are molecules formed by covalent bonds between the central metal atom or metal ion (Lewis acid) and neutral molecules or anions, called ligands (Lewis base), where the number of points to which the ligand binds to metal is called the coordination number [2, 3]. These complexes may be electrically neutral or charged and may have monodentate, ambidentate, bidentate, tri, etc., ligands. Thus, inorganic complexes are characterized by the nature of the central metal atom or ion, the oxidation state, and the number, type, and arrangement of ligands [2–4].

C. L. C. Carvalho · A. M. B. F. Soares · J. R. da Silva Alves · G. de Andrade Rodrigues · N. J. S. Furtado · G. P. dos Santos · J. L. Magalhães (✉)
Department of Chemistry, Federal University of Piauí, Teresina, PI 64049-550, Brazil
e-mail: janildo@ufpi.edu.br

F. N. Crespilho (ed.), *Advances in Bioelectrochemistry Volume 5*,
https://doi.org/10.1007/978-3-031-10832-7_4

The attention given to inorganic complexes is due to the presence of different physical and chemical properties, such as color, magnetic susceptibility, solubility and volatility, capacity to undergo oxidation–reduction reactions, and catalytic activity. The size, charge, and electronic configuration are some of the properties of the metallic ion, while the ligands present as properties the size and charge, steric and electronic factors, and among others. The main types of coordination compounds are the aquo complexes, halo, carbonyl, nitrosyl, cyano and isocyano, organometallic, isopoly, and heteropoly anions [5].

Coordination compound reactions include acid–base, substitution, lability and inertness, isomerization, and oxidation reduction. Various methods are used in the synthesis of inorganic complexes: single solution reaction, diffusion reaction and mechanical grinding reaction, Schlenk line techniques, hydrothermal/solvothermal method and in situ metal/binder reaction approach, assemblies and self-assembly, electrochemical methods, microwave heating, and biphasic synthesis [5–14]. Different geometric structures are possible depending on the coordination number of the compounds, which can be linear, flat triangle, tetrahedral, octahedral, and among others. When the coordination number of the complex is six, tetragonal distortions can occur for compounds of the trans-$[MA_4B_2]$ type. Tetragonal distortions also appear in regular octahedrons with asymmetric electron configuration, as in Cu^{2+} compounds, d_9, due to the Jahn–Teller effect [2, 3].

Some complex properties, such as stability and reactivity in a chemical or biological environment, are modified by isomerism [15, 16]. Coordination compounds have different types of isomerism: geometric, optical, binding, coordination, ligand, ionization, and hydration. In structural isomerism, the structure of the compound is changed, while in spatial isomerism or stereoisomerism, the ligands differ in their spatial arrangement. For example, $[MA_4B_2]$-type complexes may present *cis* and *trans* geometric isomers, while $[MA_3L_3]$-type compounds may present meridional (mer) and facial (fac) geometric isomers [15–18]. Optical isomers have the same physical properties, but they differ from polarized light, as these enantiomers are optically active compounds that do not have a plane of symmetry and can shift polarized light to the right (right-hand) or to the left (levorotary) [15, 19]. Bond isomerism occurs when the compound has an ambidentate ligand, such as the nitrite ion (NO_2^-) for example, in which the bond with the metal can be by nitrogen (M-NO_2) or oxygen (M-ONO) [20, 21]. When two ligands that form coordination compounds with different metals, one being a cationic complex ion, and the other an anionic complex ion, can behave as counterions to each other forming coordination isomers [22, 23]. If the ligand has isomers, these can form two compounds, resulting in ligand isomerism. Ionization isomerism occurs when one of the ligands and the counterion can act as both a ligand and a counterion. Hydration isomerism is similar to ionization isomerism, but in this case, the ligands are water and an ion that will be a counterion in one isomer and a ligand in the other [22–26].

The theories of valence bonds, crystalline field, binding field, and molecular orbitals were developed in order to understand the chemistry of coordination compounds. These theories complement each other in ways that fill gaps in each other,

helping to understand the characteristics and properties of inorganic complexes, but these theories will not be covered in this chapter [27].

Several coordination compounds stand out for their role in nature, the human body, health, and industry (Fig. 1). Complexes of natural origin are essential for the execution of certain biological processes [28]. For instance, hemoglobin acts in the transport of oxygen, as it has iron-porphyrin complexes in which the iron atoms coordinate the oxygen molecules in a reversible way. Metalloenzymes (metal complexes) regulate biological processes, chlorophyll (magnesium–porphyrin complex), a natural pigment present in plant chloroplasts, and Vitamin B_{12} (cobalt complex-corrin), essential for the normal functioning of the nervous system and red blood cell maturation are also part of this class of compounds that have biological relevance [29].

In industry, Prussian blue ($Fe_4[Fe(CN)_6]_3$) which was discovered at the beginning of the eighteenth century, but whose structure was determined more than three hundred years later, continues to be widely used as a dye and pigment due to its intense coloration [30]. Inorganic complexes are also used in electroplating, metal extraction from ores, to estimate water hardness and as catalysts [27].

Inorganic complexes have been used in medicine to treat various diseases, such as cancer, arthritis, acting as antimicrobial agents, metalloenzyme inhibitors, and among others. Among these complexes, cisplatin is one of the main coordination compounds used in the treatment of testicular, ovarian, neck, head, bladder, and lung cancer.

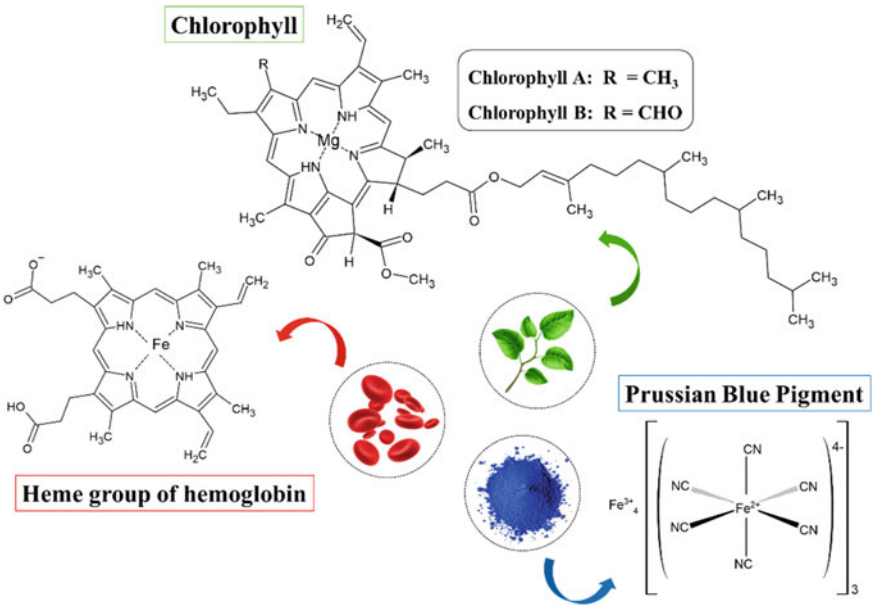

Fig. 1 Some inorganic complexes relevant to health, nature, and industry: iron-porphyrin complex present in hemoglobin, chlorophyll (magnesium-porphyrin complex) present in plants, and Prussian Blue, synthetic pigment

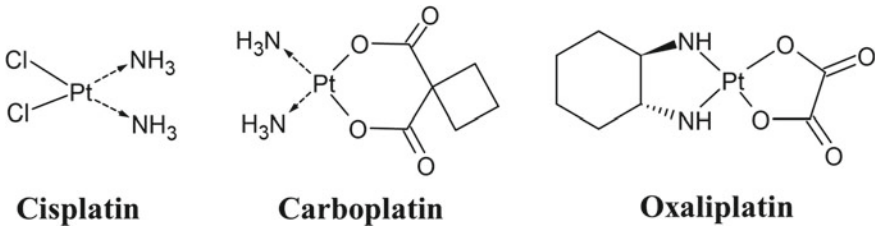

Fig. 2 Structures of three clinically approved Pt(II)-based anticancer drugs. Reprinted with permission from Ref. [35]. Copyright 2019 Elsevier

The discovery of cisplatin allowed the study and use of new complexes, including platinum, ruthenium, gold, and copper, in order to obtain effective and safe drugs [31]. Currently, almost half of cancer patients undergoing chemotherapy undergo treatment with Pt(II) complexes such as cisplatin, carboplatin, or oxaliplatin (Fig. 2). These drugs have antitumor activity because they form stable adducts with DNA (Pt–DNA), resulting in the interference of replication and transcription processes, thus inducing apoptosis. These complexes also react with RNA, mitochondrial DNA, and proteins [32–38].

The chemical industry performs the synthesis of organic polymers of great commercial importance, which are the raw materials for the production of medicines, plastics, and other components. These synthetic organic polymers need catalysts to be produced, and therefore, inorganic complexes are an important class of catalysts used in these processes. For example, Ziegler and Natta won the Nobel Prize in 1963 for the development of a titanium-based catalyst (with $TiCl_3$ and $Al(C_2H_5)_2Cl$), which was used in the polymerization of alkenes at atmospheric pressure and room temperature [39]. Furthermore, biotechnological or organocatalytic methods can be used to reduce or eliminate the production of harmful substances [40]. Ligand inner bands, *d-d* bands, and charge transfer bands are some interesting spectral characteristics of coordination compounds. Furthermore, depending on the oxidation state of the metal and the strength of the binding field, the complexes can be diamagnetic and paramagnetic, with high *spin* or *low spin*, resulting in their magnetic properties. Coupled with this, the optical, electrochemical, and catalytic properties make the inorganic complexes excellent candidates for photoluminescent, electrochemical, and electrochemiluminescent applications, as well as in disease diagnosis, among other biomedical applications [4, 41, 42]. Discrete coordination compounds and coordination polymers are sources of interest in research due to their range of applications, including adsorption, separation, catalysis, electrical, magnetic, and optical applications. Porous coordination polymers (PCPs) or metal–organic structures (MOFs) stand out for their applications including adsorption and separation, catalysis, luminescence, detection, and molecular magnets [5]. The properties of inorganic complexes allow their use in the diagnosis of diseases. Their low molecular weight, catalytic and photophysical properties, as well as tuning ability contribute to

their application as signal generation probes in photoluminescence, electrochemistry, and electrochemiluminescence for the detection of substances [41, 43–47]. Coordination compounds that exhibit photoluminescence have interesting properties such as long-lasting phosphorescence, significant stokes changes, and emission by ligand composition [48–50].

2 Metal-Based Nanomaterials

Metallic nanoparticles are part of the nanomaterials that arouse interest due to the possibility of different applications, such as in catalysis, electronics, and biomedicine. The properties that these nanomaterials may have include magnetic, electrochemical, thermal, catalytic, electronic, optical, and reactive properties [51, 52]. Some examples of metallic nanoparticles are shown in Fig. 3. They can be classified as metal nanoparticles (silver, gold, platinum, palladium, zinc, iron, etc.), nanoparticles of metal oxide (e.g., titanium dioxide and zinc oxide), doped metal/metal and metal/metal oxide nanoparticles, metal sulfide nanomaterials, and MOFs [52].

AuNPs are very attractive due to their photothermal and optical properties, as well as low toxicity, ease of preparation, and favorable binding with biological molecules, allowing their use in detection and diagnosis, biomarking, drug delivery, photovoltaics, catalysis, and other applications [52–54]. Likewise, nanostructured metal oxides have attracted attention because they have nanomorphological, functional, biocompatible, non-toxic, and catalytic properties. These properties allow their use as immobilizing matrices for the development of biosensors [55]. TiO_2, for example, is an n-type semiconductor widely explored in the areas of photocatalysis, biosensors,

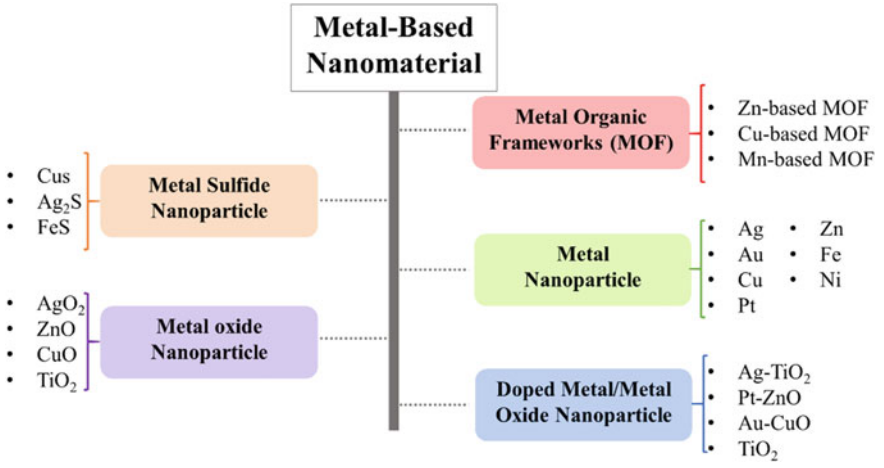

Fig. 3 Different types of metal-based nanomaterials. Adapted and reprinted with permission from Ref. [52].. Copyright 2019 Elsevier

photovoltaics or energy storage due to its properties, which include high chemical stability, biocompatibility, and morphological versatility [56]. In general, metal oxide nanoparticles are used as catalysts, superconductors, semiconductors, ceramics, and gas sensors, as well as in biomedicine for their potential antibacterial activity [55].

The doped metal/metal and metal/metal oxide nanoparticles are capable of improving the efficiency of metal oxides in biomedical applications, due to safety and increased stability. Siriwong et al. [57] compared the activity of Fe-doped TiO_2, WO_3-doped ZnO, and Fe-doped CeO_2 nanomaterials, and found that doped metal oxides can improve the photocatalytic activity of pure metal oxides. These metal oxides are almost inactive under visible light illumination. Doping with transition metals can lead to conspicuous absorption in the visible region and thus makes the photocatalysis process more attractive as it is possible to use visible light or irradiation of sunlight. In place of expensive UV lighting. Other applications resulting from metal oxide nanoparticles doping include photocurrent generation, H_2 production, antibacterial treatment, gas sensing, photocatalytic degradation, O_2 evolution, light-induced cell death, and reduction of CO_2 [58].

MOFs are compounds that have large surface areas, large pore volume, adjustable structure, thermal and chemical stability, and functionality, being applied in electrochemistry and other areas, such as catalysis. Metalophthalocyanines (Fig. 4a) have in their structure four isoindole units, linked by nitrogen in the aza position, in which the center of the molecule is a metallic atom [59], resulting in a molecule with a flat, highly conjugated structure, high chemical and thermal stability, rich surface chemistries and well defined, excellent redox activities, which has electrochemical properties, semiconductivity, and photoconductivity [60, 61]. The intense coloration of metallophthalocyanines occurs due to the π-π^* transitions of the conjugated ring of the macrocycle, as well as the transitions between the ground state A_1g (a_1u_2) and the first singlet excited state with Eu symmetry (of configuration a_1u_1 eg_1) [62].

Metalloporphyrins (Fig. 4b) are another class of compounds that have similar characteristics, such as stability, intense color, and conjugated system, resulting in biological, photophysical, and photochemical properties [63–66]. These macromolecules have four pyrrole units, linked by carbons in the meso position, with Mn and Cr linked to the basic principles of the macrocycle. The busiest orbitals, a_1u and a_2u, are nearly degenerate, but have two different electron distributions and two different orbits. The

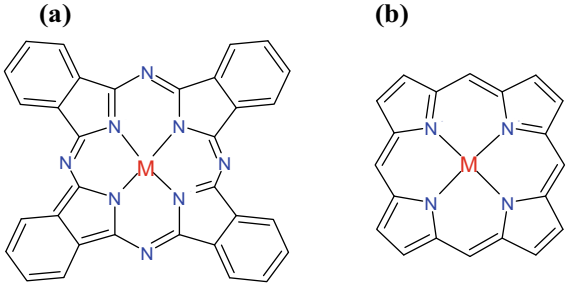

Fig. 4 Molecular structure of **a** metal phtalocyanine (MPc, M=Fe, Co) and **b** metal porphyrin (MP, M=Fe, Co)

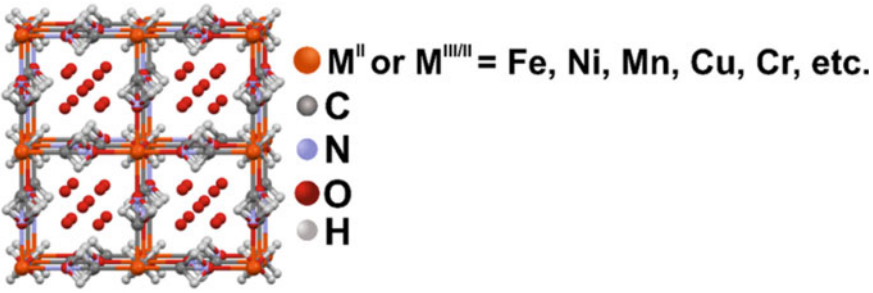

Fig. 5 Representation of the cubic structure of Prussian blue and Prussian blue analog. Adapted and reprinted with permission from Ref. [76]

properties of metalloporphyrins allow their use as contrast agents for MRI, photodynamic cancer therapy, bioimaging, and other applications, as well as in catalysis, pigments, and sensors [59, 63–66]. Iron-porphyrin-based MOFs, for example, can be applied as artificial enzymes for catalytic oxidation, such as hydroxylation and epoxidation of hydrocarbons [67].

Prussian blue (PB) or iron(III) hexacyanoferrate(II) ($Fe_4[Fe(CN)_6]_3$) is a dark blue pigment that was discovered in the early eighteenth century, but which had the structure determined more than three hundred years later, it is still widely used as a dye and pigment, in addition to other applications. [30] This compound is synthesized by the co-precipitation method in water through the reaction of de $[Fe^{III}(CN)_6]_3^-$ and a Fe^{II} salt or by mixing $[Fe^{II}(CN)_6]_4^-$ with a Fe^{III} salt.[68] The intense coloration of PB occurs due to the transfer of a metal-to-metal charge with an intense interval around 700 nm associated with Fe^{2+} –CN– Fe^{3+}. [69] PB is a mixed-valence coordination compound that has a face-centered cubic unit cell (cfc), alternating Fe^{3+} and Fe^{2+} bonded by a cyanide bridge. Ligands influence the solubility of PB: when Prussian blue presents cyanides and water molecules as binders, it is insoluble, while if the binders are only cyanides, PB is soluble [70]. The replacement of Fe(II) and/or Fe(III) by other transition metals, such as manganese, cobalt, nickel, and copper, in the PB structure results in Prussian blue analogues (PBAs) (Fig. 5) of general formula $A_xM^J[M^K(CN)_6] \cdot n\ H_2O$ (A = alkali metal ion—Na^+, Li^+, or K^+, M^J and M^K = transition metal ions, Fe^{2+}, Co^{2+}, Cu^{2+}, Zn^{2+}, Mn^{3+}, Fe^{3+}, Co^{3+}, and Cr^{3+}), with different applications such as energy storage, sensors, medicine and catalysis [69, 71–73]. Thus, PB and its analogs are useful in the electrochemical, biochemical, biomedical, and electromagnetic fields [73–75].

3 Electrochemistry of Inorganic Compounds

The structural properties of inorganic complexes and metal-based nanomaterials described in the previous section play an important role in electrochemical behavior

of these inorganic compounds. For this reason, the fundamentals the metal-based compounds electrochemistry must be known to investigate the performance of sensors for biomarkers. The electrochemistry of inorganic compounds can be defined like the one that investigates the redox reactions or electrochemical properties of inorganic species which contains at least one metal center in their chemical structure. Thus, transition metal complexes (hexacyanometallates) and metal-based materials (metal and metal oxide nanoparticles) are inorganic compounds that showed unique electrochemical behavior due to their exceptional properties such as good electrical conductivity, electrocatalytic activities, large surface areas, tunable pores, and modifiable surface [77–80]. From understanding of these advantageous properties, we wish to focus our discussion here in the inherent electrochemical properties, in particular, the well-defined redox processes this metal-based materials [81]. In this case, the term "inherent electrochemistry" is used to describe the standard electrochemical behavior of different inorganic compounds when used as electrode modifiers in applications that involves electrochemical biosensing and electrocatalysis [81]. Nonetheless, electrochemical behavior of the inorganic material-modified electrodes is guided by oxidation/reduction of the metallic center. Importantly, these charge-transfer reactions depended of experimental conditions such as pH, ionic force, nature of the electrolyte, and potentials applied [81].

In general, the redox processes of metal and metal oxide nanoparticles involve the charge-transfer reactions (in basic electrolyte) between metallic species and their transition metal-base oxides ($M + OH^- \leftrightharpoons MO + e^-$) or between metal oxide and their derivates ($MO + OH^- \leftrightharpoons MOOH + e^-$), where M is usually Ag, Au, Cu, and Co [82, 83]. Moosavifard et al. observed a well-defined electrochemical behavior of nanoporous CuO electrodes in KOH aqueous electrolyte with strong redox pair of anodic and cathodic peak in 0.40 V and 0.10 V (vs. SCE, saturated calomel electrode) [84]. Despite of the defined electrochemical behavior, few researches use these redox reactions as central question of the applications in electrocatalysis and electroanalytical. For instance, for studies of electrochemical detection of a target analyte, generally the metal and metal oxide nanoparticles can act as electrocatalysts, improving the transport of electrons of the oxidation/reduction (redox) reactions of analyte onto electrode surface. In this case, metal and metal oxide nanoparticles act as electrocatalysts, improving the transport of electrons of the redox reactions of analyte. This electrocatalytic effect is evidenced by increase of the current densities and decrease in the redox potential, which enhance the sensitivity and selectivity of target product selectivity, minimizing energy loss. [85] This performance in the electrocatalysis and electrochemical biosensing because increase of electroactive surface, mass-transport rate, smallest charge-transfer energy, and fast electron transfer [78, 82, 85, 86].

Among the mixed-valence transition metal complexes, Prussian blue and its analogs have attracted attention of the scientific community due large specific surfaces areas, diverse morphologies, adjusted pore diameters, and easily controllable size [77, 87]. Also, PB and PBA show unique properties (e.g., excellent electrocatalytic activities and well-defined redox reactions) and act as efficient electron transfer mediators in a wide spectrum of electrochemical applications [77, 88]. The open-framework structure with cubic wide channels nanoporous can insert alkali and

alkali earth metals that are useful in the reactions of charge-transfer reactions [88]. Thus, the general electrochemistry behavior of the PB and PBA is represented by Eq. 1: [88]

$$A_x M^J\left[M^K(\mathrm{CN})_6\right]_{1-y} \cdot n\mathrm{H_2O} + A^+ + e^- \rightleftharpoons A_{x+1} M^J\left[M^{K-1}(\mathrm{CN})_6\right]_{1-y} \cdot n\mathrm{H_2O} \quad (1)$$

were value of y representing the fraction of vacancies of the metal hexacyanometallate ion (the primary lattice defect). To this class of inorganic compounds, the well-defined redox process occurs in acid and neutral electrolyte. Consequently, PB and PBAs can be used for indirect electrochemical detection of (bio)analyte onto electrode surface. This means that the electrochemical properties (e.g., decrease of peak current densities) of the transition metal complexes can change because of specific interactions between the analyte structure and mettalic center [89]. Regarding other applications, the insertion of ions in the open framework along with the corresponding redox reaction of the transition metals influence in the electrochemical performance energy storage device [90, 91]. Therefore, the physico/chemical properties of inorganic compounds are crucial aspects in the electroactive behavior of metallic center. The control of these properties can allow create a favorable microenvironment to occur well-defined redox reactions with good performance various fields of electrochemistry (Fig. 6).

In particular, electronic structure of PB and PBAs causes two types of redox processes more common, the metal-to-ligand (MLCT) and ligand-to-metal charge-transfer (LMCT) reactions onto electrode surface [93, 94]. For example, the cyanido-bridged bimetallic coordination structure defined by $A_x\mathrm{Co}_y[\mathrm{Fe(CN)_6}] \cdot n\mathrm{H_2O}$ (A: alkaline metal) occurs charge-transfer processes between the cobalt and iron centers. In this case, the electron transfer (MLCT) involves the alternation between paramagnetic ($\mathrm{Fe_{LS}}^{\mathrm{III}}{}_{(S=1/2)}$–CN–$\mathrm{Co_{HS}}^{\mathrm{II}}{}_{(S=3/2)}$) and diamagnetic ($\mathrm{Fe_{LS}}^{\mathrm{II}}{}_{(S=0)}$–CN–$\mathrm{Co_{LS}}^{\mathrm{III}}{}_{(S=0)}$) entities (were LS: Low spin state and HS: High spin state) [94]. Jiménez and collaborators reported the charge transfer behavior the cyanide-bridged cubic switch containing a Cs^+ cation (Cs $\subset\{\mathrm{Mn_4Fe_4}\}$) as a molecular model of the mixed-valence of $\mathrm{Mn}_x[\mathrm{Fe(CN)_6}]_y$ PBA [95]. As a results, the cyclic voltammogramms of Cs $\subset\{\mathrm{Mn_4Fe_4}\}$ showed four quasi-reversible redox assigned to the oxidation/reduction of the four iron ions of the cubic structure. The $\mathrm{Fe_2}^{\mathrm{II}}\mathrm{Fe_2}^{\mathrm{III}}$ structure is referent to initial state that can display LMCT of type $\mathrm{Fe_2}^{\mathrm{II}}\mathrm{Fe_2}^{\mathrm{III}} \rightarrow \mathrm{Fe_4}^{\mathrm{III}}$ in the $\{\mathrm{Fe}^{\mathrm{III}}(\mathrm{Tp})\mathrm{CN_3}\}$units and MLCT ($\mathrm{Fe_2}^{\mathrm{II}}\mathrm{Fe_2}^{\mathrm{III}} \rightarrow \mathrm{Fe_4}^{\mathrm{II}}$) $\{\mathrm{Fe}^{\mathrm{II}}(\mathrm{Tp})\mathrm{CN_3}\}$units, where Tp = hydrotris(pyrazol-1-yl)borate [95].

The charge-transfer processes of PB and PBA-based nanostructure are important to investigate the mechanisms of electrochemical (bio) sensing in the clinical diagnostic fields [96, 97]. A nanocomposite constituted by toluidine blue (TB) functionalized NiFe Prussian blue analog nanocubes (NiFe PBA nanocubes@TB) was used as a signal amplifier for the detection of procalcitonin (PCT) [98]. The glassy carbon electrode (GCE) was modified with NiFe PBA nanocubes@TB and glutaraldehyde (GA) that used as cross linker of procalcitonin antibody (PCT Ab), bovine serum albumin

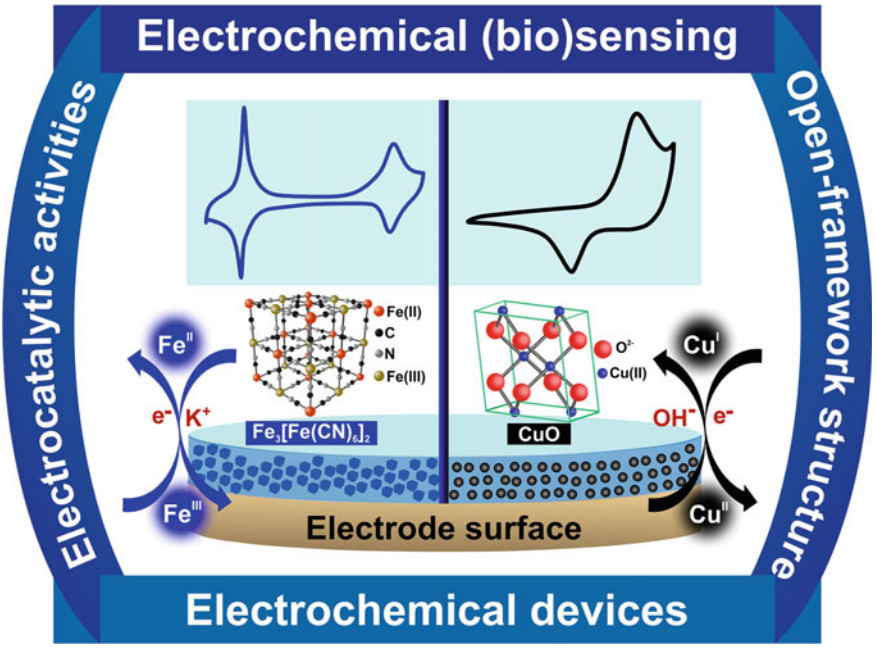

Fig. 6 Scheme of the well-defined electrochemical behavior, structures and properties of main inorganic compounds. Adapted and reprinted with permission from Refs. [84, 92]. Copyright (2015, 2021) ACS publications and Elsevier

(BSA) and procalcitonin antigen (PCT Ag), respectively (Fig. 7). The signal generation mechanism and electrochemical detection onto surface of the PCT Ag/BSA/PCT Ab/GA/NiFe PBA nanocubes@TB/GCE bioelectrode was based in the metallic fragments Ni^{2+}–CN–Fe^{2+} were near the surface of the nanocubes [98]. In this case, the covalent interaction between TB and NiFe PBA increased the concentration of $[Fe(CN)_6]^{4-}$ species and improve electrochemical response of as-prepared nanomaterials with signal current significantly amplified. Moreover, NiFe PBA nanocubes with open-framework showed large electrochemically active surface area to load abundant antibodies. Electrochemical behavior of bioactive surface exhibited signal current decreased with the increase of PCT contents from 0.001 to 25 ng mL^{-1}.

3.1 Electrochemistry of Prussian Blue and Analog

Metal hexacyanoferrates (MHCF) have interesting electrochemical properties that allow applications in several areas of chemistry, mainly in electrochemistry. For this reason, it is necessary to know the fundamental studies present in the obtaining these complexes on the surface of carbon electrode by electrochemical methods. It

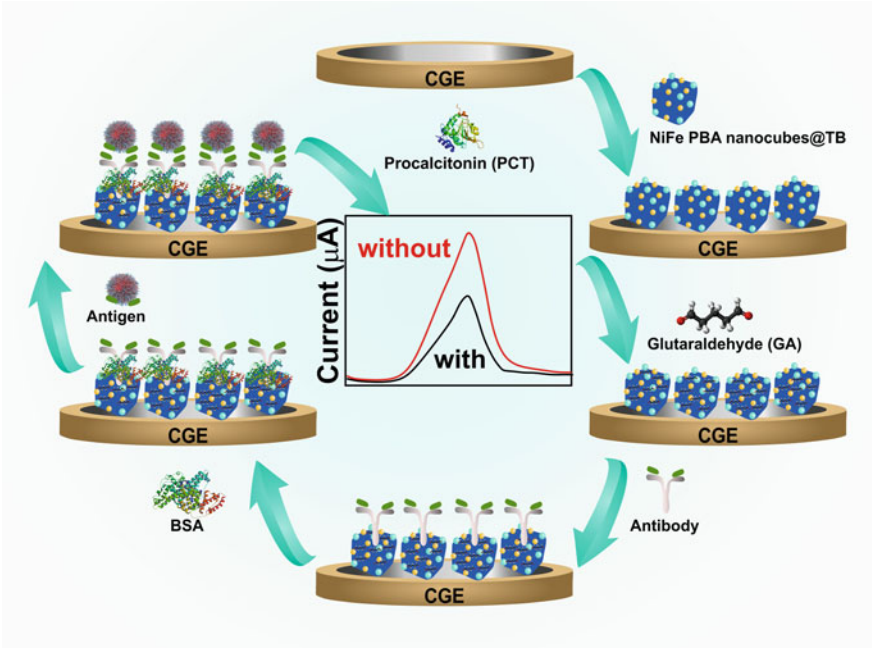

Fig. 7 Schematic representation of preparation of the PCT Ag/BSA/PCT Ab/GA/NiFe PBA nanocubes@TB/GCE bioelectrode. Adapted and reprinted with permission from Reference [98]. Copyright 2019 Elsevier

is also important to attribute the redox processes and redox reactions of MHCF on the electrode surface, the proposition of possible redox mechanisms to obtain these complexes in new systems, as well as the first investigations in chemically modified electrodes (CMEs) with MHCF to propose future applications in electrochemical sensors.

3.1.1 Obtaining of Prussian Blue and Cobalt Hexacyanoferrate by Electrosynthesis

The MHCF has zeolite-shaped structure, which is important for the selection of certain metal ion, being great redox mediators in electroanalytical applications. [99–101] The surface modification of electrodes with metal hexacyanoferrate (MHCF) is efficient for electrochemical investigations and to propose future applications of these CMEs. CMEs with MHCF are obtained by deposition of this metal complex on the electrode surface [102], photochemical synthesis in the presence of $[Fe^{III}(CN)_6]^{3-}$ [103] layer-by-layer self-assembly with a metal ion solution and $[Fe^{III}(CN)_6]^{3-}$ [104], combination of electrodeposition and chemical methods [105], and also electrodeposition in the solution of metal ion and $[Fe^{III}(CN)_6]^{3-}$ [106]. It is noteworthy

that the MHCF obtained by electrosynthesis has aroused interest in electrochemical research, as it is known that CMEs with MHCF acquire an increase in the electroactive area and have excellent electrocatalytic activities [101, 107].

The PB and cobalt hexacyanoferrate (CoHCF) are examples of MHCF that stand out for being used to modify the surface of electrodes for applications such as voltammetric, amperiometric [101, 108], and potentiometric [109] sensors. The use of electrosynthesis to obtain CMEs with PB and CoHCF is advantageous because it provides an increase in the electroactive area of the electrode surface, a smaller number of reaction steps, and because it allows the *in-situ* formation of CMEs.

Electrodeposition is the main electrochemical route for the formation of PB [110], CoHCF [111] and the hybrid complex of PB and CoHCF (Fe-CoHCF) [112]. In this electrosynthesis procedure, solutions of Fe^{3+} salts and ferricyanide $[Fe^{III}(CN)_6]^{3-}$ are used for electroforming PB in the presence of electrolytes containing K^+ ion. The solution of the Co^{2+} and $[Fe^{III}(CN)_6]^{3-}$ salt in an electrolyte containing Na^+ ion is used in the electrochemical formation of CoHCF. The hybrid complex of Fe-CoHCF is obtained by electrosynthesis in electrolytes containing solutions K^+ and Na^+ ions, as well as Co^{2+}, Fe^{3+}, and $[Fe^{III}(CN)_6]^{3-}$ ions. The literature also reports the electroformation of PB in acidic solution (pH < 2) containing only $[Fe^{III}(CN)_6]^{3-}$ [105]. An electrodeposition procedure adopted in the electroforming of PB in HCl-KCl at pH 2.0 electrolyte is illustrated in Fig. 8. The use of an acid electrolyte containing K^+ ion is important for the efficient formation and adsorption of PB on the electrode surface and for obtaining defined redox processes for the Fe^{2+}/Fe^{3+} and Fe^{3+}/Fe^{2+} transitions. In this electrosynthesis procedure, redox scans are applied in the range of −0.600 V to 1.00 V at 50 mVs^{-1}, in which the increase of the scan cycles provides PB electroformation on the electrode surface, obtaining in situ an CMEs with PB.

3.1.2 Electrosynthesis of CMEs with MHCF

A procedure for simultaneous obtaining of PB and CoHCF by electrosynthesis was proposed by Furtado and Magalhães [113], where CMEs with PB and CoHCF was obtained. In this method, an edge-plane pyrolytic graphite electrodes (EPPGE) modified nanoparticle of $CoFe_2O_4$/Chit/PTCA (where $CoFe_2O_4$ = cobalt ferrite, Chit = chitosan, and PTCA = Perylene-3,4,9,10-tetracarboxylic acid) was used. Where the source of Fe^{3+} and Co^{2+} ions were the intrinsic metals of this nanoparticle.

In the proposed electrosynthesis procedure, the EPPGE surface must be cleaned for adsorption of the $CoFe_2O_4$/Chit/PTCA nanoparticle as follows: First, it is polished using fine sandpaper (2000 μm porosity) and with an alumina suspension (0.50 μm porosity), then the EPPGE is sonicated in isopropyl alcohol for 20 min. The efficiency of the cleaning process must be evaluated by cyclic voltammetry measurements between −0.600 and +0.800 V. Then, an aliquot of 10 μL of the aqueous dispersion at 1.25 g L^{-1} of the nanoparticle is deposited on the surface of EPPGE and dried in an oven at 40 °C for 40 min (see Fig. 9).

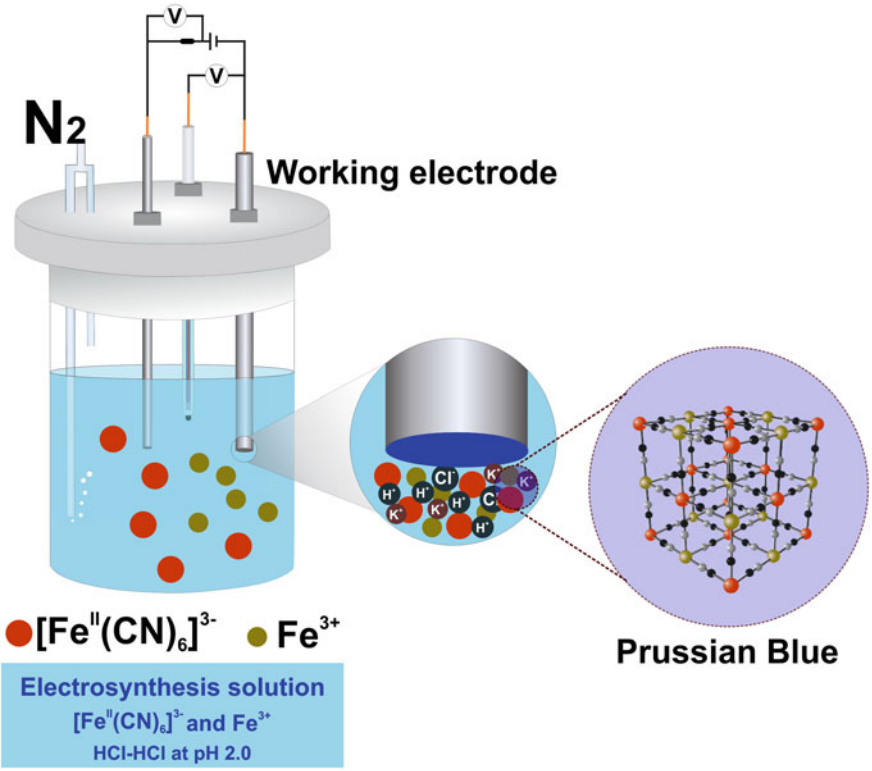

Fig. 8 Hypothetical illustration of the electrochemical formation of PB in a solution containing Fe^{3+} and $[Fe^{III}(CN)_6]^{3-}$ ions in the presence of KCl–HCl electrolyte

In the following steps, the precursor electrode III′ (EPPGE/ $CoFe_2O_4$/Chit/PTCA) is immersed in BR buffer pH 1.60, then cyclic voltammograms (CVs) is recorded in the potential range between −0.600 V to +0.800 V at 50 mV s^{-1}. This procedure is performed to know the voltammetric profile of the electrode III′ in Britton-Robinson (BR) buffer at pH 1.60 before electrosynthesis. The PB and CoHCF are obtained by electrosynthesis by immersing the electrode III′ in a solution of $K_4[Fe(CN)_6]\cdot 3H_2O$ at 1.00 mmol L^{-1} dissolved in BR buffer pH 1.60 and applying 100 scan cycles of the redox potential between −0.600 and +0.800 V at 50 mV s^{-1}. After 100 scan cycles, the electrode III produced must be washed with jets of ultrapure water and immersed only in BR buffer at pH 1.60. CVs are registered in the same redox potential interval and scan rate, verifying in the CVs of electrode III (III'/PB/CoHCF) the voltammetric profile of redox peaks attributed the presence of PB and CoHCF, showing simultaneous electroformation of these MHCF. Vishnu and Kumar [114] used the intrinsic iron present in the impurity of the graphite pencil lead and obtained PB on the surface of pencil graphite electrode (PGE), the procedure used is summarized in Fig. 10. This electrode of PGE modified with PB obtained by electrosynthesis was

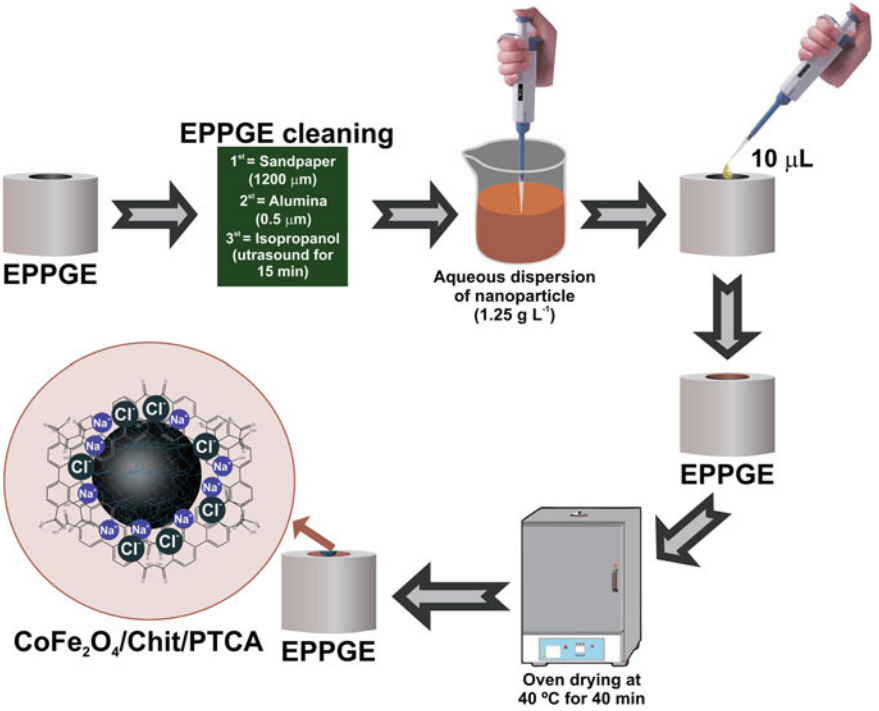

Fig. 9 Illustration of the EPPGE modification with $CoFe_2O_4$/Chit/PTCA, forming the precursor electrode III′ (EPPGE/$CoFe_2O_4$/Chit/PTCA)

used for the determination of H_2O_2, showing that the PGE/PB has application with electrochemical sensor.

Electrochemical Behavior of CMEs with PB and CoHCF

The CMEs with PB and CoHCF obtained by simultaneous electrosynthesis have very characteristic redox peaks and are well known in the literature of MHCF. In Fig. 11a, b, A1/C1 redox peak observed between +0.300 to −0.400 V is attributed to the Fe^{3+}/Fe^{2+} redox reaction characteristic of the transition from PB to Prussian White (PW) [115–117], in the soluble (Eq. 2) and insoluble (Eq. 3) form of PB. These same redox peaks were also found for hybrid film of PB and CoHCF (Fe-CoHCF) modifying a ceramic carbon electrode (CCE) [112], as shown in Fig. 11b.

$$NaFe^{III}\left[Fe^{II}(CN)_6\right]\text{ (PB)} + Na^+ + e^- \rightleftharpoons Na_2Fe^{II}\left[Fe^{II}(CN)_6\right]\text{ (PW)} \quad (2)$$

$$Fe_4^{III}\left[Fe^{II}(CN)_6\right]_3\text{(PB)} + 4Na^+ + 4e^- \rightleftharpoons Na_4Fe_4^{II}\left[Fe^{II}(CN)_6\right]_3\text{ (PW)} \quad (3)$$

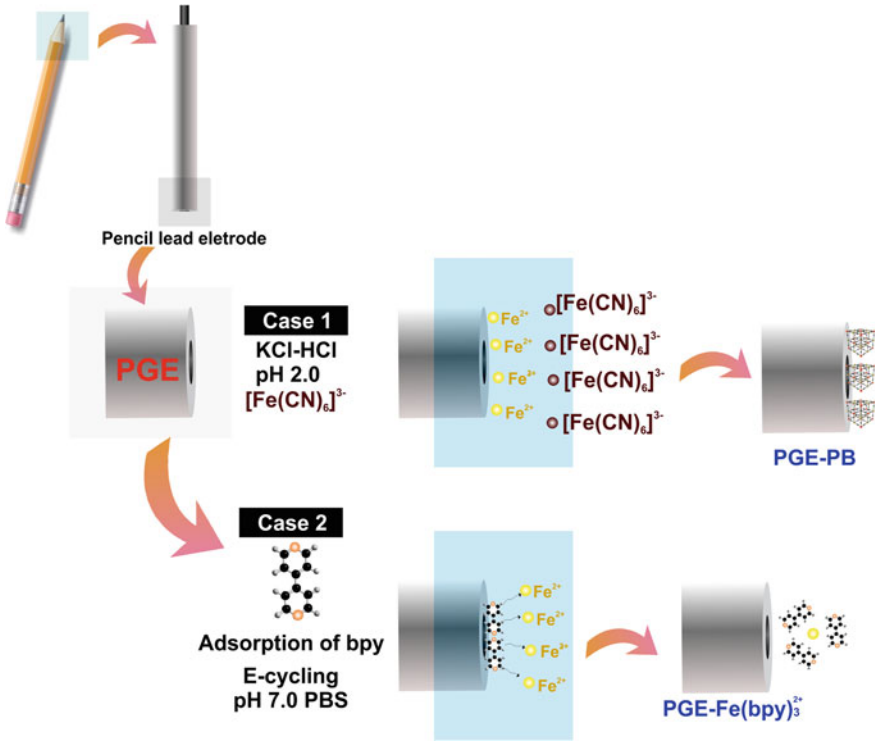

Fig. 10 Cartoon for the role of intrinsic iron in pencil lead electrode for the in-situ electrochemical derivatization as PGE-PB (case-1) and PGE-Fe(bpy)$_3^{2+}$ (case-2) hybrids with Fe(CN)$_6^{3-}$ and surface adsorbed bpy precursors. Inset cartoon is the structure of graphite and clay in the pencil lead. Reprinted with permission from Reference. [114]. Copyright 2017 Elsevier

The electrochemical formation of CoHCF was suggested by the presence of the A3/C3 redox peak pair between +0.300 to +0.600 V. This pair redox peaks is attributed to the Co^{3+}/Co^{2+} reactions (Eqs. 4 and 5), Fe^{3+}/Fe^{2+} (Eqs. 6 and 7) of CoHCF formed by electrosynthesis in the presence of a solution with Co^{2+}, $[Fe^{III}(CN)6]^{3-}$ and Na^+ ion of the electrolyte.

$$NaCo^{III}\left[Fe^{II}(CN)_6\right] + Na^+ + e^- \rightleftarrows Na_2Co^{II}\left[Fe^{II}(CN)_6\right] \tag{4}$$

or

$$Co_3^{III}\left[Fe^{II}(CN)_6\right]_2 + 2\,Na^+ + 3e^- \rightleftarrows Na_2Co_3^{II}\left[Fe^{II}(CN)_6\right]_2 \tag{5}$$

$$NaCo^{II}\left[Fe^{III}(CN)_6\right] + Na^+ + e^- \rightleftarrows Na_2Co^{II}\left[Fe^{II}(CN)_6\right] \tag{6}$$

or

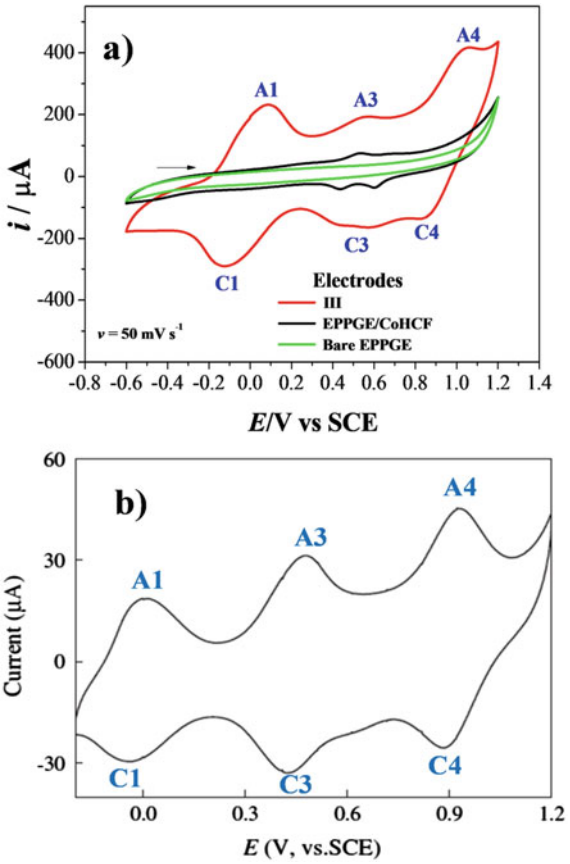

Fig. 11 Cyclic voltammograms: **a** in BR buffer at pH 1.60. Adapted and reprinted with permission from Ref. [113]. Copyright 2020 Elsevier. **b** The hybrid cobalto-iron hexacyanoferrate nanoparticles modified electrode ceramic carbon electrode (CCE) in 0.10 mol L^{-1} NaCl + 0.05 mol L^{-1} HAc-NaAc buffer at scan rates 20 mV s^{-1}. Adapted and reprinted with permission from Reference. [112] Copyright 2013 Elsevier

$$Co_3^{II}\left[Fe^{III}(CN)_6\right]_2 + 2Na^+ + 2e^- \rightleftarrows Na_2Co_3^{II}\left[Fe^{II}(CN)_6\right]_2 \quad (7)$$

It is also observed in Fig. 11a that there is no redox peak in the cyclic voltammogram of bare EPPGE when it is immersed only in BR buffer at pH 1.60. However, for electrode III, there are three pairs redox peaks, two being assigned to PB (A1/C1 and A4/C4) and one to CoHCF (A3/C3). The A4/C4 redox peak with $E_{1/2} = +0.947$ V refers to the Fe^{3+}/Fe^{2+} transition from Prussian Green (PG) to PB [110, 118], as represented in Eq. 8.

$$Fe^{III}\left[Fe^{III}(CN)_6\right]\text{ (PG)} + Na^+ + e^- \rightleftarrows NaFe^{III}\left[Fe^{II}(CN)_6\right]\text{ (PB)} \quad (8)$$

The presence of A3/C3 redox peak with $E_{1/2} = 0.548$ V in the EPPGE/CoHCF (Fig. 11a) also suggests the electroformation of CoHCF on the surface of the bare EPPGE. This observation shows that this redox peak in the EPPGE/CoHCF is located in the same potential range in which the A3/C3 redox peak in electrode III was verified, giving evidence that PB and CoHCF are formed simultaneously during

electrosynthesis. The electrode systems modified with Fe and Co hexacyanoferrates have applications in the area of electrochemical sensors, and to know the feasibility of these systems, some initial investigations need to be carried out, and this will be addressed in the next item of this chapter.

3.1.3 Applications of PB and CoHCF

The interaction of the redox chemical species $[Fe(CN)_6]^{4-/3-}$ on the surface of modified electrodes is used to know the electrochemical properties of these electrodes in comparison to the bare electrode and also to evaluate the binding between peptides in biosensors used in the determination of biomarkers.[119] In Fig. 12, electrode III has a higher anodic (i_{pa}) and cathodic (i_{pc}) peak current value which is attributed to the increase in the estimated area increase value electroactivity of this modified electrode compared to bare EPPGE. The well-defined $[Fe(CN)_6]^{4-/3-}$ redox processes (Fig. 12), showing that the preparation steps were efficient to obtain modified electrodes with better electrochemical properties (for example, electrode with higher electroactive area) [113], which is necessary for future research applications focused in ion exchange system [120], electrochemical and potentiometric sensors [109].

Ceramic carbon electrode (CCE) modified with PB and CoHCF hybrid films (Co-FeHCF/MWCNT/CCE) showed excellent electrocatalytic activity for isoniazid oxidation [112]. The large increase in i_p values is observed in Fig. 13 due to the presence of MHCF on the electrode surface. This modified electrode also has similar characteristics to electrode III in Fig. 12. This feature shows that this system is promising as an electrochemical sensor for isoniazid determination and that it can also be tested for other analytes.

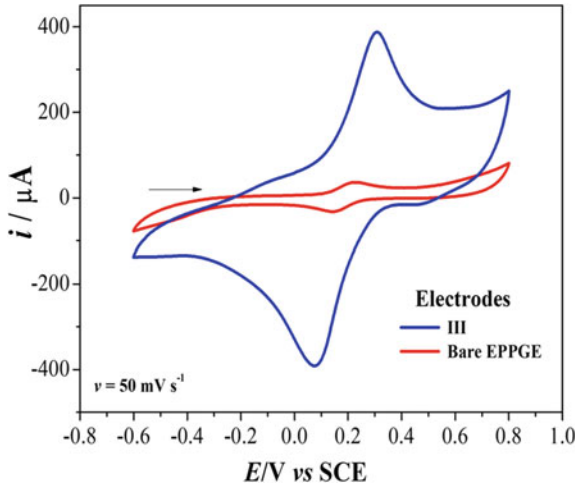

Fig. 12 Cyclic voltammograms of different electrodes in 0.10 mol L^{-1} KCl containing 1.00 mmol L^{-1} $[Fe(CN)_6]^{4-/3-}$

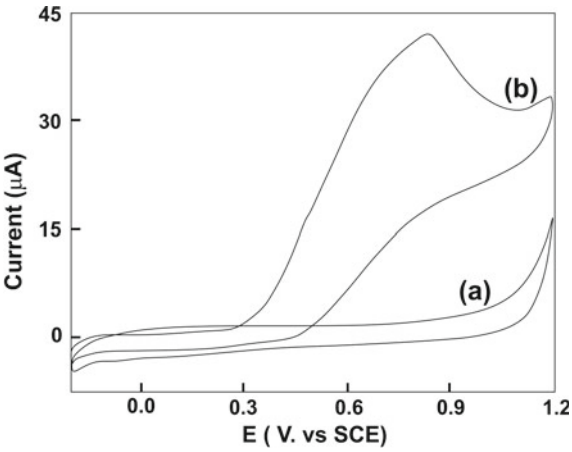

Fig. 13 Cyclic voltammograms of MWCNT/CCE in 0.10 mol L^{-1} NaCl + 0.05 mol L^{-1} HAc–NaAc buffer with the presence (**a**) and absence (**b**) of 2.5 mM isoniazid, scan rate, 20 mV s^{-1}. Reprinted with permission from Ref. [112]. Copyright 2013 Elsevier

The literature shows the development of electrochemical sensors [100, 105, 121], electrochemical immunosensor [122], and biosensors [99] made with different hexacyanoferrates and their application in the determination of different analytes. In a stage of the development of electrochemical sensors, studies with cyclic voltammetry are necessary to know the voltammetric profile of the electroactive chemical species that are modifying the electrode surface. Cyclic voltammogram of Fig. 14 shows electrode III (black line) in the presence of BR buffer pH at 1.60, where only the redox pairs A1/C1 and A3/C3 referring to PB and CoHCF, respectively, were evidenced. It was observed in Fig. 14 that the increase in the dopamine (DA) concentration caused an increase in the i_p values referring to the DA redox pair, thus making it possible to correlate the DA concentration with the i_p values. This suggests the possibility of using a more sensitive voltammetric technique [123, 124], such as differential pulse or square wave voltammetry, to construct a calibration curve, aiming at the development of a future electrochemical sensor for DA determination in matrices of interest.

In the detection of biomarkers, the literature presents electrochemical immunosensors system that contain MHCF in its composition. Xiaoran Gao et al. [125] used PB nanoparticles for tumor diagnosis and provided in his paper a summary of strategies that employ PB nanoparticles as a mediator of electron transfer and also being important for biomedical applications involving tumors. In the following items, other modified electrode systems will be presented as sensors for the determination of some biomarkers.

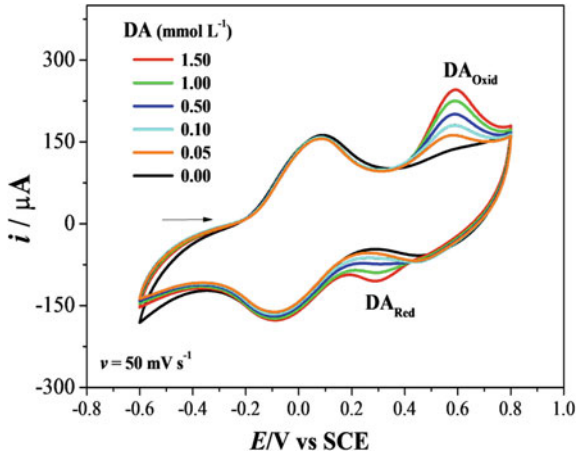

Fig. 14 Cyclic voltammograms of electrode III in the presence of different DA concentrations

3.2 Eletrochemistry of Metal-Based Nanomaterials

Currently, the electrochemistry of metal-based nanomaterials (NMs) has aroused the interest of researchers in multidisciplinary areas, due to its applications in catalysis, energy conversion and storage, and sensors [126–131]. The activity of NMs depends strongly on their size, shape, and surface morphology [132–136]. Furthermore, high surface area to mass ratio and high density of active sites are key factors in electrodic reactions [137, 138]. Among the variety of NMs available, metal-based nanomaterials, e.g., silver, gold, and platinum, are among the main sensing materials for electrochemical, biological, and biomedical applications (Fig. 15) [139, 140]. In particular, these nanomaterials are effectively applied in electrochemistry due to high chemical stability and offer advantages in electrode preparation for electrochemical sensors, such as ease of preparation and simple manufacturing process [141–144].

Advancement of nanotechnology has favored the growth in the number of applications of silver nanomaterials (Ag–NMs) in the environmental, biomedical, industrial, and electrochemical areas [134, 138–140]. In electrochemistry, a large number of various sensors based on Ag–NMs are being developed based on nanoparticle detection interfaces functionalized by polymers or molecular and for the construction of different biosensors, including enzyme-based electrodes and immunosensors [138–140].

Metallic nanomaterials are widely used to modify electrode surfaces to significantly increase the electrode's ability to transport electrons and improve the adsorption of substances [139, 140]. In this sense, Ozkan and colleagues showed through electrochemical methods that a glassy carbon electrode (GCE) modified with carboxylate-functionalized multiwalled carbon nanotube (COOH-fMWCNT) and AgNPs exhibited better selectivity and greater sensitivity for emedastine difumarate (EDD) when compared to AgNPs/GCE, MWCNT/GCE, or COOH-fMWCNT/GCE.

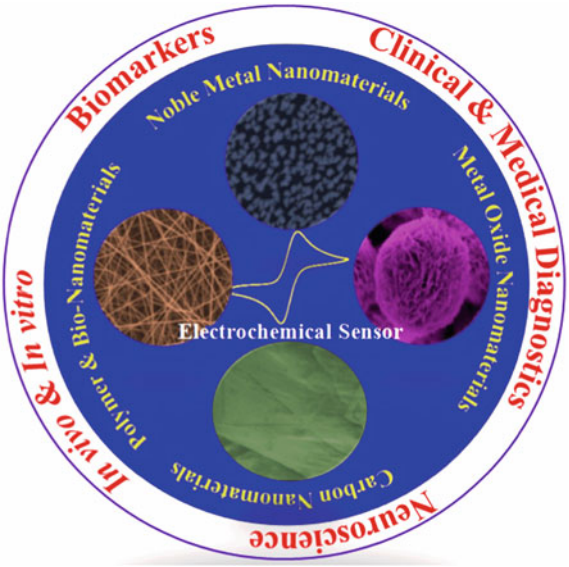

Fig. 15 Schematic illustration of nanomaterials employed as sensing materials for electrochemical, biological, and biomedical applications. Reprinted with permission from Ref. [140]. Copyright 2018 Elsevier

Figure 16 show the electrochemical behavior of EDD compound using cyclic voltammetry (CV) method in 5 mM $K_3[Fe(CN)_6]/K_4Fe[(CN)_6]$, solution as redox probe for glassy carbon electrode (GCE) modified. It is possible to observe that Ag-based nanomaterials increase the conductivity of the composite on the GCE surface which make COOH-fMWCNT/AgNPs/GCE nanosensor sensitive and good electrocatalytic activity toward emedastine difumarate electro-oxidation [141].

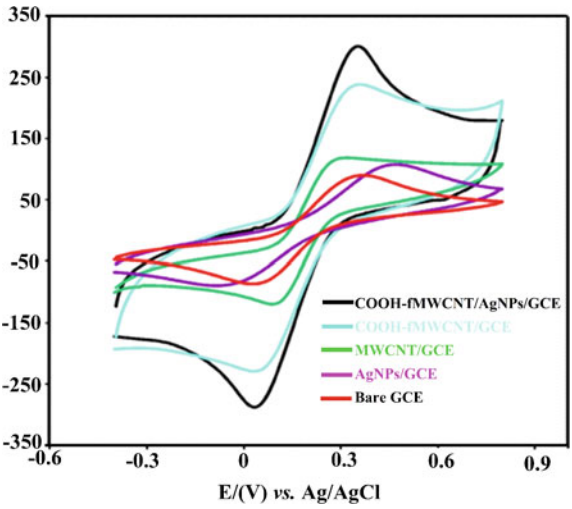

Fig. 16 CVs of bare GCE (red line), AgNPs/GCE (magenta line), MWCNT/GCE (green Line), COOH-fMWCNT/GCE (cyan line), and COOH-fMWCNT/AgNPs/GCE (black line) in 5 mM $K_3[Fe(CN)_6]/K_4Fe[(CN)_6]$ of 0.1 mM EDD in 0.1 M PB solution pH 2.0 [140]. Copyright 2020 Elsevier

In the case of biosensors for DNA, gold nanomaterials (Au-NMs). The physical and chemical characteristics of Au-NMs favor the immobilization of biomolecules, as shown in the schematic of Fig. 17. In this sense, use of Au-NMs possible obtain electrochemical biosensors, one of the most representative of all biosensors, with further sensitivity and excellent analytical performance, favoring the bioactivity of the device [138, 142, 143].

These nanomaterials acting as "electron wires" can facilitate the direct transfer of electrons between redox proteins and bulk electrode materials, thus allowing electrochemical detection without redox mediators [144–146]. Redox center of most oxido reductases is electrically insulated by the protein. In this sense, different strategies are proposed to develop enzymatic electrodes based on Au-NMs, such as: immobilization of the enzyme directly on the electrode surface [147, 148], direct attachment by the use of cysteine [149, 150], via thiol linkers [151–153], and through covalent bonds [154, 155]. Zhang and co-workers (2018) developed a sensitive and selective electrochemical biosensor for polynucleotide kinase (PNK) using gold nanoparticles (AuNPs) [144]. The preparation of this device occurred as shown in Fig. 18

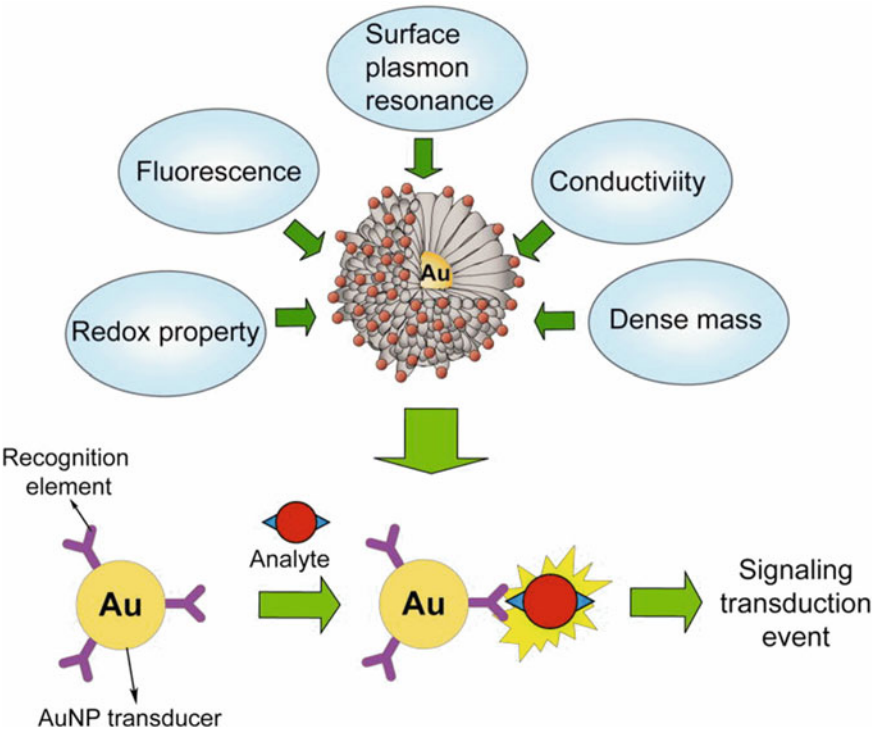

Fig. 17 Physical properties of AuNPs and schematic illustration of a AuNP-based detection system. Reprinted with permission from Ref. [141]. Copyright 2011 American Chemical Society

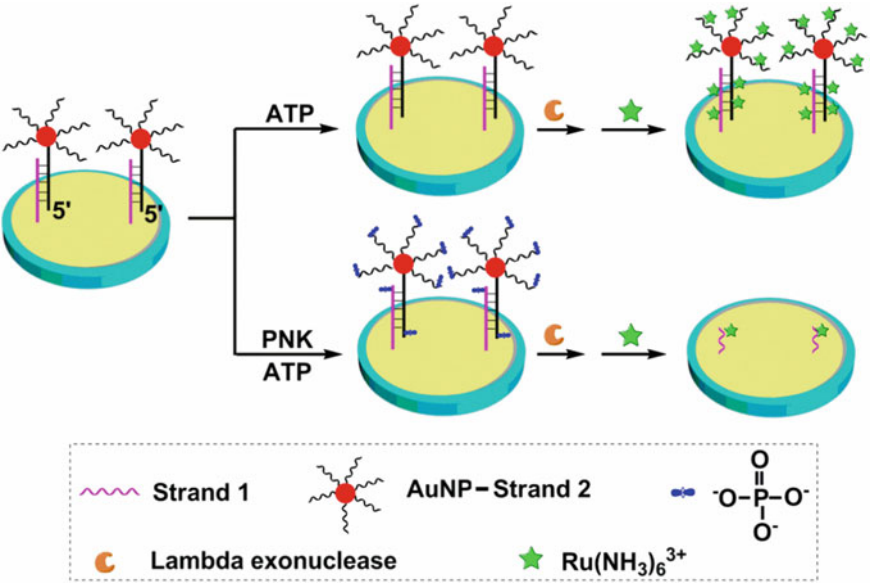

Fig. 18 Schematic illustration of an electrochemical biosensor for PNK assay based on AuNP-mediated lambda exonuclease cleavage-induced signal amplification. Reprinted with permission from Ref. [144]. Copyright 2018 Elsevier. Society

Briefly, mercaptohexanol was immobilized via gold sulfur chemistry onto gold electrode surface ($d = 2$ mm). Then, DNA strands (i.e., strand 1 and strand 2) interacted with AuNP to form AuNP-strand 2 conjugates. Thus, strand 2- modified electrode surface can form AuNP-strand 2- strand 1 conjugates. The $[Ru(NH_3)_6]^{3+}$ was used as electrochemically active indicator to electrostatically interact with the DNA strands immobilized on electrode surface.

P3T film doped with Ag showed a high sensitivity compared to those doped with other metallic particles such as Cu, Co, Au, and Pd, also the detection using square wave voltammetry (SWV) increases the oxidation signals than cyclic voltammetry (CV). A sensitivity and oxidation process these electrodes were investigated by cyclic voltammetry and square wave voltammetry (SWV). Among the prepared electrodes, the P3T film doped with Ag showed a high sensitivity compared to those doped with other metallic particles such as Cu, Co, Au, and Pd, also the detection using SWV increases the oxidation signals than CV, as shown in Fig. 19a, b [161]. All electrodes show the peak of irreversible oxidation of AA obtained on a platinum, in a potential range from 0.443 to 0.089 V (Fig. 19a). The difference in potential values corresponding to the peaks of AA oxidation may be related to the electrocatalytic activity of the material immobilized on the electrode. The good sensitivity of the P3T-Ag film in relation to the target molecule AA, due to the high electronic conductivity and good stability of silver nanoparticles in aqueous solution [162]. Furthermore, the authors showed that the developed electrochemical sensor (P3T-Ag) is selective for

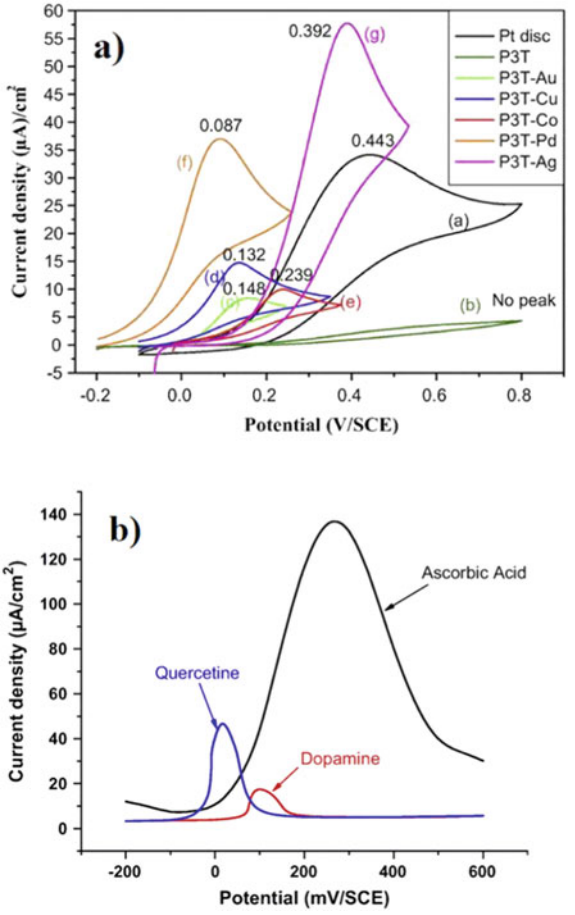

Fig. 19 **a** cyclic voltammograms responses corresponding to the electroanalysis of AA (5 mM) in the solution (PBS, 0.1 M, pH 7.4) using working electrode: Platinum disk (*a*), unmodified P3T film (*b*), P3T–Au (*c*), Cu–P3T (*d*), Co–P3T (*e*), P3T–Pd (*f*), and P3T–Ag (*g*). **b** Selectivity: electrochemical responses of ascorbic acid, dopamine and quercetin at P3T–Ag films using square wave voltammetry. Adapted and reprinted with permission from Ref. [162]. Copyright 2015 Elsevier

other molecules such as ascorbic acid, dopamine, and quercetin (Fig. 19b). Therefore, NMs and metal-based compounds are excellent materials that can be applied to modify electrode surfaces used in electrochemical analysis [163–165]. A more detailed discussion about modified electrodes will be presented in item 4 of this chapter.

4 Electrodes Modified with Inorganic Compounds

The search for improvement in the selectivity and sensitivity of sensors and biosensors has aroused the interest of the scientific community over the years [166]. Thus, the use of inorganic compounds for the modification of electrode surfaces appears as an alternative to improve the electrochemical response of sensors and biosensors,

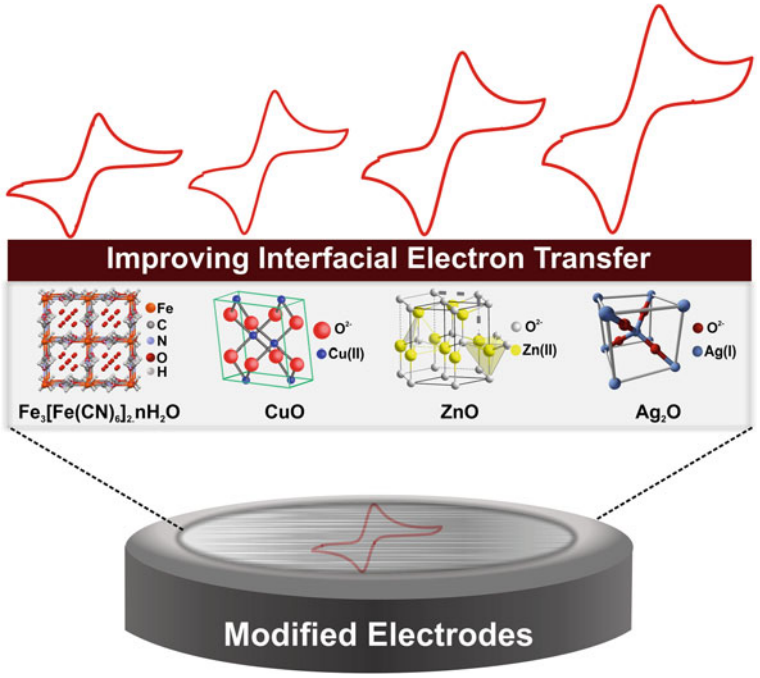

Fig. 20 Schematic representation of main inorganic compounds used for modified electrode surfaces. Source of structures from Refs. [167–169], public domain

thus reducing their limitations. Figure 20 shows the schematic representation of main inorganic compounds used for modified electrode surfaces.

PB and PBA complexes show promise for modifying the surface of electrodes, due to their thermal, structural, and electrochemical properties [170, 171]. Katic et al. [172] modified the surface of the 3D printed graphene electrode with Prussian Blue (3DGrE/PB) and after characterization, compared the performance of 3DGrE/PB with conventional electrodes: glassy carbon, gold, and platinum in real samples. The anchoring of PB nanoparticles on the surface of the graphene electrode was made possible by the oxygenated functional groups formed by the electrochemical treatment undergone by the electrode, which allows electrostatic interactions between the Fe^{3+} cations of the PB NPs and negatively charged oxygen of the treated graphene. The electrochemical performance of 3DGrE/PB was satisfactory compared to conventional electrodes, demonstrating that it is promising for detecting molecular targets [172].

Another group of inorganic compounds widely used for surface modification of electrodes, due to their excellent electrocatalytic properties are metallic phthalocyanines (PcM). These molecules can shift sensor selectivity toward the desired analyte [173]. In this sense, Sánchez-Calvo et al. [174] used cobalt (II) phthalicin

(CoPc) suspended in an aqueous medium to modify the surface of paper-based electrodes initially modified with carbon-based nanomaterials. The authors combined CoPc nanoparticles with different carbon-based nanomaterials to form hybrids with catalytic performance. Paper electrodes based on graphene oxide modified with cobalt phthalicin (GO-CoPc) demonstrated better results in the sensing of glucose and H_2O_2 compared to the other developed electrodes [174]. On the other hand, Nantaphol et al. [175] used cobalt phytalocyanin II (CoPc) to modify a screen-printed carbon electrode forming a new, inexpensive, simple, and sensitive paper-based electrochemical device (CoPc-SPCE) for determination of 8-hydroxyquinoline (8-HQ). Figure 21 shows (a) image of the developed device. The authors also investigated the electrochemical behavior of 8-HQ in the electrode modified with CoPc by cyclic voltammetry. The 8-HQ anode peak potential shifted to more negative values (from 0.46 to 0.39 V), as shown in Fig. 21b. This is due to the rapid transfer of electrons on the surface of the modified electrode, resulting in a reduction in the over potential for the oxidation of 8-HQ and an increase in the oxidation current. Therefore, according to the results obtained, the reaction mechanism for the oxidation of 8-HQ in CoPc-SPCE was proposed in Fig. 21c. CoPc-SPCE also showed good linear correlation and low detection limit (0.89 μM) [175].

Nanostructured materials are among the most suitable when you want to improve the performance of a sensor (detection limit, sensitivity, and response time). Among the nanostructured semiconductor oxides, ZnO shows promise for applications in (bio)sensing due to its chemical stability, cost-effectiveness, non-toxicity, and its high isoelectric point [176]. Thus, Manavalan et al. [177] used ZnO nanostars linked to graphene oxide nanosheets to modify a screen-printed carbon electrode (SPCE). The modified SPCE had a wide linear dynamic range (0.03–670 μM), low detection limit (1.2 nM; at $S/N = 3$), a comparatively low working voltage (−0.69 V vs. Ag/AgCl); and excellent sensitivity (16.5 μA μM^{-1} cm^{-2}). The excellent electrochemical performance of the modified electrode was attributed to the high conductivity of graphene oxide and the catalytic activities of zinc oxide [177]. On the other hand, Bahrami et al. [166] used the electrodeposition technique to develop a new voltammetric biosensor by modifying pencil graphite electrodes (PGEs) with Cu/Cu_xO nanoparticles. The developed electrode presented a low detection limit (LOD) of 1.06 μM, high sensitivity of 0.51 μA/μM and high selectivity (EUA − EDA = 0.14 V) for the detection of dopamine showing itself more efficient than biosensors modified by rod-shaped CuO, ZnO, TiO_2 and AuNPs already reported in the literature [166].

Properties such as high surface area, small size, good conductivity, and catalytic properties give nanoparticles the possibility of being used as electrode modification agents. In this sense, Muhammad et al. [178] developed a screen-printed electrochemical sensor (SPE) modified with carbon nanotubes (CNTs) and gold nanoparticles (Au NPs) using ethylenediamine (en) as a crosslinker. The modified electrode, SPE/CNT/en/AuNPs, Fig. 22a, was sensitive for the determination of thiamphenicol (TAP), with a wide linear range (0.1–30 μM), low detection limit (0.003 μM) in addition to of good stability, reproducibility, repeatability and high sensitivity. When investigating the electrochemical behavior of SPE as well as during modifications

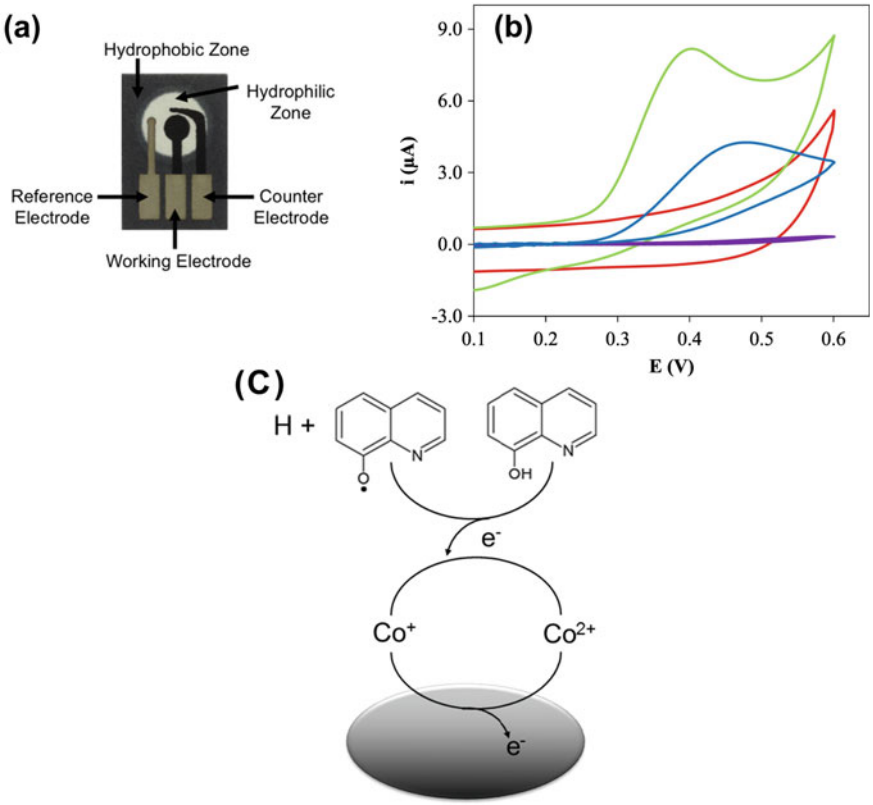

Fig. 21 **a** A photograph of electrochemical paper-based analytical device consisting of screen-printed working, reference, and counter electrodes. **b** CVs of the unmodified SPCE (purple line) and CoPc-SPCE (red line) in a ratio of 85:15 of Britton–Robinson buffer (pH 7):ethanol. CVs of the oxidation of 0.1 mM 8-HQ at the unmodified SPCE (blue line) and CoPc-SPCE (green line). Scan rate: 50 mV s^{-1} and **c** Electrochemical oxidation mechanism of 8-HQ at a CoPc-SPCE. Adapted and reprinted with permission from Ref. [175]. Copyright 2019 Elsevier

with CNTs and AuNPs (1 mM CV, 0.1 M KCl) the authors observed for SPE a pair of discrete redox peaks due to low electron transfer rate and surface area limited, Fig. 22a. On the other hand, when there is modification with CNTs, Fig. 22b, there is an increase in peak currents due to the versatile properties of CNTs that improve conductivity and surface area. After modification with CNT/en/AuNPs, there is an even more pronounced increase in peak currents, due to the synergistic effect between AuNPs and CNTs that caused an increase in electron transfer and effective surface area, Fig. 22b. The authors also proposed the charge transport mechanism that takes place on the surface of the modified electrode, Fig. 22 c, since, with the data obtained, it can be concluded that there is an oxidation reaction of TAP in SPE/CNT/en/AuNPs involves two protons and two electrons [178].

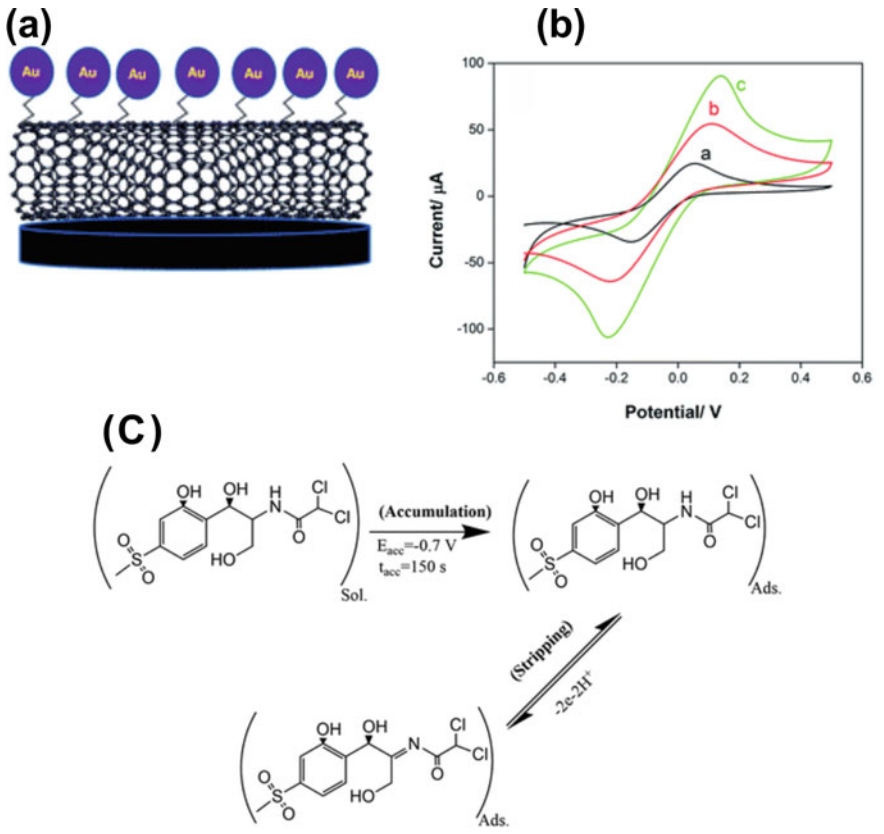

Fig. 22 **a** Illustration of electrode modified; **b** CVs of bare SPE (**a**), SPE/CNTs (**b**), and SPE/CNT/en/AuNPs (**c**) in $K_3Fe(CN)_6$ (1 mM, 0.1 M KCl); **c** The proposed mechanism for determination of TAP based on the adsorptive stripping voltammetry on the surface SPE/CNTs/en/AuNPs. Reproduced from Ref. [178] with permission from the Royal Society of Chemistry

5 Inorganic Compounds Applied to the Detection of Biomarkers

A fast and accurate diagnosis is essential for pathogen identification and appropriate treatment. The application of inorganic complexes and metal-based nanomaterials is an excellent strategy in the development of diagnostic platforms that allow rapid and cost-effective early detection of diseases through electrochemical devices [179], as illustrated in Fig. 23.

Among the diseases that most affect women are breast cancer [180]. Carcinoembryonic antigen (CEA) is a substance found on the surface of some cells. In a normal, healthy adult, the level is relatively low unless certain diseases, including certain forms of cancer, are present. Lin and colleagues proposed the construction of an unlabeled electrochemical immunosensor (Ab/Au/pDA/Au–PB/CNT/GCE) for the

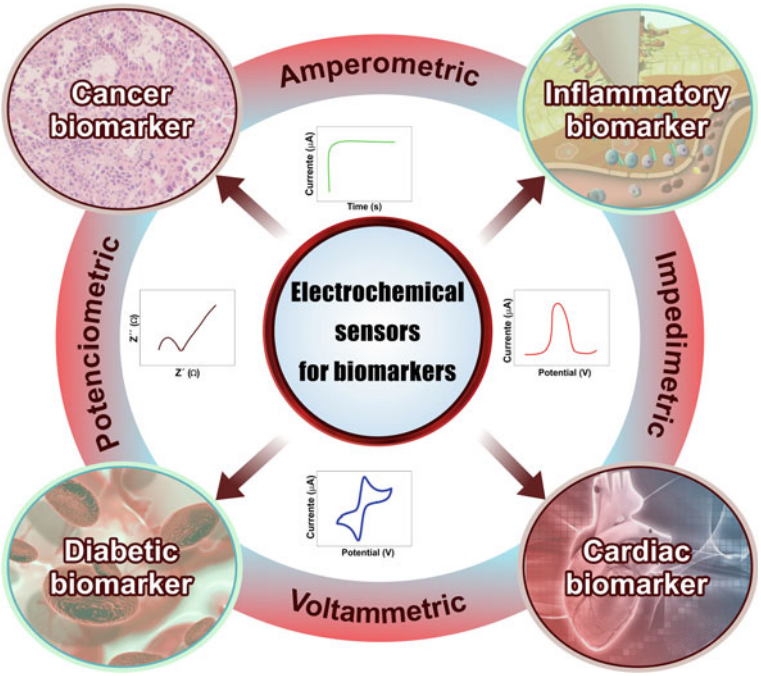

Fig. 23 Schematic illustration of the main applications of sensors for biomarkers

early and effective diagnosis of cancer based on tumor biomarkers. The electrochemical immunoassay platform was constructed using a glassy carbon electrode (GCE) modified with carbon nanotubes (CNT). The nanocomposite of PB and Au nanoparticles (Au–PB) was prepared by electrochemical coprecipitation on the modified glassy carbon electrode CNT/GCE, Fig. 24a). While PB is used as a redox probe, Au nanoparticles (AuNPs) were used to facilitate electrical conductivity. The stability of the Au–PB nanocomposite was improved by an in situ polymerized polydopamine (pDA) layer, as a bifunctional ligand which also acts as a reducing agent for the subsequent deposition of the second layer of Au nanoparticles. Then, the recognition antibody was attached to Au nanoparticles, which provide the recognition interface. The manufactured immunosensor has good stability and is capable of detecting CEA without reagent over a wide range (0.005–50 ng mL^{-1}) with high reproducibility. The detection mechanism of the marker-free electrochemical immunosensor is based on the reduction of the PB signal measured by cyclic voltammetry (CV) and differential pulse voltammetry (DPV) due to the increase of the isolation on the electrode surface by the formation of the CEA-antibody compound, as shown in Fig. 24b) [181].

C-reactive protein (CRP) is an essential protein that appears to have high concentrations during inflammatory conditions. Early detection of inflammatory mediators, including C-reactive protein, is of great diagnostic importance in many human diseases [97].

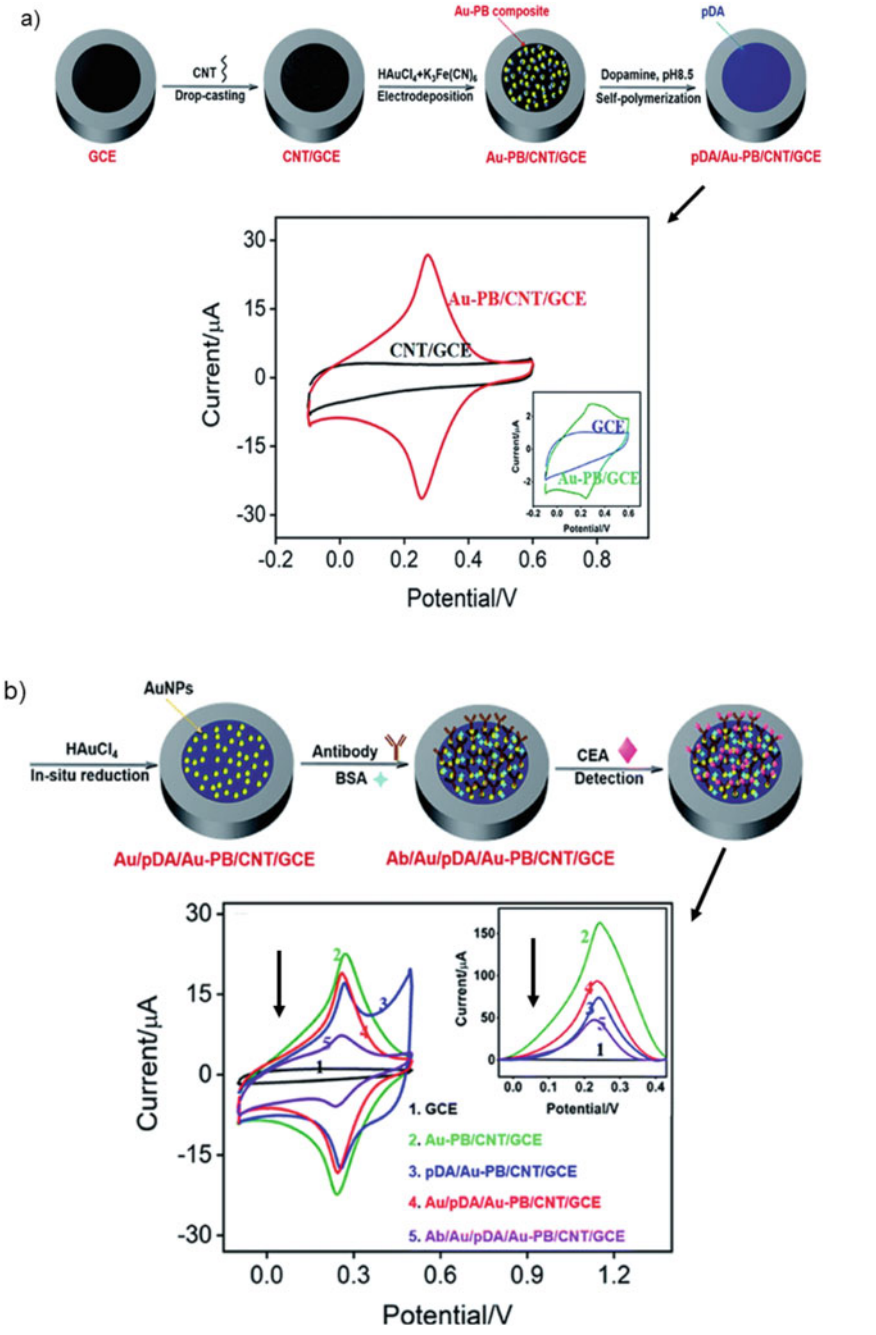

Fig. 24 Illustrative scheme of electrode construction (Ab/Au/pDA/Au–PB/CNT/GCE). **a** Increase in load transfer caused by the presence of AuNP and CNT. **b** Reduction of the PB signal measured by CV and DPV, after the formation of the CEA-antibody compound. Adapted and reprinted with permission from Ref. [181]. Copyright 2020, The Royal Society of Chemistry

To increase specificity and sensitivity in C-reactive protein electrochemical biosensor measurements, Dong et al. [183] developed a new electrochemical immunosensor based on ZnO in a porous carbon matrix (ZnO/MPC) through thermolysis of a mixed ligand metal–organic framework (MOF) (Zn-BDC-TED). The excellent properties of ZnO nanostructures such as low toxicity, high surface-to-volume ratio, excellent biocompatibility, chemical stability, and electrochemical activities, in addition to electrostatic interactions with enzymes or proteins, combined with the excellent properties of carbon structures, arouse great interest in applications of these hybrid materials in electrochemical sensors. The electrochemical immunosensor for C-reactive protein (CRP) was prepared as show the Fig. 25a). The ZnO/MPC nanocomposite interacted with ionic liquid (IL) in the carbon paste electrode (CPE) to form ZnO/MPC/ILCPE. Then, antibodies (anti-CRP) were absorbed for specifically interact with CRP. The analytical performance of immunosensor based on ZnO/MPC against the various concentrations of CRP was evaluated by DPV, as shown in Fig. 25b). It is observed that, with increasing CRP concentration (0.01–1000 ng·mL−1), the immunosensor current peaks decrease, which indicates the formation of the immune complex on the electrode surface, thus having a blocking electron transport, which occurs because the insulating properties of antibodies make it difficult for interfacial electrons to move [182].

Heart disease affects thousands of people around the world [183]. Myocardial infarction (MI) is a leading cause of human death, in which it is caused when the coronary arteries become completely blocked in certain areas of the myocardium and do not receive enough blood and oxygen to the related ischemic regions [184]. The troponin plays an essential role in the cardiac contraction system [185]. Troponin I (TnI) is considered an inhibitor of actomyosinATPase, in which increased levels of cardiac TnI can be seen in the patient's bloodstream after myocardial injury due to an MI, being used as a cardiac biomarker in the diagnosis of myocardial damage [186]. Negahdary describes the use of an electrochemical troponin I aptasensors using a sheet metal from titanium (Ti) as a working electrode modified with gold NPs. Subsequently, a high-affinity TnI thiol-functionalized aptamer was prepared and immobilized on the surface of the Ti/Au NPs electrode. The sulfhydryl group of the aptamer formed a covalent bond bond Au–S with the gold NPs and a self-assembled monolayer of TnI aptamer was formed on the surface of the working electrode, Fig. 26. The detection mechanism was based on decreasing the electrocatalytic activity (oxidation signal) of $[Fe(CN)_6]^{3-/4-}$ as a redox marker. When TnI was present in the environment, the negatively charged TnI molecules were captured by the aptamer strands and led to a further decrease in the TnI current voltammetry of differential pulse (DPV) related to the redox marker. The range of linear detection of this signaling aptasensor was from 1 to 1100 pM with an LOD of 0.18 pM [187].

Prostate cancer is one of the main male health concerns in the world, being the second most common type of cancer among men. The use of screening and early detection testing, such as prostate-specific antigen (PSA), is one of the common methods to reduce prostate cancer mortality rates, where it is possible to verify the emergence of the tumor by monitoring PSA levels in biological fluids, in particular blood. PSA is a 32–33 kDa single-chain glycoprotein produced by the prostate that is

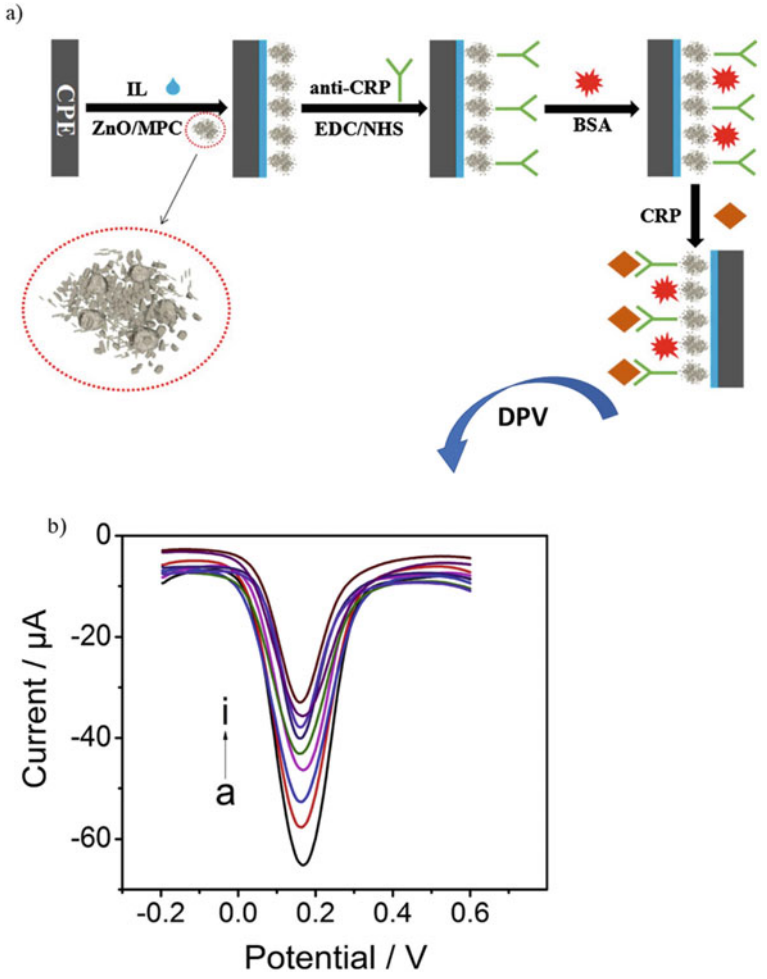

Fig. 25 **a** Schematic diagram of the processes to prepare CRP immunosensor. **b** DPV responses of BSA/anti-CRP/ZnO/MPC/IL-CPE to different CRP concentration (0.01, 0.1, 1, 10, 50, 100, 300, 500, 1000 ng·mL^{-1}). Adapted and reprinted with permission from Ref. [182]. Copyright 2016, Elsevier

present in serum, seminal plasma and benign hyperplastic and prostatic fluids; therefore, it is a special tumor biomarker for prostate cancer screening and post-treatment monitoring [188]. Akbariand co-workers (2019) proposed the construction of an electrochemical biosensor (GO/AuNPs/Ab1), Fig. 27a) in the presence of $[Fe(CN)_6]^{3-/4-}$ as a redox marker for prostate-specific antigen (PSA) detection. The voltammograms (Fig. 27b) showed an increase in the active surface area, indicating that GO/AuNPs increased the active surface of the electrode for the conjugation of more biomarker (curve a). Immobilization of antibodies and antigens on the electrode surface leads

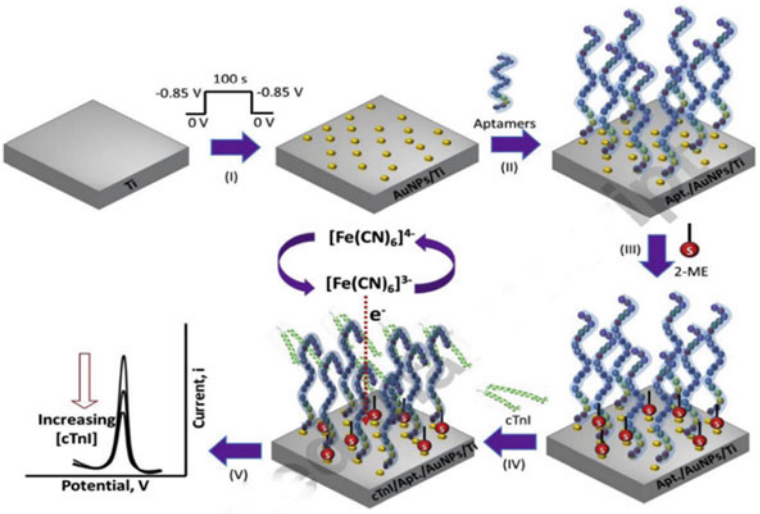

Fig. 26 Schematic representation of apt sensor based on gold NPs, PB NP for the detection of TnI. Adapted and reprinted with permission from Ref. [187]. Copyright 2016, Elsevier

to a decrease in the active surface area of the electrode due to the hampering effect on the electron transfer rate which results in the attenuation of redox peaks. (c–e curves), demonstrating that this biosensor can be used as a diagnostic tool for the detection of tumor markers, prostate cancer, and clinical analyzes [189].

Prion diseases (or transmissible spongiform encephalopathies) are a group of invariably fatal neurodegenerative diseases characterized by progressive dementia and motor dysfunction and may be spontaneous, genetic, or acquired [190]. Prion diseases in mammals are associated with a conformational transition of the cellular prion protein from its native conformation (PrP^{C}) to a pathological isoform called "scrapie prion protein" (PrP^{Sc}). Its abnormal shape, called prion protein (PrP^{C}) forms fibers that accumulate inside the cell, affecting its function, spread to neighboring cells, causing brain damage and, ultimately, the death of the organism [191]. Li and collaborators proposed the construction of a immunosensor for the sensitive detection of (PrP^{C}) based on nanocubes of Prussian blue analogs Co–Co (Co–Co PBA), modified by gold nanoparticles (PBA-AuNPs) with the presence of the antibody (Ab2) of immobilized PrP^{C} on the surface (Ab2-PBA-AuNPs), Fig. 28a). In this study, the authors state that the biosensor shows a linear dependence of the peak currents in the DPV with the increase of the PrPC concentration, as shown in Fig. 28b), with a concentration varying between 0.075 and 100 pg mL^{-1} and a detection limit of 0.014 pg mL^{-1} [192].

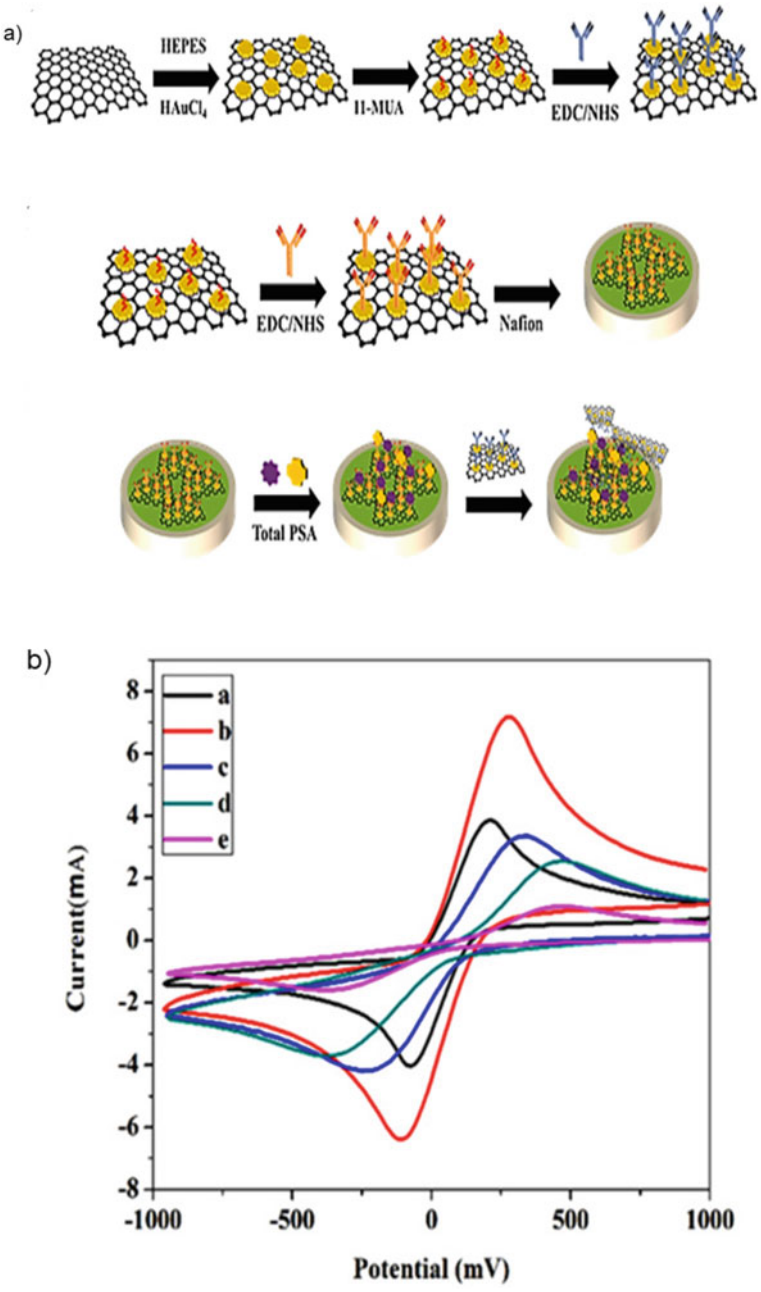

Fig. 27 **a** Schematic representation of the construction of the electrochemical biosensor for detection of prostate-specific antigen (PSA). **b** Electrochemical behavior of the electrode surface: *a* single GC, *b* G/GNP, *c* G/GNP/Ab1, *d* G/GNP/Ab1/Ag, and *e* G/GNP/Ab1/Ag/Ab2. Adapted and reprinted with permission from Ref. [189]. Copyright 2019, WILEY–VCH Verlag GmbH & Co

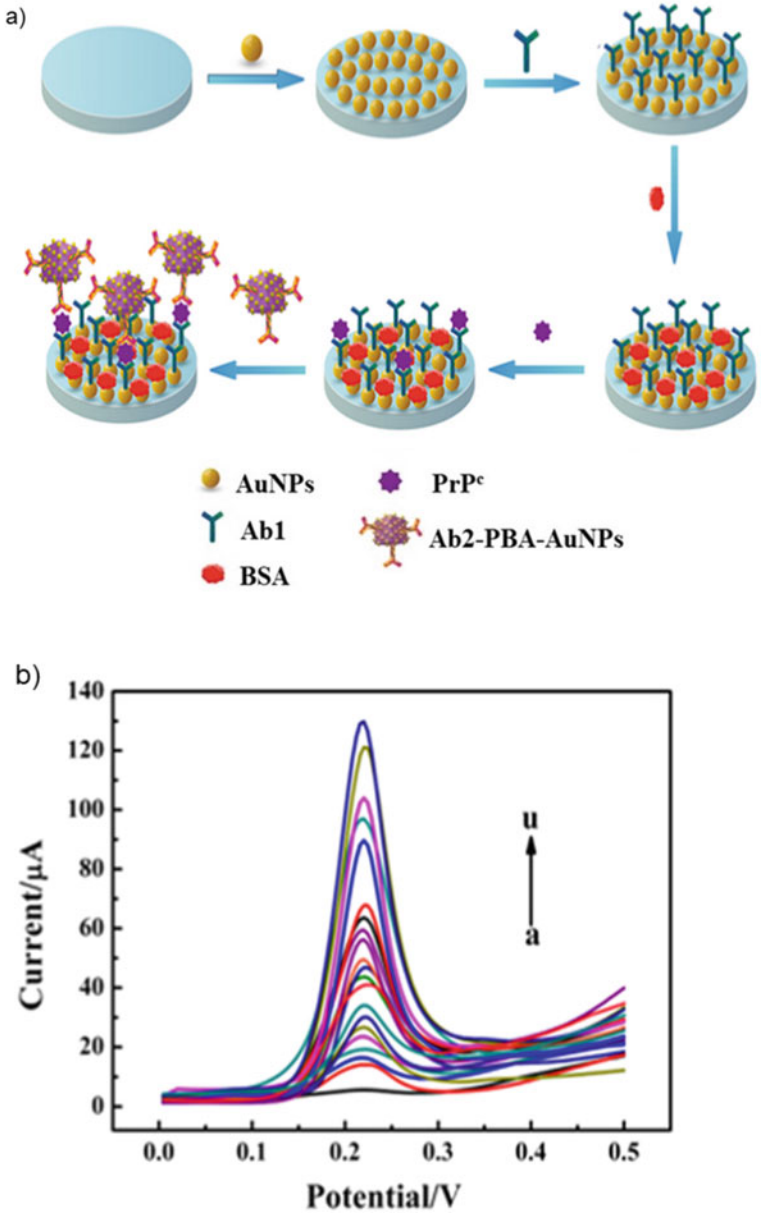

Fig. 28 **a** Schematic representation of the construction of the immunosensor (Ab2-PBA-AuNPs) for detection prion protein (PrPC). **b** Electrochemical response of the dependence of I on logarithmic values of concentrations (PrP^C). Adapted and reprinted with permission from Ref. [192]. Copyright 2016, Elsevier

6 Prospects and Challenges

This chapter reviews inorganic complexes and metal-based as excellent candidates for the development of biomarkers sensors. For this purpose, various compounds are employed in the modification of the electrodes' surface, such as Prussian Blue and analog, hexacyanoferrate and analog, nanoparticles of Au, Ti, ZnO, and metal-modified NTCs. We were highlighted that the appropriate choice of inorganic complex, strategy mechanism of functionalization of electrodes, and optimization of the organizational structure play a fundamental role in designing new biomarkers sensors for fast and accurate diagnosis. Thus, researchers in this area seek to develop essentials tools for the identification and more appropriate treatment of diseases. Moreover, this chapter also points out more suitable ways to build more efficient devices.

Acknowledgements The financial support from CAPES and CNPq is gratefully acknowledged.

References

1. Werner A (2012) Beitrag zur konstitution anorganischer verbindungen. BoD–Books on Demand
2. Shriver DF, Atkins PW, Langford CH (1999) Inorganic chemistry
3. Jorgensen CK (2012) Inorganic complexes. Elsevier
4. Wells AF (2012) Structural inorganic chemistry. Oxford University Press
5. Tong M-L, Chen X-M (2017) Synthesis of coordination compounds and coordination polymers. In: Modern inorganic synthetic chemistry. Elsevier
6. Lawrance GA (2010) Introduction to coordination chemistry. Wiley, Australia
7. McCleverty JA, Meyer TJ (2005) Comprehensive coordination chemistry II: transition metal groups 7 and 8
8. Kole GK, Vittal JJ (2013) Solid-state reactivity and structural transformations involving coordination polymers. Chem Soc Rev 42:1755–1775
9. Davis CM, Curran KA (2007) Manipulation of a Schlenk line: preparation of tetrahydrofuran complexes of transition-metal chlorides. J Chem Educ 84:1822–1823
10. Konar S, Clearfield A (2008) Solvothermal synthesis and characterization of two high-nuclearity mixed-valent manganese phosphonate clusters. Inorg Chem 47:3489–3491
11. Chen XM, Tong ML (2007) Solvethermal in situ metal/ligand reactions: a new bridge between coordination chemistry and organic synthetic chemistry. Acc Chem Res 40:162–170
12. Leininger S, Olenyuk B, Stang PJ (2000) Self-assembly of discrete cyclic nanostructures mediated by transition metals. Chem Rev 100:853–907
13. Takahashi K et al (2008) Evidence of the chemical uniaxial strain effect on electrical conductivity in the spin-crossover conducting molecular system: [FeIII(qnal)2][Pd(dmit)2]5·acetone. J Am Chem Soc 130:6688–6689
14. Higham L et al (1998) Formation and X-ray structure of a novel water-soluble tertiary–secondary phosphine complex of ruthenium (ii): [Ru{P(CH_2 OH)$_3$}$_2$ {P(CH_2 OH) 2H} 2Cl_2]. Chem Commun 443:1107–1108
15. Pantalon Juraj N, Kirin SI (2021) Inorganic stereochemistry: Geometric isomerism in bis-tridentate ligand complexes. Coord Chem Rev 445

16. Dabb SL, Fletcher NC (2015) Mer and fac isomerism in tris chelate diimine metal complexes. Dalt. Trans. 44:4406–4422
17. Andreini C, Cavallaro G, Lorenzini S (2012) FindGeo: a tool for determining metal coordination geometry. Bioinformatics 28:1658–1660
18. Cremades E, Echeverría J, Alvarez S (2010) The trigonal prism in coordination chemistry. Chem Eur J 16:10380–10396
19. Von Zelewsky A (1996) Stereochemistry of coordination compounds. Wiley
20. Eslami A, Hasani, N. Thermoanalytical study of linkage isomerism in coordination compounds. Part III: A DSC study on the effect of counterion on the solid state isomerization of nitro and nitrito linkage isomers of pentaamminecobalt(III) complexes. Thermochim. Acta 575, 114–121 (2014).
21. Sabbani S, Das SK (2009) Reversible nitro-nitrito inter-conversion in a simple mono-nuclear nickel(II) complex [NiII{C6H4(NH2)2}2(NO2)2] in the solid state. Inorg Chem Commun 12:364–367
22. Kauffman GB (2013) Alfred Werner: founder of coordination chemistry. Springer Science & Business Media
23. Lawrance GA (2013) Introduction to coordination chemistry. Wiley
24. Kauffman GB (2011) Coordination chemistry: history. Encycl Inorg Bioinorg Chem. https://doi.org/10.1002/9781119951438.eibc0046
25. Kauffman GB (1973) Alfred Werner's research on structural isomerism. Coord Chem Rev 11:161–188
26. Constable EC, Housecroft CE (2013) Coordination chemistry: the scientific legacy of Alfred Werner. Chem Soc Rev 42:1429–1439
27. Fromm KM (2000) Coordination compounds, vol 7. Kirk-Othmer Encyclopedia of Chemical Technology
28. Bertini G, Gray HB, Gray H, Valentine JS, Stiefel EI, Stiefel E (2007) Biological inorganic chemistry: structure and reactivity. University Science Books
29. García-Sánchez MA et al (2013) Crossed and linked histories of tetrapyrrolic macrocycles and their use for engineering pores within sol-gel matrices. Molecules 18:588–653
30. Turner DR, Batten SR, Neville SM (2009) Coordination polymers: design, analysis and applications. RSC Publishing, Cambridge
31. Trudu F, Amato F, Vaňhara P, Pivetta T, Peña-Méndez EM, Havel J (2015) Coordination compounds in cancer: past, present and perspectives. J Appl Biomed
32. Arnesano F et al (2011) Probing the interaction of cisplatin with the human copper chaperone atox1 by solution and in-cell NMR spectroscopy. J Am Chem Soc 133:18361–18369
33. Jamieson ER, Lippard SJ (1999) Structure, recognition, and processing of cisplatin—DNA adducts
34. Brabec V (2002) DNA modifications by antitumor platinum and ruthenium compounds: their recognition and repair. Prog Nucleic Acid Res Mol Biol 71:1–68
35. Farrer NJ, Griffith DM (2020) Exploiting azide–alkyne click chemistry in the synthesis, tracking and targeting of platinum anticancer complexes. Curr Opin Chem Biol 55:59–68
36. Göschl S et al (2017) Comparative studies of oxaliplatin-based platinum(iv) complexes in different in vitro and in vivo tumor models. Metallomics 9:309–322
37. Riddell IA, Lippard SJ (2018) Cisplatin and oxaliplatin: our current understanding of their actions. In: Metallo-drugs: development and action of anticancer agents
38. Galluzzi L et al (2014) Systems biology of cisplatin resistance: past, present and future. Cell Death Dis 5:1–18
39. Marusak RA, Doan K, Cummings SD (2007) Integrated approach to coordination chemistry: an inorganic laboratory guide. Wiley
40. Malinowski J, Zych D, Jacewicz D, Gawdzik B, Drzeżdżon J (2020) Application of coordination compounds with transition metal ions in the chemical industry—a review. Int J Mol Sci 21:1–26
41. Ma DL et al (2016) Metal complexes for the detection of disease-related protein biomarkers. Coord Chem Rev 324:90–105

42. Smith BR, Gambhir SS (2017) Nanomaterials for in vivo imaging. Chem Rev 117:901–986
43. Meggers E (2009) Targeting proteins with metal complexes. Chem Commun, 1001–1010. https://doi.org/10.1039/b813568a
44. Xiong E et al (2017) Triple-helix molecular switch electrochemical ratiometric biosensor for ultrasensitive detection of nucleic acids. Anal Chem 89:8830–8835
45. Lin S et al (2017) The application of a G-quadruplex based assay with an iridium(iii) complex to arsenic ion detection and its utilization in a microfluidic chip. J Mater Chem B 5:479–484
46. Katayama Y, Ohgi T, Mitoma Y, Hifumi E, Egashira N (2016) Detection of influenza virus by a biosensor based on the method combining electrochemiluminescence on binary SAMs modified Au electrode with an immunoliposome encapsulating Ru (II) complex. Anal Bioanal Chem 408:5963–5971
47. Zhou B, Zhu M, Qiu Y, Yang P (2017) Novel Electrochemiluminescence-Sensing Platform for the Precise Analysis of Multiple Latent Tuberculosis Infection Markers. ACS Appl Mater Interfaces 9:18493–18500
48. Zhao Q, Li F, Huang C (2010) Phosphorescent chemosensors based on heavy-metal complexes. Chem Soc Rev 39:3007–3030
49. Zhao J et al (2012) Transition metal complexes with strong absorption of visible light and long-lived triplet excited states: from molecular design to applications. RSC Adv 2:1712–1728
50. Markwalter CF, Kantor AG, Moore CP, Richardson KA, Wright DW (2019) Inorganic complexes and metal-based nanomaterials for infectious disease diagnostics. Chem Rev 119:1456–1518
51. Khoshnevisan K et al (2019) Nanomaterial based electrochemical sensing of the biomarker serotonin: a comprehensive review. Microchim Acta 186
52. Yaqoob AA et al (2020) Recent advances in metal decorated nanomaterials and their various biological applications: a review. Front Chem 8:1–23
53. Yin D, Li X, Ma Y, Liu Z (2017) Targeted cancer imaging and photothermal therapy via monosaccharide-imprinted gold nanorods. Chem Commun 53:6716–6719
54. Elahi N, Kamali M, Baghersad MH (2018) Recent biomedical applications of gold nanoparticles: a review. Talanta 184:537–556
55. Solanki PR, Kaushik A, Agrawal VV, Malhotra BD (2011) Nanostructured metal oxide-based biosensors. NPG Asia Mater. 3:17–24
56. Şerban I, Enesca A (2020) Metal oxides-based semiconductors for biosensors applications. Front Chem 8:1–8
57. Siriwong C, Wetchakun N, Inceesungvorn B, Channei D, Samerjai T, Phanichphant S (2012) Doped-metal oxide nanoparticles for use as photocatalysts. Prog Cryst Growth Charact Mater 58:145–163
58. Medhi R, Marquez MD, Lee TR (2020) Visible-light-active doped metal oxide nanoparticles: review of their synthesis, properties, and applications. ACS Applied Nano Materials 3:6156–6185
59. Sun S, Jiang N, Xia D (2011) Density functional theory study of the oxygen reduction reaction on metalloporphyrins and metallophthalocyanines. J Phys Chem C 115:9511–9517
60. Akyüz D, Keleş T, Biyiklioglu Z, Koca A (2017) Electrochemical pesticide sensors based on electropolymerized metallophthalocyanines. J Electroanal Chem 804:53–63
61. Amsterdam SH et al (2019) Electronic coupling in metallophthalocyanine-transition metal dichalcogenide mixed-dimensional heterojunctions. ACS Nano 13:4183–4190
62. Zhou Q, Liu ZF, Marks TJ, Darancet P (2021) Electronic structure of metallophthalocyanines, MPc (M = Fe Co, Ni, Cu, Zn, Mg) and fluorinated MPc. J Phys Chem A 125:4055–4061
63. Imran M, Ramzan M, Qureshi AK, Azhar Khan M, Tariq M (2018) Emerging applications of porphyrins and metalloporphyrins in biomedicine and diagnostic magnetic resonance imaging. Biosensors 8:1–17
64. Ptaszyńska AA et al (2018) Porphyrins inactivate *Nosema* spp. microsporidia. Sci Rep 8:1–11
65. Varchi G et al (2015) Engineered porphyrin loaded core-shell nanoparticles for selective sonodynamic anticancer treatment. Nanomedicine 10:3483–3494

66. Pereira MM, Dias LD, Calvete MJF (2018) Metalloporphyrins: bioinspired oxidation catalysts. ACS Catal, 10784–10808. https://doi.org/10.1021/acscatal.8b01871
67. Liu L, Zhou Y, Liu S, Xu M (2018) The applications of metal−organic frameworks in electrochemical sensors. ChemElectroChem 5(1):6–19
68. Tokoro H, Ohkoshi SI (2011) Novel magnetic functionalities of Prussian blue analogs. Dalt Trans 40:6825–6833
69. Catala L, Mallah T (2017) Nanoparticles of Prussian blue analogs and related coordination polymers: from information storage to biomedical applications. Coord Chem Rev 346:32–61
70. Herren, F., Fischer, P. & Ludi, A. Molecules and Long-Range Magnetic Order. 956–959 (1980).
71. Samain L et al (2013) Relationship between the synthesis of Prussian blue pigments, their color, physical properties, and their behavior in paint layers. J Phys Chem C 117:9693–9712
72. Kjeldgaard S et al (2021) Strategies for synthesis of Prussian blue analogues. R Soc Open Sci 8
73. Nai J, Lou XW (2019) Hollow structures based on Prussian blue and its analogs for electrochemical energy storage and conversion. Adv Mater 31:1–20
74. Johansson A, Widenkvist E, Lu J, Boman M, Jansson U (2005) Fabrication of high-aspect-ratio Prussian blue nanotubes using a porous alumina template. Nano Lett 5:1603–1606
75. Hoffman HA, Chakrabarti L, Dumont MF, Sandler AD, Fernandes R (2014) Prussian blue nanoparticles for laser-induced photothermal therapy of tumors. RSC Adv 4:29729–29734
76. Wikimedia Commons c2022. Available in: https://commons.wikimedia.org/wiki/File:Hydrated-Prussian-blue-unit-cell-a-centroids-all-OH-3D-bs-17.png/. Accessed on: 14 Feb 2022
77. Zakaria MB, Chikyow T (2017) Recent advances in Prussian blue and Prussian blue analogues: synthesis and thermal treatments. Coord Chem Rev 352:328–345
78. Sawan S, Maalouf R, Errachid A, Jaffrezic-Renault N (2020) Metal and metal oxide nanoparticles in the voltammetric detection of heavy metals: a review. TrAC—Trends Anal Chem 131:116014
79. Maduraiveeran G, Sasidharan M, Jin W (2019) Earth-abundant transition metal and metal oxide nanomaterials: synthesis and electrochemical applications. Prog Mater Sci 106:100574
80. Pal J, Pal T (2015) Faceted metal and metal oxide nanoparticles: design, fabrication and catalysis. Nanoscale 7:14159–14190
81. Chia X, Eng AYS, Ambrosi A, Tan SM, Pumera M (2015) Electrochemistry of nanostructured layered transition-metal dichalcogenides. Chem Rev 115:11941–11966
82. Lu L (2019) Nanoporous noble metal-based alloys: a review on synthesis and applications to electrocatalysis and electrochemical sensing. Microchim Acta 186
83. Giziński D et al (2020) Nanostructured anodic copper oxides as catalysts in electrochemical and photoelectrochemical reactions. Catalysts 10:1–38
84. Moosavifard et al (2015) Designing 3D highly ordered nanoporous CuO electrodes for high-performance asymmetric supercapacitors. ACS Appl Mater Interfaces 7:4851–4860
85. Liu F, Zhang L, Wang L, Cheng F (2021) The electrochemical tuning of transition metal-based materials for electrocatalysis. Electrochem Energy Rev. 4:146–168
86. Zhu Y et al (2020) Metal oxide-based materials as an emerging family of hydrogen evolution electrocatalysts. Energy Environ Sci 13:3361–3392
87. Li J, Yan X, Li X, Zhang X, Chen J (2018) A new electrochemical immunosensor for sensitive detection of prion based on Prussian blue analogue. Talanta 179:726–733
88. Hurlbutt K, Wheeler S, Capone I, Pasta M (2018) Prussian blue analogs as battery materials. Joule 2:1950–1960
89. Carvalho CLC et al (2021) Effect of Ibuprofen on the electrochemical properties of Prussian blue/single-walled carbon nanotubes nanocomposite modified electrode. Surfa Interfaces 25
90. Niel P, Shen L, Luo H, Ding B, Xu G, Wang J, Zhang X (2014) Prussian blue analogues: a new class of anode materials for lithium ion batteries. J Mater Chem A 2:5852–5857
91. Wang B et al (2018) Prussian blue analogs for rechargeable batteries. iScience 3:110–133
92. Carvalho et al (2021) Effect of Ibuprofen on the electrochemical properties of Prussian blue/single-walled carbon nanotubes nanocomposite modified electrode. Surf Interfaces 25:101–276

93. Bonhommeau S et al (2008) Metal-to-ligand and ligand-to-metal charge transfer in thin films of Prussian blue analogues investigated by X-ray absorption spectroscopy. Phys Chem Chem Phys 10:5882–5889
94. Aguila D et al (2016) Switchable Fe/Co Prussian blue networks and molecular analogues. Chem Soc Rev 45:203–224
95. Jiménez J-R et al (2020) Electron transfer in the Cs {Mn4Fe4} cubic switch: a soluble molecular model of the MnFe Prussian Blue Analogs (PBAs). Angewandte Chemie 18:8089–8093
96. Zhou N et al (2018) Core−shell heterostructured CuFe@FeFe Prussian blue analogue coupling with silver nanoclusters via a one-step bioinspired approach: efficiently nonlabeled aptasensor for detection of bleomycin in various aqueous environments. Anal Chem 90:13624–13631
97. Lin J et al (2020) Reagentless and sensitive determination of carcinoembryonic antigen based on a stable Prussian blue modified electrode. RSC Adv 10:38316–38322
98. Gao Z et al (2020) An enzyme-free immunosensor for sensitive determination of procalcitonin using NiFe PBA nanocubes@TB as the sensing matrix. Anal Chim Acta 1097:169–175
99. Yao Y, Bai X, Shiu K-K (2012) Spontaneous deposition of Prussian Blue on multi-walled carbon nanotubes and the application in an amperometric biosensor. Nanomaterials 2:428–444
100. Crespilho FN et al (2006) A strategy for enzyme immobilization on layer-by-layer dendrimer-gold nanoparticle electrocatalytic membrane incorporating redox mediator. Electrochem Commun 8:1665–1670
101. Sattarahmady N, Heli H, Moradi SE (2013) Cobalt hexacyanoferrate/graphene nanocomposite—application for the electrocatalytic oxidation and amperometric determination of captopril. Sens Actuators, B Chem 177:1098–1106
102. Wang J et al (2018) Synthesis of hybrid-metal hexacyanoferrates nanoparticle films and investigation of its hybrid vigor. J Electroanal Chem 810:191–198
103. Gimenes DT, Nossol E (2017) Effect of light source and applied potential in the electrochemical synthesis of Prussian blue on carbon nanotubes. Electrochim Acta 251:513–521
104. Deng K et al (2015) Electrochemical preparation, characterization and application of electrodes modified with nickel-cobalt hexacyanoferrate/graphene oxide-carbon nanotubes. J Electroanal Chem 755:197–202
105. Tao W et al (2005) An amperometric hydrogen peroxide sensor based on immobilization of hemoglobin in poly(o-aminophenol) film at iron-cobalt hexacyanoferrate-modified gold electrode. Anal Biochem 338:332–340
106. Abbaspour A, Ghaffarinejad A (2008) Electrocatalytic oxidation of L-cysteine with a stable copper-cobalt hexacyanoferrate electrochemically modified carbon paste electrode. Electrochim Acta 53:6643–6650
107. Haghighi B, Hamidi H, Gorton L (2010) Electrochemical behavior and application of Prussian blue nanoparticle modified graphite electrode. Sens Actuators, B Chem 147:270–276
108. Heli H, Majdi S, Sattarahmady N (2010) Ultrasensitive sensing of N-acetyl-L-cysteine using an electrocatalytic transducer of nanoparticles of iron (III) oxide core-cobalt hexacyanoferrate shell. Sens Actuators, B Chem 145:185–193
109. Giorgetti M et al (2001) Nickel hexacyanoferrate membrane as a coated wire cation-selective electrode. Analyst 126:2168–2171
110. Itaya K (1982) Electrochemistry of Prussian blue modified electrodes: an electrochemical preparation method. J Electrochem Soc 129:1498–1500
111. Chen S-M (1998) Characterization and electrocatalytic properties of cobalt hexacyanoferrate films. Electrochim Acta 43:3359–3369
112. Yu H et al (2013) Preparation of hybrid cobalto-iron hexacyanoferrate nanoparticles modified multi-walled carbon nanotubes composite electrode and its application. J Electroanal Chem 700:47–53
113. Furtado NJS, Magalhães JL (2020) Cobalt ferrite nanoparticles as a source of intrinsic metals for simultaneous electrosynthesis of Prussian blue and cobalt hexacyanoferrate. J Electroanal Chem 871:114315

114. Vishnu N, Kumar AS (2017) Development of Prussian Blue and Fe(bpy)$_3^{2+}$ hybrid modified pencil graphite electrodes utilizing its intrinsic iron for electroanalytical applications. J Electroanal Chem 786:145–153
115. Karyakin AA (2001) Prussian blue and Its analogues: electrochemistry and analytical applications. Electroanalysis 13:813–819
116. Abbaspour A, Kamyabi MA (2005) Electrochemical formation of Prussian blue films with a single ferricyanide solution on gold electrode. J Electroanal Chem 584:117–123
117. Lisowska-Oleksiak A, Nowak AP, Jasulaitiene V (2006) Poly(3,4-ethylenedioxythiophene)-Prussian blue hybrid material: evidence of direct chemical interaction between PB and pEDOT. Electrochem Commun 8:107–112
118. Sharma MK, Aggarwal SK (2013) Simultaneous formation of Prussian blue and copper hexacyanoferrate from a solution of Cu^{2+} and $K_3[Fe(CN)_6]$ in presence of $HAuCl_4$. J Electroanal Chem 705:64–67
119. Negahdary M, Heli H (2019) An electrochemical peptide-based biosensor for the Alzheimer biomarker amyloid-β(1–42) using a microporous gold nanostructure. Microchim Acta 186:775–783
120. Sciacca R et al (2021) Stable films of zinc-hexacyanoferrate: electrochemistry and ion insertion capabilities. J Solid State Electrochem 26:63–72
121. Guimaraes GAA et al (2020) Development and application of electrochemical sensor of boron-doped diamond (BDD) modified by drop casting with tin hexacyanoferrate. J Solid State Electrochem 24:1769–1779
122. Zhang L et al (2019) FeS_2-AuNPs nanocomposite as mimicking enzyme for constructing signal-off sandwich-type electrochemical immunosensor based on electroactive nickel hexacyanoferrate as matrix. Electroanalysis 31:1–8
123. Bard AJ, Faulkner LR (2001) Electrochemical methods, fundamentals and applications. Wiley, New York
124. Brett CMA, Brett AMO (1993) Electrochemistry. Principles, methods and applications. Oxford, Great Britain
125. Gao et al (2020) The application of Prussian blue nanoparticles in tumor diagnosis and treatment. Sensors 20:6905
126. Mirkin MV, Sun T, Yu Y, Zhou M (2016) Electrochemistry at One Nanoparticle. Acc Chem Res, 2328–2335
127. Yang H, Xu W, Zhou Y (2019) Signal amplification in immunoassays by using noble metal nanoparticles: a review. Microchim Acta 186(12):1–22
128. Zamborini FP, Bao L, Dasari R (2012) Nanoparticles in measurement science. Anal Chem 84:541–576
129. Kleijn SE, Lai SC, Koper MT, Unwin PR (2014) Electrochemistry of nanoparticles. Angew Chem, Int Ed 53:3558−3586
130. Campbell FW, Compton RG (2010) The use of nanoparticles in electroanalysis: an updated review. Anal Bioanal Chem 396(1):241–259
131. Antuña-Jiménez D, González-García MB, Hernández-Santos D, Fanjul-Bolado P (2020) Screen-printed electrodes modified with metal nanoparticles for small molecule sensing. Biosensors 10(2):9
132. Anker J, Hall W, Lyandres O et al (2008) Biosensores com nanosensores plasmônicos. Natureza Mater 7:442–453
133. Hernández-Santos D, González-García MB, García AC (2002) Metal-nanoparticles based electroanalysis. Electroanalysis 14(18):1225–1235
134. Chen S, Yuan R, Chai Y et al (2013) Electrochemical sensing of hydrogen peroxide using metal nanoparticles: a review. Microchim Acta 180:15–32
135. Rodrıguez-Sanchez ML, Rodrıguez MJ, Blanco MC, Rivas J, Lopez-Quintela MA (2005) Kinetics and mechanism of the formation of Ag nanoparticles by electrochemical techniques:a plasmon and cluster time-resolved spectroscopic study. J Phys Chem B 109:1183–1191
136. Qaseem A, Chen F, Wu X, Johnston RL (2016) Pt-free silver nanoalloy electrocatalysts for oxygen reduction reaction in alkaline media. Catal Sci Technol 6(10):3317–3340

137. Zhao S, Jin R, Jin R (2018) Opportunities and challenges in CO_2 reduction by gold-and silver-based electrocatalysts: from bulk metals to nanoparticles and atomically precise nanoclusters. ACS Energy Lett 3(2):452–462
138. Sun D, Xu X, Qin Y, Jiang SP, Shao Z (2020) Rational design of Ag-based catalysts for the electrochemical CO_2 reduction to CO: a review. Chemsuschem 13(1):39–58
139. Maduraiveeran G, Sasidharan M, Ganesan V (2018) Electrochemical sensor and biosensor platforms based on advanced nanomaterials for biological and biomedical applications. Biosens Bioelectron 103:113–129
140. Imanzadeh H, Bakirhan NK, Habibi B, Ozkan SA (2020) A sensitive nanocomposite design via carbon nanotube and silver nanoparticles: selective probing of Emedastine Difumarate. J Pharm Biomed Anal 181:113096
141. Saha K, Agasti SS, Kim C, Li X, Rotello VM (2012) Gold nanoparticles in chemical and biological sensing. Chem Rev 112(5):2739–2779
142. Yang X, Yang M, Pang B, Vara M, Xia Y (2015) Gold nanomaterials at work in biomedicine. Chem Rev 115(19):10410–10488
143. Doria G, Conde J, Veigas B, Giestas L, Almeida C, Assunção M, Rosa J, Baptista PV (2012) Noble metal nanoparticles for biosensing applications. Sensors 12(2):1657–1687
144. Cui L, Li Y, Lu M, Tang B, Zhang CY (2018) An ultrasensitive electrochemical biosensor for polynucleotide kinase assay based on gold nanoparticle-mediated lambda exonuclease cleavage-induced signal amplification. Biosens Bioelectron 99:1–7
145. Murata K, Suzuki M, Kajiya K, Nakamura N, Ohno H (2009) High performance bioanode based on direct electron transfer of fructose dehydrogenase at gold nanoparticle-modified electrodes. Electrochem Commun 11(3):668–671
146. Li F, Feng Y, Wang Z, Yang L, Zhuo L, Tang B (2010) Direct electrochemistry of horseradish peroxidase immobilized on the layered calcium carbonate–gold nanoparticles inorganic hybrid composite. Biosens Bioelectron 25(10):2244–2248
147. Xiang C, Zou Y, Sun LX, Xu F (2009) Direct electrochemistry and enhanced electrocatalysis of horseradish peroxidase based on flowerlike ZnO–gold nanoparticle–Nafion nanocomposite. Sens Actuators, B Chem 136(1):158–162
148. Stine KJ (2017) Enzyme immobilization on nanoporous gold: a review. Biochemistry Insights 10
149. Ansari SA, Husain Q (2012) Potential applications of enzymes immobilized on/in nano materials: a review. Biotechnol Adv 30:512–523
150. Andreescu S, Luck LA (2008) Studies of the binding and signaling of surface-immobilized periplasmic glucose receptors on gold nanoparticles: a glucose biosensor application. Anal Biochem 375(2):282–290
151. Li Y, Schluesener HJ, Xu S (2010) Gold nanoparticle-based biosensors. Gold Bulletin 43(1):29–41
152. Li Y, Schluesener HJ, Xu S (2010) Biossensores baseados em nanopartículas de ouro. Touro de Ouro 43:29–41
153. Lei CX, Hu SQ, Gao N, Shen GL, Yu RQ (2004) Bioelectrochemistry 65:33
154. Zhang S, Wang N, Yu H, Niu Y, Sun C (2005) Covalent attachment of glucose oxidase to an Au electrode modified with gold nanoparticles for use as glucose biosensor. Bioelectrochemistry 67(1):15–22
155. Pingarrón JM, Yañez-Sedeño P, González-Cortés A (2008) Gold nanoparticle-based electrochemical biosensors. Electrochim Acta 53(19):5848–5866
156. Antoine O, Bultel Y, Durand R (2001) Oxygen reduction reaction kinetics and mechanism on platinum nanoparticles inside Nafion®. J Electroanal Chem 499(1):85–94
157. Chen A, Holt-Hindle P (2010) Platinum-based nanostructured materials: synthesis, properties, and applications. Chem Rev 110(6):3767–3804
158. Govindhan M, Liu Z, Chen A (2016) Design and electrochemical study of platinum-based nanomaterials for sensitive detection of nitric oxide in biomedical applications. Nanomaterials 6(11):211

159. Harriman A, Millward GR, Neta P, Richoux MC, Thomas JM (1988) Interfacial electron-transfer reactions between platinum colloids and reducing radicals in aqueous solution. J Phys Chem 92(5):1286–1290
160. Welch CM, Compton RG (2006) The use of nanoparticles in electroanalysis: a review. Anal Bioanal Chem 384(3):601–619
161. Maouche N, Nessark B, Bakas I (2019) Platinum electrode modified with polyterthiophene doped with metallic nanoparticles, as sensitive sensor for the electroanalysis of ascorbic acid (AA). Arab J Chem 12(8):2556–2562
162. Lia CY, Cai YJ, Yang CH, Wu CH, Wei Y, Wen TC, Wang TL, Shieh YT, Line WC, Chen WJ (2011) Highly sensitive and selective electrochemical determination of dopamine and ascorbic acid at Ag/Ag_2S modified electrode. Electrochim Acta 56:1955–1959
163. Bilge S, Dogan-Topal B, Atici EB, Sınağ A, Ozkan SA () Rod-like CuO nanoparticles/waste masks carbon modified glassy carbon electrode as a voltammetric nanosensor for the sensitive determination of anti-cancer drug pazopanib in biological and pharmaceutical samples. Sens Actuators B Chem 343:130109
164. Sensors and Actuators B: Chemical, 343, 130109.
165. Yu X, Li Y, Li Y, Liu S, Wu Z, Dong H, Xu Z, Li X, Liu Q (2022) An electrochemical amplification strategy based on the ferrocene functionalized cuprous oxide superparticles for the detection of NSE. Talanta 236:122865
166. Martins, B.; Sampaio, T.; de Farias, A.; Martins, R.d.P.; Teixeira, R.; Oliveira, R.; Oliveira, C.; da Silva, M.; Rodrigues, V.; Dantas, N.; et al. Immunosensor Based on Zinc Oxide Nanocrystals Decorated with Copper for the Electrochemical Detection of Human Salivary Alpha-Amylase. Micromachines, 12, 657, (2021).
167. Bahrami E, Amini R, Vardak S (2021) Electrochemical detection of dopamine via pencil graphite electrodes modified by Cu/Cu_xO nanoparticles. J Alloy Compd 855:157292–157330
168. https://commons.wikimedia.org/wiki/File:Copper(II)-oxide-unit-cell-3D-balls.png (accessed on 30 January 2022).
169. https://commons.wikimedia.org/wiki/File:Wurtzite_polyhedra.png (accessed on 30 January 2022).
170. https://commons.wikimedia.org/wiki/File:Silver(I)-oxide-unit-cell-3D-balls.png (accessed on 30 January 2022).
171. Goda ES, Lee S, Sohail M, Yoon KR (2020) Prussian blue and its analogues as advanced supercapacitor electrodes. J Energy Chem 50:206–229
172. Carvalho CLC, Silva ATB, Luz RAS, Castro GMB, da Luz Lima C, Mastelaro VR, da Silva RR, Oliveira ON, Cantanhêde W (2018) Development of $Co_3[Co(CN)_6]_2/Fe_3O_4$ Bifunctional Nanocomposite for Clinical Sensor Applications. ACS Applied Nano Materials 1:4283–4293
173. Katic V, dos Santos PL, dos Santos MF, Pires BM, Loureiro HC, Lima AP, Queiroz JCM, Landers R, Muñoz RAA, Bonacin JA (2019) 3D Printed Graphene Electrodes Modified with Prussian Blue: Emerging Electrochemical Sensing Platform for Peroxide Detection. ACS Appl Mater Interfaces 11:35068–35078
174. Coelho MKL, da Silva DN, Pereira AC (2019) Development of electrochemical sensor based on carbonaceal and metal phthalocyanines materials for determination of ethinyl estradiol. Chemosensors 7:1–28
175. Sánchez-Calvo A, Costa-García A, Blanco-López MC (2020) Paper-based electrodes modified with cobalt phthalocyanine colloid for the determination of hydrogen peroxide and glucose. Analyst 145:2716–2724
176. Nantaphol S, Jesadabundit W, Chailapakul O, Siangproh W (2019) A new electrochemical paper platform for detection of 8-hydroxyquinoline in cosmetics using a cobalt phthalocyanine-modified screen-printed carbon electrode. J Electroanal Chem 832:480–485
177. Napi MLM, Sultan SM, Ismail R, How KW, Ahmad MK (2019) Electrochemical-based biosensors on different zinc oxide nanostructures: A review. In Materials 12:1–34
178. Manavalan S, Veerakumar P, Chen SM, Lin KC (2020) Three-dimensional zinc oxide nanostars anchored on graphene oxide for voltammetric determination of methyl parathion. Microchim Acta 187:5–13

179. Muhammad A, Hajian R, Yusof NA, Shams N, Abdullah J, Woi PM, Garmestani H (2018) A screen printed carbon electrode modified with carbon nanotubes and gold nanoparticles as a sensitive electrochemical sensor for determination of thiamphenicol residue in milk. RSC Adv 8(5):2714–2722
180. Ma, DL. *et al.* Metal complexes for the detection of disease-related protein biomarkers. coordinate Chem. Rev. 324, 90–105 (2016).
181. Thwaites, RS. *et al.* Info _Outline. Crit. Rev. Clin. Lab. Sci. 8, 1–5 (2020).
182. Ridker, PM. A test in context: High-sensitivity C-reactive protein.*J. Am. Coll. Cardiol.*67, 712–723 (2016).
183. Dong S, Zhang D, Cui H, Huang T (2019) ZnO/porous carbon composite from a mixed-ligand MOF for ultrasensitive electrochemical immunosensing of C-reactive protein. Sensors Actuators, B Chem. 284:354–361
184. Han W et al (2020) The effects of the wenyang huoxue method on coronary heart disease heart failure: A protocol for systematic review. Med. (United States) 99:1–4
185. Ito, R. *et al.* Clinical Differences of Recent Myocardial Infarction Compared with Acute Myocardial Infarction — Insights from the Tokyo CCU Network Multicenter Registry —. circ. J. 84, 1511–1518 (2020).
186. Thiruganasambandamoorthy V et al (2020) Use of conventional cardiac troponin assay for diagnosis of non-ST-elevation myocardial infarction: "The Ottawa Troponin Pathway." PLoS ONE 15:1–15
187. JACC Review Topic of the Week (2019) Sandoval, Y. & Jaffe, AS Type 2 Myocardial Infarction. J Am Coll Cardiol 73:1846–1860
188. Negahdary M (2020) Aptamers in nanostructure-based electrochemical biosensors for cardiac biomarkers and cancer biomarkers: A review. Biosens Bioelectron 152:112018
189. Liu, R., Wu, S., Zhang, B., Guo, M. & Zhang, Y. The association between sleep duration and prostate cancer: A systematic review and meta-analysis.*Medicine (Baltimore).*99, e21180 (2020).
190. Akbari jonous, Z.*et al.* An electrochemical biosensor for prostate cancer biomarker detection using graphene oxide–gold nanostructures. Eng. Life Sci. 19, 206–216 (2019).
191. Rosener, NS *et al.* Clustering of human prion protein and α-synuclein oligomers requires the prion protein N-terminus. common Biol. 3, 1–12 (2020).
192. Baral PK, Yin J, Aguzzi A, James MNG (2019) Transition of the prion protein from a structured cellular form (PrPC) to the infectious scrapie agent (PrPSc). Protein Sci 28:2055–2063
193. Li J, Yan X, Li X, Zhang X, Chen J (2018) A new electrochemical immunosensor for sensitive detection of prion based on Prussian blue analogue. Talanta 179:726–733

Bioelectrodes with Enzyme Cascade Reactions

Jefferson Honorio Franco and Adalgisa R. De Andrade

Abstract We will discuss different approaches toward obtaining deep or total fuel oxidation in biofuel cells. We will explore the reactions involved in enzyme cascades (two or more enzymes) and hybrid configurations (which combine an organic catalyst with an enzyme, to cleave carbon–carbon bonds and to harvest all electrons from fuels) adopted in enzymatic biofuel cells (EBFCs) to catalyze the oxidation of fuels with high energy density. We will focus on the recent developments in catalytic cascades in EBFCs aimed at enhanced energy production. We will also discuss EBFC stability and lifetime. The fundamental knowledge gained about EBFCs will soon allow them to be applied in portable or implantable electronic devices. Finally, we will discuss future directions based on the development and evaluation of a novel and suitable EBFC design for potential applications.

Keywords Enzymatic fuel cell · Enzyme cascade · Hybrid system · Electrochemical oxidation · Catalytic activity; power sources

1 Introduction

1.1 Biofuel Cells—Concepts and General Considerations

1.1.1 Fuel Cells (FCs)

FCs are electrochemical devices that convert chemical energy to electrical energy [1]. FCs produce energy by oxidizing compounds at the anode and reducing oxygen at the cathode. Noble metals are usually employed to oxidize fuels (such as hydrogen [2], methanol [3], ethanol [4], glycerol [5], and glucose [6]) at the anode compartment. Electron transfer to the cathode side occurs through an external circuit, and electricity

J. H. Franco · A. R. De Andrade (✉)
Departamento de Química, Faculdade de Filosofia Ciências e Letras de Ribeirão Preto, Universidade de São Paulo, Ribeirão Preto, São Paulo, Brazil
e-mail: ardandra@ffclrp.usp.br

F. N. Crespilho (ed.), *Advances in Bioelectrochemistry Volume 5*,
https://doi.org/10.1007/978-3-031-10832-7_5

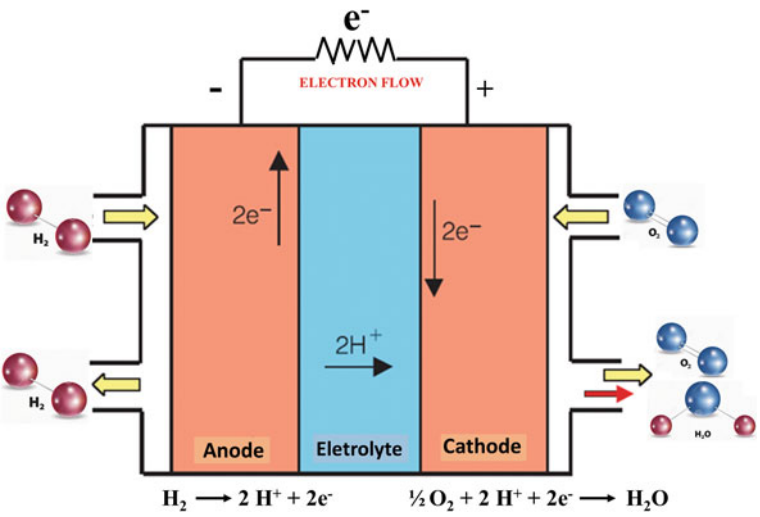

Fig. 1 Simplified schematic diagram of a hydrogen–oxygen fuel cell

production is completed via reaction with an oxidant, commonly oxygen. Both reactions take place simultaneously [7]. Figure 1 displays a schematic representation of an FC.

Overall, FCs produce high energy and power rates. However, some factors limit their application: Noble metal catalysts (based on Pt, Pd, and other noble metals) are expensive, catalysts can be poisoned, electrodes can be passivated, and noble metals will soon become scarce in the Earth's crust [7–9]. An important drawback of FCs that operate at average temperatures (<100 °C) is that noble metals cannot oxidize more complex products or oxidize the fuel completely because these metals cannot cleave the fuel carbon–carbon bond in this condition [10].

1.1.2 Biofuel Cells (BFCs)

In addition to FCs based on metallic catalysts, there are BFCs, which are divided into three classes: enzymatic, microbial, and organelle-based fuel cells [11]. BFCs use biocatalysts instead of metals to oxidize high energy density fuels and hence produce energy [12]. Biocatalysts are advantageous because they are renewable and easy to produce, do not depend on finite reserves, and do not require extreme pH values or high temperatures [9]. BFCs have drawn the attention of research groups working in the field of bioelectrochemistry because they generate high energy. This allows them to be applied in small electronic devices, where they act as a small battery [13]. In 1911, Potter et al. used a *Saccharomyces cerevisiae* culture to produce energy [14]. In 1964, Yahiro et al. reported the first enzymatic fuel cell based on the enzymes

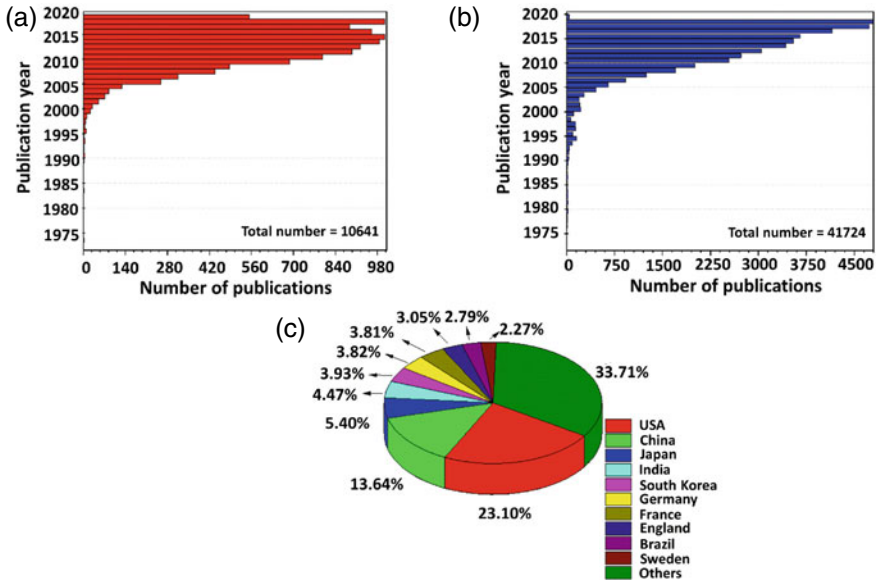

Fig. 2 Publications in the Web of Science™ database for the subject biofuel cell (**a**). Data from the Science direct database for publications for the subject biofuel cell (**b**) and countries of origin of these publications (**c**)

glucose oxidase (GOx) and D-amino acid oxidase to catalyze glucose and D-alanine oxidation, respectively [15].

Despite these advances, research into BFCs did not increase significantly from the 1960s to the 1980s. Nevertheless, in the late 1990s, BFCs reawakened researchers' interest. Figure 2 shows that the number of scientific publications on BFCs grew significantly after the 2000s, due to technological improvements in the areas of nanomaterials [16], enzyme immobilization [17], hybrid systems [18], and molecular engineering [19] and to the urgency about obtaining alternative sources of energy generation. Therefore, researchers have focused on producing small devices that require low power [20] including self-powered sensors [8] and implantable [21] or wearable devices [22].

1.1.3 Enzymatic Biofuel Cells (EBFCs)

EBFCs employ enzymes as catalysts to oxidize fuels or to reduce oxygen [23]. Enzymes are attractive catalysts because they present high catalytic activity and specificity; they allow membraneless EBFC devices to be constructed, thereby avoiding complications due to cross-over reactions [24]; they are renewable; they can be produced on large scale; unlike noble metals, they do not need finite natural reserves;

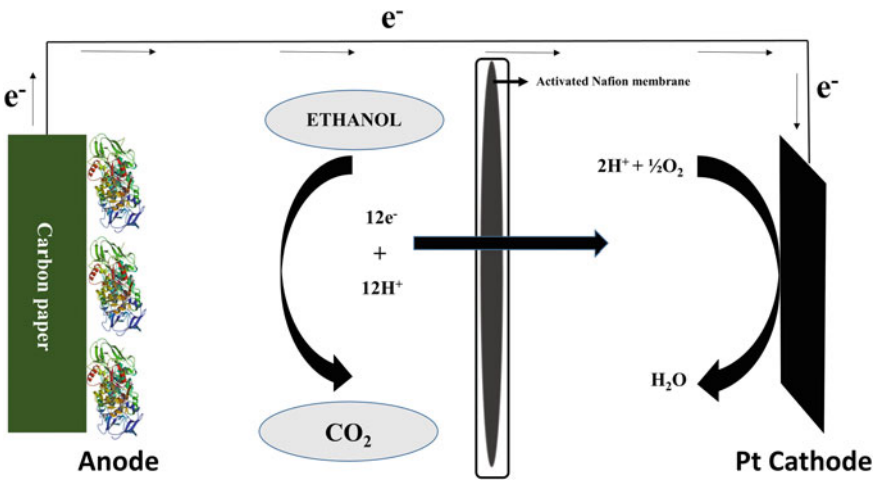

Fig. 3 Schematic representation of an ethanol enzymatic biofuel cell operating at a semi-bio condition (note that the cathode still employs a Pt-catalyst)

and they enable EBFCs to operate at physiological pH and room temperature, providing a mild and safe reaction medium [24, 25].

Figure 3 shows an example of a cascade reaction for ethanol oxidation in an EBFC, where a group of enzymes acts as catalysts at the anode, to oxidize the fuel completely; oxygen is reduced at the cathode side.

The energy generated by EBFCs is lower than the energy generated by metal-based FCs [7], so EBFCs surely will not be used to generate power in battle tanks, aircraft, or giant batteries for city supplies. In fact, EBFCs have potential applications in the range of μA and mA, which makes them a promising energy source in small devices. When it comes to EBFCs, one of the researcher's main goals is to obtain the maximum energy from the employed fuel, to increase the delivered energy.

2 First Steps in EBFC Development

Researchers have used EBFCs to oxidize several fuels. Given that most enzymes are highly selective, pioneering investigators employed only one enzyme to produce the bio-enzymatic film at the electrode, which allowed oxidation to occur in a single catabolic step, with two electrons being collected from the fuel.

Nanomaterials like carbon nanotubes (CNTs) are used to enhance performance in diverse research fields; for example, CNTs help to improve the electronic, thermal, and mechanical properties of electrochemical systems and make these systems more compatible with enzymes [26, 27]. CNTs have high electrical conductivity, so they have promising applications in EBFCs. Furthermore, they can be modified with functional groups, to which biomolecules can be immobilized [26, 27]. CNTs can

increase the electron transfer rate between the enzyme active site and the electrode surface by either direct electron transfer (DET) or mediated electron transfer (MET, which occurs by using a mediator molecule) [28, 29]. Although MET generates a higher power density, DET provides a simpler architecture and lower loss of EBFC performance [28]. Thus, integrating CNTs into the bioelectrode improves the electronic and catalytic properties of said electrode, affording synergistic power sources that are potentially applicable in EBFCs [30].

One example of integrating CNTs into EBFCs is the combination of GOx with modified multi-walled carbon nanotubes (MWCNTs) immobilized on the electrode surface, to oxidize glucose to gluconolactone (two electrons). The presence of MWCNTs in the EBFC facilitates direct electron transfer between the enzyme active site and the electrode surface, which could help to simplify and to miniaturize an effective and reliable membraneless EBFC. However, more detailed studies on the electrocatalytic rate, lifetime, and reproducibility of this EBFC during glucose oxidation are needed [31].

The literature contains good reviews on enhanced lifetime and communication between the enzyme and the electrode surface in EBFCs [23, 24, 32].

3 Key Issues Faced During EFBC Development

One of the most important concerns during EBFC development is achieving high current and power density values to make its commercial application viable. As discussed previously, EBFC lifetime and efficiency issues must be faced before this technology can be accepted in the market [25]. Moreover, for an outstanding catalytic activity to be obtained, the total energy available in the fuel must be harnessed; that is, all the electrons from the oxidation reaction must be collected. Because of the high selectivity of most enzymes bearing in mind, the energy metabolism of all living organisms more than one enzyme must be used in an EBFC for complete fuel oxidation to be achieved.

4 Enzyme Cascades in EBFCs

At least two catabolic steps are required to obtain high energy and complete fuel oxidation through harvesting of all the electrons from the fuel molecule. For this purpose, an enzyme cascade, involving at least two enzymes, is necessary to improve the oxidation reaction pathway [33]. Indeed, researchers have used enzyme cascades to achieve complete fuel oxidation [12, 34, 35].

Palmore et al. [36] reported the first enzyme cascade-based EBFC for complete alcohol oxidation; more specifically, these authors employed a series of three enzymes to harvest all the electrons from methanol. First, NAD^+-dependent alcohol dehydrogenase (ADH) oxidized methanol to formaldehyde, collecting two electrons.

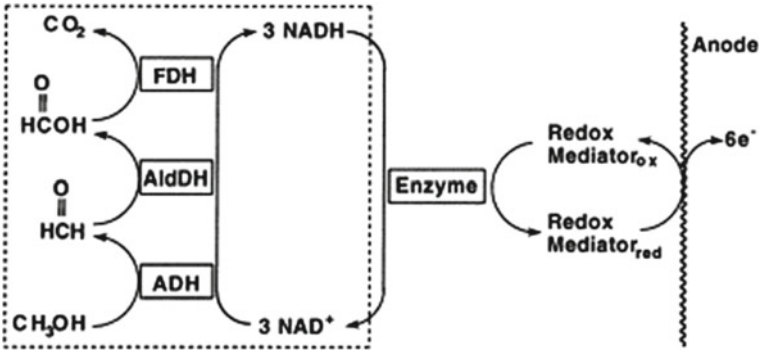

Fig. 4 Methanol oxidation to carbon dioxide catalyzed by NAD^+-dependent alcohol-(ADH), aldehyde-(AldDH), and formate-(FDH) dehydrogenases (shown within the box) proposed by Palmore et al. [36]. Reprinted with permission from Palmore et al. (1998). A methanol/dioxygen biofuel cell that uses NAD^+-dependent dehydrogenases as catalysts: Application of an electro-enzymatic method to regenerate nicotinamide adenine dinucleotide at low overpotentials. Journal of Electroanalytical Chemistry, v. 443, p. 155–161. Copyright 2022, Elsevier

Then, NAD^+-dependent aldehyde dehydrogenase (AldDH) oxidized formaldehyde to formic acid, collecting two more electrons. Finally, NAD^+-dependent formate dehydrogenase (FDH) oxidized formic acid to the final product, carbon dioxide (CO_2), collecting two additional electrons. NAD^+ was electro-enzymatically regenerated by coupling an enzyme to the anode via a redox mediator. Figure 4 shows the scheme of the proposed methanol EBFC [36].

Xu et al. reported an enzyme cascade involving six enzymes—glucose dehydrogenase, gluconate 2-dehydrogenase, aldolase, ADH, AldDH, and oxalate oxidase—to obtain deep glucose oxidation [37], as represented in Fig. 5. Compared to the cascade involving only two enzymes, the power (6.74 ± 1.43 $\mu W\ cm^{-2}$) and current density (31.5 ± 6.5 $\mu A\ cm^{-2}$) were 46.8 and 33.9 times higher, respectively [37]. In 2017, Wu et al. used an enzyme cascade involving the enzymes ADH, AldH, and FDH immobilized on carbon nanodots (CNDs) for methanol oxidation [38]. As in the pioneering work of Palmore et al. [36], this bioanode was coated with a redox mediator, polymerized methylene blue, to lower the overpotential for NADH oxidation. The biocatalytic system reached an OCP of 0.71 ± 0.02 V and a power density of 68.7 ± 0.4 $\mu W\ cm^{-2}$, confirming that the CNDs enhanced the catalytic activity by improving electron transfer and producing highly conductive EFC architectures [38].

Another elegant approach in enzyme cascades entails mimicking the citric acid metabolic cycle for ethanol oxidation [39]. To this end, 10 enzymes were immobilized on a membrane layer consisting of quaternary ammonium bromide salt-modified Nafion® placed on the electrode surface. The power density value of this cascade was nine times higher than the value achieved with a single enzyme [39]. Later, Sokic-Lazic et al. applied a similar enzyme cascade comprising eight enzymes (pyruvate dehydrogenase, succinyl CoA synthetase, fumarase, aconitase, isocitrate dehydrogenase, malate dehydrogenase, citrate synthase, and α-ketoglutarate dehydrogenase)

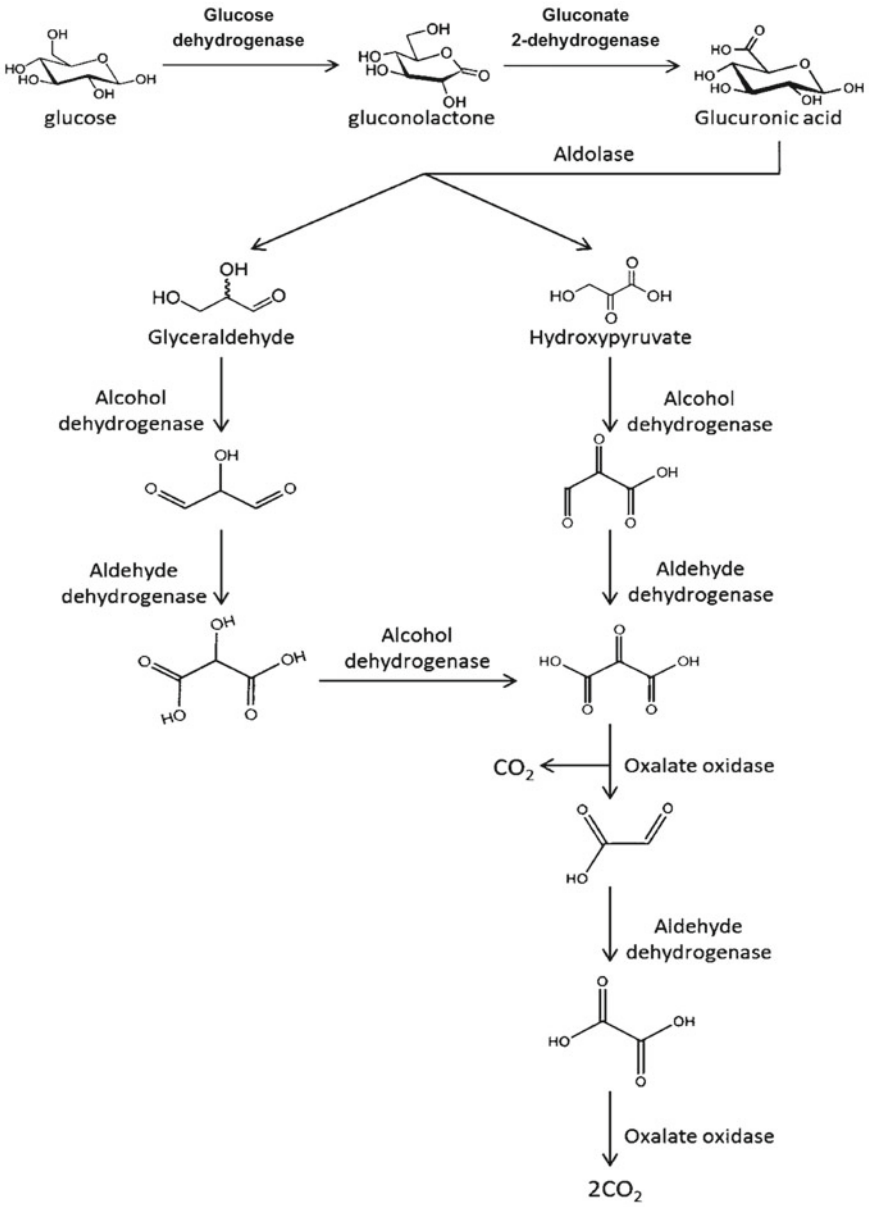

Fig. 5 Schematic representation of a six-enzyme cascade for glucose oxidation. Reprinted with permission from Xu and Minteer [37]. Copyright 2022, ACS Publications

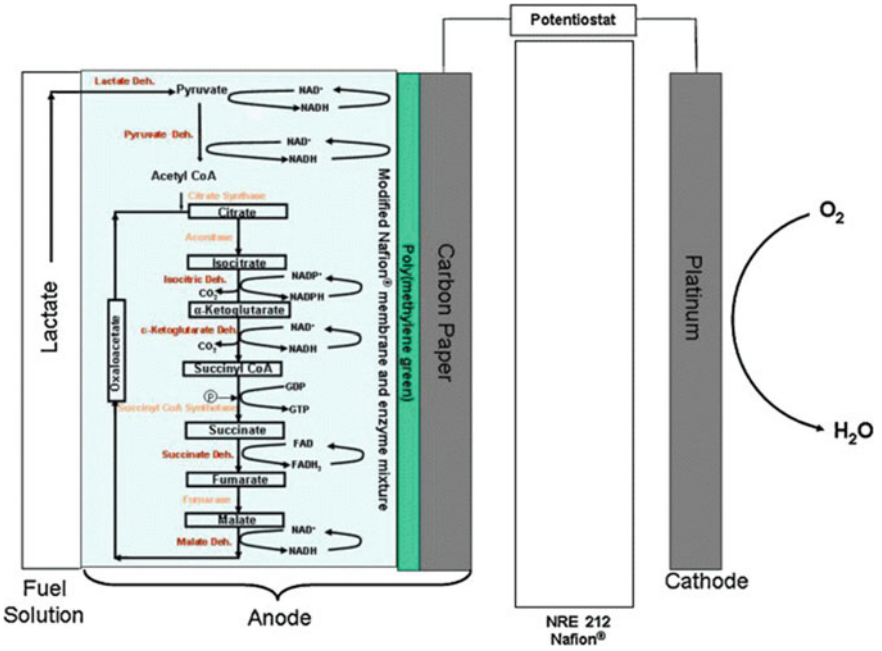

Fig. 6 Deep lactate oxidation in the lactate/air biofuel cell. Reprinted with permission from Sokic-Lazic D, de Andrade AR, Minteer SD (2011). Utilization of enzyme cascades for complete oxidation of lactate in an enzymatic biofuel cell. Electrochimica Acta, v. 56, p. 10,772–10,775. Copyright 2022, Elsevier

to oxidize lactate completely (Fig. 6) [40]. The cascade gave 18- and 21-times higher power density (827 ± 21 μW cm^{-2}) and current density (3.32 ± 0.11 mA cm^{-2}) values, respectively, than the system containing only one enzyme.

Zhang et al. applied an in vitro pathway involving 15 enzymes for simultaneous oxidation of glucose, sucrose, and fructose (mixed sugars present in soft drinks) and obtained Faradaic efficiency of 95% and maximum power density between 0.80 and 1.08 mW cm^{-2} [41]. Although the enzyme cascade operated with great fuel flexibility, the authors reported that lifetime, stability, and power density enhancement must be further investigated [41].

Numerous investigations have shown that the amount of energy subtracted from fuels increases with the number of enzymes on the electrode surface, as depicted in Fig. 7a for lactate oxidation. However, fuel concentration generally affects power and current density values, impacting EBFC performance. For instance, Fig. 7b demonstrates that power density initially increases with fuel concentration, but it plunges at higher fuel concentrations, indicating that the ionic strength generated by the increasing fuel concentration affects the enzyme kinetics and impairs EBFC performance. Therefore, new enzyme cascades that tolerate high fuel concentrations must be developed [40].

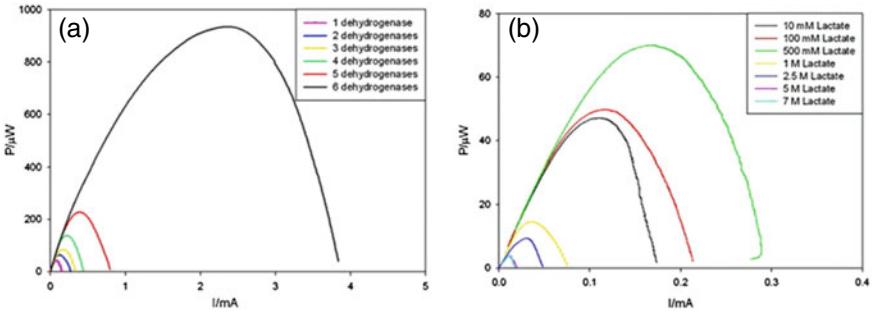

Fig. 7 Power curves for lactate enzymatic biofuel cell for **a** successive additions of different dehydrogenases in 100 mM sodium lactate. **b** bioanode containing one enzyme (LDH) in the presence of different lactate concentrations. Reprinted with permission from Sokic-Lazic D, de Andrade AR, Minteer SD (2011). Utilization of enzyme cascades for complete oxidation of lactate in an enzymatic biofuel cell. Electrochimica Acta, v. 56, p. 10,772–10,775. Copyright 2022, Elsevier

Enzyme cascades usually generate high energy when deep oxidation is achieved [42]. Nevertheless, when the number of enzymes immobilized on the electrode surface increases, there is a fine balance between electron gain and stability loss. Thus, building a complex and robust architecture capable of accommodating a large number of enzymes for effective and complete fuel oxidation becomes a difficult task [12]. Neto et al. showed that an increase in the number of enzymes immobilized on the electrode surface decreased the cascade stability [10]. These authors immobilized seven enzymes, namely ADH, AldDH, aconitase, citrate synthase, isocitric, S-acetyl-CoA, and synthetase, on the electrode surface by using the linear ethyleneimine polymer (LEIP) as immobilization matrix and ethylene glycol diglycidyl ether (EGDGE) as a crosslinking agent, to obtain complete ethanol oxidation. The third step of the cascade performed less efficiently than the first two steps when ADH and AldDH were employed. This confirmed that the addition of several enzymes to a complex immobilization structure decreases the power density and hence the EBFC catalytic activity, a consequence of steric hindrance to fuel approach to the enzyme catalytic sites [10].

As reviewed by Sokic-Lazic et al. [42], the specific activity of each enzyme involved in the cascade is another important issue. Ideally, bottlenecks between enzymes must be avoided so that a continuous cycle is maintained. However, this will only be possible if all the enzymes have similar enzymatic activity—units/mg (1U means that the enzyme converts one mol of the substrate (fuel) per minute), but such a cascade is not easy to project. One example of such cascade can be observed in Fig. 8, which illustrates the enzymes involved in the Krebs cycle employed for deep oxidation of ethanol [39], lactate [40], and pyruvate [43].

Although metabolic enzyme cascades work perfectly for the total oxidation of several fuels, there is a lack of energy/electron generation in this kind of EBFC. Most enzymes used in these cascades are non-oxidoreductase enzymes, implying

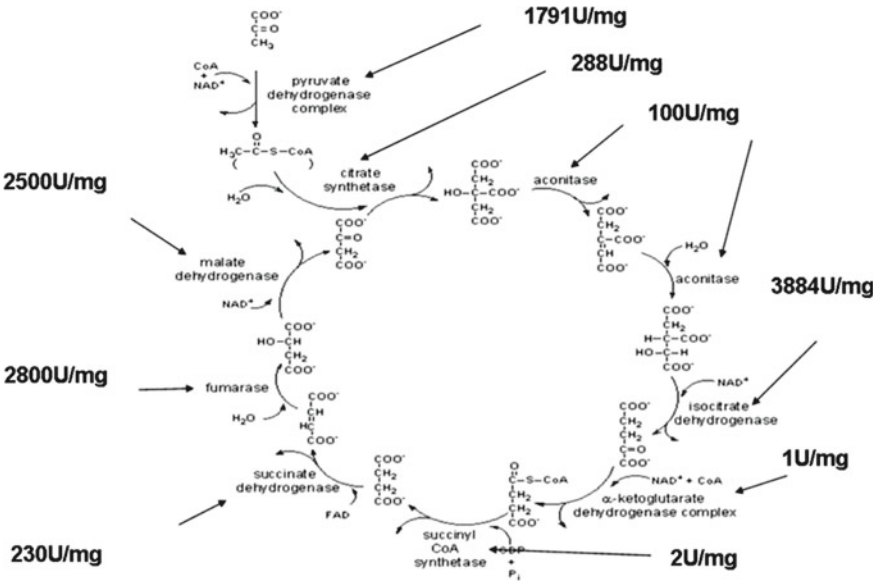

Fig. 8 Specific activity of the enzymes involved in the mimetic Krebs cycle. Reprinted with permission from Sokic-Lazic D, Arechederra RL, Treu BL, Minteer SD (2010). Oxidation of biofuels: Fuel Diversity and Effectiveness of Fuel Oxidation through Multiple Enzyme Cascades. Electroanalysis, v. 22, p. 757–764. Copyright 2022, Wiley Online Library

that the electrode demands low power density [37]. The amount of energy delivered in an EBFC cascade can be optimized by employing oxidoreductase enzymes.

Therefore, when it comes to deep fuel oxidation in EBFCs, two main challenges must be faced: specific activities of the enzymes and stabilization of the multienzyme cascade immobilized on the electrode surface. Overcoming these challenges is complex and depends on factors such as type of enzyme immobilization, the addition of implemented nanostructures to increase electron transfer between the enzymes and the electrode surface, and electrode surface area [1].

One of the great advantages of EBFCs is that sugars or alcohols, with low toxicity and high energy density, can be employed as fuel [42]. However, using two or more enzymes in the cascade might fail to oxidize the fuel completely, probably due to cascade inhibition by reaction products or intermediates. This could culminate in low energy density and efficiency, which are essential parameters for energy sources. Thus, researchers must engineer enzyme cascades with a degree of complexity that can generate high energy rates while allowing EBFCs for practical applications to be developed [44].

Table 1 summarizes some enzyme cascades for various fuels; the number of enzymes involved in the cascade and the generated power is emphasized.

Table 1 Enzyme cascades in enzymatic biofuel cells

Number of enzymes in the cascade	Fuel	OCP (V)	Maximum power density ($\mu A\ cm^{-2}$)	I_{max} ($\mu A\ cm^{-2}$)	Reference
3	Methanol	0.71	68.7 ± 0.4	220 ± 0.8	[38]
3	Methanol	0.80	670 ± 6.0	*	[36]
3	Methanol	*	261 ± 7.6	845 ± 35.5	[45]
2	Glycerol	*	1210 ± 0.15	2250 ± 0.25	[34]
2	Ethanol	0.82	2040 ± 0.05	2730 ± 0.15	[46]
10	Ethanol	*	1010 ± 0.01	3600 ± 0.23	[39]
6	Lactate	*	3320 ± 110	827 ± 21	[40]
6	Glucose	0.571	6.74 ± 1.43	31.5 ± 6.5	[37]
2	Glucose	*	322 ± 0.017	*	[47]
5	Pyruvate	*	3920 ± 0.48	931 ± 0.09	[43]
15	Sucrose	0.80	690	*	[41]

* Unreported value

5 New Approach in EBFCs: Use of Hybrid Cascades to Improve Electrooxidation Pathways

As discussed above, several enzymes used in enzymatic cascade studies are limited by their stability, high specificity, and operating conditions (pH, temperature, and electrolytes). Hybrid systems, which combine the advantages of enzymatic oxidation with another organic or inorganic catalyst, can help to overcome the stability issues that arise when a large number of enzymes are immobilized on the electrode surface. Studies on such hybrid systems have described the use of an abiotic catalyst, which only acts to improve characteristics including electrode area and conductivity. However, this type of catalyst does not act together with the enzyme or directly on fuel oxidation [19, 48, 49]. In other studies, metallic electrocatalysts have been added to systems containing enzymes to increase the biofuel cell energy output [48, 50]. For example, Kwon et al. combined gold-modified cotton fibers with GOx for glucose oxidation, to achieve a power density of 3.7 mW cm^{-2}. The authors claimed that the metallic fibers increased the conductivity between the enzyme and the electrode [51]. For hydrogen oxidation, the amino acid arginine was incorporated into the nickel bis-diphosphine complex ($[Ni^{II}(P^{Cy}_2N^{Arg}_2)_2]^{7+}$) and immobilized onto CNTs modified with naphthoic acid groups [52]. Nevertheless, hybrid systems combining an abiotic catalyst and an enzyme still have deficiencies like low power density and failure in collecting all electrons—fuel oxidation is incomplete because these systems cannot break the fuel carbon–carbon bonds.

To address this problem, the enzyme oxalate oxidase (OxOx) has been employed to cleave carbon–carbon bonds of acids and oxalate. OxOx catalyzes oxalate oxidation to two CO_2 molecules [53, 54]. The analogous enzyme oxalate decarboxylase

(OxDc), which catalyzes oxalate carbon–carbon cleavage, to give formate and CO_2, has also been applied [55]. These enzymes have similar function and activity [56, 57] and have been satisfactorily used in the total oxidation of alcohols such as glycerol [58], glucose [37], and ethanol [59].

In the case of alcohol oxidation, the OH groups must be oxidized first, which can be achieved with the organic catalyst N-oxyl-2,2,6,6-tetramethylpiperidine (TEMPO). This organic catalyst has been used to oxidize groups containing oxygen, nitrogen, and sulfur [58], such as alcohols and aldehydes [60], and to oxidize amines to aldehydes, ketones, or nitriles to their respective acids [61] at room temperature. TEMPO and its derivatives are widely applied in syntheses because they are safe and inexpensive [62]; they are also employed in some specific oxidations [63]. Figure 9 illustrates the mechanism of action of TEMPO. The catalytically active oxoammonium cation originates from the nitroxyl radical (I). Then, oxoammonium (II) is reduced to the hydroxylamine (III) form, which performs the second oxidation and regenerates the oxyammonium cation [64, 65]. TEMPO modification improves the catalyst properties for the desired application in EBFCs [65].

Concomitant use of TEMPO and OxOx or OxDc in the hybrid cascade overcomes the individual limitations of these catalysts and enables total electron harvesting from fuels [66, 67]. This hybrid system is more robust and employs less protein, facilitating biofilm formation and stabilization [59].

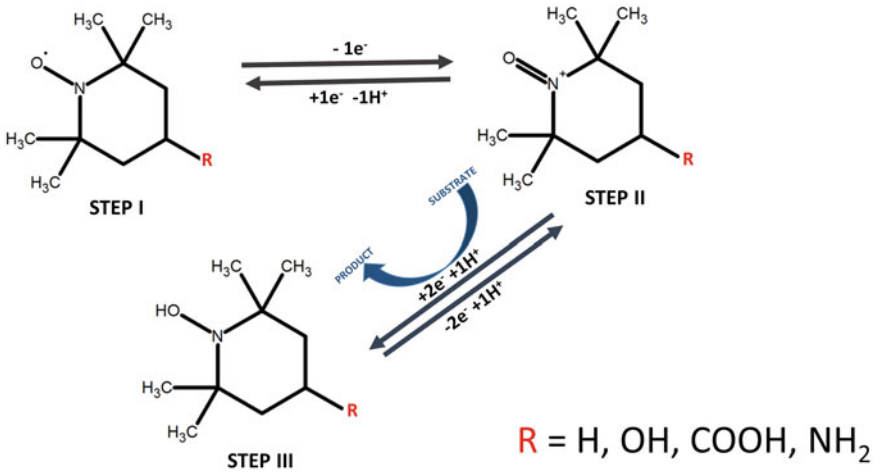

Fig. 9 Schematic representation of the TEMPO oxidation mechanism. Step I—nitroxyl radical. Step II—oxoammonium cation. Step III—hydroxylamine

5.1 Recent Studies Using Hybrid Cascade Systems for Complete Oxidation

Given the need to improve how complex electrooxidative cascades perform, researchers have studied hybrid catalytic motifs. Hu et al. developed a hybrid system by combining TEMPO and GOx for glucose oxidation. The hybrid bioelectrode harvested four electrons from glucose and gave a maximum power density of 38.1 $\mu W\ cm^{-2}$, showing that the joint action of TEMPO and GOx enhanced catalytic activity, opening possibilities for developing a more promising energy conversion device [68].

Many studies on such hybrid systems are focused on alcohols such as glycerol and ethanol. Hickey et al. [58] applied the organic catalyst 4-amino-TEMPO (TEMPO-NH_2) and OxOx in the glycerol//O_2 EBFC. Nuclear magnetic resonance (13C NMR) analyzes identified CO_2, confirming complete glycerol oxidation. The authors stated that an important approach is to combine different catalysts under conditions where both operate under their maximum activity (pH, temperature). This hybrid system allowed an enhanced bi-catalytic cascade for complete glycerol oxidation to be developed [58].

A similar strategy has been reported for lactate oxidation: A hybrid biofilm containing TEMPO-NH_2/OxDc oxidized lactate to a high degree, with high catalytic activity (0.15 mA cm^{-2}) [69]. Important features of this hybrid bioanode were its higher stability and efficiency. The synergistic action of the organic catalyst and the enzyme provided complete lactate oxidation, confirming that the hybrid architecture can operate in the catabolic steps of several fuels [69].

Despite the satisfactory results obtained by combining TEMPO-NH_2 and enzymes such as OxOx and OxDc to oxidize glycerol [58], lactate [69], and ethanol [70], new approaches are required to promote cascade reactions that provide high-performance EBFCs, enabling practical and efficient applications [70]. Therefore, researchers have explored different ways to immobilize the organic catalyst, so that system performance is enhanced even further. In this context, covalent TEMPO immobilization onto a linear ethyleneimine polymer (LEIP) backbone crosslinked onto a carbon electrode has been proposed for oxidation of many fuels [71, 72]. Based on the results, higher current density was achieved as compared to the analogous system involving homogeneous TEMPO. The new material presented promising characteristics for oxidation of several fuels, facilitating improvement of the catabolic reaction for hybrid catalytic cascades [66, 71].

A tri-catalytic-motif architecture has been developed for glycerol oxidation [67], with the hybrid system TEMPO-LEIP/MWCNT/(OxDc) providing increased electrocatalytic activity. According to the results, TEMPO-LEIP oxidized the first five glycerol oxidation steps, MWCNTs-OxDc cleaved the mexolate carbon–carbon bonds, and catalyzed oxalate decarboxylation, to give formate and CO_2. Thus, this tri-catalytic system increased current density by collecting all the 14 electrons from the glycerol molecule and represents an opportunity for constructing a promising bioanode architecture for deep electrochemical oxidation of fuels [67].

Complete ethanol oxidation has been demonstrated by employing an immobilized hybrid system containing MWCNT-COOH, TEMPO-LEIP, and OxOx [59]. This catalytic system relied on the synergistic effect of its components. Current density increased by 3- and 2.5-fold as compared to the MWCNT-COOH/OxOx and MWCNT-COOH/TEMPO-LEIP systems, respectively. Electrochemical and chromatographic experiments confirmed that OxOx was able to cleave the acetic acid C–C bond efficiently, generating formic acid. In turn, TEMPO acted on formic acid oxidation, producing CO_2 and harvesting all the 12 electrons from ethanol [59]. Figure 10 illustrates complete ethanol oxidation by the hybrid system MWCNT-COOH/TEMPO-LEIP/OxOx, through which all the catabolic steps occurring in the presence of the catalysts combined on the electrode surface can be followed.

Countless efforts have been made to produce complex and efficient systems for application in the field of bioelectrochemistry. Recent studies have shown the use of organic catalysts tethered to pyrene and of organic catalysts as non-covalent anchors based on π–π stacking interactions between pyrene and CNTs [18, 67]. For example, the catalytic activity of pyrene-TEMPO/MWNCT was higher compared to TEMPO-NH_2, generating more energy due to enhanced electrochemical oxidation [73, 74].

Andersen and collaborators developed an electroanalytical system based on paper-based platforms to evaluate deep glycerol oxidation in multi-step reactions [75]. The electrochemical platforms allowed for fast characterization of the intermediate

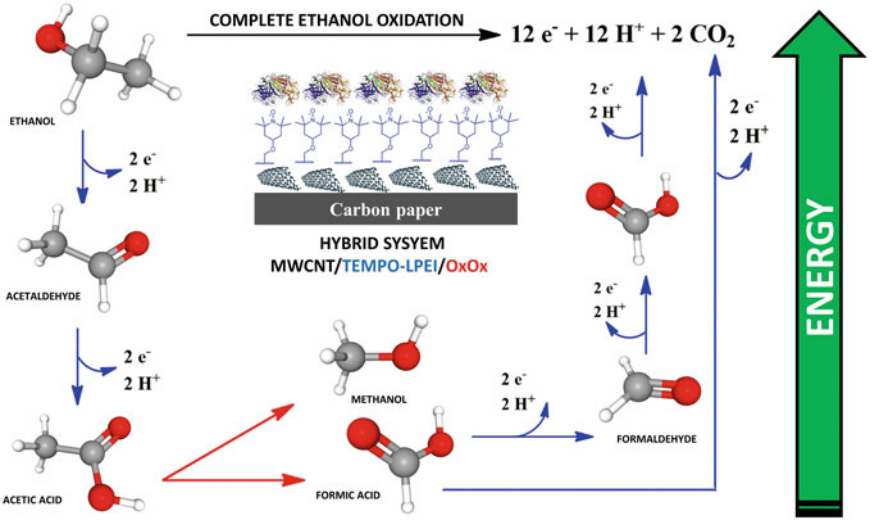

Fig. 10 Proposed scheme for complete ethanol oxidation at the hybrid system MWCNT-COOH/TEMPO-LEIP/OxOx. The blue arrow represents the oxidation mediated by the organic catalyst TEMPO, and the red arrow represents the bio-enzymatic oxidation due to the action of the enzyme OxOx

Table 2 Hybrid cascade systems in enzymatic biofuel cells

System	Fuel	OCP (V)	Power density($\mu A\ cm^{-2}$)	I_{max} ($\mu A\ cm^{-2}$)	Reference
GAAuNPs/CNFs	Glucose	*	91.4	304	[76]
TEMPO/GOx	Glucose	*	38.1	651.4	[68]
TEMPO-NH_2 + OxOx	Glycerol	*	*	875	[58]
MWCNT/TEMPO-LEIP/OxDc	Glycerol	*	*	1300	[67]
$Pt_{65}Sn_{35}$/MWCNTs + OxOx	Ethylene glycol	0.643	332	930	[77]
MG/MWCNTs/TEMPO-LPEI/ADH + AldDH + NAD^+	Ethanol	0.649	378.2	1087	[66]
MWCNT-COOH/TEMPO-LEIP/OxOx	Ethanol	0.492	302.5	821.1	[59]
MWCNT-COOH/Pyrene-TEMPO/OxDc	Ethanol	0.598	388	690	[18]
TEMPO-NH_2/OxDc	Ethanol	0.468	78	353	[70]
ADH/TiO_2NTs-TCPP	Ethanol	1.13	270	360	[78]
Poly-(MG-PYR) + MWCNTs + Nafion + ADH/AldDH/NAD +	Ethanol	0.503	275	1040	[79]
MWCNTs-COOH-Au/ADH	Ethanol	0.61	155	990	[48]

* Unreported value

products formed during the triple catalytic cascade comprising the organic catalyst pyrene-TEMPO, metallic palladium supported on 3D graphene nanosheets (Pd-GNS), and OxDc. This paper-based microfluidic device can be used in environmental and clinical analyses [75].

Despite the advances in EBFCs in recent years, they are not yet fully effective for application as an autonomous energy source. A detailed study of the energy storage capacity of these hybrid systems is crucial. Table 2 lists the literature papers describing the use of hybrid cascades in EBFC development.

6 Enzymatic Cascades Applied for Operating Power Sources

6.1 Wearable Devices for EBFCs

EBFCs can be applied in glucose sensors, pacemakers, and wearable devices [44]. A direct consequence of using hybrid catalytic cascades is their application in wearable electronic devices [80]. These devices have become commercially attractive—the development of small devices such as smartwatches, fitness bands, and wearable detectors has drawn the attention of the population because they consume little power

and are suitable, body-compliant power sources [81]. Wang et al. developed the first example of a fully imprinted and stretchable bifunctional biosupercapacitor to collect and to store energy generated by lactate from sweat [82]. The hybrid system proved to be self-charging via the redox reactions of the lactate biofuel cell, providing high power density (0.343 mW cm^{-2}). The wearable electronic device can be produced with low-cost materials such as elastic adhesive films, allowing contact with the human skin during rigorous exercise, thereby acting as a powerful energy source (Fig. 11). Although the epidermal device provides a simple and efficient design, future studies must be carried out to adjust the stability of the system, so that the large-scale production of a wearable device that generates energy through human sweat produced during physical exercise can soon be implemented [82].

A biosensor that can detect the alcohol content in the body through sweat has also been reported [83], paving the way for the development of devices that can detect alcohol in other fluids such as tears and saliva for real-time alcohol monitoring [81, 83, 84].

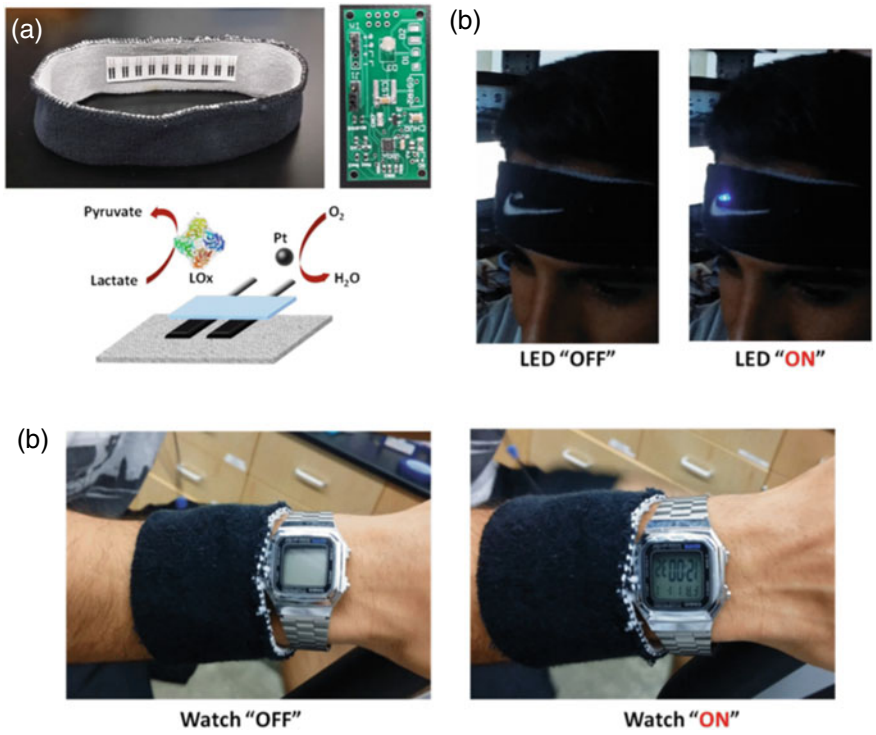

Fig. 11 **a** Image of a headband-based textile biofuel cell and the DC/DC converter along with a scheme of the half-cell reaction taking place at the two electrodes. Real-time generation of usable electrical energy from human sweat to power **b** LED and **c** wrist-watch. Reprinted with permission from Bandodkar AJ, Wang J (2016). Wearable Biofuel Cells: A Review. Electroanalysis, v. 28, p. 1188–1200. Copyright 2022, Wiley Online Library

6.2 EFC Self-powered Biosensors

Since the pioneering work of Adam Heller, who employed a miniaturized glucose EBFC to monitor and to convert blood sugar to energy, many improvements have been made in this field [85, 86]. There have been continuous efforts to increase the energy production, lifetime, and stability of miniaturized enzymatic biofuel cells (mEBFCs) [85]. A self-powered glucose sensor to measure glucose in body fluids has been proposed: The sensor combines a miniaturized organic electrochemical transistor (OECT) and an EBFC that uses redox enzymes to generate energy [86]. This autonomous biosensor is stable, easy to prepare, and inexpensive, and it has a wide detection range (10–20 mM). It also acts as an organic electrochemical transistor, generating high energy rates upon contact with relevant glucose concentrations in the human fluid. Remarkably, the new design acts as a technological advance for self-powered micrometric-scale sensory devices for glucose detection [86].

Gouranlou et al. built an ethanol EBFC by immobilizing ADH with poly-diallyldimethylammonium chloride (PDDA) and MWCNTs on the anode. The supporting agent (PDDA) acted as a polyelectrolyte that dispersed the MWCNTs and prolonged the ADH activity, improving bioanode performance. The EBFC produced power density and open-circuit potential (OCP) equal to 1.713 mW cm^{-2} and 0.281 V, respectively. The hybrid system PDDA/MWCNT/ADH improved the surface area electronic conductivity, making the system promising for future commercial applications [87].

The field of bioelectrochemistry has received growing attention. Parameters such as different types of enzyme immobilization [88] and study of other important factors aiming to improve electron transfer between the enzyme and electrode [48] and catalytic activity [78, 89] are fundamental steps to obtain robust EBFCs.

Autonomous self-powered biodevices have focused mainly on systems that have low power. In this case, EBFCs can simultaneously be employed as a power source and biosensor [90]. The major advantage of these sensors is that they do not need an external power source. Katz and Willner were the first to report on self-powered biosensors: They determined analyte concentration by measuring the power or current output generated by the EBFC [91]. The analyte was detected by increasing or decreasing the EFC power output. A self-powered device can replace large, expensive types of equipment and reduces the need for high technical training [92]. This type of sensor has been reported for several analytes, including ethanol [20], lactate [93], nitroaromatic explosives [94], glucose [95], acetaldehyde [96], and cholesterol [97].

The most promising advancement reported recently has been the development of hybrid supercapacitor/biofuel cells (SC-EBFCs), which combine strategies to improve energy storage and conversion [98]. One advantage of SCs is their rapid charge–discharge, allowing for instantaneous energy generation. These new concept SC-EBFCs combine a hybrid bi-catalytic bioelectrode with a charge-store energy matrix, which is expanded to develop an SC-EBFC device [99]. This system efficiently acts as a self-powered device for energy storage and generation—the enzyme

can recharge the system, eliminating the need for an external source [100]. These promising features will allow implantable or usable small bioelectronic devices to be produced [100, 101]. Furthermore, despite the advances in SC-EBFCs, finding biocompatibility between two complex systems remains a challenge [100, 102, 103]. Notably, constructing new improved systems is a new strategy to obtain efficient and suitable elements that store charge in the SC through robust energy generation by the EBFC, opening a new design for the fabrication of high-performance bioelectrochemical systems.

7 Conclusions and Futures Perspective

We have shown that deep or total oxidation of complex fuels requires a complete enzymatic cascade or a hybrid system. These systems furnish higher power density as compared to the single-enzyme counterpart. Biofilm complexity directly affects stability and the amount of delivered power. Hybrid systems are simpler because they demand a smaller amount of catalyst to provide the same outcome as a large number of enzymes (>6–10). Notwithstanding the efficient approaches employed in the bi-catalytic bioelectrode for cascade reactions, some crucial issues such as short lifetime, low stability, and unsatisfactory power density need to be solved. Overall, the main possibility for EBFCs to move from fundamental research to the market may go through its coupling with SC in self-powered electronic devices, which has potential application in the future.

Funding The authors are grateful for the financial support obtained from the Brazilian research funding agency FAPESP (2021/ 01134-7) (2017/20431-7) (2014/50945-4) and CAPES (001).

Conflicts of Interest The authors declare no conflict of interest

References

1. Xiao X, Xia H, Wu R et al (2019) Tackling the challenges of enzymatic (bio)fuel cells. Chem Rev 119:9509–9558. https://doi.org/10.1021/acs.chemrev.9b00115
2. Manoharan Y, Hosseini SE, Butler B et al (2019) Hydrogen fuel cell vehicles; current status and future prospect. Appl Sci 9:2296. https://doi.org/10.3390/app9112296
3. Gong L, Yang Z, Li K et al (2018) Recent development of methanol electrooxidation catalysts for direct methanol fuel cell. J Energy Chem 27:1618–1628. https://doi.org/10.1016/j.jechem.2018.01.029
4. Akhairi MAF, Kamarudin SK (2016) Catalysts in direct ethanol fuel cell (DEFC): an overview. Int J Hydrogen Energy 41:4214–4228. https://doi.org/10.1016/j.ijhydene.2015.12.145
5. Antolini E (2019) Glycerol electro-oxidation in alkaline media and alkaline direct glycerol fuel cells. Catalysts 9:980. https://doi.org/10.3390/catal9120980

6. Brouzgou A, Tsiakaras P (2015) Electrocatalysts for glucose electrooxidation reaction: a review. Top Catal 58:1311–1327. https://doi.org/10.1007/s11244-015-0499-1
7. Sharaf OZ, Orhan MF (2014) An overview of fuel cell technology: fundamentals and applications. Renew Sustain Energy Rev 32:810–853. https://doi.org/10.1016/j.rser.2014.01.012
8. Kirubakaran A, Jain S, Nema RK (2009) A review on fuel cell technologies and power electronic interface. Renew Sustain Energy Rev 13:2430–2440. https://doi.org/10.1016/j.rser.2009.04.004
9. Aquino Neto S, De AAR (2013) New energy sources: the enzymatic biofuel cell. J Braz Chem Soc 24:1891–1912. https://doi.org/10.5935/0103-5053.20130261
10. Aquino Neto S, Minteer SD, de Andrade AR (2017) Developing ethanol bioanodes using a hydrophobically modified linear polyethylenimine hydrogel for immobilizing an enzyme cascade. J Electroanal Chem. https://doi.org/10.1016/j.jelechem.2017.09.001
11. Cooney MJ, Svoboda V, Lau C et al (2008) Enzyme catalysed biofuel cells. Energy Environ Sci 1:320–337. https://doi.org/10.1039/B809009B
12. Macazo FC, Minteer SD (2017) Enzyme cascades in biofuel cells. Curr Opin Electrochem 5:114–120. https://doi.org/10.1016/j.coelec.2017.07.010
13. Wang L, Wu X, Su BSQ et al (2021) Enzymatic biofuel cell: opportunities and intrinsic challenges in futuristic applications. Adv Energy Sustain Res 2:2100031. https://doi.org/10.1002/aesr.202100031
14. Potter MC, Waller AD (1911) Electrical effects accompanying the decomposition of organic compounds. Proc R Soc Lond Ser B, Containing Papers of a Biological Character 84:260–276. https://doi.org/10.1098/rspb.1911.0073
15. Yahiro AT, Lee SM, Kimble DO (1964) Bioelectrochemistry: I. Enzyme utilizing bio-fuel cell studies. Biochimica et Biophysica Acta (BBA)—Specialized Section on Biophysical Subjects 88:375–383. https://doi.org/10.1016/0926-6577(64)90192-5
16. Zhao C, Gai P, Song R et al (2017) Nanostructured material-based biofuel cells: recent advances and future prospects. Chem Soc Rev 46:1545–1564. https://doi.org/10.1039/C6CS00044D
17. Lee JY, Shin HY, Lee JH et al (2009) A novel enzyme-immobilization method for a biofuel cell. J Mol Catal B Enzym 59:274–278. https://doi.org/10.1016/j.molcatb.2008.10.008
18. Franco JH, Klunder KJ, Lee J et al (2020) Enhanced electrochemical oxidation of ethanol using a hybrid catalyst cascade architecture containing pyrene-TEMPO, oxalate decarboxylase and carboxylated multi-walled carbon nanotube. Biosens Bioelectron 154.https://doi.org/10.1016/j.bios.2020.112077
19. Yang X-Y, Tian G, Jiang N, Su B-L (2012) Immobilization technology: a sustainable solution for biofuel cell design. Energy Environ Sci 5:5540–5563. https://doi.org/10.1039/C1EE02391H
20. Franco JH, Minteer SD, De Andrade AR (2021) Ethanol biofuel cells: hybrid catalytic cascades as a tool for biosensor devices. Biosensors 11:41. https://doi.org/10.3390/bios11020041
21. Guo KW (2012) Green nanotechnology of trends in future energy: a review. Int J Energy Res 36:1–17. https://doi.org/10.1002/er.1928
22. Gamella M, Koushanpour A, Katz E (2018) Biofuel cells—activation of micro- and macro-electronic devices. Bioelectrochemistry 119:33–42. https://doi.org/10.1016/j.bioelechem.2017.09.002
23. Karim NA, Yang H (2021) Mini-review: recent technologies of electrode and system in the enzymatic biofuel cell (EBFC). Appl Sci 11:5197. https://doi.org/10.3390/app11115197
24. Ramesh M, Balakrishnan P, Dhanaprabhu SS et al (2021) Enzyme-modified electrodes for biofuel cells: a comprehensive review. Mater Today: Proc 46:3495–3501. https://doi.org/10.1016/j.matpr.2020.11.922
25. Minteer SD, Liaw BY, Cooney MJ (2007) Enzyme-based biofuel cells. Curr Opin Biotechnol 18:228–234. https://doi.org/10.1016/j.copbio.2007.03.007

26. Feng W, Ji P (2011) Enzymes immobilized on carbon nanotubes. Biotechnol Adv 29:889–895. https://doi.org/10.1016/j.biotechadv.2011.07.007
27. Wang Y, Liu L, Li M et al (2011) Multifunctional carbon nanotubes for direct electrochemistry of glucose oxidase and glucose bioassay. Biosens Bioelectron 30:107–111. https://doi.org/10.1016/j.bios.2011.08.038
28. Bullen RA, Arnot TC, Lakeman JB, Walsh FC (2006) Biofuel cells and their development. Biosens Bioelectron 21:2015–2045. https://doi.org/10.1016/j.bios.2006.01.030
29. Kavanagh P, Leech D (2013) Mediated electron transfer in glucose oxidising enzyme electrodes for application to biofuel cells: recent progress and perspectives. Phys Chem Chem Phys 15:4859. https://doi.org/10.1039/c3cp44617d
30. Vincent KA, Li X, Blanford CF et al (2007) Enzymatic catalysis on conducting graphite particles. Nat Chem Biol 3:761–762. https://doi.org/10.1038/nchembio.2007.47
31. Ivnitski D, Branch B, Atanassov P, Apblett C (2006) Glucose oxidase anode for biofuel cell based on direct electron transfer. Electrochem Commun 8:1204–1210. https://doi.org/10.1016/j.elecom.2006.05.024
32. Rasmussen M, Abdellaoui S, Minteer SD (2016) Enzymatic biofuel cells: 30 years of critical advancements. Biosens Bioelectron 76:91–102. https://doi.org/10.1016/j.bios.2015.06.029
33. Franco JH, Minteer SD, de Andrade AR (2018) Product analysis of operating an ethanol/O_2 biofuel cell shows the synergy between enzymes within an enzymatic cascade. J Electrochem Soc 165:H575–H579. https://doi.org/10.1149/2.0931809jes
34. Arechederra RL, Treu BL, Minteer SD (2007) Development of glycerol/O_2 biofuel cell. Journal of Power Sources 173:156–161. https://doi.org/10.1016/j.jpowsour.2007.08.012
35. Ricca E, Brucher B, Schrittwieser JH (2011) Multi-enzymatic cascade reactions: overview and perspectives. Adv Synth Catal 353:2239–2262. https://doi.org/10.1002/adsc.201100256
36. Palmore GTR, Bertschy H, Bergens SH, Whitesides GM (1998) A methanol/dioxygen biofuel cell that uses NAD^+-dependent dehydrogenases as catalysts: application of an electroenzymatic method to regenerate nicotinamide adenine dinucleotide at low overpotentials. J Electroanalyt Chem 443:155–161. https://doi.org/10.1016/S0022-0728(97)00393-8
37. Xu S, Minteer SD (2012) Enzymatic biofuel cell for oxidation of glucose to CO_2. ACS Catal 2:91–94. https://doi.org/10.1021/cs200523s
38. Wu G, Gao Y, Zhao D et al (2017) Methanol/oxygen enzymatic biofuel cell using laccase and NAD^+-dependent dehydrogenase cascades as biocatalysts on carbon nanodots electrodes. ACS Appl Mater Interfaces 9:40978–40986. https://doi.org/10.1021/acsami.7b12295
39. Sokic-Lazic D, Minteer SD (2008) Citric acid cycle biomimic on a carbon electrode. Biosens Bioelectron 24:939–944. https://doi.org/10.1016/j.bios.2008.07.043
40. Sokic-Lazic D, de Andrade AR, Minteer SD (2011) Utilization of enzyme cascades for complete oxidation of lactate in an enzymatic biofuel cell. Electrochim Acta 56:10772–10775. https://doi.org/10.1016/j.electacta.2011.01.050
41. Zhu Z, Ma C, Percival Zhang Y-H (2018) Co-utilization of mixed sugars in an enzymatic fuel cell based on an in vitro enzymatic pathway. Electrochim Acta 263:184–191. https://doi.org/10.1016/j.electacta.2017.11.083
42. Sokic-Lazic D, Arechederra RL, Treu BL, Minteer SD (2010) Oxidation of biofuels: fuel diversity and effectiveness of fuel oxidation through multiple enzyme cascades. Electroanalysis 22:757–764. https://doi.org/10.1002/elan.200980010
43. Sokic-Lazic D, Minteer SD (2009) Pyruvate/air enzymatic biofuel cell capable of complete oxidation. Electrochem Solid-State Lett 12:F26. https://doi.org/10.1149/1.3170904
44. Hickey DP, Gaffney EM, Minteer SD (2018) Electrometabolic pathways: recent developments in bioelectrocatalytic cascades. Top Curr Chem 376:43. https://doi.org/10.1007/s41061-018-0221-4
45. Addo PK, Arechederra RL, Minteer SD (2010) Evaluating enzyme cascades for methanol/air biofuel cells based on NAD+-dependent enzymes. Electroanalysis 22:807–812. https://doi.org/10.1002/elan.200980009
46. Akers NL, Moore CM, Minteer SD (2005) Development of alcohol/O_2 biofuel cells using salt-extracted tetrabutylammonium bromide/Nafion membranes to immobilize dehydrogenase enzymes. Electrochim Acta 50:2521–2525. https://doi.org/10.1016/j.electacta.2004.10.080

47. Zhu Z, Sun F, Zhang X, Zhang Y-HP (2012) Deep oxidation of glucose in enzymatic fuel cells through a synthetic enzymatic pathway containing a cascade of two thermostable dehydrogenases. Biosens Bioelectron 36:110–115. https://doi.org/10.1016/j.bios.2012.04.001
48. Aquino Neto S, Almeida TS, Palma LM et al (2014) Hybrid nanocatalysts containing enzymes and metallic nanoparticles for ethanol/O_2 biofuel cell. J Power Sources 259:25–32. https://doi.org/10.1016/j.jpowsour.2014.02.069
49. Le TXH, Bechelany M, Engel AB et al (2016) Gold particles growth on carbon felt for efficient micropower generation in a hybrid biofuel cell. Electrochim Acta 219:121–129. https://doi.org/10.1016/j.electacta.2016.09.135
50. Aquino Neto S, Milton RD, Crepaldi LB et al (2015) Co-immobilization of gold nanoparticles with glucose oxidase to improve bioelectrocatalytic glucose oxidation. J Power Sources 285:493–498. https://doi.org/10.1016/j.jpowsour.2015.03.121
51. Kwon CH, Ko Y, Shin D et al (2018) High-power hybrid biofuel cells using layer-by-layer assembled glucose oxidase-coated metallic cotton fibers. Nat Commun 9:4479. https://doi.org/10.1038/s41467-018-06994-5
52. Gentil S, Lalaoui N, Dutta A et al (2017) Carbon-nanotube-supported bio-inspired nickel catalyst and its integration in hybrid hydrogen/air fuel cells. Angew Chem Int Ed 56:1845–1849. https://doi.org/10.1002/anie.201611532
53. Aguilar C, Urzúa U, Koenig C, Vicuña R (1999) Oxalate oxidase from ceriporiopsis subvermispora: biochemical and cytochemical studies. Arch Biochem Biophys 366:275–282. https://doi.org/10.1006/abbi.1999.1216
54. Moussatche P, Angerhofer A, Imaram W et al (2011) Characterization of Ceriporiopsis subvermispora bicupin oxalate oxidase expressed in *Pichia pastoris*. Arch Biochem Biophys 509:100–107. https://doi.org/10.1016/j.abb.2011.02.022
55. Svedružić D, Jónsson S, Toyota CG et al (2005) The enzymes of oxalate metabolism: unexpected structures and mechanisms. Arch Biochem Biophys 433:176–192. https://doi.org/10.1016/j.abb.2004.08.032
56. Tanner A, Bowater L, Fairhurst SA, Bornemann S (2001) Oxalate decarboxylase requires manganese and dioxygen for activity. J Biol Chem 276:43627–43634. https://doi.org/10.1074/jbc.M107202200
57. Escutia MR, Bowater L, Edwards A et al (2005) Cloning and sequencing of two *Ceriporiopsis subvermispora* bicupin oxalate oxidase allelic isoforms: implications for the reaction specificity of oxalate oxidases and decarboxylases. Appl Environ Microbiol 71:3608–3616. https://doi.org/10.1128/AEM.71.7.3608-3616.2005
58. Hickey DP, McCammant MS, Giroud F et al (2014) Hybrid enzymatic and organic electrocatalytic cascade for the complete oxidation of glycerol. J Am Chem Soc 136:15917–15920. https://doi.org/10.1021/ja5098379
59. Franco JH, de Almeida PZ, Abdellaoui S et al (2019) Bioinspired architecture of a hybrid bifunctional enzymatic/organic electrocatalyst for complete ethanol oxidation. Bioelectrochemistry 130:107331. https://doi.org/10.1016/j.bioelechem.2019.107331
60. Pozzi G, Cavazzini M, Quici S et al (2004) Poly(ethylene glycol)-supported TEMPO: an efficient, recoverable metal-free catalyst for the selective oxidation of alcohols. Org Lett 6:441–443. https://doi.org/10.1021/ol036398w
61. Semmelhack MF, Schmid CR (1983) Nitroxyl-mediated electro-oxidation of amines to nitriles and carbonyl compounds. J Am Chem Soc 105:6732–6734. https://doi.org/10.1021/ja00360a042
62. De Luca L, Giacomelli G, Masala S, Porcheddu A (2003) Trichloroisocyanuric/TEMPO oxidation of alcohols under mild conditions: a close investigation. J Org Chem 68:4999–5001. https://doi.org/10.1021/jo034276b
63. Zhou Z, Liu L (2014) TEMPO and its derivatives: synthesis and applications. Curr Org Chem 18:459–474. https://doi.org/10.2174/13852728113176660151
64. Abdellaoui S, Knoche KL, Lim K et al (2016) TEMPO as a promising electrocatalyst for the electrochemical oxidation of hydrogen peroxide in bioelectronic applications. J Electrochem Soc 163:H3001–H3005. https://doi.org/10.1149/2.0011604jes

65. Ciriminna R, Palmisano G, Pagliaro M (2015) Electrodes functionalized with the 2,2,6,6-tetramethylpiperidinyloxy radical for the waste-free oxidation of alcohols. ChemCatChem 7:552–558. https://doi.org/10.1002/cctc.201402896
66. Franco JH, Neto SA, Hickey DP et al (2018) Hybrid catalyst cascade architecture enhancement for complete ethanol electrochemical oxidation. Biosens Bioelectron 121:281–286. https://doi.org/10.1016/j.bios.2018.09.011
67. Macazo FC, Hickey DP, Abdellaoui S et al (2017) Polymer-immobilized, hybrid multi-catalyst architecture for enhanced electrochemical oxidation of glycerol. Chem Commun 53:10310–10313. https://doi.org/10.1039/C7CC05724E
68. Li G, Wu Z, Xu C, Hu Z (2022) Hybrid catalyst cascade for enhanced oxidation of glucose in glucose/air biofuel cell. Bioelectrochemistry 143:107983. https://doi.org/10.1016/j.bioelechem.2021.107983
69. Franco JH, Grattieri M, de Andrade AR, Minteer SD (2021) Unveiling complete lactate oxidation through a hybrid catalytic cascade. Electrochim Acta 376:138044. https://doi.org/10.1016/j.electacta.2021.138044
70. Franco JH, Klunder KJ, Russell V, et al (2019) Hybrid enzymatic and organic catalyst cascade for enhanced complete oxidation of ethanol in an electrochemical micro-reactor device. Electrochimica Acta 135254. https://doi.org/10.1016/j.electacta.2019.135254
71. Hickey DP, Milton RD, Chen D et al (2015) TEMPO-modified linear poly(ethylenimine) for immobilization-enhanced electrocatalytic oxidation of alcohols. ACS Catal 5:5519–5524. https://doi.org/10.1021/acscatal.5b01668
72. Hepperle JAM, Mitschang F, Bier AK et al (2013) Immobilization of catalysts in poly(p-xylylene) nanotubes. RSC Adv 3:25976. https://doi.org/10.1039/c3ra43647k
73. Andersen NI, Artyushkova K, Matanović I et al (2019) Spectro-electrochemical microfluidic platform for monitoring multi-step cascade reactions. ChemElectroChem 6:246–251. https://doi.org/10.1002/celc.201800578
74. Das A, Stahl SS (2017) Noncovalent immobilization of molecular electrocatalysts for chemical synthesis: efficient electrochemical alcohol oxidation with a pyrene–TEMPO conjugate. Angew Chem Int Ed 56:8892–8897. https://doi.org/10.1002/anie.201704921
75. Andersen NI, Artyushkova K, Matanović I et al (2019) Modular microfluidic paper-based devices for multi-modal cascade catalysis. ChemElectroChem 6:2448–2455. https://doi.org/10.1002/celc.201900211
76. Wang Z, Xia L, Xia J et al (2016) Direct energy harvesting from starch by hybrid enzymatic and non-enzymatic cascade bioanode. RSC Adv 6:26421–26424. https://doi.org/10.1039/C6RA02059C
77. Antonio JGR, Franco JH, Almeida PZ et al (2021) Carbon Nanotube PtSn nanoparticles for enhanced complete biocatalytic oxidation of ethylene glycol in biofuel cells. ACS Materials Au. https://doi.org/10.1021/acsmaterialsau.1c00029
78. Zhang L, Bai L, Xu M et al (2015) High performance ethanol/air biofuel cells with both the visible-light driven anode and cathode. Nano Energy 11:48–55. https://doi.org/10.1016/j.nanoen.2014.10.020
79. Bonfin CS, Franco JH, de Andrade AR (2019) Ethanol bioelectrooxidation in a robust poly(methylene green-pyrrole)-mediated enzymatic biofuel cell. J Electroanalyt Chem 844.https://doi.org/10.1016/j.jelechem.2019.04.075
80. Huang X, Zhang L, Zhang Z et al (2019) Wearable biofuel cells based on the classification of enzyme for high power outputs and lifetimes. Biosens Bioelectron 124–125:40–52. https://doi.org/10.1016/j.bios.2018.09.086
81. Bandodkar AJ, Wang J (2016) Wearable biofuel cells: a review. Electroanalysis 28:1188–1200. https://doi.org/10.1002/elan.201600019
82. Lv J, Yin L, Chen X et al (2021) Wearable biosupercapacitor: harvesting and storing energy from sweat. Adv Func Mater 31:2102915. https://doi.org/10.1002/adfm.202102915
83. Campbell AS, Kim J, Wang J (2018) Wearable electrochemical alcohol biosensors. Curr Opin Electrochem 10:126–135. https://doi.org/10.1016/j.coelec.2018.05.014

84. Bandodkar AJ, Jeerapan I, Wang J (2016) Wearable chemical sensors: present challenges and future prospects. ACS Sens 1:464–482. https://doi.org/10.1021/acssensors.6b00250
85. Heller A, Feldman B (2008) Electrochemical glucose sensors and their applications in diabetes management. Chem Rev 108:2482–2505. https://doi.org/10.1021/cr068069y
86. Ohayon D, Nikiforidis G, Savva A et al (2020) Biofuel powered glucose detection in bodily fluids with an n-type conjugated polymer. Nat Mater 19:456–463. https://doi.org/10.1038/s41563-019-0556-4
87. Gouranlou F, Ghourchian H (2016) Enhancement of ethanol–oxygen biofuel cell output using a CNT based nano-composite as bioanode. Biosens Bioelectron 78:337–343. https://doi.org/10.1016/j.bios.2015.11.064
88. Fenga PG, Cardoso FP, Aquino Neto S, De Andrade AR (2013) Multiwalled carbon nanotubes to improve ethanol/air biofuel cells. Electrochimica Acta 106:109–113. https://doi.org/10.1016/j.electacta.2013.05.046
89. Ramanavicius A, Kausaite A, Ramanaviciene A (2008) Enzymatic biofuel cell based on anode and cathode powered by ethanol. Biosens Bioelectron 24:761–766. https://doi.org/10.1016/j.bios.2008.06.048
90. Nasar A, Perveen R (2019) Applications of enzymatic biofuel cells in bioelectronic devices—a review. Int J Hydrogen Energy 44:15287–15312. https://doi.org/10.1016/j.ijhydene.2019.04.182
91. Katz E, Bückmann AF, Willner I (2001) Self-powered enzyme-based biosensors. J Am Chem Soc 123:10752–10753. https://doi.org/10.1021/ja0167102
92. Grattieri M, Minteer SD (2018) Self-powered biosensors. ACS Sens 3:44–53. https://doi.org/10.1021/acssensors.7b00818
93. Xiao X, Siepenkoetter T, Conghaile PÓ et al (2018) Nanoporous gold-based biofuel cells on contact lenses. ACS Appl Mater Interfaces 10:7107–7116. https://doi.org/10.1021/acsami.7b18708
94. Germain MN, Arechederra RL, Minteer SD (2008) Nitroaromatic actuation of mitochondrial bioelectrocatalysis for self-powered explosive sensors. J Am Chem Soc 130:15272–15273. https://doi.org/10.1021/ja807250b
95. Cinquin P, Gondran C, Giroud F et al (2010) A glucose biofuel cell implanted in rats. PLoS ONE 5:e10476. https://doi.org/10.1371/journal.pone.0010476
96. Zhang L, Zhou M, Dong S (2012) A self-powered acetaldehyde sensor based on biofuel cell. Anal Chem 84:10345–10349. https://doi.org/10.1021/ac302414a
97. Sekretaryova AN, Beni V, Eriksson M et al (2014) Cholesterol self-powered biosensor. Anal Chem 86:9540–9547. https://doi.org/10.1021/ac501699p
98. Agnès C, Holzinger M, Le Goff A et al (2014) Supercapacitor/biofuel cell hybrids based on wired enzymes on carbon nanotube matrices: autonomous reloading after high power pulses in neutral buffered glucose solutions. Energy Environ Sci 7:1884–1888. https://doi.org/10.1039/C3EE43986K
99. Knoche KL, Hickey DP, Milton RD et al (2016) Hybrid glucose/O_2 biobattery and supercapacitor utilizing a pseudocapacitive dimethylferrocene redox polymer at the bioanode. ACS Energy Lett 1:380–385. https://doi.org/10.1021/acsenergylett.6b00225
100. Shleev S, González-Arribas E, Falk M (2017) Biosupercapacitors. Curr Opin Electrochem 5:226–233. https://doi.org/10.1016/j.coelec.2017.09.023
101. Conzuelo F, Ruff A, Schuhmann W (2018) Self-powered bioelectrochemical devices. Curr Opin Electrochem 12:156–163. https://doi.org/10.1016/j.coelec.2018.05.010
102. Pankratov D, Blum Z, Suyatin DB et al (2014) Self-charging electrochemical biocapacitor. ChemElectroChem 1:343–346. https://doi.org/10.1002/celc.201300142
103. Shen F, Pankratov D, Pankratova G et al (2019) Supercapacitor/biofuel cell hybrid device employing biomolecules for energy conversion and charge storage. Bioelectrochemistry 128:94–99. https://doi.org/10.1016/j.bioelechem.2019.03.009

(Bio)electrodes on Paper Platforms as Simple and Portable Analytical Tools for Bioanalytical Applications

Habdias A. Silva-Neto, Danielly S. Rocha, Lauro A. Pradela-Filho, Thiago R. L. C. Paixão, and Wendell K. T. Coltro

Abstract Conductive material based on carbon particles is the most usual structure fully incorporated upon cellulose microfibers due to intrinsic properties such as low-electrical resistivity, accessibility, low-cost, dispersion on solvents, and high-contact surface. In this chapter, we introduced the most popular examples of microfabrication protocols for manufacturing paper-based electrodes. The procedure step-by-step for transferring or creating conductive sites on a paper will be indicated. In addition, this chapter also discusses in detail the main examples reported in literature associated with paper-based electrodes and bioanalytical applications. Some strategies of electrode modification, redox activities, and electrochemical analysis involving biomarkers of diabetes, cancer, Alzheimer's disease, and COVID-19 will be explored.

Keywords Cellulose substrate · Carbon allotrope · Material transference · Paper-based electrochemical sensor · Bioanalysis

1 Introduction

Suitable interconnects between conductive particles and cellulose-based substrates have been powerful in producing compact electrochemical devices [1–3]. Traditional electronic devices can be utilized for realizing the interfacing between the target molecule present on chemical samples and analytical detectors. The electrodes surface, when induced by potentiostat, can be catalyzed directly or indirectly by the electrochemical reaction of the target molecule. Then, the electron flow from reactions is monitored by the software. In the last years, the conductive materials,

H. A. Silva-Neto · D. S. Rocha · W. K. T. Coltro (✉)
Instituto de Química, Universidade Federal de Goiás, Goiânia, GO 74690-900, Brazil
e-mail: wendell@ufg.br

L. A. Pradela-Filho · T. R. L. C. Paixão
Departamento de Química Fundamental, Instituto de Química, Universidade de São Paulo, São Paulo, SP 05508-000, Brazil

T. R. L. C. Paixão · W. K. T. Coltro
Instituto Nacional de Ciência E Tecnologia de Bioanalítica, Campinas, SP 13084-971, Brazil

F. N. Crespilho (ed.), *Advances in Bioelectrochemistry Volume 5*,
https://doi.org/10.1007/978-3-031-10832-7_6

including polymers, metals, and carbon allotropes, are the most standard components for creating conductive structures with suitable electron transfer performance in the modern electrochemistry field. While material composed of cellulose is huge recommended as a substrate due to due to accessibility, chemical stability, mechanical resistance, capillarity and ly to, presence of fibers, and greater adherence with conductive inks [2, 4–9].

Material combination through solid–solid and liquid–solid processes is the most traditional for constructing paper-based electrodes, also nominated as electrochemical paper-based analytical devices (ePAD). Manufacturing strategies that can transfer or generating conductive structures upon paper substrates includencil printing, [10] pencil drawing [11], and laser scribing [12]. These protocols are the best examples that can be successfully employed in the microfabrication field due to the use low-cost and accessible materials, and the Fig. 1 illustrates the above-mentioned techniques. Highlighted literature showed many examples of these devices for high-impact sensing applicationss such as forensic, pharmaceutical, food, environmental, and clinical. However, this chapter is dedicated to reviewing recent tendencies in bioanalysis on a paper.

The construction of electrodes on paper is quite attractive to day-to-day uses in the modern analytical chemistry. Considering relevant clinical analysis, the ePAD associated with electrochemical responses has been provided as an interesting alternative for solving infinite situation involving bioanalysis [13]. The key to success of these analytical devices is probably associated with the portability and the possibility of integrating with some detector, as amperometry, square wave voltammetry (SWV), and differential pulse voltammetry (DPV), per example. Another suitable technique

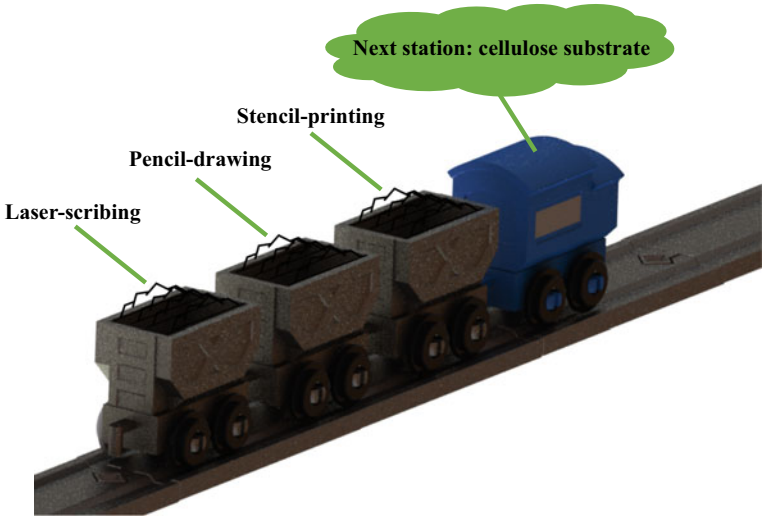

Fig. 1 Illustration of most popular microfabrication protocols for constructing paper-based electrodes

is electrochemical impedance spectroscopy (EIS) which is traditionally coupled with biosensors.

The above-mentioned electrochemical methods exhibited similar performance in terms of detectability from found responses through traditional analytical instrumentation such as UV–VIS spectrophotometry, HPLC–MS, and ICP-MS, for example [14, 15]. In contrast, some methodologic challenges observed in conventional instrumentatio, such as the calibration steps, sample preparation, and long analyst train time, are not found when employing the electrochemical methods [16]. It is important to mention that when the surface of ePADs exhibited inefficient sensing performance, some additional steps are recommended to improve the target analysis, including proposing activations of the electrode surface and modifying the electrode surface with nanocomposites biomaterials. Examples of modification included graphene oxide, carbon nanotube, aptamer, and enzymes [5, 16].

The electrochemical bioanalysis traditionally catalyzed on electrodes is realized in biological matrices collected in two distinct fluids, such as invasive and non-invasive. Invasive sampling from human blood can be pre-treated converting in plasm and serum to reduce the solid-phase interferences. Non-invasive samples can be collected in sweat, tear, urine, saliva, and swab.

This chapter introduced the last information on the paper-based electrodes dedicated to bioanalysis. The main properties of cellulose-based material and the most popular manufacturing techniques employed for constructing ePADs will be carefully demonstrated. Considering the most popular bioanalysis, the advances in sensing performance and clinically relevant application are also discussed. Posteriorly, we conclude this chapter indicating some notes and challenges observed in their devices for realizing bioanalysis.

2 Cellulose-Based Substrate

Paper substrate is a material of varying porositconsisting of cellulose, the most abundant natural renewable polymer [17]. While a raw material, it can be obtained from numerous sources, including biomaterials such as trees, plants, vegetables, and some wastes. Cellulose is classified as a polysaccharide consisting of numerous D-glucose units through unbranched bonds of the type $\beta(1 \rightarrow 4)$.[18, 19] In terms of chemical properties, cellulose can be characterized as hydrophilic with both intermolecular and intramolecular hydrogen bonds and van der Waals forces [19]. Figure 2 presents a real image of the structures of the fiber in a cellulose-based substrate from the scanning electron microscopy (SEM) technique (a), a schematic representation of the fibers, as well as the structure of the chains of the cellulose molecule (b).

A few intrinsic characteristics of the paper substrate include flexibility, high availability, biocompatibility, portability, biodegradability, versatility, recyclability and being considered a low-cost material [9, 20, 21]. Furthermore, the paper is naturally tasteless, odorless, with high-chemical resistance to solvents, and has a surface that is easily and adaptable with biological recognition agents [9, 22]. In this way, all

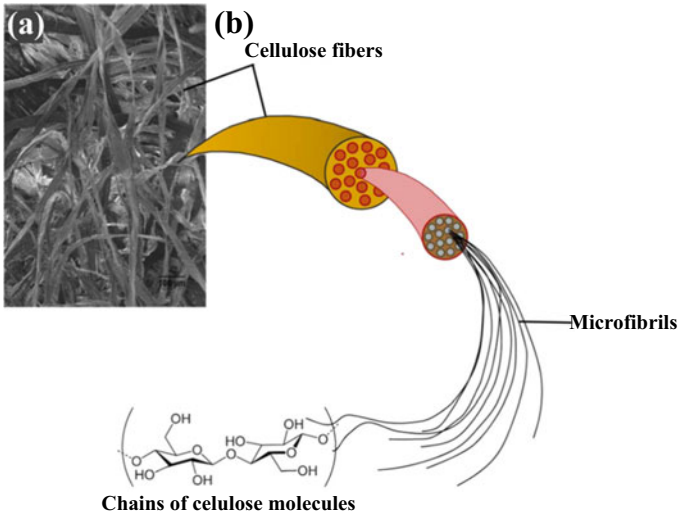

Fig. 2 **a** Scanning electron microscopy analysis showing the cellulose fibers on the paper surface. **b** Structural representation of cellulose fiber. It was reprinted from [18] with permission of American Chemical Society

these attractive properties mentioned above have consolidated the paper substrate as a promising platform for constructing analytical devices for numerous applications in the field of analytical chemistry.

3 Fabrication of Paper-Based Electrodes

In the last years, paper-based electrodes have been successfully manufactured and applied in the most relevant bioanalytical field. In this way, this section is totally dedicated for demonstrating the main examples of microfabrication protocols associated with constructing ePADs which consist of a working electrode (WE), reference electrode (RE), and auxiliary electrode (AE). Fabrication methods, including stencil printing, pencil drawing, and laser scribing, will be carefully discussed. It is possible to see in Fig. 3 that the schematic illustrates most usual protocols used for creating paper-based electrodes.

3.1 Stencil Printing

Stencil printing is a simple and low-cost approach used to produce disposable electrochemical sensors. Figure 4 shows a schematic representation of the most popular

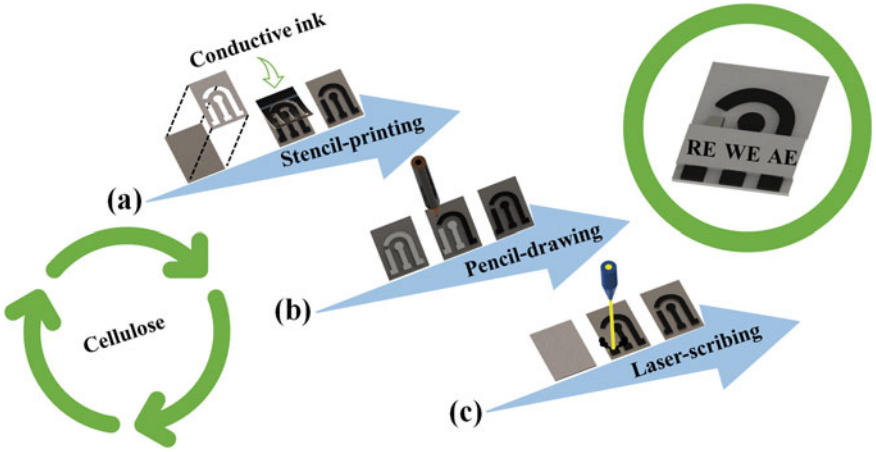

Fig. 3 Schematic representation of process to construct paper-based electrodes. **a** Stencil printing strategy; **b** pencil drawing approach; **c** laser scribing method. Reference electrode (RE); working electrode (WE); auxiliary electrode (AE)

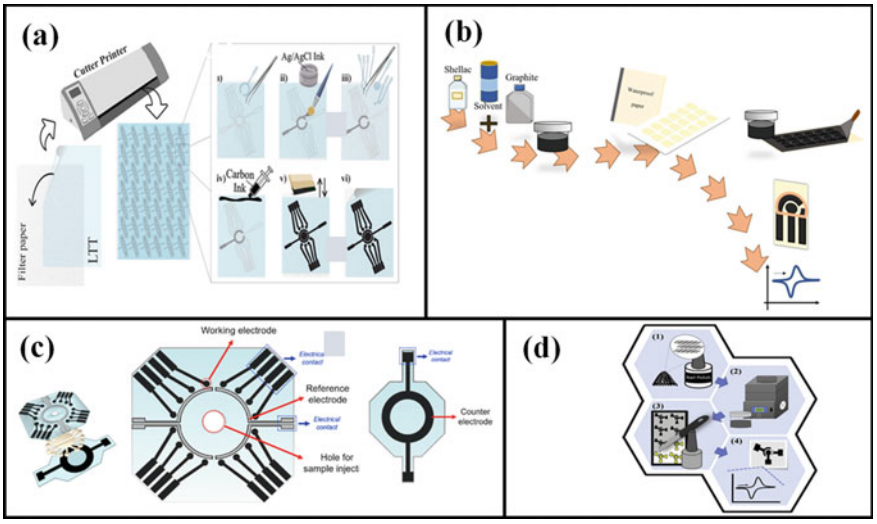

Fig. 4 Schematic representation of the electrode fabrication using the stencil printing technique. **a** Reprinted from [23] with permission of Elsevier; **b** reprinted from [24] with permission of Elsevier; **c** reprinted from [26] with permission of Elsevier; **d** reprinted from [25] with permission of Elsevier

examples of stencil-printed electrodes manufactured on paper [23–26]. Considering the step-by-step fabrication, the procedure initially involves attaching an open mask to the paper substrate. This mask is made of adhesive tape or transparent film used as a mold. This is important to design the shape and size of the electrodes. The

conductive ink with high viscosity is then applied to the top of the mask using a syringe. This ink is spread on the mask using a squeegee, filling the exposed paper area. The mask is subsequently removed from the substrate. Silver ink is applied onto the reference electrode (RE) using a small paintbrush, generating the silver pseudo-RE. After drying, wax is stamped on the back of the paper device, resulting in hydrophobic barriers to define the area of the electrochemical cell.

The above-mentioned fabrication method is similar to the screen printing approach. However, stencil printing does not depend on sophisticated screen apparatus, [1] making this technique feasible to produce disposable sensors in resource-limited laboratories. Higher viscosity inks are necessary to avoid their dispersion across the mask boundaries, ensuring the conductive ink remains uniformly spread only on the exposed paper areas. Conductive inks are commercially available with different prices and compositions [27]. Considering an excess of conductive ink is required to make the electrodes, the fabrication process can be limited depending on the ink price. Inks based on carbon sources have received considerable attention due to their good electrical conductivity and ease of making with alternative materials, significantly decreasing ink costs. The carbon source is combined with a binder to produce the conductive ink, adhering to the substrate. Nail polish, [28] glass varnish, [15, 29] shellac glue, [24] and cellulose acetate [30] are examples of binders used to produce low-cost conductive inks. The ink formulation can help to modulate the electrochemical response of the sensors. Higher carbon percentages typically provide better electrical conductivity, enhancing the electrochemical performance of the sensors [28]. However, it is important to find the best ratio between the binder and carbon-based particle since higher conductive particle percentages can also compromise the mechanical stability of the conductive track, generating fragile sensors. The ink viscosity is controlled by the ratio between the ink and solvent.

Through the stencil printing method is possible to produce disposable electrochemical sensors with paper or plastic materials as substrates [31]. The popularity of the paper substrate is associated with its intrinsic characteristics previously discussed in this chapter and the ability to generate flow without external pumps due to its capillary properties. This feature, in special, makes this material a great substrate for producing portable microfluidic platforms. Plastic materials also have attractive characteristics, such as flexibility, hydrophobicity, and transparency. Overhead projector sheets are examples of plastic sources used to fabricate disposable electrochemical sensors [32]. They are thin films composed of polyvinyl alcohol polyester. Despite the possibility of using different substrates, the choice will depend on the analytical application since each material can provide extra features to the resulting sensors [33].

Wang et al. [34] produced paper-based electrochemical devices using the stencil printing technique. The proposed system, made using the principle of origami, is composed of a detection zone and sampling and reaction zone in a single device. The fabrication process involved six steps: (i) the fabrication of microfluidic channels onto chromatographic paper using wax printing; (ii) stencil printing electrodes using graphite ink; (iii) immobilization of enzyme and cofactor into the reaction zone; (iv)

drying the system for 6 h at 4 °C in the dark; (v) cutting the paper; (vi) and folding the paper device, generating an origami-like device.

3.2 Pencil Drawing

The fabrication process of electrochemical sensors using the pencil drawing technique occurs through a mechanical friction between the pencil and the cellulose fibers to promote suitable deposition of graphite flakes upon the substrate surface. The transfer method can be considered simples, economically viable, and ecologically correct [35–38]. Furthermore, the pencil drawing procedure uses accessible materials making possible the day-to-day applicability. The first study that successfully explored this approach was reported by Dossi et al. [39]. The most popular examples of ePADs reported in the literature are summarized in Figs. 6 and 7. These protocols indicate that the fabrication time occurs between 5 and 15 min with an estimated cost per sensor *c.a* 0.001–0.1 USD [35, 37, 38, 40–43].

Traditional materials used for creating pencil drawn electrodes include paper substrate, plastic pre-molds, and pencil, and additionally, hydrophobic binder promotes the delimitation of the geometric area from the sensor. Regarding the paper substrate, the literature highlights filter paper, watercolor paper, office paper, corrugated fiberboard, vegetal paper, and alumina sandpaper [1]. For producing the pre-molds on paper, the traditional holder can be utilized includes stainless-steel mold, stencil, polyester mask, and adhesive paper label. In terms of available commercially pencils, there is a popular model nominated as grade B highlighting models 4B, 6B, and 9B [44, 45]. For delimitating the geometric area from electrodes, manual deposition of hydrophobic binds, utilization of polyester films wax barrier, self-adhesive tape, and even reusable barrier can be explored.

The choice of the paper substrate and pencil model can be fundamental and reflect on device performance. In general, substrates with the a large presence of porous and pencil with a high number of conductive particles are most recommended to promote low-electrical resistivity on a modified paper surface [44].

The carbon atoms present in graphite (carbon allotrope) are formed through arrangements that results a planar hexagonal structure linked through covalent bonds. This implies that the carbon atoms of the aforementioned system are connected to three other atoms resulting in an angle of 120° and bond lengths of a magnitude of approximately 1.42 Å. This structure (formed by stacks of parallel two-dimensional (2D) graphene sheets) is extremely important to confer suitable electrical resistivity [46–48].

Additional information on graphite-based structures can be performed using Raman spectroscopy analysis and demonstrate microstructures with domains of D, G e 2D bands at 1350, 1579, and 2700 cm^{-1}, respectively [49]. On the other hand, scanning electron microscopy (SEM) measurements upon electrode surface indicated the large presence of microfibers fully incorporated with graphite flakes (See Fig. 5).

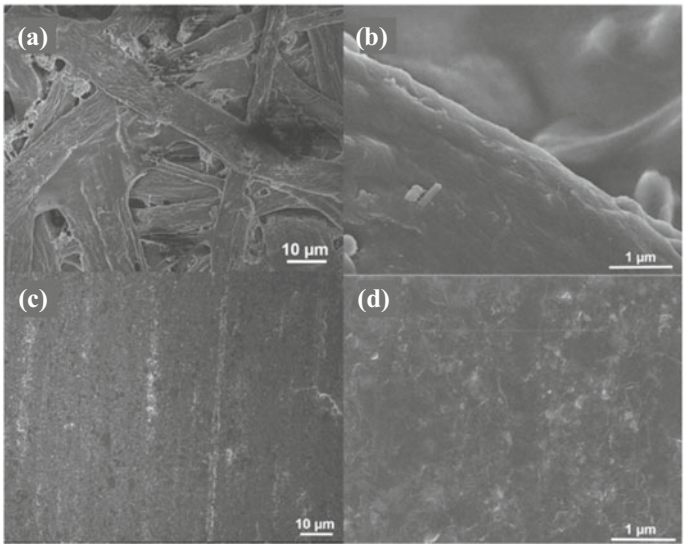

Fig. 5 SEM images at different magnifications of 1000 × and 20,000 × showing **a** office paper. **b** Paper fibers. **c** Electrode manufactured using the pencil drawing technique. **d** Graphite flakes. Reprinted from [50] with permission of Royal Society of Chemistry

3.3 Laser Scribing

The laser scribing technique uses a CO_2 laser source [12, 53]. The carbonization process generates carbon conductive tracks, promising candidates to produce electrochemical sensors. Unlikely stencil printing, this technique does not require a mask. The CO_2 laser machine is controlled by a microcomputer, which is managed by the software used to engineer the geometry and size of the electrodes. The laser induction achieves high-local temperatures (>2500 ºC) on the substrate, resulting in the carbonization process depending on the material. Materials as paper, [12] polyimide, [54] and phenolic resins [55] are examples of substrates carbonized by this technique. The carbonization process can also release gas, leading to porous structures.

Araujo et al. [12] described the fabrication of electrochemical sensors using the laser scribing technique and paperboard as substrate (Fig. 8a). The authors reported the formation of graphene-like structures on the paperboard, providing high-electrical conductivity to the resulting materials. During the fabrication, the carbonization parameters have shown a strong influence on the electrical conductivity of the carbon path, affecting the electrochemical properties of the sensors. The parameters include laser power, scan rate, and distance between the substrate and laser tip. Besides these parameters, the paper type is also considered for the fabrication process since it is commercially available with different compositions, structures, hydrophobicity, and grammage (mass per unit area), impacting the stability and robustness of the sensors.

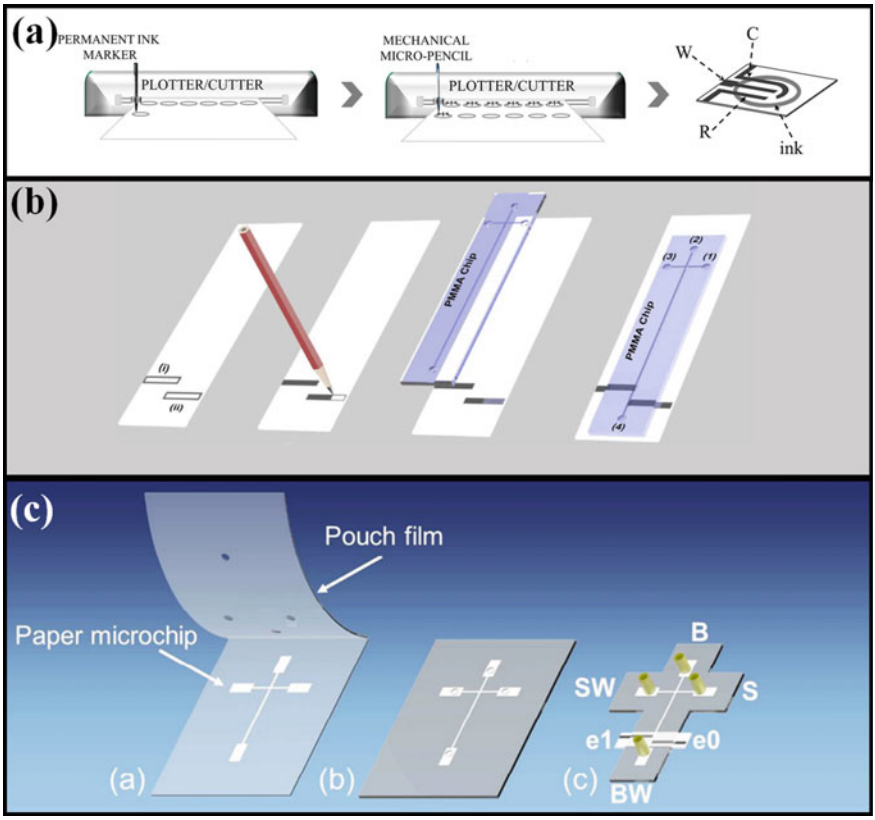

Fig. 6 Schematic illustration of pencil drawing approach. **a** Automatic fabrication of conductive sites upon paper. Reprinted from [51] with permission of American Chemical Society Wiley; **b** manufacturing process of ePAD through direct pencil friction upon paper for creating electrophoresis chip. Reprinted from [38] with permission of Adapted with permission of Wiley; **c** representation of fully electrode fabrication on a paper platform. It was reprinted from [52] with permission of Royal Society of Chemistry

The manufacturing performance of electrodes exhibited reproducibility responses in term of RSD $\leq$4%, using the redox activity of picric acid as model reaction.

The system proposed by Tasic et al. [57] consisted of a three-electrode electrochemical cell. Once carbonized, silver ink was applied to the reference electrode, generating a silver pseudo-RE. The ink was also used to paint the electrical contact of the electrodes to enhance the connection with the instrumentation. The detection zone was delimited with glue, and then, the sensors were ready to use (Fig. 8c). More examples of pyrolyzed electrodes upon paper substrate can be observed in Fig. 8.

Laser scribing does not rely on chemical reagents and controlled atmospheric conditions, resulting in a greener route to producing paper-based electrochemical sensors. In addition, laser-scribed sensors might be used in different situations, which can be advantageous to ink-based electrodes. Stencil-printed electrodes, for example,

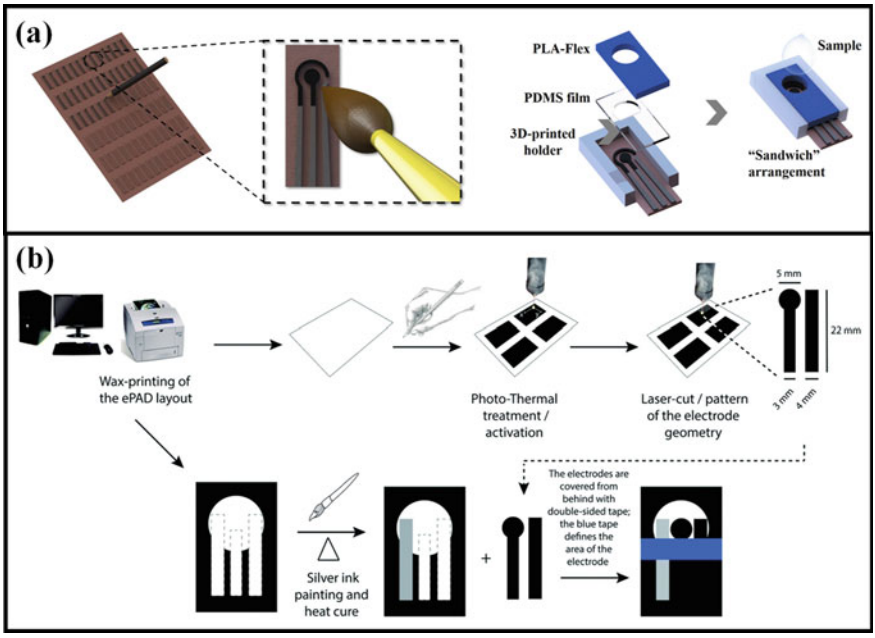

Fig. 7 **a** Illustration of fabrication process to construct ePAD on a sandpaper substrate and assembling of device with 3D-printed holder. Reprinted from [49] with permission of Elsevier; **b** schematic representation of step-by-step ePADs fabrication with surface treatment using CO_2 laser. Reprinted from [50] with permission of Royal Society of Chemistry

normally have low stability in organic solvents due to ink dissolution. This effect is considered a drawback for electroanalysis involving sensors designed for long-term use. Even though few works have reported the applicability of the paper-based sensors fabricated by laser scribing, this technique has great potential to become popular once it allows mass-production scale due to its automated nature associated with high reproducibility [54, 58].

4 Bioanalytical Application

As mentioned above, the three most popular approaches for manufacturing conductive structures upon paper fibers aim to create disposable electrode. Through these devices are possible to see numerous opportunities of sensing including cases as forensic, environmental, food, pharmaceutical, and clinical issues. The literature has been showing many studies that contrast the relevance of ePAD in the modern analytical chemistry. However, the intention of this section is carefully demonstrated only the prominent examples of ePADs dedicated to bioanalysis, and Fig. 9 indicates some examples of clinical applications. Key information from the target analyte as

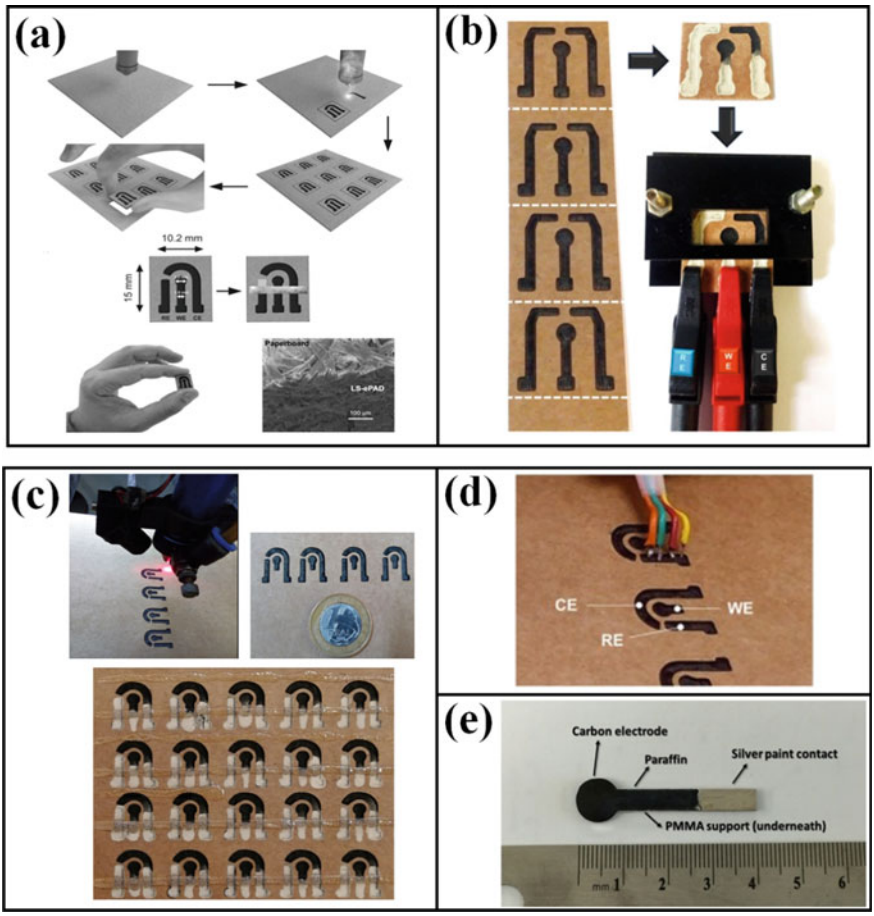

Fig. 8 Examples of laser scribing electrodes manufactured on a paper platform. **a** Manufacture process of ePADs. Reprinted from [12] with permission of Wiley; **b** real image of laser scribing electrodes. Reprinted from [56] with permission of Elsevier; **c** fabrication and delimitation of geometric region of electrochemical cell. Reprinted from [57] with permission of Elsevier; **d** real image of ePADs. Reprinted from [58] with permission of Elsevier; **e** final image of working electrode constructed on a paper by laser scribing method. Reprinted from [3] with permission of Elsevier;

biological relevance and redox activity will be presented. In addition, bioanalysis's analytical parameters, including electrochemical technique, the limit of detection (LOD), selectivity, matrix effect, and analysis time, will also be discussed.

Dungchai et al. [7] reported the pioneers study employed ePADs in association with amperometry for multianalytes detection in biological fluid. The authors fabricated microfluidic devices integrated with three carbon-based electrochemical cells and showed that the working electrodes surface, when anchored with enzymes glucose oxidase, lactate oxidase, and uricase, can be successfully explored for selective detection of glucose and lactate and uric acid in the human serum sample,

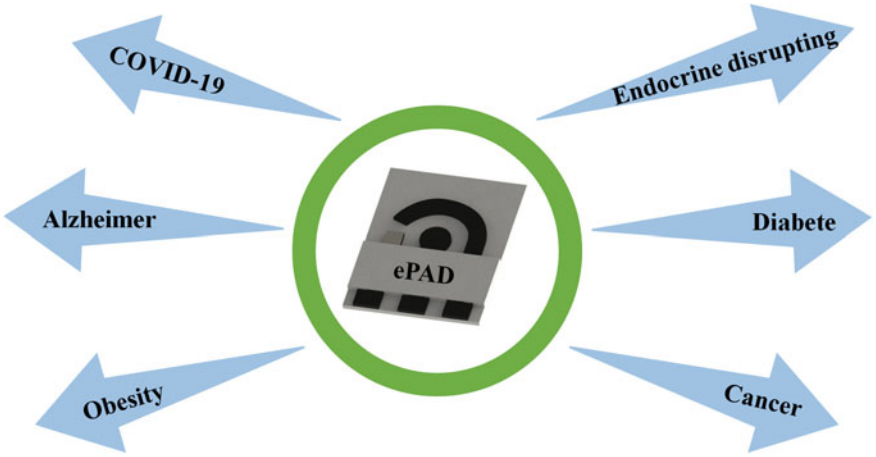

Fig. 9 Schematic demonstration of main bioanalysis examples that can be realized by using ePADs

respectively. In addition, the study indicated that the simultaneous redox activities of target biomolecules occur at potential 0.0 V versus Ag/AgCl for 100 s and reported detectable levels in terms of LOD ranging from 0.21 and 1.38 mmol L^{-1}.

Probably motivated by the high impact of the above-mentioned study, Nie et al. [8] exhibited that ePADs can be also performed for electrochemical analysis of organic specie in complex urine samples. They reported that the carbon-based electrode incorporated with glucose oxidase and redox mediator ($[Fe(CN)_6]^{3-}$) can be promoted the sensing performance of glucose at 0.3 V versus Ag/AgCl for 20 s. The calculated value of LOD for the analyte was 0.22 mmol L^{-1} and demonstrated that the bioanalysis of glucose in urine samples does not interfere with bovine serum albumin (BSA).

Following the tendency that paper-based devices showed affordable analytical performance for bioanalysis, other studies combined the versatility of cellulose-based structuresed with disposable electrodes for realizing the separations and detection in sequence of biomolecules emerging then, the paper-based separation devices. Carvalhal et al. [59] proposed the chromatographic separation and detection of molecules ascorbic (AA) and uric (UA) acids by using the microfluidics channels integrated with gold electrodes. In the above study, the molecules AA and UA were successfully separated through 10 × 7 mm paper-column and electrochemically detected applied potential at 0.4 V versus Au for 16 min. The calculated value of LOD for both molecules AA and UA was 0.02 mmol L^{-1}.

Dossi et al. [39] proposed ePAD in association with the amperometric detector for performing the separation and analysis of AA and sunset yellow. The authors evidenced that the oxidation of target molecules occurs at 0.9 V versus graphite, and the calculated values of LOD were 30 and 90 μmol L^{-1} for AA and sunset yellow, respectively.

Chagas et al. [38] combined PMMA electrophoresis chip with alternative capacitively coupled contactless conductivity detection (C^4D) on paper-based electrodes for realizing the separations and measurements of inorganic cations ions (K^+ and Na^+) in human tear. The migration time for cations ions separation was 64.5 ± 1.5 and 80.5 ± 1.8 s. Moreover, the analytical parameters as LOD and linear concentration range were (4.9 and 6.8 μmol L^{-1}) and (6–26 and 120–170 μmol L^{-1}), respectively. The reported protocol showed satisfactory accuracy performance with quantitative measurements of K^+ and Na^+ ranged between 83.4 and 103.4%. In another study, Chagas et al. [52] constructed ePADs integrated with C^4D detector to make possible the separation and detection of BSA and creatinine molecules in clinical compounds. The reported separation performance in terms of migration time showed very reproducible values, and RSD ≤2% considering both chemical species. In addition, the detectable levels for BSA and creatinine were 20 and 35 mmol L^{-1}, respectively.

Pradela et al. [60] developed microfluidic paper-based devices (μPAD) under a constant support electrolyte flow inspired by flow injection analysis. The system was composed of paper-based devices coupled with thermoplastic electrodes. Amperometry was used as the analytical technique. Continuous flow generation is a challenge for paper devices due to the increase of the drag force through the microfluidic channel, affecting the analytical signal. The system consisted of two reservoirs connected to the microfluidic channel (Fig. 10a). The inlet reservoir was constantly filled with supporting electrolytes, which flowed by gravity and capillarity. This solution flows through the detection system, reaching an outlet reservoir. The outlet reservoir is a fan-shaped paper responsible for wicking the carrier fluid. The analyte solution (2 μL) was injected at a specific point between the inlet reservoir and the electrochemical detector. The electrochemical measurements were started when the

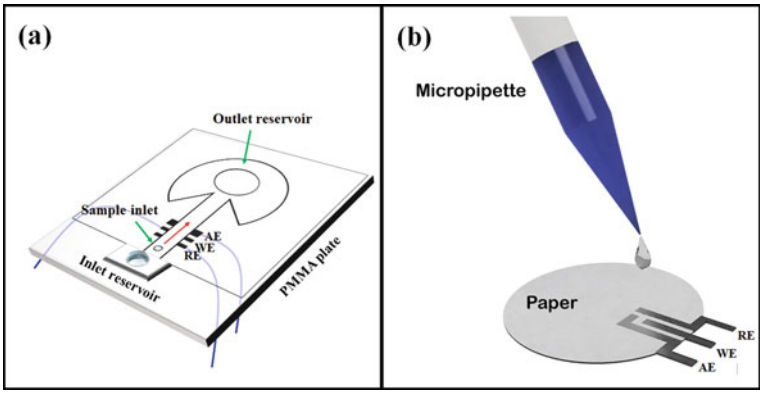

Fig. 10 Schematic representations of the paper-based microfluidic device proposed by **a** Pradela et al. [60] and **b** Arantes et al. [61]. RE: carbon pseudo-reference electrode; WE: working electrode; AE: auxiliary electrode. Reprinted from [60, 61] with permission of American Chemical Society and Elsevier, respectively

supporting electrolyte reaches the outlet reservoir since the drag force is considerably decreased at this point, controlling the flow rate. Keeping a constant flow in this system is important to ensure signal reproducibility. The proposed device was used for amperometric determination of caffeic acid in tea samples through detection potential at 0.4 V versus C. The linear concentration range reported values and LOD was 10 to 500 and 2.5 μmol L^{-1}, respectively.

Arantes et al. [61] reported another interesting approach with microfluidic devices (Fig. 10b). The system involved the combination of batch injection analysis with μPAD. The tree-electrode electrochemical system was fabricated on a circular paper substrate using the pencil drawn technique combined with CO_2 laser pretreatment. The analyte solution with supporting electrolyte was directly injected onto the working electrode surface, generating transient signals associated with the analyte oxidation. During the experiment, the analyte solution (15 μL) gradually spreads on the edges of the paper by capillarity.

Consequently, sequential injections can be performed into the microfluidic device. The proposed system was used to determine paracetamol in pharmaceutical samples. Paper-based microfluidic devices are promising analytical platforms for field analyzes since they combine low-cost and portability with rapid analyzes. In addition, they typically require small sample volumes, which is a great feature for analytical quantification in biological samples.

As discussed above, the ePADs can be applied for realizing the separation and/or detection of sugars, cations ions, organic acids, and analgesic. Figures 11, 12, and 13 outlined the most recent examples of ePADs in association with portable electrochemical detectors for realizing bioanalysis. When is considerable the last five years, these devices also demonstrated high potentiality for realizing bioanalysis in the most

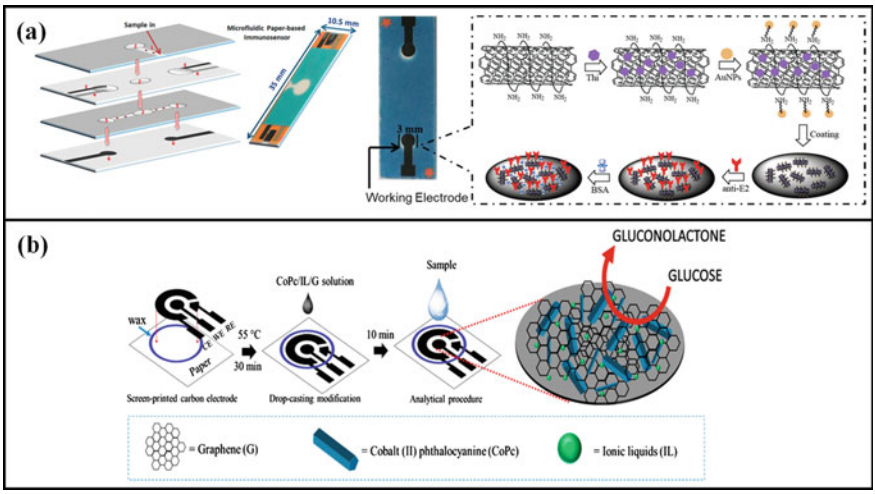

Fig. 11 Examples of ePADs successfully utilized for hormone (**a**) and glucose (**b**) detections in biological samples and reprinted from [62] and [63] with permission of Elsevier

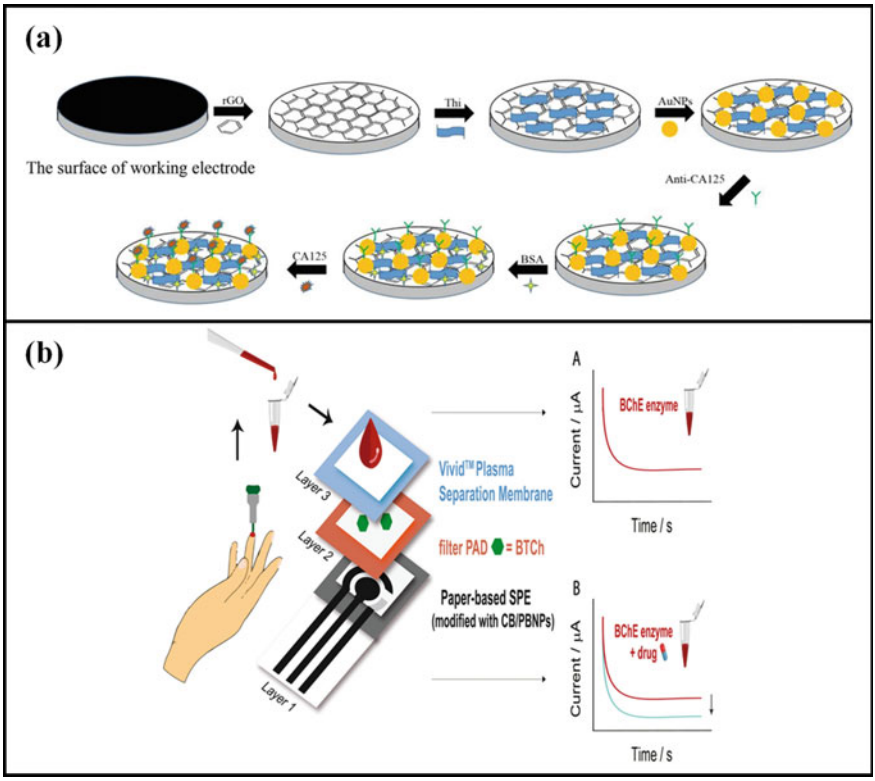

Fig. 12 Schematic demonstration of ePADs utilized for realizing the detections of cancer antigen 125 (**a**) and enzyme butyrylcholinesterase, (**b**) reprinted [64] and [65] with permission of Elsevier

different areas of clinical diagnosis, included endocrine disruption, diabetes, cancer, obesity, Alzheimer, and COVID-19, per example.

The paper-based electrodes can be applied for performing analysis of 17β-estradiol (E2) in serum samples [62]. The molecule E2 is a type of hormone produced by human ovaries. Their presence on organism is attributed to some important biological functions such as fertility and growth maturation of the female reproductive. Also, the presence of molecule E2 can be associated to other vital functions such as the development of bones, maintenance, and enhancement of skeletal muscles, per example. In this way, the quantification of molecule E2 in biological samples it is extremally important and can be realized electronically through immunosensor on a paper. As indicated in Fig. 11a, the reported μPADs surface was modified with MWCNTs/thionine/AuNPs nanocomposites followed by anti-E2. Before starting the electrochemical measurements, the above surface was cleaner with 1% BSA solution to block any possible target adsorption. The proposed method successfully showed an analysis of E2 in serum samples via DPV responses at −0.2 V versus Ag/AgCl,

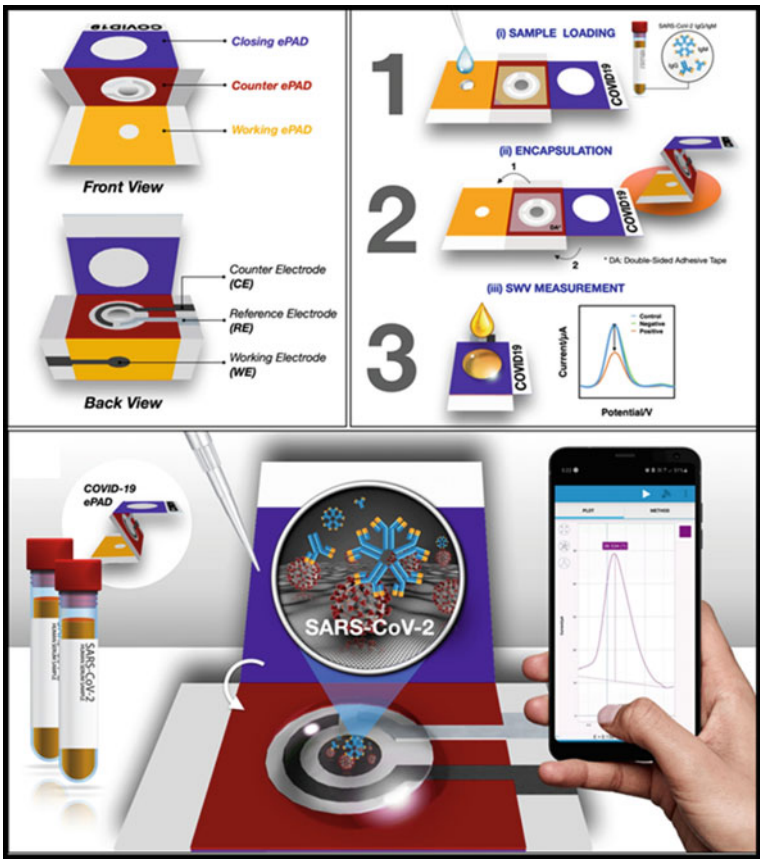

Fig. 13 Schematic representation of paper-based electrodes dedicated for performing the diagnosis of COVID-19 and reprinted from [66] with permission of Elsevier

with a reported value of LOD ~10 pg mL^{-1} and the absence of interferences involving organic acid species.

As denotated in Fig. 11b, Chaiyo et al. [63] manufactured ePAto realize amperometric glucose measurements in blood serum samples. The presence of molecule glucose when detected in dysfunctional blood levels can be associated with diabetes diagnosis. This critical issue mentioned above is a large vector of death and disability in the human species. Diabetes patients can be indicated several disorders such as blindness, nerve degeneration, and kidney failure. For this reason, the diagnosis of diabetes is extremely important, and the reported study revealed that the paper-based electrodes, when incorporated with graphene and cobalt(II) phthalocyanine nanocomposite, are realized selective and sensitive amperometric detection of glucose at 0.7 versus C. The authors showed one of the best analytical performances in reported literature with values of LOD ~0.64 μmol L^{-1} and a linear range between 0.01 and 1.3 mmol L^{-1}.

It is observed in Fig. 12a that the ePADs reported by Fan et al. [64] can be explored for the detection of cancer antigen 125 in serum samples. The antigen 125 is traditionally related to ovarian cancer, and the recommended for healthy human serum is lass then 35 U mL^{-1}. In addition, the mentioned biomarker can be attributed to other cancer like lung cancer, endometrial cancer, and breast cancer. For the target detection, the authors anchored the paper surface with r-GO/thionine/AuNPs and realized the DPV measurements through scanning voltage between − 0.5 V and 0.3 V versus Ag/AgCl and using electrolyte supporting composed of 0.1 mol L^{-1} PBS. The reported electrochemical analysis of cancer antigen indicated an LOD value of 0.01 U mL^{-1}. It was also compared in parallel experiments by using ELISA approach, and the both found quantification values of antigen 125 were statically similar, indicating the high performance of the paper-based electrodes. It is important to mention that the reported method realized full analysis in time less than 25 min.

In another study, Caratelli et al. [65] constructed ePAD compose of carbon black paste and applied the device as precision medicine for Alzheimer's disease (AD), see Fig. 12b. The AD is neurodegenerative situation that is characterized by some disturbances such as memory loss and in several cases losing control of bodily function, per example. The main legacy of the AD is the progressive degradation of social relationships formed over long periods. The main biomarkers of AD are the enzymes acetylcholinesterase (AChE) and butyrylcholinesterase (BChE), and there are presented poor redox activity. For improving their sensing performance, the authors incorporated the electrode surface with nanocomposites based on Prussian blue. The target electrochemical detection was performed through the redox behavior of enzyme BChE in the presence of inhibitor butyrylthiocholine prepared in 0.05 mol L^{-1} PBS and 0.1 mol L^{-1} KCl. The amperometry technique as selected with detection potential at 0.3 V versus Ag/AgCl and the real samples composed by human blood (blood dilution: 1:2 (v/v)). The reported analytical performance exhibited suitable detectability of enzyme BChE with LOD and repeatability values of 0.005 μ mol L^{-1} and 4.2%, respectively.

It is possible to see in Fig. 13, and the schematic illustration employed ePAD is dedicated to realizing the detection of SARS-CoV-2 spike protein in biological samples. SARS-CoV-2 virus can affect the respiratory system and promote other infection, fever, and headaches from vomiting and diarrhea, per example. The pandemic situation involving COVID-19 caused several problems to public health, with over 32 million infected cases. In this way, Yakoh et al. [66] manufactured paper-based electrodes in combination with SWV responses and the redox mediator $[Fe(CN)6]^{3-/4-}$. The construction of biosensors involved the incorporations of GO following to activation of carboxyl groups in the presence of EDC/NHS (proportion: 1:2 (v/v)). Then, the electrodes were exposed to a washing step with 0.01 PBS mol L^{-1} and blocked with skim milk. Before the target detection, the authors reported that the serum samples previously dopped with antibodies were added onto the electrode surface and incubated at room temperature before the target detection. Finally, the electrode was washed with PBS, and the indirect detection of spike protein was realized through redox activity of $[Fe(CN)6]^{3-/4-}$. The peak potential attributed to oxidation of redox mediator occurred at ~0.2 V versus Ag/AgCl, with the stability of

responses ranging from 95 to 105% and a value of LOD ~0.11 ng mL^{-1}. The authors also indicated the clinical possibility through analysis of 17 serum samples, and the reported responses were statistically similar to found results in ELISA test kit.

5 Conclusion and Perspectives

This chapter revised the most important information about low-cost manufacturing strategies for constructing paper-based electrodes. Electrode fabrication through stencil printing, pencil drawing, and laser scribing has been recommended for creating disposable electrochemical devices. The main conductive materials successfully used are based on carbon allotropes. The manufacture steps performed for constructing paper-based electrodes indicated that the stencil printing and laser scribing are more robust and reproducible. On the other hand, the pencil drawing approach is extremally simple and instrumental-free. The microfabrication challenges observed in stencil, pencil, and laser techniques had the viscosity control from conductive ink, adherence of graphite particles upon cellulose substrate, and increase in mechanical resistance of pyrolyzed electrodes, respectively. As reviewed in the bioanalysis examples, the ePADs play suitable analytical performance in detectability, repeatability, and selectivity. Most important, the paper-based electrode surface can be employed to catalyze an infinite of redox bioactivity, including chemical markers for diabetes, cancer, and SARS-CoV-2 virus, for example. If the bare surface of electrodes is poor for realizing the sensing performance, the most popular examples successfully suggested some electrode modification strategies that can drastically improve the faradaic current of the target bioanalysis. These points stated that the ePADs are versatile, accessible, portable, and exhibit potential for solving the most bioanalytical challenges observed in modern analytical chemistry.

Acknowledgements The authors would like to thank CAPES, CNPq (grants 307554/2020-1, 142412/2020-1 and 405620/2021-7), FAPESP (2019/16491-0, 2021/00205-8, 2018/08782-1), and INCTBio (grant 465389/2014-7) for the financial support and granted scholarships.

References

1. Stefano JS, Orzari LO, Silva-Neto HA, de Ataíde VN, Mendes LF, Coltro WKT, Paixão TRLC, Janegitz BC (2022) Different approaches for fabrication of low-cost electrochemical sensors. Curr Opin Electrochem 32:100893. https://doi.org/10.1016/j.coelec.2021.100893
2. Ataide VN, Mendes LF, Gama LILM, de Araujo WR, Paixão TRLC (2020) Electrochemical paper-based analytical devices: ten years of development. Anal Methods 12:1030–1054. https://doi.org/10.1039/c9ay02350j
3. Giuliani JG, Benavidez TE, Duran GM, Vinogradova E, Rios A, Garcia CD (2016) Development and characterization of carbon based electrodes from pyrolyzed paper for biosensing applications. J Electroanal Chem 765:8–15. https://doi.org/10.1016/j.jelechem.2015.07.055

4. Torrinha Á, Morais S (2021) Electrochemical (bio)sensors based on carbon cloth and carbon paper: an overview. TrAC—Trends Anal Chem 142. https://doi.org/10.1016/j.trac.2021.116324
5. Ozer T, McMahon C, Henry CS (2020) Advances in paper-based analytical devices. Annu Rev Anal Chem 13:85–109. https://doi.org/10.1146/annurev-anchem-061318-114845
6. Liana DD, Raguse B, Justin Gooding J, Chow E (2012) Recent advances in paper-based sensors. Sensors 12:11505–11526. https://doi.org/10.3390/s120911505
7. Dungchai W, Chailapakul O, Henry CS (2009) Electrochemical detection for paper-based microfluidics. Anal Chem 81:5821–5826
8. Nie Z, Nijhuis CA, Gong J, Chen X, Kumachev A, Martinez AW, Narovlyansky M, Whitesides GM (2010) Electrochemical sensing in paper-based microfluidic devices. Lab Chip 10:477–483. https://doi.org/10.1039/b917150a
9. Nery EW, Kubota LT (2013) Sensing approaches on paper-based devices: a review. Anal Bioanal Chem 405:7573–7595. https://doi.org/10.1007/s00216-013-6911-4
10. Afonso AS, Uliana CV, Martucci DH, Faria RC (2016) Simple and rapid fabrication of disposable carbon-based electrochemical cells using an electronic craft cutter for sensor and biosensor applications. Talanta 146:381–387. https://doi.org/10.1016/j.talanta.2015.09.002
11. Dossi N, Petrazzi S, Terzi F, Toniolo R, Bontempelli G (2019) Electroanalytical cells pencil drawn on PVC supports and their use for the detection in flexible microfluidic devices. Talanta 199:14–20. https://doi.org/10.1016/j.talanta.2019.01.126
12. de Araujo, Reis W, Frasson CMR, Ameku WA, Silva JR, Angnes L, Paixão TRLC (2017)Single-step reagentlesslaser scribing fabrication of electrochemical paper-based analytical devices. Angewandte Chemie—Int Edition, 15309–15313
13. Solhi E, Hasanzadeh M, Babaie P (2020) Electrochemical paper-based analytical devices (ePADs) toward biosensing: Recent advances and challenges in bioanalysis. Anal Methods 12:1398–1414. https://doi.org/10.1039/d0ay00117a
14. Mettakoonpitak J, Volckens J, Henry CS (2020) Janus electrochemical paper-based analytical devices for metals detection in aerosol samples. Anal Chem 92:1439–1446. https://doi.org/10.1021/acs.analchem.9b04632
15. Silva-Neto HA, Cardoso TMG, McMahon CJ, Sgobbi LF, Henry CS, Coltro WKT (2021) Plug-and-play assembly of paper-based colorimetric and electrochemical devices for multiplexed detection of metals†. Analyst 146. https://doi.org/10.1039/d1an00176k
16. Noviana E, McCord C, Clark K, Jang I, Henry C (2019) Electrochemical paper-based devices: sensing approaches and progress toward practical applications. Lab on a Chip. https://doi.org/10.1039/C9LC00903E
17. Kalia S, Dufresne A, Cherian BM, Kaith BS, Avérous L, Njuguna J, Nassiopoulos E (2011) Cellulose-based bio- and nanocomposites: a review. Int J Polym Sci 2011. https://doi.org/10.1155/2011/837875
18. Mahadeva SK, Walus K, Stoeber B (2015) Paper as a platform for sensing applications and other devices: A review. ACS Appl Mater Interfaces 7:8345–8362. https://doi.org/10.1021/acsami.5b00373
19. Zainal SH, Mohd NH, Suhaili N, Anuar FH, Lazim AM, Othaman R (2021) Preparation of cellulose-based hydrogel: a review. J Market Res 10:935–952. https://doi.org/10.1016/j.jmrt.2020.12.012
20. Martinez AW, Phillips ST, Butte MJ, Whitesides GM (2007) Patterned paper as a platform for inexpensive, low-volume, portable bioassays. Angew Chem 119:1340–1342. https://doi.org/10.1002/ange.200603817
21. Pelton R (2009) Bioactive paper provides a low-cost platform for diagnostics. TrAC—Trends Anal Chem 28:925–942. https://doi.org/10.1016/j.trac.2009.05.005
22. Luo X, Zhang L (2013) New solvents and functional materials prepared from cellulose solutions in alkali/urea aqueous system. Food Res Int 52:387–400. https://doi.org/10.1016/j.foodres.2010.05.016
23. de Oliveira TR, Fonseca WT, de Oliveira SG, Faria RC (2019) Fast and flexible strategy to produce electrochemical paper-based analytical devices using a craft cutter printer to create wax barrier and screen-printed electrodes. Talanta 195:480–489. https://doi.org/10.1016/j.talanta.2018.11.047

24. Melo Henrique J, Rocha Camargo J, Gabriel de Oliveira G, Santos Stefano J, Campos Janegitz B (2021) Disposable electrochemical sensor based on shellac and graphite for sulfamethoxazole detection. Microchem J 170. https://doi.org/10.1016/j.microc.2021.106701
25. Camargo JR, Andreotti IAA, Kalinke C, Henrique JM, Bonacin JA, Janegitz BC (2020) Waterproof paper as a new substrate to construct a disposable sensor for the electrochemical determination of paracetamol and melatonin. Talanta 208:120458. https://doi.org/10.1016/j.talanta.2019.120458
26. Fava EL, Silva TA, do Prado TM, de Moraes FC, Faria RC, Fatibello-Filho O (2019) Electrochemical paper-based microfluidic device for high throughput multiplexed analysis. Talanta 203:280–286. https://doi.org/10.1016/j.talanta.2019.05.081
27. Kava AA, Henry CS (2021) Exploring carbon particle type and plasma treatment to improve electrochemical properties of stencil-printed carbon electrodes. Talanta 221:121553. https://doi.org/10.1016/j.talanta.2020.121553
28. Pradela-Filho LA, Araújo DAG, Takeuchi RM, Santos AL (2017) Nail polish and carbon powder: an attractive mixture to prepare paper-based electrodes. Electrochim Acta 258:786–792. https://doi.org/10.1016/j.electacta.2017.11.127
29. Pradela-Filho LA, Andreotti IAA, Carvalho JHS, Araújo DAG, Orzari LO, Gatti A, Takeuchi RM, Santos AL, Janegitz BC (2020) Glass varnish-based carbon conductive ink: a new way to produce disposable electrochemical sensors. Sens Actuators, B Chem 305:127433. https://doi.org/10.1016/j.snb.2019.127433
30. Santhiago M, Bernardes JS, Pereira MP, Oliveira JM, Strauss M, Bufon CCB (2017) Flexible and foldable fully-printed carbon black conductive nanostructures on paper for high-performance electronic, electrochemical, and wearable devices. ACS Appl Mater Interfaces 9:24365–24372. https://doi.org/10.1021/acsami.7b06598
31. Noviana E, McCord CP, Clark KM, Jang I, Henry CS (2020) Electrochemical paper-based devices: sensing approaches and progress toward practical applications. Lab Chip 20:9–34. https://doi.org/10.1039/c9lc00903e
32. Araújo DAG, Camargo JR, Pradela-Filho LA, Lima AP, Muñoz RAA, Takeuchi RM, Janegitz BC, Santos AL (2020) A lab-made screen-printed electrode as a platform to study the effect of the size and functionalization of carbon nanotubes on the voltammetric determination of caffeic acid. Microchem J 158:105297. https://doi.org/10.1016/j.microc.2020.105297
33. Camargo JR, Orzari LO, Araújo DAG, de Oliveira PR, Kalinke C, Rocha DP, Luiz dos Santos A, Takeuchi RM, Munoz RAA, Bonacin JA, Janegitz BC (2021) Development of conductive inks for electrochemical sensors and biosensors. Microchem J 164. https://doi.org/10.1016/j.microc.2021.105998
34. Wang CC, Hennek JW, Ainla A, Kumar AA, Lan WJ, Im J, Smith BS, Zhao M, Whitesides GM (2016) A paper-based pop-up electrochemical device for analysis of beta-hydroxybutyrate. Anal Chem 88:6326–6333. https://doi.org/10.1021/acs.analchem.6b00568
35. Dossi N, Toniolo R, Pizzariello A, Impellizzieri F, Piccin E, Bontempelli G (2013) Pencil-drawn paper supported electrodes as simple electrochemical detectors for paper-based fluidic devices. Electrophoresis 2085–2091
36. Oliveira VXG, Dias AA, Carvalho LL, Cardoso TMG, Colmati F, Coltro WKT (2018) Determination of ascorbic acid in commercial tablets using pencil drawn electrochemical paper-based analytical devices. Anal Sciencesiences 34:91–95
37. Dias AA, Cardoso TMG, Chagas CLS, Oliveira VXG, Munoz RAA, Henry CS, Santana MHP, Paixão TRLC, Coltro WKT (2018) Detection of analgesics and sedation drugs in whiskey using electrochemical paper-based analytical devices. Electroanalysis 30:2250–2257. https://doi.org/10.1002/elan.201800308
38. Chagas CLS, Costa Duarte L, Lobo-Júnior EO, Piccin E, Dossi N, Coltro WKT (2015) Hand drawing of pencil electrodes on paper platforms for contactless conductivity detection of inorganic cations in human tear samples using electrophoresis chips. Electrophoresis 36:1837–1844. https://doi.org/10.1002/elps.201500110
39. Dossi N, Toniolo R, Pizzariello A, Impellizzieri F, Piccin E, Bontempelli G (2013) Pencil-drawn paper supported electrodes as simple electrochemical detectors for paper-based fluidic devices. Electrophoresis 34:2085–2091. https://doi.org/10.1002/elps.201200425

40. Koga H, Nagashima K, Huang Y, Zhang G, Wang C, Takahashi T, Inoue A, Yan H, Kanai M, He Y, Uetani K, Nogi M, Yanagida T (2019) Paper-based disposable molecular sensor constructed from oxide nanowires, cellulose nanofibers, and pencil-drawn electrodes. ACS Appl Mater Interfaces 11:15044–15050. https://doi.org/10.1021/acsami.9b01287
41. Kanaparthi S (2017) Pencil-drawn paper-based non-invasive and wearable capacitive respiration sensor. Electroanalysis 29:2680–2684. https://doi.org/10.1002/elan.201700438
42. Orzari LO, de Araujo Andreotti IA, Bergamini MF, Marcolino LH, Janegitz BC (2018) Disposable electrode obtained by pencil drawing on corrugated fiberboard substrate. Sensors Actuators B: Chem 264:20–26. https://doi.org/10.1016/j.snb.2018.02.162
43. Santhiago M, Strauss M, Pereira MP, Chagas AS, Bufon CCB (2017) Direct drawing method of graphite onto paper for high-performance flexible electrochemical sensors. ACS Appl Mater Interfaces 9:11959–11966. https://doi.org/10.1021/acsami.6b15646
44. Kurra N, Kulkarni GU (2013) Pencil-on-paper: electronic devices. Lab Chip 13:2866–2873. https://doi.org/10.1039/c3lc50406a
45. Foster CW, Brownson DAC, Ruas De Souza AP, Bernalte E, Iniesta J, Bertotti M, Banks CE (2016) Pencil it Pencil drawn electrochemical sensing platforms. Analyst 141:4055–4064. https://doi.org/10.1039/c6an00402d
46. McAllister MJ, Li JL, Adamson DH, Schniepp HC, Abdala AA, Liu J, Herrera-Alonso M, Milius DL, Car R, Prud'homme RK, Aksay IA (2007) Single sheet functionalized graphene by oxidation and thermal expansion of graphite. Chem Mater 19:4396–4404. https://doi.org/10.1021/cm0630800
47. Unwin PR, Güell AG, Zhang G (2016) Nanoscale electrochemistry of sp2 carbon materials: from graphite and graphene to carbon nanotubes. Acc Chem Res 49:2041–2048. https://doi.org/10.1021/acs.accounts.6b00301
48. de Ataide V, Arantes I, Mendes L, Baldo T, Rocha D, Paixão TRLC, Coltro WKT (2022) Review—a pencil drawing overview: from graphite to electrochemical sensors/biosensors applications. J Electrochem Soc. https://doi.org/10.1149/1945-7111/ac68a0
49. Rocha DS, Duarte LC, Silva-Neto HA, Chagas CLS, Santana P, Filho NRA, Coltro WKT (2021) Sandpaper-based electrochemical devices assembled on a reusable 3D-printed holder to detect date rape drug in beverages. Talanta. https://doi.org/10.1016/j.talanta.2021.122408
50. Ataide VN, Ameku WA, Bacil RP, Angnes L, de Araujo WR, Paixão TRLC (2021) Enhanced performance of pencil-drawn paper-based electrodes by laser-scribing treatment. RSC Adv 11:1644–1653. https://doi.org/10.1039/d0ra08874a
51. Dossi N, Petrazzi S, Toniolo R, Tubaro F, Terzi F, Piccin E, Svigelj R, Bontempelli G (2017) Digitally controlled procedure for assembling fully drawn paper-based electroanalytical platforms. Anal Chem 89:10454–10460. https://doi.org/10.1021/acs.analchem.7b02521
52. Chagas CLS, de Souza FR, Cardoso TMG, Moreira RC, da Silva JAF, de Jesus DP, Coltro WKT (2016) A fully disposable paper-based electrophoresis microchip with integrated pencil-drawn electrodes for contactless conductivity detection. Anal Methods 8:6682–6686. https://doi.org/10.1039/c6ay01963c
53. Damasceno S, Corrêa CC, Gouveia RF, Strauss M, César C, Bufon B, Santhiago M (2020) Delayed capillary flow of elastomers: an efficient method for fabrication and nanofunctionalization of flexible foldable, twistable, and stretchable electrodes from pyrolyzed paper. Adv Electron Mater 1900826:1–10. https://doi.org/10.1002/aelm.201900826
54. Lin J, Peng Z, Liu Y, Ruiz-Zepeda F, Ye R, Samuel ELG, Yacaman MJ, Yakobson BI, Tour JM (2014) Laser-induced porous graphene films from commercial polymers. Nat Commun 5:5–12. https://doi.org/10.1038/ncomms6714
55. Zhang Z, Song M, Hao J, Wu K, Li C, Hu C (2018) Visible light laser-induced graphene from phenolic resin: a new approach for directly writing graphene-based electrochemical devices on various substrates. Carbon N Y 127:287–296. https://doi.org/10.1016/j.carbon.2017.11.014
56. Tasić N, Bezerra Martins A, Yifei X, Sousa Góes M, Martín-Yerga D, Mao L, Paixão TRLC, Moreira Gonçalves L (2020) Insights into electrochemical behavior in laser-scribed electrochemical paper-based analytical devices. Electrochem Commun 121. https://doi.org/10.1016/j.elecom.2020.106872

57. Tasić N, Sousa de Oliveira L, Paixão TRLC, Moreira Gonçalves L (2020) Laser-pyrolysed paper electrodes for the square-wave anodic stripping voltammetric detection of lead. Medical Devices Sensors 3. https://doi.org/10.1002/mds3.10115
58. Bezerra Martins A, Lobato A, Tasić N, Perez-Sanz FJ, Vidinha P, Paixão TRLC, Moreira Gonçalves L (2019) Laser-pyrolyzed electrochemical paper-based analytical sensor for sulphite analysis. Electrochem Commun 107:106541. https://doi.org/10.1016/j.elecom.2019.106541
59. Carvalhal RF, Kfouri MS, de Piazetta MHO, Gobbi AL, Kubota LT (2010) Electrochemical detection in a paper-based separation device. Anal Chem 82:1162–1165. https://doi.org/10.1021/ac902647r
60. Pradela-Filho LA, Noviana E, Araújo DAG, Takeuchi RM, Santos AL, Henry CS (2020) Rapid analysis in continuous-flow electrochemical paper-based analytical devices. ACS Sensors. 5:274–281. https://doi.org/10.1021/acssensors.9b02298
61. Arantes IVS, Paixão TRLC (2022) Couple batch-injection analysis and microfluidic paper-based analytical device: a simple and disposable alternative to conventional BIA apparatus. Talanta 240. https://doi.org/10.1016/j.talanta.2021.123201
62. Wang Y, Luo J, Liu J, Li X, Kong Z, Jin H, Cai X (2018) Electrochemical integrated paper-based immunosensor modified with multi-walled carbon nanotubes nanocomposites for point-of-care testing of 17β-estradiol. Biosens Bioelectron 107:47–53. https://doi.org/10.1016/j.bios.2018.02.012
63. Chaiyo S, Mehmeti E, Siangproh W, Hoang TL, Nguyen HP, Chailapakul O, Kalcher K (2018) Non-enzymatic electrochemical detection of glucose with a disposable paper-based sensor using a cobalt phthalocyanine–ionic liquid–graphene composite. Biosens Bioelectron 102:113–120. https://doi.org/10.1016/j.bios.2017.11.015
64. Fan Y, Shi S, Ma J, Guo Y (2019) A paper-based electrochemical immunosensor with reduced graphene oxide/thionine/gold nanoparticles nanocomposites modification for the detection of cancer antigen 125. Biosens Bioelectron 135:1–7. https://doi.org/10.1016/j.bios.2019.03.063
65. Caratelli V, Ciampaglia A, Guiducci J, Sancesario G, Moscone D, Arduini F (2020) Precision medicine in Alzheimer's disease: An origami paper-based electrochemical device for cholinesterase inhibitors. Biosens Bioelectron 165:112411. https://doi.org/10.1016/j.bios.2020.112411
66. Yakoh A, Pimpitak U, Rengpipat S, Hirankarn N, Chailapakul O, Chaiyo S (2021) Paper-based electrochemical biosensor for diagnosing COVID-19: detection of SARS-CoV-2 antibodies and antigen. Biosens Bioelectron 176:112912. https://doi.org/10.1016/j.bios.2020.112912